Source Apportionment and Trend Analysis of Air Particulate Matter in the Auckland Region

July 2017

Technical Report 2017/001

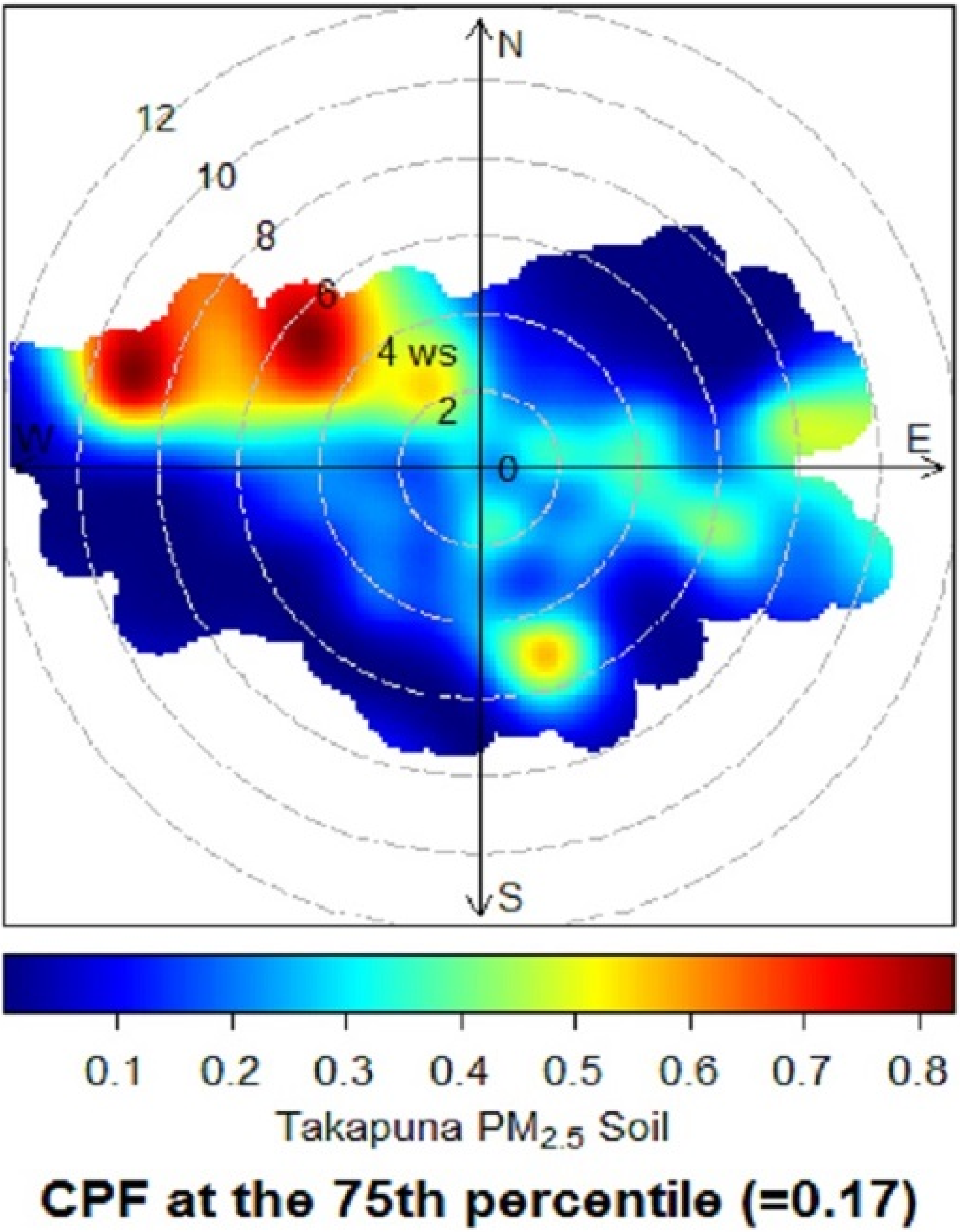

Auckland Council
Te Kaunihera o Tāmaki Makaurau

Source apportionment and trend analysis of air particulate matter in the Auckland region

July 2017 Technical Report 2017/001

P K Davy
W J Trompetter
T Ancelet
A Markwitz

Institute of Geological and Nuclear Sciences Ltd, GNS Science

Auckland Council
Technical Report TR2017/001
ISSN 2230-4525 (Print)
ISSN 2230-4533 (Online)

ISBN 978-1-98-852940-0 (Print)
ISBN 978-1-98-852941-7 (PDF)

This report has been peer reviewed by the Peer Review Panel.

Review completed on 11 July 2017
Reviewed by one reviewer

Approved for Auckland Council publication by:

Name: Dr Lucy Baragwanath

Position: Manager, Research and Evaluation (RIMU)

Name: Simon Tredgett

Position: Manager, Environmental Monitoring, Research and Evaluation (RIMU)

Date: 11 July 2017

Recommended citation

Davy, P. K., Ancelet, T., Trompetter, W. J and Markwitz, A (2017). Source apportionment and trend analysis of air particulate matter in the Auckland region. Prepared by the Institute of Geological and Nuclear Sciences Ltd, GNS Science for Auckland Council. Auckland Council technical report, TR2017/001

Date that GNS Science can use associated data: August 2014
GNS Science Consultancy Report 2014/194, July 2017

Cover image: Figure 6.20 Takapuna $PM_{2.5}$ crustal matter CPF analysis (see page 59)

© 2017 Auckland Council

This publication is provided strictly subject to Auckland Council's copyright and other intellectual property rights (if any) in the publication. Users of the publication may only access, reproduce and use the publication, in a secure digital medium or hard copy, for responsible genuine non-commercial purposes relating to personal, public service or educational purposes, provided that the publication is only ever accurately reproduced and proper attribution of its source, publication date and authorship is attached to any use or reproduction. This publication must not be used in any way for any commercial purpose without the prior written consent of Auckland Council.

Auckland Council does not give any warranty whatsoever, including without limitation, as to the availability, accuracy, completeness, currency or reliability of the information or data (including third party data) made available via the publication and expressly disclaim (to the maximum extent permitted in law) all liability for any damage or loss resulting from your use of, or reliance on the publication or the information and data provided via the publication. The publication, information, and data contained within it are provided on an "as is" basis.

CONTENTS

FIGURES

TABLES

APPENDICES

APPENDIX FIGURES

EXECUTIVE SUMMARY

This report presents an analysis of airborne particle samples from an ongoing sampling programme collected from 2006 to 2013 at five ambient air quality monitoring sites across the Auckland Region. Exposure to air pollution from airborne particles can result in significant adverse health effects for the resident population. Understanding the composition and identifying the sources of air pollution is vital for effective air quality management and policy implementation.

The main objectives of the study were to:

- identify the sources contributing to air pollution episodes;
- estimate the contribution of sea salt and other natural particulate matter sources to ambient concentrations;
- estimate the contribution of secondary particulate matter sources to ambient concentrations;
- distinguish between the contribution of home heating and motor vehicle emission sources;
- determine the variation of source contributions by season;
- examine inter-annual variations in source contributions;
- observe the trends in source contributions over time.

Airborne particles are composed of many elements and compounds from many different sources and, by analysing these components, the sources and their relative contributions to air pollution can be identified. This study represents the largest source apportionment study undertaken in New Zealand to date and provides results of benefit for air quality management in both the Auckland region and New Zealand as a whole.

Two size fractions of particles were collected for the study:

1. Samples of particulate matter less than 2.5 micrometres in diameter (denoted as $PM_{2.5}$) were collected onto filters at Takapuna, Queen Street, Khyber Pass Road and Penrose air quality monitoring sites.
2. Samples of particulate matter less than 10 micrometres in diameter (denoted as PM_{10}) were collected onto filters at Takapuna, Queen Street, Khyber Pass Road, Penrose and Henderson air quality monitoring sites.

Average source contributions to particulate matter in Auckland

The analysis of the particulate matter sample sets identified five common source contributors to both $PM_{2.5}$ and PM_{10} for the sites where samples were collected. These were

1. biomass burning;
2. motor vehicles;
3. secondary sulphate,
4. marine aerosol and;
5. crustal matter.

At some sites local industrial emissions were also identified but were found to be relatively minor contributors to particulate matter concentrations. Emissions from ships were found to be impacting on the Auckland CBD.

Average source contributions to $PM_{2.5}$ indicate that biomass burning and motor vehicle emissions are the predominant sources of $PM_{2.5}$ across all sites in Auckland. However, for the Takapuna and Queen Street sites, marine aerosol was also found to be a significant contributor. This result has implications for air quality management since marine aerosol is a naturally generated source and therefore cannot be effectively manged.

For PM_{10} (which also included the Henderson site), average source contributions show that marine aerosol and motor vehicle emissions are the predominant sources of PM_{10} across all sites in Auckland. Motor vehicle contributions to PM_{10} were significantly higher than for $PM_{2.5}$ due to the associated coarse particle road dust component. Figure ES1 presents the average source contributions to $PM_{2.5}$ and PM_{10} mass concentrations respectively.

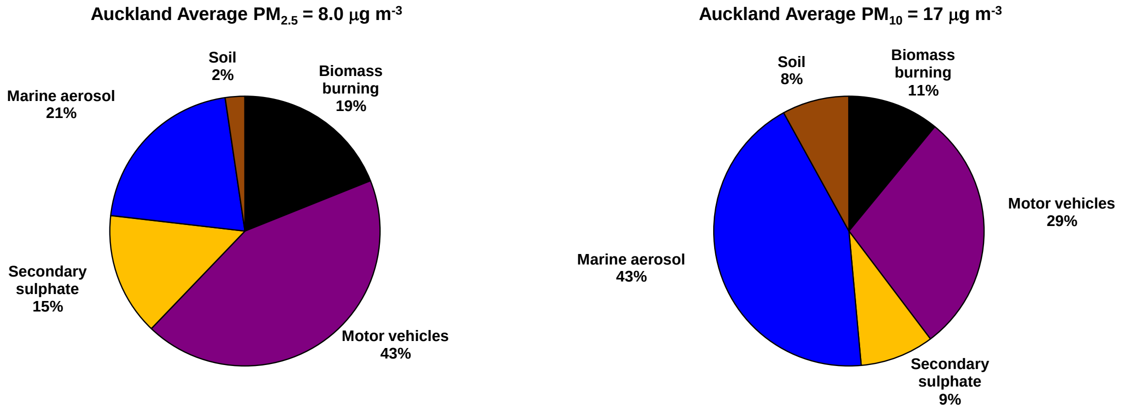

Figure ES1 Pan-Auckland average source contributions to $PM_{2.5}$ (left), and PM_{10} (right)

Biomass burning emissions, primarily due to the use of solid fuel fires for domestic heating was the dominant source during the winter months at Takapuna and Penrose with motor vehicle emissions the next significant source contributor. However, at Queen Street and Khyber Pass Road the converse was found where motor vehicle emissions were the primary source during winter due the proximity to busy roadways. The data shows that motor vehicle emissions were the primary anthropogenic source contributor during all other seasons at all sites.

Secondary sulphate and marine aerosol concentrations were highest at all sites during the spring and summer months. Crustal matter was present as a minor contributor at all sites and largely dependent on the nature of local dust generating activities.

Inter-annual trends in source contributions to particulate matter in Auckland

Over the monitoring period it was found that $PM_{2.5}$ concentrations decreased at all monitoring sites and for some sites (e.g. Queen Street) the decrease was more marked than others due to significant changes in emission source activities. Similar to $PM_{2.5}$, trend analysis showed PM_{10} concentrations have also decreased across all monitoring locations.

It would appear that decreasing $PM_{2.5}$ concentrations are largely responsible (approximately 70 %) for the observed decrease in PM_{10}. Understanding the drivers for the observed decrease in particulate matter concentrations across the Auckland urban area is necessary from both regulatory and policy perspectives in order to measure the effectiveness of policy implementation. The following individual source trend observations were made:

1. Biomass burning source contributions to urban particulate matter concentrations (both $PM_{2.5}$ and PM_{10}) in Auckland were found to be increasing. The Biomass burning source is primarily related to use of solid fuel fires for domestic heating during the winter. The reasons for the increase in source contributions are unclear since reductions might be expected with widespread introduction of alternative space heating technologies (such as heat pumps).
2. Particulate matter associated with motor vehicle emissions were found to have markedly decreased at all sites over the monitoring period for both $PM_{2.5}$ and PM_{10}. Reductions in motor vehicle associated $PM_{2.5}$ concentrations were driving the commensurate decrease in PM_{10}. Detailed analysis of the data from individual sites suggests that tailpipe emissions reductions from diesel vehicles are largely responsible for the observed trends, most likely through improvements in fuel formulation and engine technology. The particulate matter fraction between $PM_{2.5}$ and PM_{10} associated with motor vehicles, primarily from re-suspension of road dusts, was not found to be decreasing, and was actually increasing at some sites (Takapuna, Khyber Pass Road, Henderson) in line with traffic volume increases. The predominance of motor vehicle sources (tailpipe emissions and associated road dust component) presents chronic exposure risk since the contributions are relatively consistent all year and the particles are composed of a combination of ultra-fine (<300 nm) carbonaceous aerosol and coarse particles that include of a range heavy metal species (Zn, Cu, Sb, Ba) from brake linings and mechanical abrasion of parts and surfaces (tyres, road surface).
3. The long term trend analysis for secondary sulphate contributions to $PM_{2.5}$ and PM_{10} shows that concentrations have been decreasing in urban particulate matter over the monitoring period. A significant influence on secondary sulphate concentrations is the production of precursor gases such as SO_2 from combustion of sulphur containing fuels in urban areas. The stepwise introduction (2006 – 2010) of low sulphur automotive fuels appears to have been the main driver of secondary sulphate reductions across the Auckland urban area.
4. Trends in marine aerosol source contributions provided one of the most interesting results from the data analysis which found that concentrations (dominated by sea salt) are trending downwards across all sites in Auckland. The marine aerosol component of urban air particulate matter is part of the ‘natural’ background and therefore is that proportion that cannot be managed. The apparent decrease therefore has implications for air quality management in Auckland. At this stage it is unclear whether the observed decreases in marine aerosol concentrations are part of a larger inter-decadal cycle related to Southern Hemisphere circulation patterns or a more permanent trend.
5. Crustal matter source contributions at the monitoring sites in Auckland were likely to be a combination of windblown soil, road dust and dust generated by earthworks, construction and road works. Concentrations were found to vary from site to site depending on meteorological conditions and local dust generating activities. The long-term trend analyses for crustal matter contributions to urban particulate matter showed that there is a small apparent decrease in contributions but this was largely site dependent and more reflective of the episodic nature of local activities.

The trend analysis of Auckland particulate matter indicates that improvements in motor vehicle emissions were responsible for approximately 50 % of the observed reduction in $PM_{2.5}$ concentrations with rest accounted for by the reduction in secondary sulphate and marine aerosol concentrations.

1.0 INTRODUCTION

This report presents the results of an extensive receptor modelling study of ten datasets of airborne particle samples sets collected at five ambient air quality monitoring sites across the Auckland Region from 2006 to 2013. The work was commissioned by the Auckland Council (AC) as part of their ambient air quality monitoring strategy.

1.1 REQUIREMENT TO MANAGE AIRBORNE PARTICLE POLLUTION

In response to growing evidence of significant health effects associated with airborne particle pollution, the New Zealand Government introduced in 2005 a National Environmental Standard (NES) of 50 μg/m^3 for particles less than 10 μm in aerodynamic cross section (denoted as PM_{10}). The NES places the onus on regional councils to monitor PM_{10} and publicly report if the air quality in their region exceeds the standard. Regional councils were originally required to comply with the standard by 2013 or face restrictions on the granting of resource consents for discharges to air that contain PM_{10}. However, the NES regulations were amended in April 2011 following a technical review, regulatory authorities are now required to comply by 2016 with a provision for no more than one exceedence annually plus exceptional events by application for exemption (e.g. dust storms, volcanic eruptions) and a requirement for offsets by industry in PM_{10} polluted airsheds replacing the restriction on industrial consents (Ministry for the Environment. 2011. *Clean Healthy Air for All New Zealanders: National Air Quality Compliance Strategy to Meet the* PM_{10} *Standard*).

Clearly then, in areas where the PM_{10} standard is exceeded, information on the sources contributing to those air pollution episodes is required in order to:

- identify ‘exceptional events’ outside of regulatory authority control;
- effectively manage air quality and;
- formulate appropriate mitigation strategies where necessary.

In addition to the PM_{10} NES, the Ministry for the Environment issued ambient air quality guidelines for air pollutants in 2002 that included a (monitoring) guideline value of 25 μg m^{-3} for $PM_{2.5}$ (24-hour average). More recently, the World Health Organisation (WHO) has confirmed a $PM_{2.5}$ ambient air quality guideline value of 25 μg m^{-3} (24-hour average) based on the relationship between 24-hour and annual PM levels. The WHO annual average guideline for $PM_{2.5}$ is 10 μg m^{-3}. These are the lowest levels at which total, cardiopulmonary and lung cancer mortality have been shown to increase with more than 95% confidence in response to exposure to $PM_{2.5}$. WHO recommends the use of $PM_{2.5}$ guidelines over PM_{10} as epidemiological studies have shown that most of the adverse health effects associated with PM_{10} is due to $PM_{2.5}$.

1.2 IDENTIFYING SOURCES OF AIRBORNE PARTICLE POLLUTION

Measuring the mass concentration of air particulate matter provides little information on the identity of the contributing sources. Airborne particles are composed of many elements and compounds from many different sources. Receptor modelling provides a means to determine the relative mass contribution of sources that impact significantly on the total mass of air particulate matter collected at a monitoring site. Firstly, gravimetric mass is determined and then a variety of methods can be used to determine the elements and compounds present in a sample. For this study elemental concentrations in the samples were determined by ion beam analysis (IBA) at the New Zealand Ion Beam Analysis Facility operated by GNS Science in Lower Hutt.

Ion beam analysis is a mature analytical technique that provides a non-destructive determination of multi-elemental concentrations present in a sample. Using elemental concentrations with appropriate statistical techniques and purpose-designed mathematical models the sources contributing to each ambient sample can be estimated. In general the more ambient samples that are included in the analysis the more robust the receptor modelling results.

The main objectives of the study were to:

- identify the sources contributing to air pollution episodes
- estimate the contribution of sea salt and other natural particulate matter sources to ambient concentrations
- estimate the contribution of secondary particulate matter sources to ambient concentrations
- distinguish between the contribution of home heating and motor vehicle emission sources
- determine the variation of source contributions by season
- examine inter-annual variations in source contributions
- observe the trends in source contributions over time.

This study represents the largest source apportionment study undertaken in New Zealand to date and provides results of benefit for both the Auckland region and New Zealand as a whole. This report describes the sampling, the results and the outcomes according to these objectives.

1.3 REPORT STRUCTURE

The report is comprised of several different parts as follows:

Chapter 2 provides a synopsis of the previous studies and an overview of the approach taken in this study (2014 analysis) of the contribution of different sources to air particulate matter pollution in the Auckland region. The information derived during the previous studies provides a background on which the current study has expanded.

Chapter 3 briefly describes the analytical techniques and methodology used for the receptor modelling analysis.

Chapter 4 presents a synopsis of the receptor modelling results from across the five sampling sites in the Auckland region. Included in this chapter are the significant results and trend analyses for sources on an Auckland-wide basis.

Chapter 5 presents an analysis of individual elements that are important contributors to particulate matter on a region-wide basis.

Chapters 6 to 10 present the receptor modelling results on a site by site basis.

2.0 SYNOPSIS OF PREVIOUS ANALYSES AND APPROACH TO THE 2014 ANALYSIS

The 2007 report *Source apportionment of airborne particles in the Auckland region* (Davy, Trompetter et al. 2007) and 2008 report Source apportionment of airborne particles in the Auckland region: 2008 Update (Davy, Trompetter et al. 2009) gathered together 14 datasets of $PM_{2.5}$ and PM_{10} filter samples collected during 2006 and 2007 at six air quality monitoring sites across the Auckland region for a receptor modelling study. Ion beam analysis was used to provide the elemental composition of the particle samples. Data analysis techniques were used to elucidate the sources that were the primary contributors to ambient $PM_{2.5}$ and PM_{10} concentrations at the Auckland air quality monitoring sites.

The results contained in the 2007 and 2008 reports showed that five common source contributors were identified for the sites where $PM_{2.5}$ samples were collected. These were biomass burning, secondary sulphate, crustal matter, motor vehicle emissions and marine aerosol. Similar to the $PM_{2.5}$ results, five common source contributors were also identified for the PM_{10} sampling locations. The 2006 and 2007 sampling data showed that source mass contributions demonstrated consistent trends between sites and that biomass burning was significant at all sites during winter, motor vehicle emission sources provided a constant level of $PM_{2.5}$ and PM_{10} across Auckland urban areas and that marine aerosol was a particularly significant contributor to PM_{10} in Auckland. The 2007 and 2008 reports provided the basis for the next report, the 2010 Analysis. The datasets analysed previously were extended to four years of sampling at all sites with the exception of the Kingsland site which was disestablished in September 2007.

The *2010 Analysis* (Davy, Trompetter et al. 2011) reanalysed all datasets from initial compilation of the analytical elemental spectra and quality assurance process through to generation of receptor modelling and source apportionment analyses. As such, the results contained in that report were essentially independent of the 2007 and 2008 reports. The expansion of the datasets provided greater confidence and consistency in the results and enabled year on year variations in source contributions to be assessed.

This report, *Source apportionment and trend analysis of air particulate matter in the Auckland Region*, has taken the previous PM_{10} and $PM_{2.5}$ datasets from five air quality monitoring sites across Auckland and added another four years of sampling results to provide a continuous eight-year sampling record. The Auckland particulate matter speciation dataset is now comprised of over 10,000 individual samples with the elemental speciation of each sample providing a database comprised of more than 250,000 individual datapoints. For this report, the data has been reanalysed from initial compilation of the analytical elemental data and quality assurance process through to generation of receptor modelling and source apportionment analyses.

The critical difference for the current study compared to the earlier analyses, was that eight years of monitoring data has provided the basis for a trend analysis of both the underlying elemental composition data and the sources contributing to air pollution in Auckland. Most significantly, the particulate matter composition database that has now been established for Auckland has enabled the identification of more minor sources (mainly industrial emissions), variations in the primary sources including the separation of emissions from petrol and diesel fuelled vehicles along with the impact of shipping emissions on the Auckland CBD. Arsenic and lead contamination data has been attributed to burning of treated timber and old painted timber respectively as fuel for domestic fires. These results have important implications for air quality management and key considerations for air quality policy formulation in the Auckland region.

3.0 METHODOLOGY

3.1 PARTICULATE MATTER SAMPLING SITES

Samples of particulate matter collected on filters from five Auckland Council monitoring sites were received by GNS Science on an annual basis. Elemental concentrations in the particle samples were determined by ion beam analysis techniques at the New Zealand Ion Beam Analysis (IBA) Facility at Gracefield, Lower Hutt. A full description of the IBA methods and data analysis techniques used in this report is provided in Appendix 1.

All particulate matter sampling and systems maintenance at sampling sites was carried out by Watercare Services Limited (WSL) on contract to Auckland Council. As such, WSL maintains all records of equipment, flow rates, filter weighing and sampling methodologies used for the particulate matter sampling regimes.

The authors of this report have previously visited all sites and noted site locations and typical activities in the surrounding area that may contribute to particulate matter concentrations. These observations are reflected in the conceptual receptor models described for each site in Chapters 6 to 10. Figure 3.1 presents the locations of each of the monitoring sites described in this study.

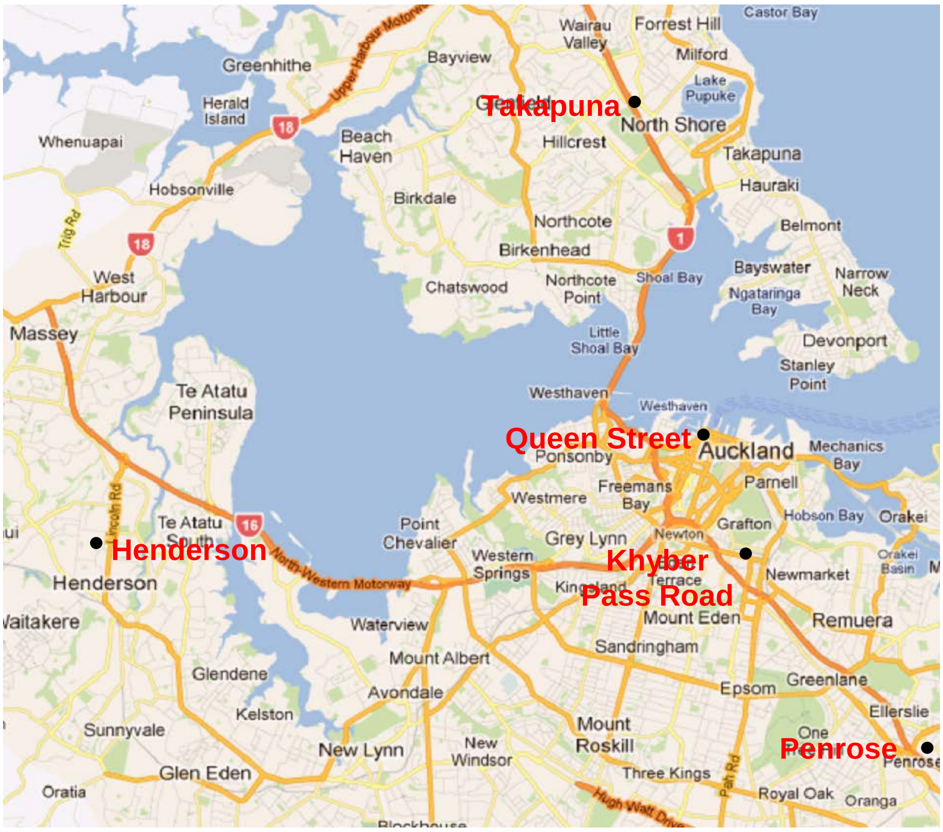

Figure 3.1 Location of the five monitoring sites (●) included in the Auckland receptor modelling study (source: Wisesmaps.co.nz)

3.2 RECEPTOR MODELLING PROCESS

The multivariate analysis of air particulate matter sample composition (also known as receptor modelling) provides groupings (or factors) of elements that vary together over time. This technique effectively ‘fingerprints’ the sources that are contributing to airborne particulate matter and the mass of each element (and the PM mass) attributed to that source. In this study the primary source contributors were determined using results from the Positive Matrix Factorisation (PMF analysis) of the particulate matter elemental composition.

A critical point for understanding the receptor modelling process is that the PMF model can produce any number of solutions, all of which may be mathematically correct (Paatero, Hopke et al. 2002). The “best” solution (eg., number of factors, etc.) is generally determined by the practitioner after taking into account the model diagnostics and a review of the available factor profiles and contributions (to check physical interpretability). Most commonly used receptor models are based on conservation of mass from the point of emission to the point of sampling and measurement (Hopke 1999). Their mathematical formulations express ambient chemical concentrations as the sum of products of species abundances in source emissions and source contributions. In other words, the chemical profile measured at a monitoring station is resolved mathematically to be the sum of a number of different factors or sources. As with most modelling approaches, receptor models based on the conservation of mass are simplifications of reality and have the following general assumptions:

1. compositions of source emissions are constant over the period of ambient and source sampling;
2. chemical species do not react with each other (i.e., they add linearly);
3. all sources with a potential for contributing to the receptor have been identified and have had their emissions characterized;
4. the number of sources or source categories is less than or equal to the number of species measured;
5. the source profiles are linearly independent of each other; and
6. measurement uncertainties are random, uncorrelated, and normally distributed.

The effects of deviations from these assumptions are testable, and can therefore allow the accuracy of source quantification to be evaluated. Uncertainties in input data can also be propagated to evaluate the uncertainty of source contribution estimates. There are a number of natural physical restraints that must be considered when developing a model for identifying and apportioning sources of airborne particles, these are (Hopke 2003):

- the model must explain the observations;
- the predicted source compositions must be non-negative;
- the predicted source contributions must be non-negative;
- the sum of predicted elemental mass contributions from each source must be less than or equal to measured mass for each element.

These constraints need to be kept in mind when conducting and interpreting any receptor modelling approach, particularly since a receptor model is still an approximation of the real-world system. A number of factors also affect the nature of a sources' particle composition and its contributions to ambient loadings (Brimblecombe 1986, Hopke 1999, Seinfeld and Pandis 2006):

1. the composition of particles emitted from a source may vary over time;
2. the composition of particles is modified in the atmosphere through a multitude of processes and interactions, for example;

- adsorption of other species onto particle surfaces;
- gas to particle conversions forming secondary particulate matter, for example the conversion of SO_2 gas to SO_4^{2-};
- volatilisation of particle components such as organic compounds or volatilisation of Cl through reaction with acidic species;
- interaction with and transformation by, solar radiation and free radicals in the atmosphere such as the OH and NO_3 species.

The analytical processes used in this study did not analyse for nitrate so the missing mass that the analysis is not explaining is likely a combination of nitrate and other unmeasured species. Measurement of the ionic components (Selleck and Keywood 2012) in $PM_{2.5}$ at the Takapuna site between 2009 and 2013 suggests that the nitrate content (as NH_4NO_3) contributes approximately 3 % to total $PM_{2.5}$ mass on average.

Analytical noise is also introduced during the species measurement process such as analyte interferences and limits of detection for species of interest. These are at least in the order of 5% for species well above its respective detection limit and 20% or more for those species near the analytical method detection limit (Hopke 1999). Further details on data analysis and dataset preparation are provided in Appendix 1.

3.3 DATA ANALYSIS AND DATA REPORTING

The results of receptor modelling have been reported in a manner that provides as much information as possible on the contributions of sources to particulate matter concentrations so that it may be used for monitoring strategies, air quality management and policy development. A useful method to illustrate the significance of ambient air quality monitoring results is to identify those days that the monitoring results fall into certain categories. This method is described by the Ministry for the Environment in the discussion document on Environmental Performance Indicators (Ministry for the Environment, October 1997). Table 3.1 provides a description of these categories.

Table 3.1 Ambient air quality categories

Category	Maximum Measured Value	Comment
Action	Exceeds Guideline	Completely unacceptable by national and international standards.
Alert	Between 66% and 100% of the guideline	A warning level which can lead to guidelines being exceeded if trends are not curbed.
Acceptable	Between 33% and 66% of the guideline	A broad category, where maximum values might be of concern in some sensitive locations, but are generally at a level that does not warrant dramatic action.
Good	Between 10% and 33% of the guideline	Peak measurements in this range are unlikely to affect air quality.
Excellent	Less than 10% of the guideline	Of little concern.

The main intention of the air quality categories is to present the results of ambient monitoring in a manner that assists in setting goals for air quality management. Sample days where particulate matter concentrations exceeded 66 % (i.e. fell within the alert or action categories) of the relevant guideline or standard have been identified and the mass concentrations of contributing sources presented for each of the sample datasets.

The data have been analysed to provide the following outputs:

1. Mass of PM and mass of elemental species apportioned to each source;
2. Source elemental profiles;
3. Average percentage PM mass apportioned to each source;
4. Temporal variation of source mass contributions (time-series plots);
5. Seasonal variations in source mass contributions. For the purposes of this study
    a. summer has been defined as December to February inclusive;
    b. autumn; March - May;
    c. winter; June – August;
    d. spring; September – November.;
6. Weekend and weekday split of source contributions to examine variations in source activity;
7. Inter-annual variations and trends;
8. Analysis of source contributions on peak PM days and the meteorology associated with peak pollution events. Peak PM days were defined as those sample days where particulate matter concentrations were higher than 66 % of either the National Environmental Standard (NES) for PM_{10} or the Ambient Air Quality Guidelines (AAQG) $PM_{2.5}$ monitoring guideline. Table 3.2 presents the relevant standards, guidelines and targets.

Table 3.2 Standards, guidelines and targets for particulate matter in Auckland

Particle size	PM_{10}		$PM_{2.5}$
Averaging Time	24 hour	Annual	24 hour
Ambient Air Quality Guideline	50 μg m^{-3}	20 μg m^{-3}	25 μg m^{-3}
National Environmental Standard	50 μg m^{-3}		
NES – allowable exceedances per year	3[1]		
MfE* ‘Acceptable’ air quality category	33 μg m^{-3}	13 μg m^{-3}	17 μg m^{-3}

*Ministry for the Environment air quality categories taken from Ministry for the Environment, October 1997. Environmental Performance Indicators: Proposals for Air, Fresh Water and Land

In addition to these analyses, the variation of source strength with wind direction has been examined using Conditional Probability Function (CPF) analysis. This method is described in Section 3.2.2. Back trajectories of air mass parcels have also been calculated using HYSPLIT (see Section 3.3 and Section 3.4) and presented where it was considered useful for understanding and rationalising results, particularly for those sources considered as resulting from long range transport or to confirm source directionality.

3.3.1 Long-term trend analyses

For all statistical analyses presented in this report, the *openair* package based on ‘R’ statistical software has been used to analyse the Nelson data for trends (Team 2011, Carslaw 2012, Carslaw and Ropkins 2012). For the trend analysis, the TheilSen function in *openair* was used (Carslaw 2012). The analysis of trends in the particulate matter concentration and source contribution data are accompanied by confidence interval estimates for the observed trends. The following paragraph describes the basis of the TheilSen function and is taken from Carslaw 2015.

> Given a set of n x, y pairs, the slopes between all pairs of points are calculated. Note, the number of slopes can increase by ≈ n^2 so that the number of slopes can increase rapidly as the length of the data set increases. The Theil-Sen estimate of the slope is the median of all these slopes. The advantage of the using the Theil-Sen estimator is that it tends to yield accurate confidence intervals even with non-normal data and heteroscedasticity (non-constant error variance). It is also resistant to outliers — both characteristics can be important in air pollution. As previously mentioned, the estimates of these parameters can be made more robust through bootstrap-resampling, which further adds to the computational burden, but is not an issue for most time series which are expressed either as monthly or annual means. Bootstrap resampling also provides the estimate of p for the slope. (Carslaw 2015)

Only those trend results with statistical significance (p) above the 90th percentile confidence intervals have been considered in the current work. All TheilSen trend analyses were generated using deseasonalised (using the functionality available within *openair*) data to remove seasonal effects.

---

[1] Revised in 2011 from one exceedence

3.3.2 Conditional probability function analysis

A useful data analysis method is to investigate the relationship between the source contributions and wind direction. Bivariate polar plots using the source contributions to particulate matter were produced using R statistical software and the *openair* package (Team 2011, Carslaw 2012, Carslaw and Ropkins 2012). Using bivariate polar plots, source contributions can be shown as a function of both wind speed and direction, providing invaluable information about potential source regions and how pollution from a specific source builds up. To produce the polar plots, wind speeds and directions were vector averaged using functions available in *openair*. A full description of the vector averaging process can be found in Carslaw (2012).

Conditional Probability Function (CPF) analysis provides a method to find the directions for which high values of source contributions are likely to be related. The probability that a source contribution originates from a given wind direction is estimated by comparing the wind direction distribution for the upper 25 % of source contributions relative to the total wind direction distribution.

$$CPF_{\Delta\theta} = \frac{m_{\Delta\theta}}{n_{\Delta\theta}} \tag{3.15}$$

Where:

$m_{\Delta\theta}$: Number of occurrences from wind sector $\Delta\theta$ for the upper 25 % of source contributions.

$n_{\Delta\theta}$: Total number of occurrences from the same wind sector.

Sources are likely to be located in the directions that have high CPF values. Because of the smoothing involved, the colour scale is only to provide an indication of overall pattern and should not be interpreted in concentration units. An example output (from Takapuna PM_{10} data – see Section 6.7) is provided in Figure 3.2 showing that the ‘Cement’ source originates from southeast of the monitoring site and that the highest concentrations occur during moderate to strong winds.

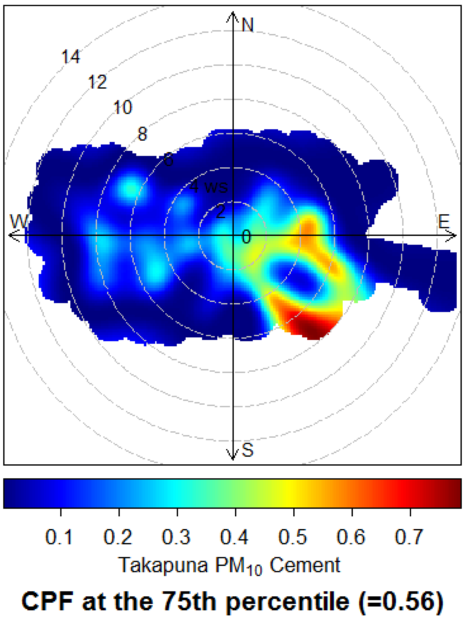

Figure 3.2 Takapuna PM$_{10}$ Cement source CPF analysis

3.3.3 HYSPLIT air-mass back- trajectories

The HYSPLIT (HYbrid Single-Particle Lagrangian Integrated Trajectory) model is a complete system, from computing simple air parcel trajectories to complex dispersion and deposition simulations (Draxler and Rolph 2003). For the purpose of this study, HYSPLIT has been used to calculate the back trajectories of air parcels for sample days of interest in order to examine long-range atmospheric transport processes and determine potential particulate matter source locations.

3.3.4 Potential source contribution function analyses

Potential source contribution function (PSCF) analysis is the conditional probability that an air parcel with a certain level of pollutant concentrations arrives at a receptor site after having passed through a specific upwind source region (Hsu, Holsen et al. 2003, Hwang and Hopke 2007). The PSCF values were obtained using the source contributions derived from PMF analyses and air-mass back trajectories produced by HYSPLIT. PSCF$_{ij}$ is defined as:

$$PSCF_{ij} = \frac{m_{ij}}{n_{ij}} \qquad (3.16)$$

where n_{ij} is the total number of endpoints that fall in the ijth cell and m_{ij} is the number of endpoints in the same cell that exceed, in this study, a threshold criterion of the average contribution from each source. If a trajectory associated with a sample has a mass contribution higher than the criterion, then a high PSCF value in a cell (1 degree latitude and longitude or 100 km x 100 km) represents a potential source area. For this study 96 hour backward trajectories were calculated every 4 hours (0, 4, 8, 12, 16, 20, 24 UTC) at 500 m above ground level using the National Centers for Environmental Prediction and the National Center for Atmospheric Research (NCEP/NCAR) global reanalysis data (http://www.arl.noaa.gov/gbl_reanalysis.php).

PART 1: OVERVIEW OF SOURCE CONTRIBUTIONS AND TREND ANALYSIS FOR AIR PARTICULATE MATTER IN AUCKLAND

4.0 INTERSITE COMPARISON OF PARTICULATE MATTER SOURCES

The receptor modelling results for the five Auckland monitoring sites have been compiled so that the results can be compared. Table 4.1 presents a summary of size fraction sampled, number of samples and monitoring period for each of the Auckland sites.

Table 4.1 Auckland monitoring site summary: size fraction, sample number and sample period

Site	PM size fraction	Instrument type	Number of filter samples included in analysis	Sample period
Takapuna	$PM_{2.5}$	RAAS speciation sampler	765	November 2006 – December 2013
	PM_{10}	Partisol 2000	877	December 2005 - December 2013
Queen Street	$PM_{2.5}$	Partisol 2000	908	December 2005 - December 2013
	PM_{10}	Partisol sequential	2622	December 2005 - December 2013
Khyber Pass	$PM_{2.5}$	Partisol 2000	921	December 2005 - December 2013
	PM_{10}	Partisol 2000	892	December 2005 - December 2013
Penrose	$PM_{2.5}$	Partisol speciation sampler	807	January 2006 - December 2013
	PM_{10}	Partisol speciation sampler	790	May 2006 - December 2013
	PM_{10}	Partisol 2000	779	January 2007 – December 2013
Henderson	PM_{10}	Partisol 2000	798	August 2006 – December 2013

Section 4.1 compares source mass contributions by average, seasonal and weekday/weekend differences.

4.1 INTERSITE COMPARISON OF SOURCE CONTRIBUTIONS

4.1.1 Average source contributions to $PM_{2.5}$

Five common source contributors were identified for the sites where $PM_{2.5}$ samples were collected. These were biomass burning, motor vehicles, secondary sulphate, marine aerosol and crustal matter. The average ambient $PM_{2.5}$ concentrations and source mass contributions common to each site are presented in Table 4.2 and Figure 4.1. In all cases the averages are for time periods for each dataset indicated in Table 4.2. Note that motor vehicle source contributions have been combined for those sites where more than one motor vehicle source contribution was determined (for the split between petrol and diesel emissions please refer to the individual sites described in Chapters 6 to 10).

Table 4.2 Average* $PM_{2.5}$ concentrations and source mass contributions for Auckland sites

Monitoring period	Site	$PM_{2.5}$ ($\mu g\ m^{-3}$)	Biomass burning ($\mu g\ m^{-3}$)	Motor vehicles ($\mu g\ m^{-3}$)	Secondary sulphate ($\mu g\ m^{-3}$)	Marine aerosol ($\mu g\ m^{-3}$)	Soil ($\mu g\ m^{-3}$)
2007-2013	Takapuna	7.0 ±0.2	1.7 ±0.2	1.7 ±0.1	0.8 ±0.06	2.3 ±0.1	0.2 ±0.05
2006-2013	Queen Street	9.5 ±0.4	0.8±0.6	3.6 ±0.7	0.9 ±0.3	2.1 ±0.4	0.1 ±0. 3
2006-2013	Khyber Pass Road	8.3 ±0.4	1.3 ±0.2	4.1 ±0.4	1.3 ±0.2	0.9 ±0.2	0.03 ±0.02
2006-2013	Penrose	7.1 ±0.5	1.5 ±0.3	2.5 ±0.3	1.0 ±0.1	0.5 ±0.1	0.3 ±0.2

*±standard deviation in mean contribution

Average contributions to $PM_{2.5}$ indicate that biomass burning and motor vehicle emissions are the predominant sources of $PM_{2.5}$ across all sites in Auckland. However for the Takapuna and Queen Street sites, marine aerosol was also found to be a significant contributor.

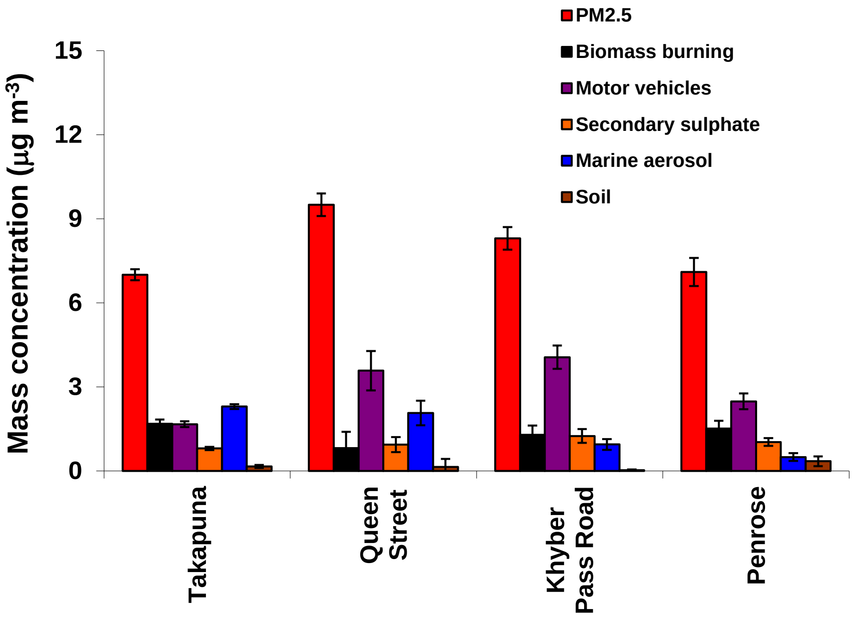

Figure 4.1 Average $PM_{2.5}$ concentrations and source mass contributions at Auckland monitoring sites

4.1.2 Average source contributions to PM_{10}

Similar to the $PM_{2.5}$ results, five common source contributors were identified for the PM_{10} sampling locations which also included the Henderson site The average PM_{10} concentrations and source contributions to PM_{10} determined for sources common to each site are presented in Table 4.3 and Figure 4.2. In all cases this represents the average across the entire dataset with the time periods as indicated in Table 4.3. Note that motor vehicle source contributions have been combined for those sites where more than one motor vehicle source contribution was determined.

Table 4.3 Average* PM_{10} concentrations and source mass contributions for Auckland sites

Monitoring period	Site	PM_{10} (µg m^{-3})	Biomass burning (µg m^{-3})	Motor vehicles (µg m^{-3})	Sulphate (µg m^{-3})	Marine aerosol (µg m^{-3})	Soil (µg m^{-3})
2006-2009	Takapuna	16.1 ±0.6	2.1 ±0. 4	3.4 ±0.5	2.2 ±0.4	6.3 ±1.5	1.0 ±0.2
2006-2009	Queen Street	17.7 ±0.4	1.2 ±0.4	5.8 ±0.7	1.0 ±0.4	6.9 ±0.6	1.0 ±0.3
2006-2009	Khyber Pass Road	18.2 ±0.6	1.4 ±0.2	4.9 ±0.6	1.7 ±0.5	7.6 ±0.5	1.4 ±0.4
2006-2009	Penrose	16.9 ±0.6	2.0 ±0.5	3.9 ±0.4	1.4 ±0.3	6.8 ±0.2	1.7 ±0.2
2007-2009	Henderson	13.7 ±0.6	2.3 ±0.3	2.0 ±0.3	1.4 ±0.5	6.0 ±0.4	1.2 ±0.1

*±standard deviation in mean contribution

Average source contributions to PM_{10} show that marine aerosol and motor vehicle emissions are the predominant sources of PM_{10} across all sites in Auckland. Figure 4.2 illustrates the importance of the marine aerosol and soil contributions to the coarse fraction of PM_{10} (i.e. $PM_{10-2.5}$). Motor vehicle contributions to PM_{10} were also significantly higher than for $PM_{2.5}$ due to the associated coarse particle road dust component.

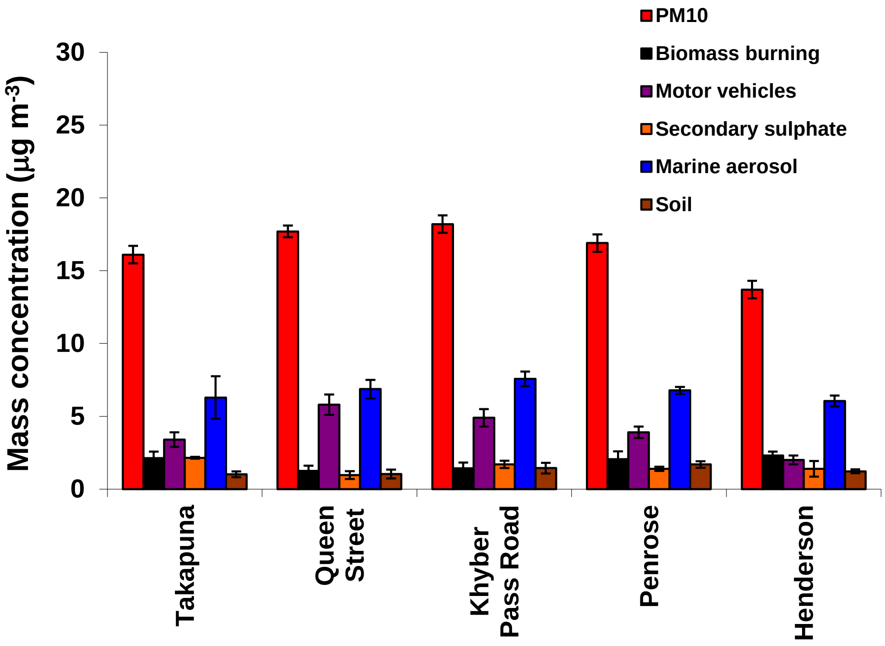

Figure 4.2 Average PM_{10} concentrations and source mass contributions at Auckland monitoring sites

4.1.3 Seasonal source contributions for $PM_{2.5}$

Five common source contributors were identified for the sites where $PM_{2.5}$ samples were collected. These were biomass burning, motor vehicles, secondary sulphate, marine aerosol and crustal matter. Figure 4.3 presents the average monthly source mass contributions at each $PM_{2.5}$ monitoring site. The monthly averages cover the entire monitoring period for each sample set as detailed in Table 4.1 and show the seasonal variations.

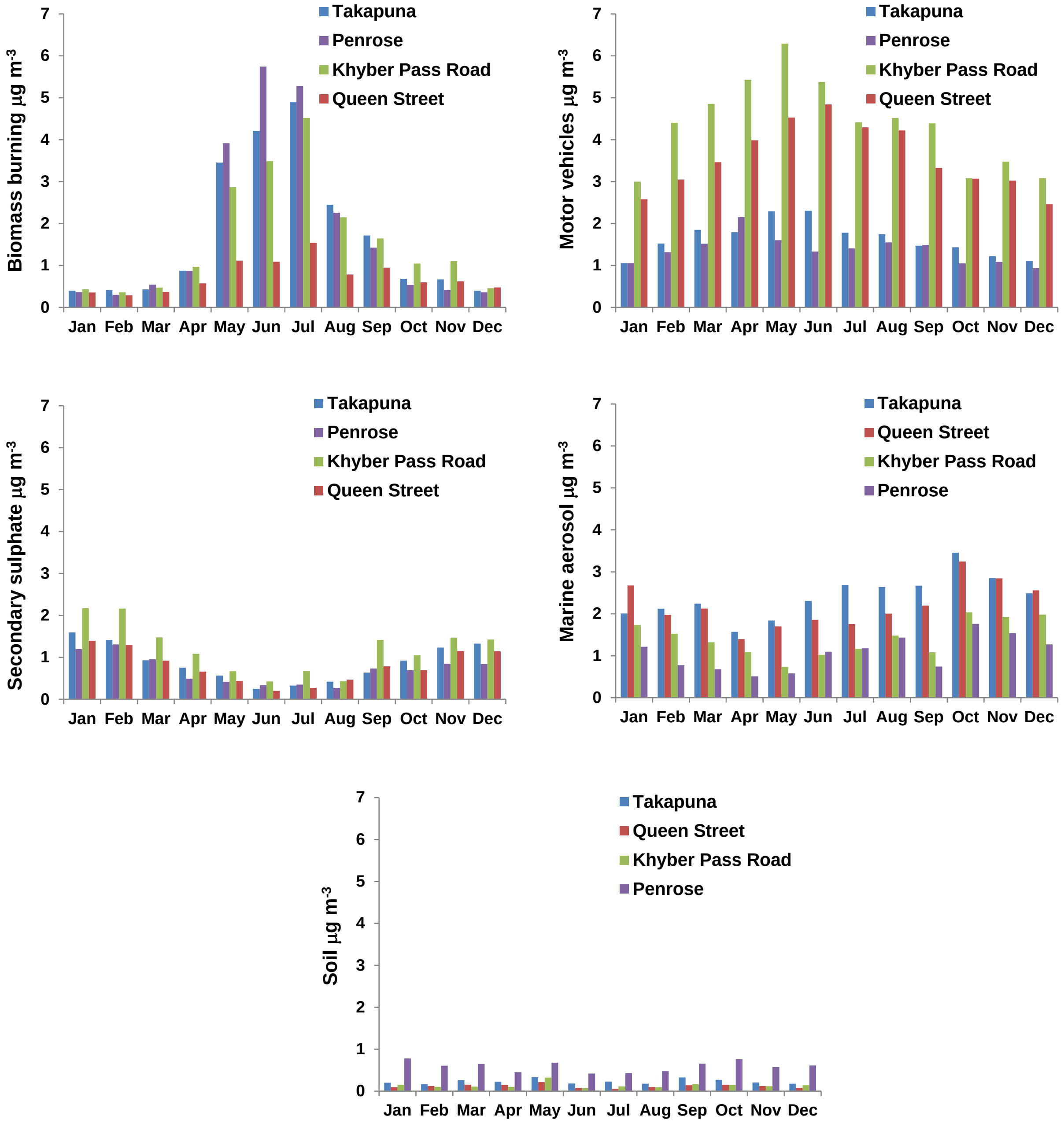

Figure 4.3 Monthly average $PM_{2.5}$ mass contributions for sources common to each AC monitoring site

Biomass burning was the dominant source during the winter months at Takapuna and Penrose with motor vehicle emissions the next significant source contributor. However, at Queen Street and Khyber Pass Road the converse was found where motor vehicle emissions were the primary source. Note that for Takapuna, Khyber Pass Road and Queen Street the two motor vehicle source contributions (Diesel vehicles + Petrol vehicles) have been combined. The data shows that motor vehicle emissions were the primary anthropogenic source contributor during all other seasons at all sites and that there is a constant baseline of 1 - 2 $\mu g\ m^{-3}$ of marine aerosol in $PM_{2.5}$.

Secondary sulphate and marine aerosol concentrations were highest at all sites during the spring and summer months. Crustal matter was present as a minor contributor at all sites except for Penrose where the crustal matter component includes contributions from nearby industrial activities.

4.1.4 Seasonal source contributions for PM_{10}

As with the $PM_{2.5}$ results, five common source contributors were identified for the PM_{10} sampling locations which also includes the Henderson site. Figure 4.4 presents the monthly average source mass contributions for PM_{10} at each monitoring site showing the seasonality in mass contributions for biomass burning, motor vehicle emissions, secondary sulphate and marine aerosol. The monthly averages cover the entire monitoring period for each sample set as detailed in Table 4.1.

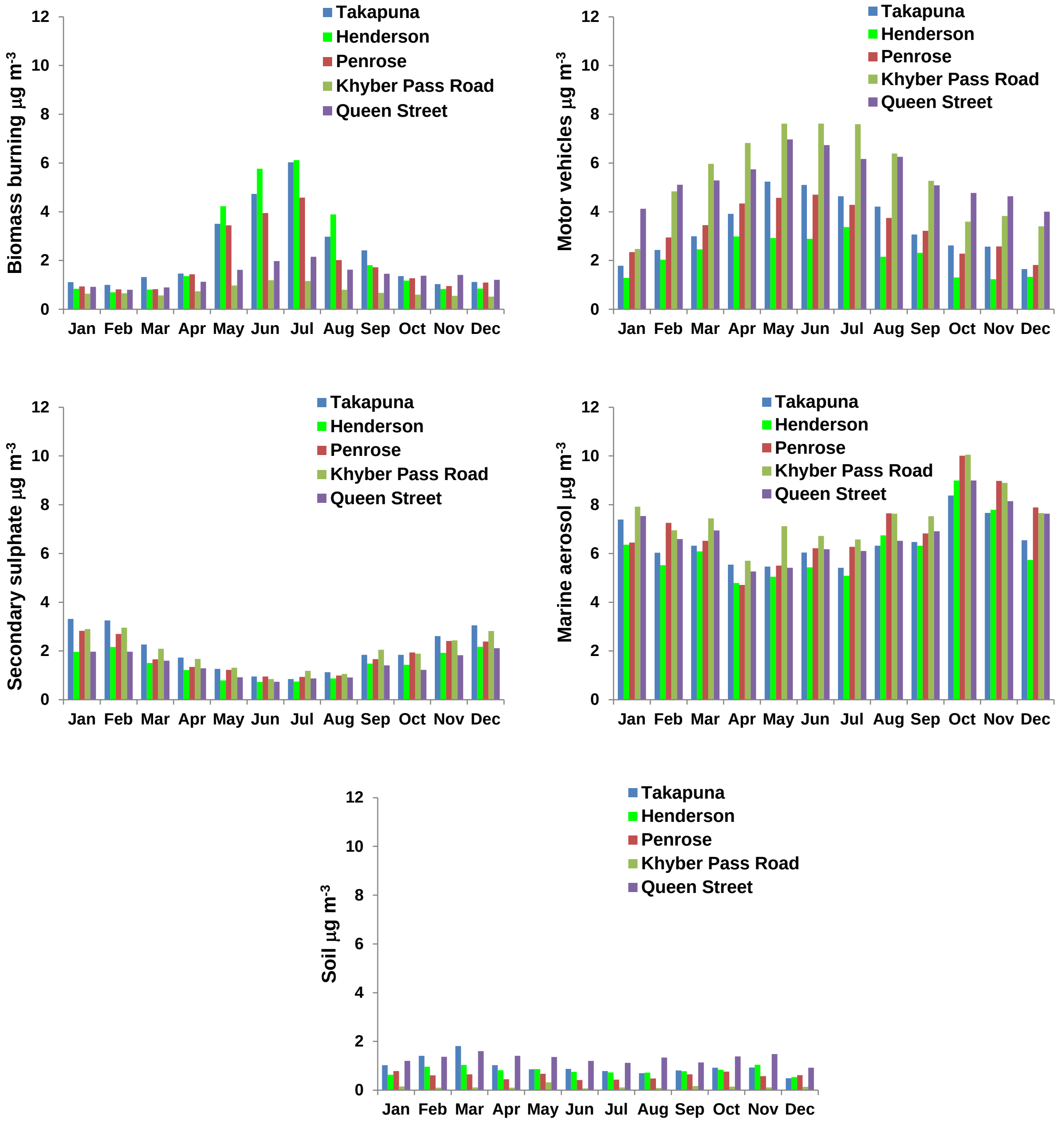

Figure 4.4 Monthly average PM_{10} mass contributions for sources common to each AC monitoring site

Biomass burning, motor vehicle emissions and marine aerosol were the primary sources of PM_{10} during winter at all sites. Motor vehicle emissions dominated at roadside monitoring locations or where major arterial routes/motorways were nearby (Takapuna, Queen Street, Khyber Pass Road and Penrose) and contributions to PM mass from biomass burning was highest at residential locations (Takapuna, Henderson) For other seasons it can be seen that those sources with airborne particles in the coarse fraction (motor vehicles/road dust and marine aerosol) have higher mass contributions, particularly in the case of marine aerosol which dominates source contributions at times. The predominance of motor vehicle sources (tailpipe emissions and associated road dust component) presents chronic exposure risk since the contributions are relatively consistent all year and the particles are composed of a combination of ultra-fine (<300 nm) carbonaceous aerosol and coarse particles that include of a range heavy metal species (Zn, Cu, Sb, Ba) from brake linings and mechanical abrasion of parts and surfaces (tyres, road surface) (Lough, Schauer et al. 2005, Schauer, Lough et al. 2006, Hays, Cho et al. 2011).

Secondary sulphate and biomass burning mass contributions to PM_{10} remained similar to that for $PM_{2.5}$ due to the particle size range produced by those sources. Monthly average PM_{10} crustal matter contributions were remarkably consistent across all sites.

4.2 LONG-TERM TRENDS IN SOURCE CONTRIBUTIONS TO PARTICULATE MATTER ACROSS AUCKLAND

The particulate matter concentration and source contribution data for all sites were combined (amalgamated into one time-series dataset) for common sources to provide a pan-urban overview of trends in particulate matter concentrations. Section 3.3.1 provides a description of the trend analyses methodology. Over the monitoring period it was found that $PM_{2.5}$ concentrations decreased at all monitoring sites and this is reflected in the combined $PM_{2.5}$ data (3400 samples) as shown in Figure 4.5.

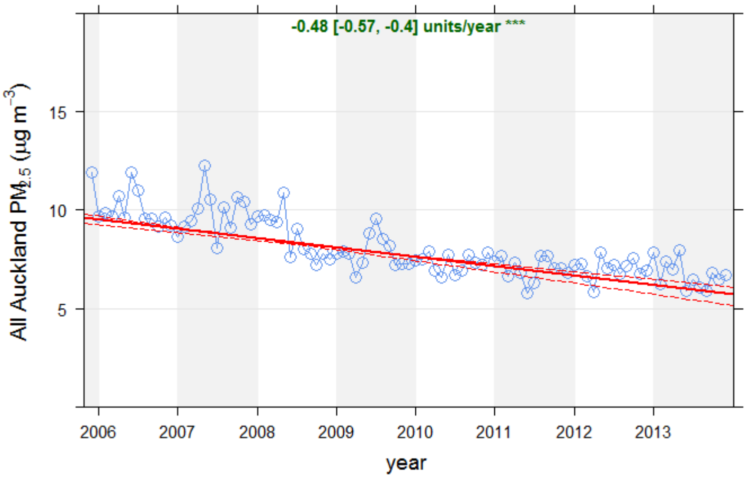

Figure 4.5 Long-term trend in pan-urban $PM_{2.5}$ concentrations for Auckland Council monitoring sites showing that concentrations have decreased (statistically significant at the 99.9 % confidence interval for all sites)

The combined $PM_{2.5}$ dataset reflects the trend analysis for individual sites, although for some sites (e.g. Queen Street) the decrease was more marked than others due to significant changes in source activities.

Similar to $PM_{2.5}$, trend analysis of PM_{10} concentrations from a combined dataset (6750 samples) have also decreased across all monitoring locations as presented in Figure 4.6.

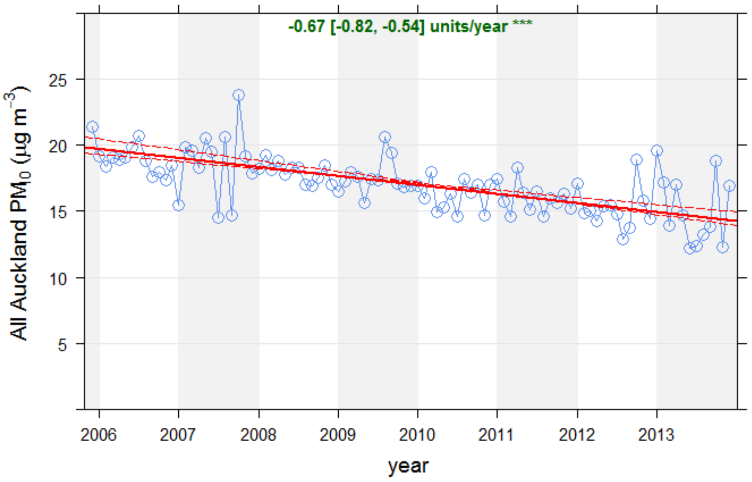

Figure 4.6 Long-term trends in pan-urban PM_{10} concentrations for Auckland Council monitoring sites showing that concentrations have decreased (statistically significant at the 99.9 % confidence intervals)

It would appear that decreasing $PM_{2.5}$ concentrations are largely responsible (approximately 70 %) for the observed decrease in PM_{10}. Understanding the drivers for the observed decrease in particulate matter concentrations across the Auckland urban area is necessary from both regulatory and policy perspectives in order to measure the effectiveness of policy implementation. Therefore, each of the predominant source types was examined for individual trends as set out in the following sections.

4.2.1 Trends in Biomass burning source contributions

Interestingly, Biomass burning source contributions to urban particulate matter concentrations (both $PM_{2.5}$ and PM_{10}) in Auckland were found to be increasing as shown by Figure 4.7and 4.8 respectively.

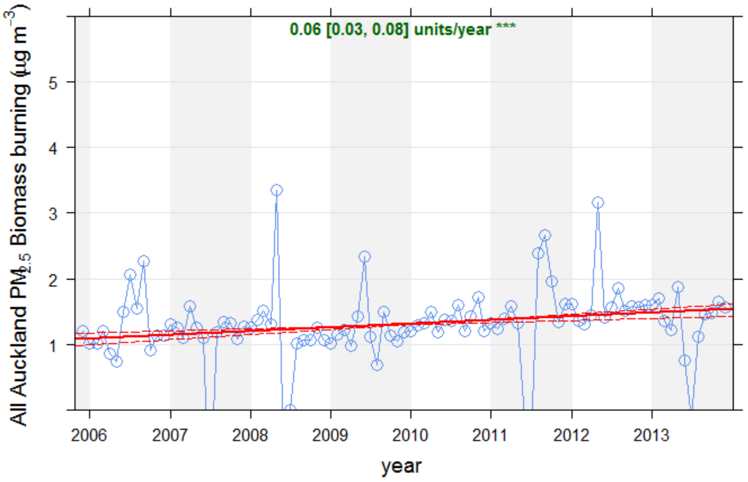

Figure 4.7 Long-term trends in $PM_{2.5}$ Biomass burning source contributions across all Auckland monitoring sites showing that concentrations have increased (statistically significant at the 99.9 % confidence interval)

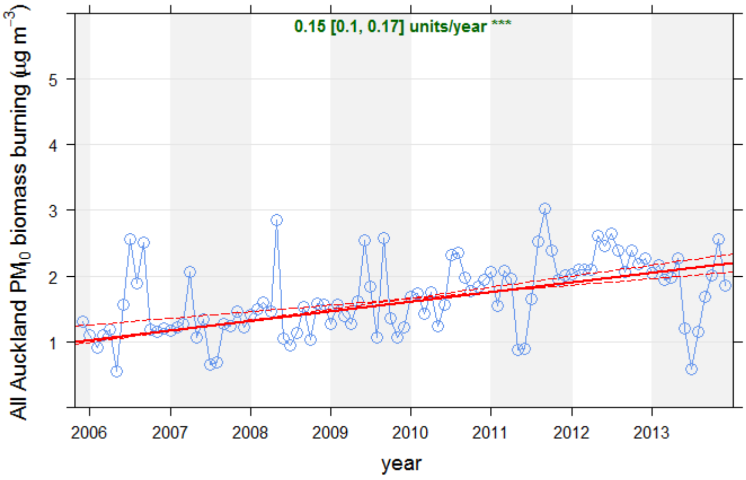

Figure 4.8 Long-term trends in PM_{10} Biomass burning source contributions across all Auckland monitoring sites showing that concentrations have increased (statistically significant at the 99.9 % confidence interval)

The Biomass burning source is primarily related to use of solid fuel fires for domestic heating during the winter. The reasons for the increase in source contributions are unclear since reductions might be expected with widespread introduction of alternative space heating technologies (such as heat pumps).

4.2.2 Trends in Motor vehicle source contributions

Particulate matter associated with motor vehicle emissions were found to have markedly decreased at all sites over the monitoring period as shown for both $PM_{2.5}$ and PM_{10} in Figure 4.9 and 4.10 respectively.

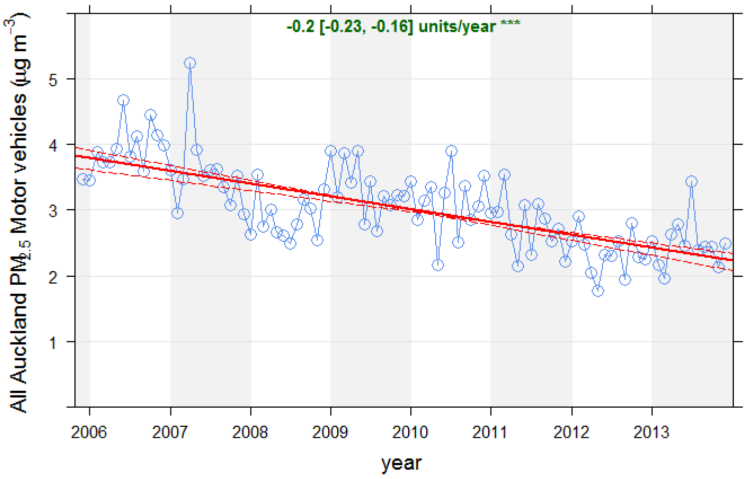

Figure 4.9 Long-term trends in $PM_{2.5}$ motor vehicle source contributions across all Auckland monitoring sites showing that concentrations have decreased (statistically significant at the 99.9 % confidence interval)

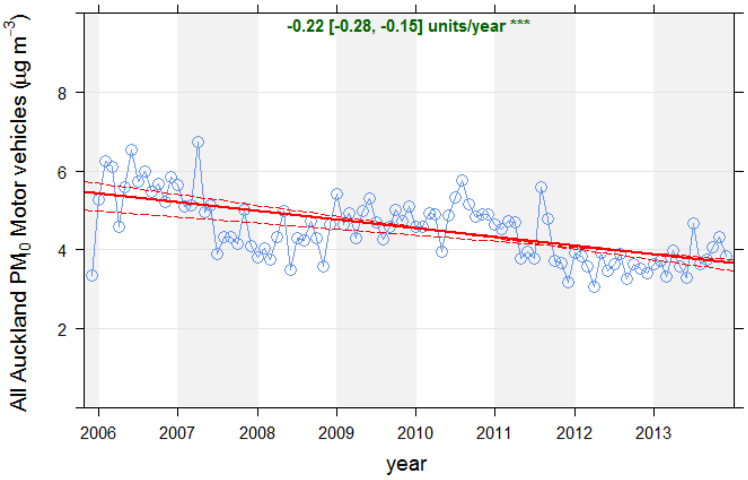

Figure 4.10 Long-term trends in PM_{10} motor vehicle source contributions across all Auckland monitoring sites showing that concentrations have decreased (statistically significant at the 99.9 % confidence interval)

It can be seen from Figure 4.9 and 4.10 that reductions in motor vehicle associated $PM_{2.5}$ concentrations are driving the commensurate decrease in PM_{10}. Detailed analysis of the data from individual sites (see for example, Chapters 6 to 9) suggests that tailpipe emissions reductions from diesel vehicles are largely responsible for the observed trends, most likely through improvements in fuel formulation and engine technology. The particulate matter fraction between $PM_{2.5}$ and PM_{10} associated with motor vehicles, primarily from re-suspension of road dusts, was not found to be decreasing, and was actually increasing at some sites in line with traffic volume increases (Xie, Davy et al. 2015). The data also suggests that the trending decrease may have plateaued in the last two years of this analysis (2012-2013).

Both the $PM_{2.5}$ and PM_{10} motor vehicle source contributions demonstrated a significant day-of-the-week concentration bias as presented in Figure 4.11. This difference was a reflection of normal workday activity and commuter behaviour and matches traffic count data.

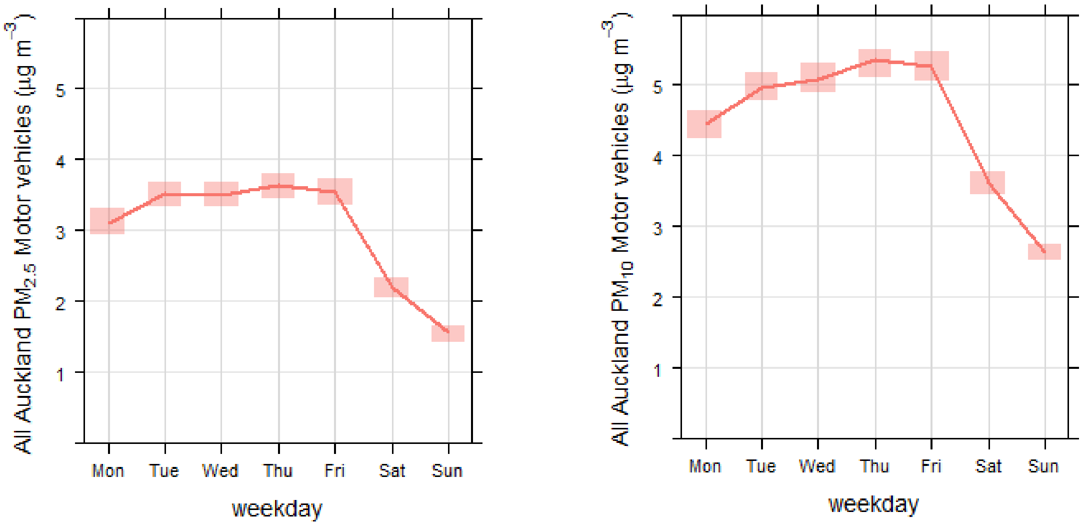

Figure 4.11 Temporal variations in motor vehicle contributions to $PM_{2.5}$ (left) and PM_{10} (right) in all Auckland samples (the shaded bars are the 95 percentile confidence limits in the mean)

4.2.3 Trends in Secondary sulphate source contributions

The long term trend analysis for secondary sulphate contributions to $PM_{2.5}$ and PM_{10} shows that concentrations have been decreasing (99.9 % confidence interval) in urban particulate matter over the monitoring period as presented in Figure 4.12 and 4.13 respectively.

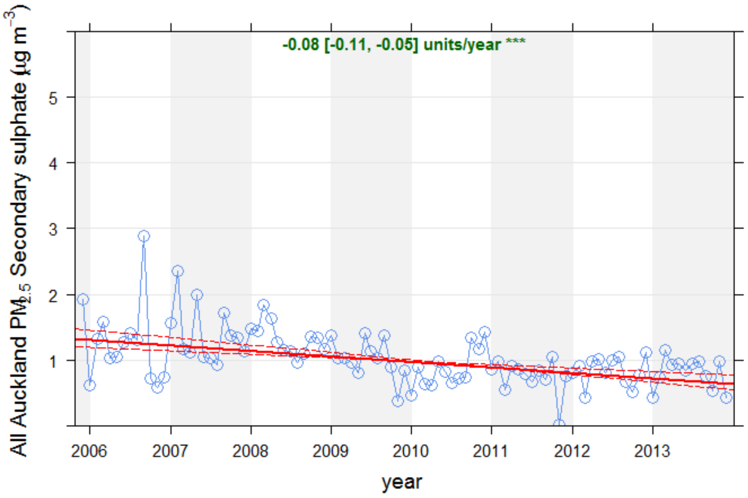

Figure 4.12 Long-term trends in $PM_{2.5}$ secondary sulphate source contributions across all Auckland monitoring sites showing that concentrations have decreased (statistically significant at the 99.9 % confidence interval)

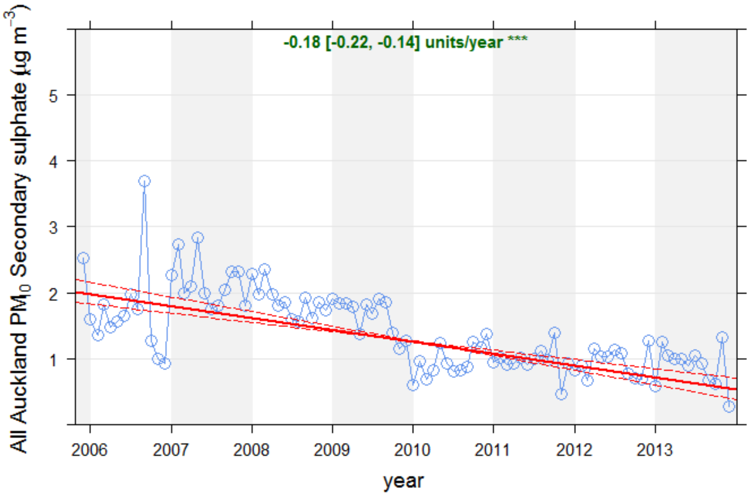

Figure 4.13 Long-term trends in PM_{10} secondary sulphate source contributions across all monitoring sites showing that concentrations have decreased (statistically significant at the 99.9 % confidence interval)

A significant influence on secondary sulphate concentrations is the production of precursor gases such as SO_2 from combustion of sulphur containing fuels in urban areas. The stepwise introduction (2006 – 2010) of low sulphur automotive fuels (especially diesel) appears to have been the main driver of secondary sulphate reductions across the Auckland urban area. Detailed discussion on this is provided in Section 5.1.3.

4.2.4 Trends in Marine aerosol source contributions

One of the most interesting results from the data analysis was the finding that marine aerosol (dominated by sea salt) concentrations are trending downwards across all sites in Auckland.

Figure 4.14 and 4.15 show respectively, that both the fine and coarse fractions of the marine aerosol component decreased over the monitoring period.

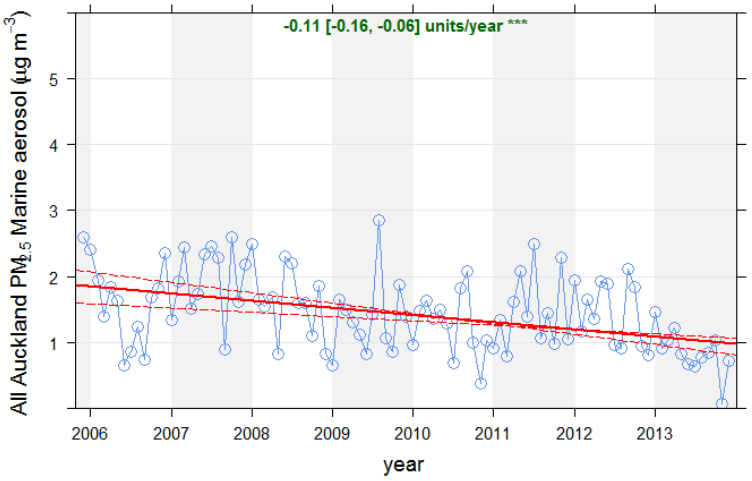

Figure 4.14 Long-term trends in $PM_{2.5}$ marine aerosol source contributions across all monitoring sites showing that concentrations have decreased (statistically significant at the 99.9 % confidence interval)

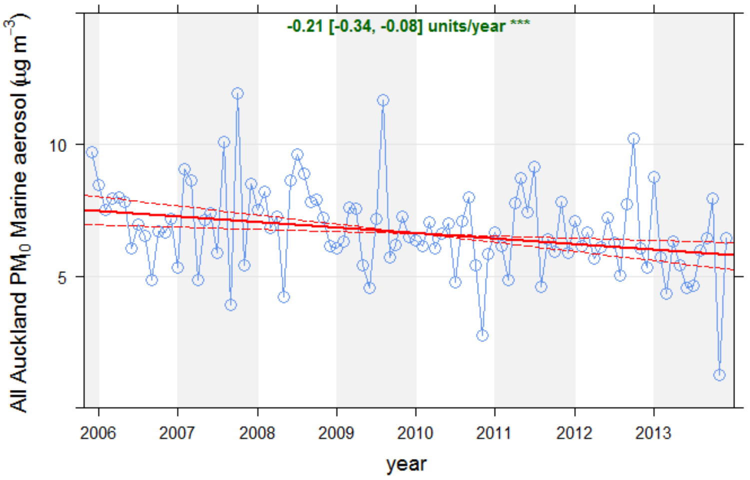

Figure 4.15 Long-term trends in PM_{10} marine aerosol source contributions across all monitoring sites showing that concentrations have decreased (statistically significant at the 99.9 % confidence interval)

The marine aerosol component of urban air particulate matter is considered to be part of the 'natural' background and therefore is that proportion that cannot be managed. The apparent decrease therefore has implications for air quality management in Auckland. It has been shown previously that the primary marine aerosol generation and source regions were in the Southern Ocean below Australia and to the northeast of Auckland out in the Pacific Ocean as shown in the PSCF presented in plot Figure 4.16 (Davy, Trompetter et al. 2011, Davy, Trompetter et al. 2011). The PSCF plot was generated using the Takapuna PM_{10} marine aerosol source contribution data using HYSPLIT back-trajectories as described in Sections 2.3.2 and 2.3.3.

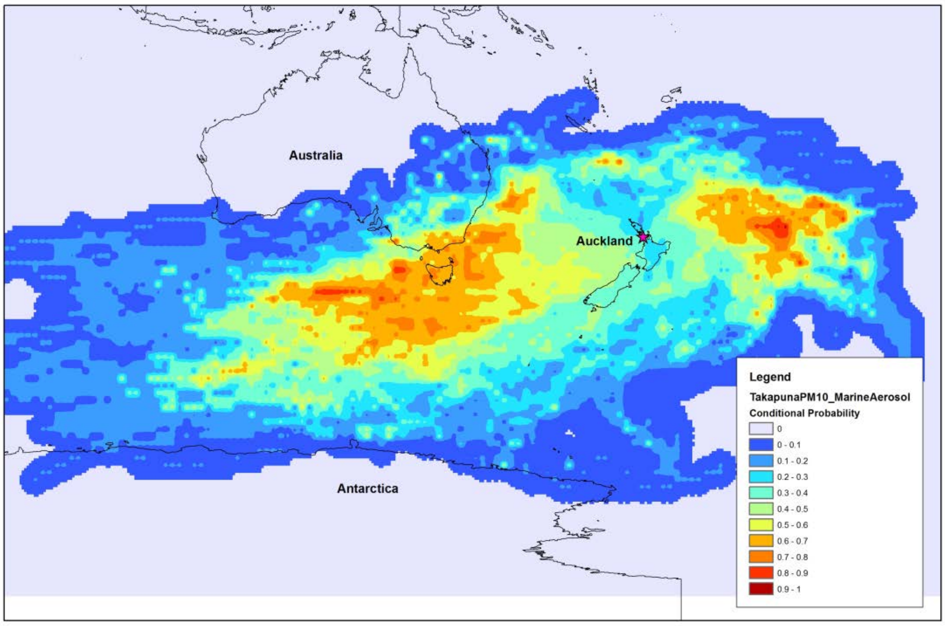

Figure 4.16 PSCF plot for the Takapuna PM_{10} marine aerosol source contribution data showing that the most likely source regions are in the Southern Ocean below Australia and Pacific Ocean to the northeast of Auckland

At this stage, it is unclear whether the observed decreases in marine aerosol concentrations are part of a larger inter-decadal cycle related to Southern Hemisphere circulation patterns or a more permanent trend.

4.2.5 Trends in Crustal matter source contributions

Crustal matter source contributions at the monitoring sites in Auckland were likely to be a combination of windblown soil, road dust and dust generated by earthworks, construction and road works. Concentrations were found to vary from site to site depending on meteorological conditions and local dust generating activities. Crustal matter sources (synonymous with Soil as a source reference) of airborne particles are derived from weathering and mechanical abrasion processes and are generally in the coarse fraction particle size range with the greatest contribution to PM_{10} and some minor contribution to $PM_{2.5}$.

In built-up urban locations, road dust may be the most significant source of crustal matter particularly for those monitoring sites at high density traffic locations (Thorpe and Harrison 2008) and this is evident in motor vehicle contributions to PM_{10} at the Queen Street and Khyber Pass Road sites. The long-term trend analyses for crustal matter contributions to urban particulate matter showed that there is a small apparent decrease in $PM_{2.5}$ contributions (90 % confidence intervals) as presented in Figure 4.17, but that there was significant variability from year to year reflecting localised influence of dust generating activities.

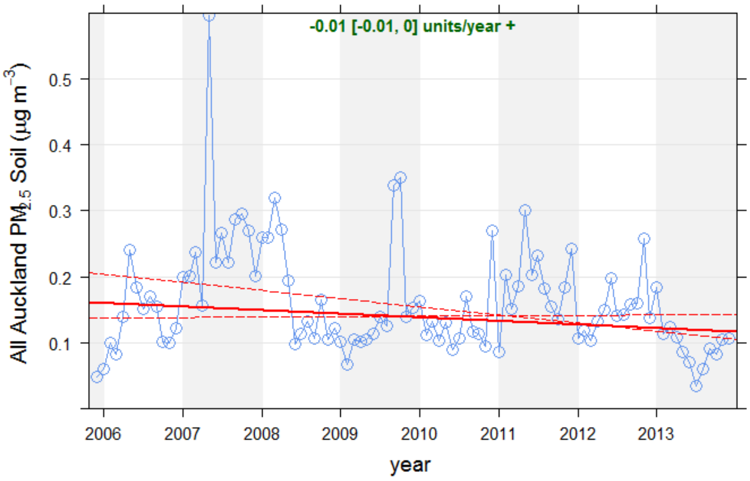

Figure 4.17 Long-term trends in $PM_{2.5}$ crustal matter source contributions across all monitoring sites showing that concentrations have decreased (statistically significant at the 90 % confidence interval)

Contributions of crustal matter to PM_{10} concentrations were an order of magnitude higher than $PM_{2.5}$ reflecting the coarse particle dominance of this source. The trend analysis showed (Figure 4.17) that concentrations had decreased over the monitoring period but as for $PM_{2.5}$, this was largely site dependent and more reflective of the episodic nature of local activities.

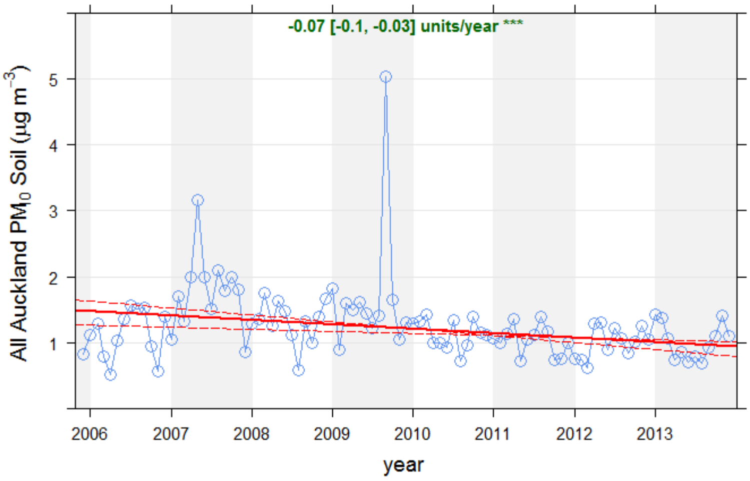

Figure 4.18 Long-term trends in PM_{10} crustal matter source contributions across all monitoring sites showing that concentrations have decreased (statistically significant at the 99.9 % confidence interval)

It can be seen from Figure 4.19 that the temporal variation for PM_{10} crustal matter contributions that concentrations during the weekend were significantly lower than during weekdays which indicates that the source emissions were primarily driven by human activity. Any randomly generated process would not show any bias for day of the week.

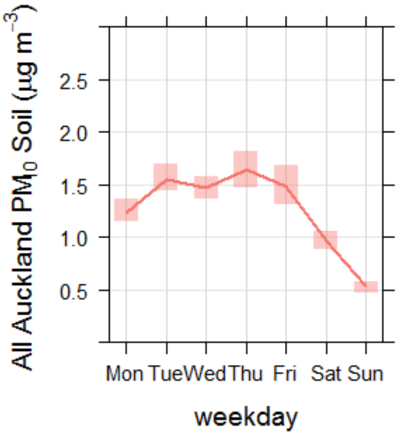

Figure 4.19 Temporal variations in crustal matter contributions for all Auckland PM_{10} samples showing lower weekend concentrations (the shaded bars are the 95 percentile confidence limits in the mean)

5.0 ANALYSIS OF KEY ELEMENTAL CONCENTRATIONS ACROSS ALL AUCKLAND SITES

5.1 ELEMENTAL CONCENTRATIONS IN AUCKLAND PARTICULATE MATTER

This section provides an overview of the elemental concentrations present in particulate matter samples from the Auckland air quality monitoring sites. Table 5.1 presents summary statistics for elemental concentrations from all Auckland PM$_{2.5}$ samples while Table 5.2 provides the statistics for all PM$_{10}$ samples. The statistical data for the disaggregated sites is presented in Chapters 6 to 10.

Table 5.1 Elemental concentrations in PM$_{2.5}$ for all Auckland sites (3200 samples)

Species	Average (ng m^{-3})	Max (ng m^{-3})	Min (ng m^{-3})	Median (ng m^{-3})	Std Dev (ng m^{-3})	Av LOD (ng m^{-3})	%>LOD
PM$_{2.5}$ (μg m^{-3})	**8**	**40**	**0**	**7**	**4**		
H	105	1238	0	87	91	44	77
BC	3137	16281	0	2885	1767	177	100
Na	577	4605	0	411	604	255	66
Mg	60	643	0	47	54	26	75
Al	26	2895	0	18	66	13	73
Si	64	4435	0	48	113	9	100
P	5	144	0	2	7	14	16
S	239	2897	0	195	165	9	100
Cl	763	7042	0	521	792	7	99
K	58	8100	0	41	161	7	99
Ca	48	3224	0	38	74	6	99
Sc	2	26	0	1	2	8	6
Ti	2	125	0	1	4	7	12
V	2	80	0	0	4	7	11
Cr	2	44	0	1	2	6	9
Mn	2	37	0	1	3	6	13
Fe	64	952	0	54	52	5	98
Co	2	18	0	1	2	9	6
Ni	2	30	0	1	3	8	9
Cu	5	235	0	4	6	10	23
Zn	18	521	0	9	31	11	49
Ga	3	41	0	0	5	17	8
Ge	4	42	0	0	6	22	6
As	5	69	0	0	9	29	8
Se	7	71	0	0	11	35	9
Br	8	103	0	0	13	45	9
Rb	14	114	0	0	21	72	9
Sr	18	238	0	0	28	91	9
Mo	45	553	0	0	78	213	11
I	7	71	0	2	10	25	10
Ba	8	364	0	4	14	28	8
Hg	10	159	0	0	18	64	4

Species	Average (ng m^{-3})	Max (ng m^{-3})	Min (ng m^{-3})	Median (ng m^{-3})	Std Dev (ng m^{-3})	Av LOD (ng m^{-3})	%>LOD
PM$_{2.5}$ (μg m^{-3})	**8**	**40**	**0**	**7**	**4**		
Pb	13	144	0	0	24	80	6

Table 5.1 shows carbonaceous species (represented by BC), sodium, chlorine and sulphur were found to dominate average PM$_{2.5}$ elemental mass concentrations indicating that combustion processes, marine aerosol and secondary sulphate species are important contributors to ambient PM$_{2.5}$ across Auckland. A number of measured species were generally close to or below the limits of detection.

Table 5.2 Elemental concentrations in PM$_{10}$ for all Auckland sites (6800 samples)

Species	Average (ng m^{-3})	Max (ng m^{-3})	Min (ng m^{-3})	Median (ng m^{-3})	Std Dev (ng m^{-3})	Av LOD (ng m^{-3})	%>LOD
PM$_{10}$ (μg m^{-3})	**17**	**130**	**0**	**16**	**6**		
H	143	1416	0	122	107	43	87
BC	3446	14964	0	3010	2152	173	99
Na	2107	9379	0	1895	1296	462	96
Mg	193	1002	0	175	109	37	98
Al	107	6415	0	78	139	16	97
Si	298	16439	22	215	370	11	100
P	17	1393	0	13	24	16	52
S	398	2471	0	362	199	12	100
Cl	3117	16774	0	2734	2026	7	100
K	127	2055	0	115	77	7	100
Ca	221	4949	1	181	205	7	100
Sc	3	49	0	2	4	10	12
Ti	14	822	0	10	19	7	62
V	2	87	0	0	5	10	8
Cr	2	401	0	0	6	8	11
Mn	5	99	0	4	5	7	35
Fe	265	4254	0	234	187	5	100
Co	4	62	0	2	5	11	13
Ni	2	107	0	1	4	9	10
Cu	11	945	0	9	15	10	52
Zn	28	2301	0	15	62	12	60
Ga	3	36	0	0	5	18	7
Ge	4	51	0	0	6	23	6
As	6	83	0	0	10	30	10
Se	7	76	0	0	11	36	9
Br	12	106	0	5	15	45	12
Rb	14	169	0	0	21	75	8
Sr	20	262	0	0	29	93	9
Mo	40	529	0	0	73	227	9
I	11	211	0	3	16	31	19
Ba	20	331	0	17	19	31	30
Hg	12	161	0	0	19	66	5

Pb	13	257	0	0	24	82	5

Table 5.2 shows that carbonaceous species (represented by BC), sodium, chlorine and sulphur were also found to dominate average PM_{10} elemental mass concentrations but that other elemental species such as Al Si, Ca, Fe and Zn were also significant components. Correlation matrices for the major elemental contributors to $PM_{2.5}$ and PM_{10} concentrations are presented in Figure 5.1 and the clustering of elements show the key relationships between them. For example, $PM_{2.5}$ is correlated with BC, H and K indicating the importance of combustion source emissions to $PM_{2.5}$ concentrations, while for PM_{10} elemental components associated with combustion sources are still important, clustered elements such as Na and Cl or Al and Si have a much stronger influence on PM_{10} concentrations. The latter two clusters of elements represent coarse particle ($PM_{10-2.5}$) marine aerosol (sea salt) and crustal matter sources respectively.

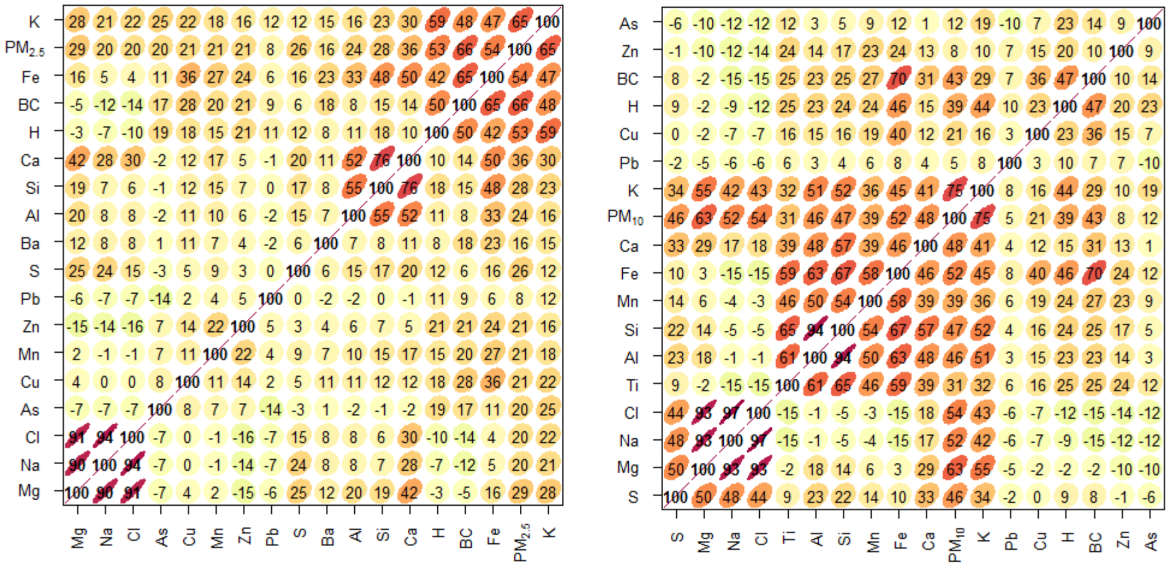

	Mg	Na	Cl	As	Cu	Mn	Zn	Pb	S	Ba	Al	Si	Ca	H	BC	Fe	$PM_{2.5}$	K
K	28	21	22	25	22	18	16	12	12	15	16	23	30	59	48	47	65	100
$PM_{2.5}$	29	20	20	20	21	21	21	8	26	16	24	28	36	53	66	54	100	65
Fe	16	5	4	11	36	27	24	6	16	23	33	48	50	42	65	100	54	47
BC	-5	-12	-14	17	28	20	21	9	6	18	8	15	14	50	100	65	66	48
H	-3	-7	-10	19	18	15	21	11	12	8	11	18	10	100	50	42	53	59
Ca	42	28	30	-2	12	17	5	-1	20	11	52	76	100	10	14	50	36	30
Si	19	7	6	-1	12	15	7	0	17	8	55	100	76	18	15	48	28	23
Al	20	8	8	-2	11	10	6	-2	15	7	100	55	52	11	8	33	24	16
Ba	12	8	8	1	11	7	4	-2	6	100	7	8	11	8	18	23	16	15
S	25	24	15	-3	5	9	3	0	100	6	15	17	20	12	6	16	26	12
Pb	-6	-7	-7	-14	2	4	5	100	0	-2	-2	0	-1	11	9	6	8	12
Zn	-15	-14	-16	7	14	22	100	5	3	4	6	7	5	21	21	24	21	16
Mn	2	-1	-1	7	11	100	22	4	9	7	10	15	17	15	20	27	21	18
Cu	4	0	0	8	100	11	14	2	5	11	11	12	12	18	28	36	21	22
As	-7	-7	-7	100	8	7	7	-14	-3	1	-2	-1	-2	19	17	11	20	25
Cl	91	94	100	-7	0	-1	-16	-7	15	8	8	6	30	-10	-14	4	20	22
Na	90	100	94	-7	0	-1	-14	-7	24	8	8	7	28	-7	-12	5	20	21
Mg	100	90	91	-7	4	2	-15	-6	25	12	20	19	42	-3	-5	16	29	28

	S	Mg	Na	Cl	Ti	Al	Si	Mn	Fe	Ca	PM_{10}	K	Pb	Cu	H	BC	Zn	As
As	-6	-10	-12	-12	12	3	5	9	12	1	12	19	-10	7	23	14	9	100
Zn	-1	-10	-12	-14	24	14	17	23	24	13	8	10	7	15	20	10	100	9
BC	8	-2	-15	-15	25	23	25	27	70	31	43	29	7	36	47	100	10	14
H	9	-2	-9	-12	25	23	24	24	46	15	39	44	10	23	100	47	20	23
Cu	0	-2	-7	-7	16	15	16	19	40	12	21	16	3	100	23	36	15	7
Pb	-2	-5	-6	-6	6	3	4	6	8	4	5	8	100	3	10	7	7	-10
K	34	55	42	43	32	51	52	36	45	41	75	100	8	16	44	29	10	19
PM_{10}	46	63	52	54	31	46	47	39	52	48	100	75	5	21	39	43	8	12
Ca	33	29	17	18	39	48	57	39	46	100	48	41	4	12	15	31	13	1
Fe	10	3	-15	-15	59	63	67	58	100	46	52	45	8	40	46	70	24	12
Mn	14	6	-4	-3	46	50	54	100	58	39	39	36	6	19	24	27	23	9
Si	22	14	-5	-5	65	94	100	54	67	57	47	52	4	16	24	25	17	5
Al	23	18	-1	-1	61	100	94	50	63	48	46	51	3	15	23	23	14	3
Ti	9	-2	-15	-15	100	61	65	46	59	39	31	32	6	16	25	25	24	12
Cl	44	93	97	100	-15	-1	-5	-3	-15	18	54	43	-6	-7	-12	-15	-14	-12
Na	48	93	100	97	-15	-1	-5	-4	-15	17	52	42	-6	-7	-9	-15	-12	-12
Mg	50	100	93	93	-2	18	14	6	3	29	63	55	-5	-2	-2	-2	-10	-10
S	100	50	48	44	9	23	22	14	10	33	46	34	-2	0	9	8	-1	-6

Figure 5.1 Clustered correlation plots for key constituent elements in $PM_{2.5}$ (left) and PM_{10} (right)

The following sections present a more in-depth analysis of elemental concentrations across Auckland based on the clustering observed in Figure 5.1.

5.1.1 Black carbon, hydrogen and potassium concentrations in particulate matter

Black carbon represents the contribution of combustion particles to particulate matter concentrations. In Auckland, combustion sources were found to be dominated by motor vehicle emissions and solid fuel fires for domestic heating. Whereas hydrogen, while largely representative of hydrocarbon compounds produced by the incomplete combustion of fuels, is also a component of secondary aerosol such as ammonium sulphate or ammonium nitrate generated by gas-to-particle atmospheric reaction processes (Pandis, Harley et al. 1992, Seinfeld and Pandis 2006). The relationship between black carbon and potassium is indicative of the contribution of Biomass burning emissions. Figure 5.2 presents time-series plots for BC, H and K showing winter peaks that are explained by both emission source activity and the influence of meteorology. Potassium concentrations show peaks at other times of the year due the influence of other sources such as crustal matter and marine aerosol. Particulate matter released by fireworks being was primarily responsible for extreme peaks in potassium concentrations. Further analysis of the influence of fireworks on elemental concentrations is provided in Chapter 8.

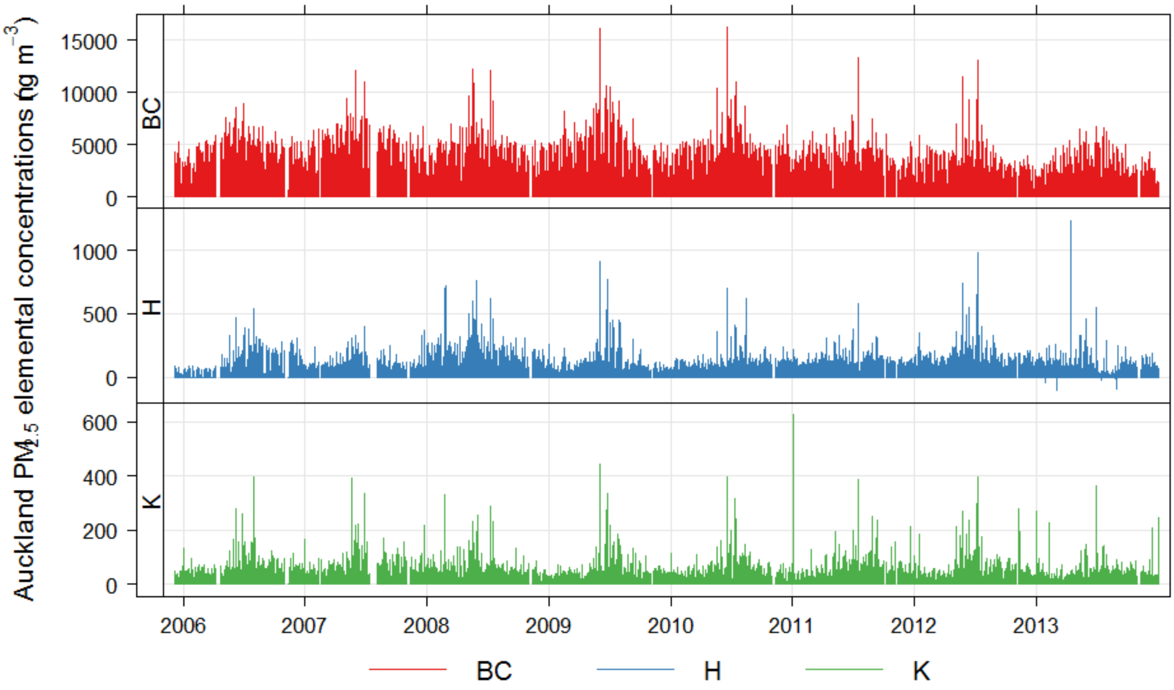

Figure 5.2 Time-series plots for BC, H and K in all Auckland PM$_{2.5}$ samples

Interestingly when the long-term trends in black carbon and hydrogen were examined it was found that there was a significant decreasing trend in BC (99.9 % CI) across Auckland while H concentrations (95 % CI) appear to be increasing. This result represents the relative contribution of sources, with BC concentrations primarily driven by motor vehicles and H concentrations are largely dictated by the amount of organic compounds released by incomplete combustion of biomass. It has been shown that up to 90% of the particulate matter released from wood fires is in the form of organic compounds (Fine, Cass et al. 2002, Fine, Cass et al. 2004, Davy, Trompetter et al. 2009).

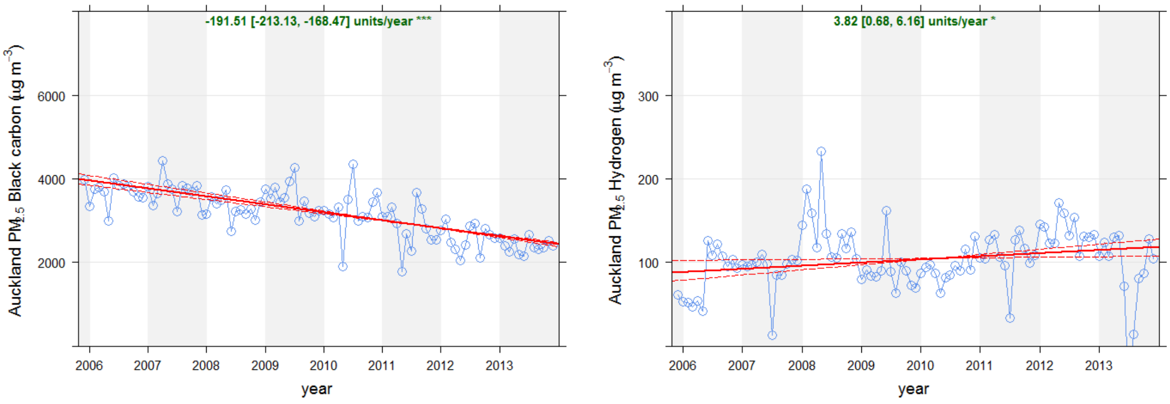

Figure 5.3 Trend analysis showing a decrease in BC (statistically significant at the 99.9 % confidence interval) (left) and increasing H (statistically significant at the 95 % confidence interval) (right) in all Auckland PM$_{2.5}$ samples

5.1.2 Sodium and chlorine concentrations in particulate matter

Sodium and chlorine are the primary constituents of sea salt and were also significant elemental contributors to both $PM_{2.5}$ and PM_{10} mass. The elements were highly correlated (as shown in Figure 5.4), present in the same ratio at peak concentrations as found in sea salt ([Na] = 0.56[Cl]) (Lide 1992) and demonstrate the relative influence of natural aerosol on urban particulate matter concentrations in Auckland due to the isolated oceanic location of the New Zealand landmass. Other sources of Na and Cl include biomass burning, motor vehicle emissions, crustal matter, fireworks and industrial emissions.

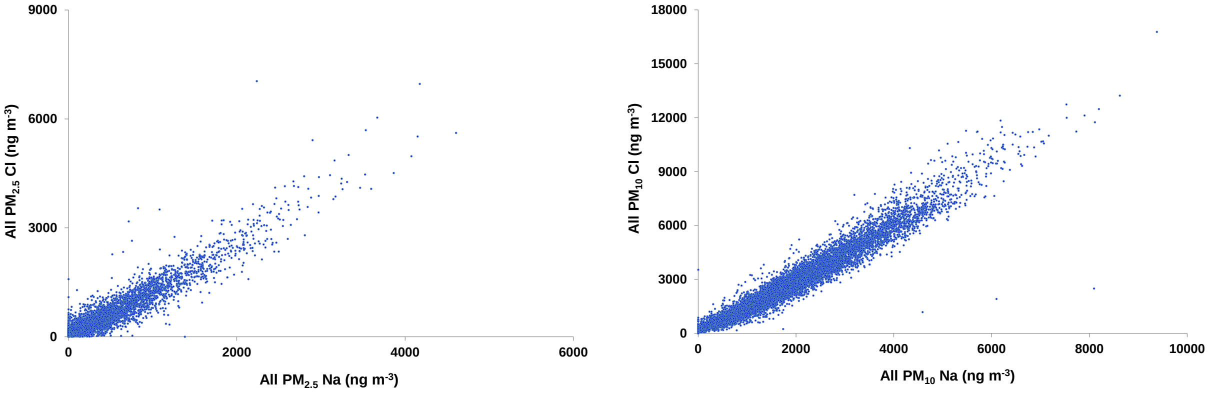

Figure 5.4 Scatterplots for sodium and chlorine in $PM_{2.5}$ (left) and PM_{10} (right) for all Auckland PM samples

The long-term trends for sodium and chlorine in particulate matter samples from Auckland show that both sodium and chlorine concentrations have decreased over the monitoring period in $PM_{2.5}$ and PM_{10} as presented in Figure 5.5 and 5.6 respectively (all at the 99.9% confidence interval). This is an unexpected but interesting result and was reflected by the similar decrease in the receptor modelling derived marine aerosol source contributions to PM as presented in Chapter 4.

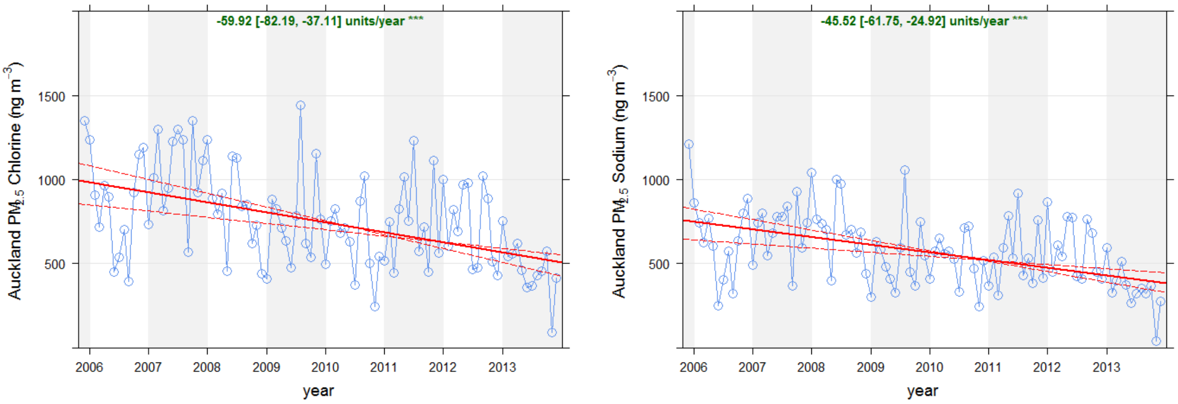

Figure 5.5 Trend analysis showing a decrease in Cl (left) and Na (right) in all Auckland $PM_{2.5}$ samples (statistically significant at the 99.9 % confidence interval)

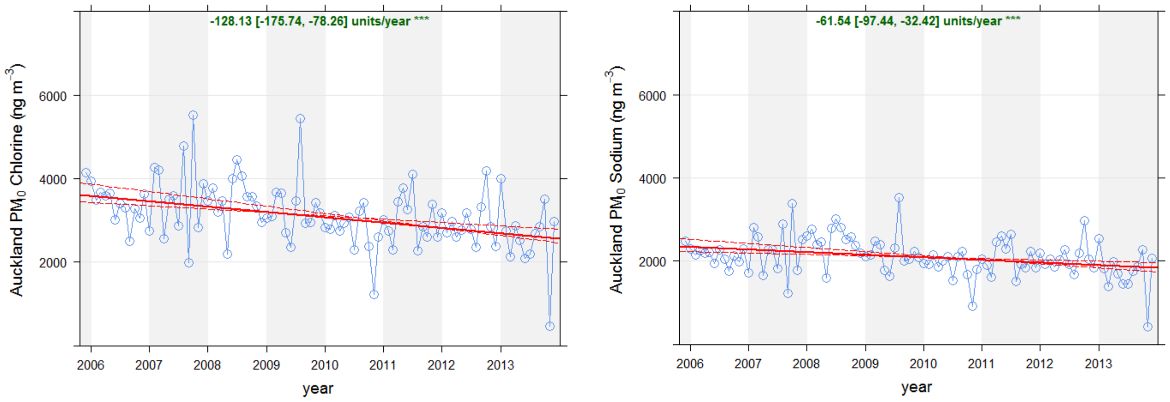

Figure 5.6 Trend analysis showing a decrease in Cl (left) and Na (right) in all Auckland PM_{10} samples (statistically significant at the 99.9 % confidence interval)

Research has shown that the concentration of marine aerosol shows a strong dependence of wind speed across the ocean surface and ranges from about 2 µg m^{-3} to as much as 50 µg m^{3} or more at wind speeds in excess of 15 m s^{-1} (Fitzgerald 1991) and the Auckland data corroborates those potential concentration ranges. Therefore it was expected that marine aerosol concentrations in Auckland would largely be influenced by meteorological and long-range transport mechanisms as shown previously (Davy, Trompetter et al. 2011) and that long-term concentrations would be relatively stable given the (assumed) random nature of marine aerosol generation from meteorological influences. The exact reasons for the decreasing urban sodium and chlorine concentrations are unclear at present, but it may be related to longer-term changes in Southern hemisphere circulation patterns or changes in surface water salinity.

5.1.3 Sulphur concentrations in particulate matter

The presence of sulphur in airborne particulate matter is generated from a variety of sources including sulphur incorporated in mineral structures of crustal matter, cell structure of trees (biomass burning), volcanic emissions, marine aerosol, automotive fuels (petrol, diesel and fuel oils used by ships) and other fossil fuels such as coal. Sulphur containing particulate matter is also derived from precursor gases such as sulphur dioxide, hydrogen sulphide or dimethyl sulphide from the gas-to-particle reaction process in the atmosphere. These reactions can take hours to days depending on the reaction pathway followed, the availability of catalytic metals (e.g. Fe, Mn), relative humidity and the strength of solar radiation (Seinfeld and Pandis 2006). Therefore, concentrations of sulphur containing particulate matter from secondary sulphate sources are likely to be highest some distance downwind of a precursor gas emission source (Polissar, Hopke et al. 2001).

Table 5.1 and 5.2 indicate that most of the sulphur present in the Auckland urban atmosphere was in the fine ($PM_{2.5}$) fraction and Section 4.2.3 showed that this was dominated by secondary sulphate aerosol. Figure 5.7 presents the time-series plot for $PM_{2.5}$ sulphur concentrations in all Auckland samples.

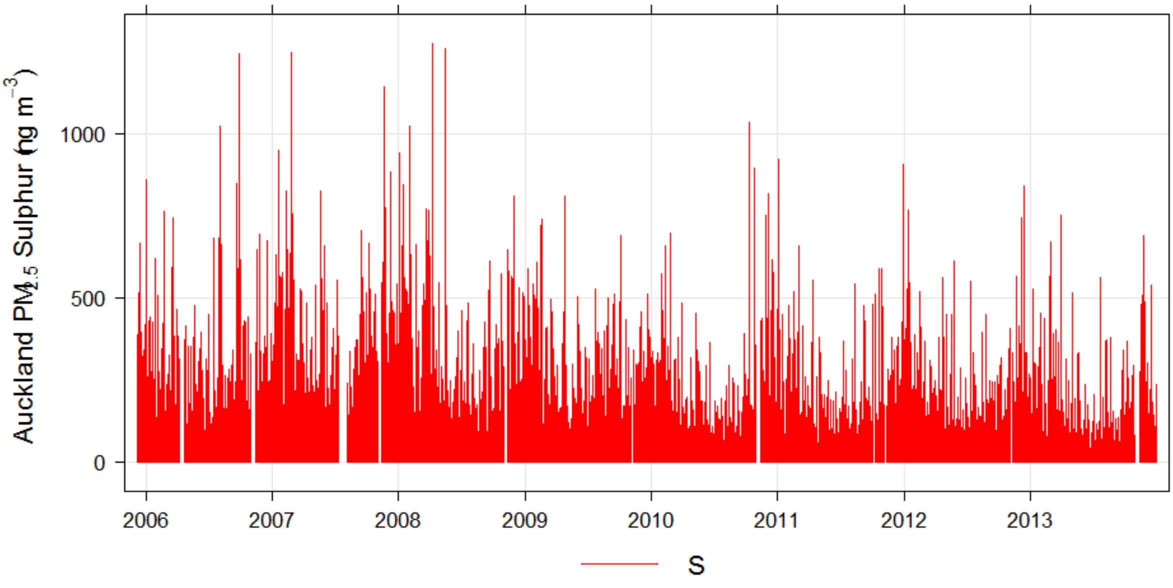

Figure 5.7 Time-series plot for sulphur in all Auckland $PM_{2.5}$ samples

The long term trend analysis for sulphur in $PM_{2.5}$ shows that concentrations have been decreasing (99.9 % confidence interval) in urban particulate matter over the monitoring period as shown Figure 5.8.

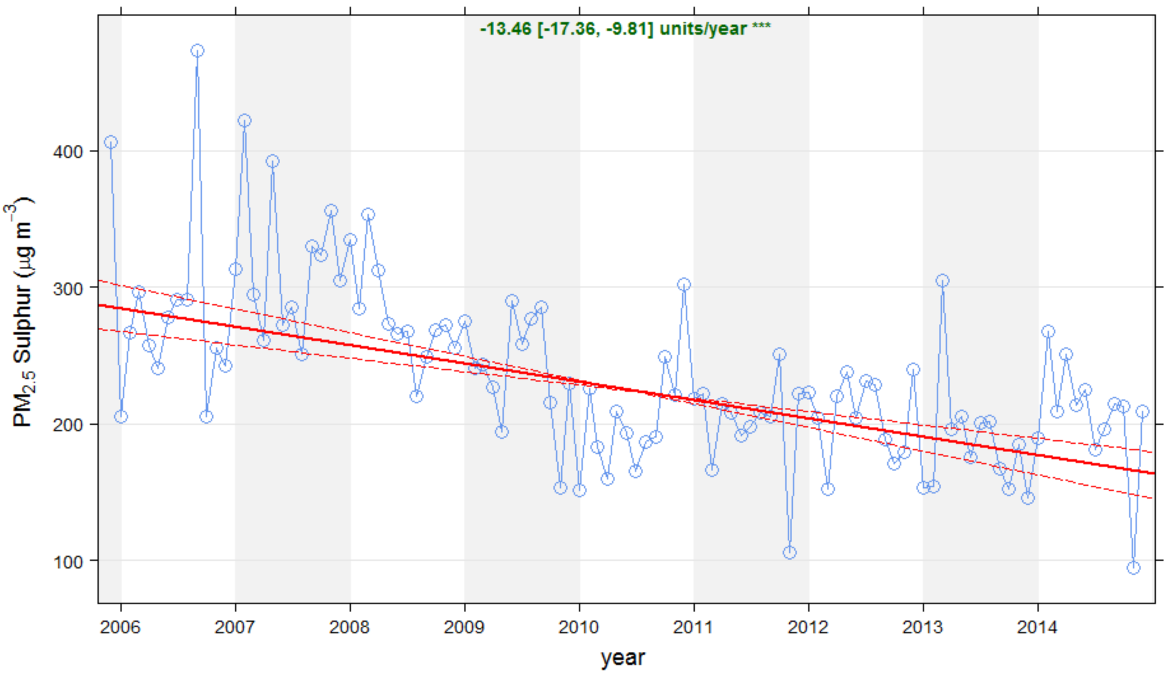

Figure 5.8 Trend analysis showing a decrease in sulphur in all Auckland $PM_{2.5}$ samples (statistically significant at the 99.9 % confidence interval)

A significant influence on secondary sulphate concentrations is the production of precursor gases such as SO_2 from combustion of sulphur containing fuels in urban areas. Over the monitoring period there have been several step-changes in automotive fuel composition in New Zealand, particularly due to the Petroleum Products Specifications Regulations 2002 which dictated the reduction of sulphur in diesel and petrol over a period of time as summarised in Table 5.3.

Table 5.3 Key dates for the reduction of sulphur in automotive fuels as specified in the Petroleum Products Specifications Regulations 2002

Year	Regular petrol (Sulphur ppm)	Premium petrol (Sulphur ppm)	Diesel (Sulphur ppm)
1998	500	500	3000
Petroleum Products Specifications Regulations 2002			
1 May 2007	150	150	50
1 January 2008	50	50	50
1 January 2009	50	50	10

The key dates identified in Table 5.3 have been marked on the trend analysis plot of sulphur concentrations over the years 2006 – 2010 as presented in Figure 5.9. This shows that the reduction in sulphur concentrations largely occurred during this period (95 % confidence interval) with no statistically significant trend in sulphur concentrations evident for the years 2010 – 2014 as shown in Figure 5.10.

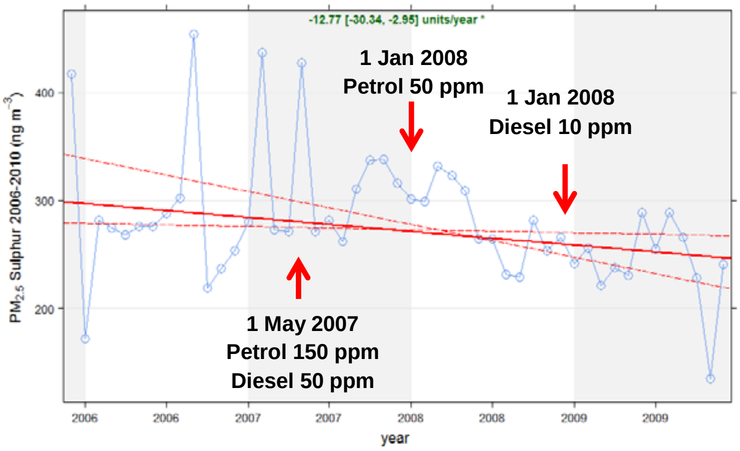

Figure 5.9 Trend analyses for 2006-2010 showing a decrease in sulphur in all Auckland $PM_{2.5}$ samples (statistically significant at the 95 % confidence limits)

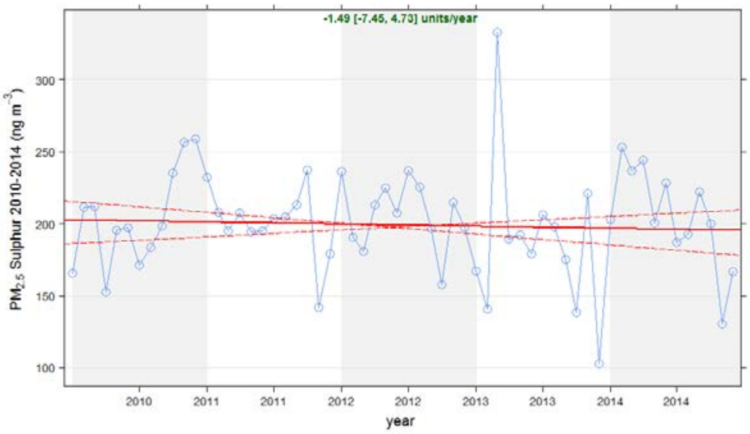

Figure 5.10 Trend analyses for 2010-2014 showing no statistically significant trend over the period for sulphur in all Auckland $PM_{2.5}$ samples

It is likely that the reduction in sulphur content in automotive fuels is also in part responsible for the observed reduction in diesel powered vehicle tailpipe emissions as discussed in Section 4.2.2. The reduction of sulphur containing aerosol is a demonstrable impact of policy (and regulation) for improving urban air pollution.

5.1.4 Aluminium and silicon concentrations - the crustal matter components of particulate matter

Aluminium and silicon concentrations were primarily associated with crustal matter (synonymous with Soil as a source reference) which is predominantly a coarse particle source generated by mechanical abrasion of surface material. In urban locations the passage of motor vehicles over roads can be the primary source of emissions. Crustal matter is primarily composed of aluminosilicate minerals and the source profiles reflect this with Al and Si being the primary constituents and Mg, K, Ca, Ti and Fe commonly present. The mass ratio of Si/Al is consistently about 3:1 for both PM_{10} and $PM_{2.5}$ size fractions across all Auckland monitoring sites and is similar to the Si/Al ratio in aluminosilicate minerals.

A specific dust event that resulted in PM_{10} exceedances across the Auckland region was identified as originating from a dust storm in the Australian desert during September 2009 (Davy, Trompetter et al. 2011), the influence of which can be seen in the time-series plots for Al and Si in all Auckland PM_{10} samples presented in Figure 5.11.

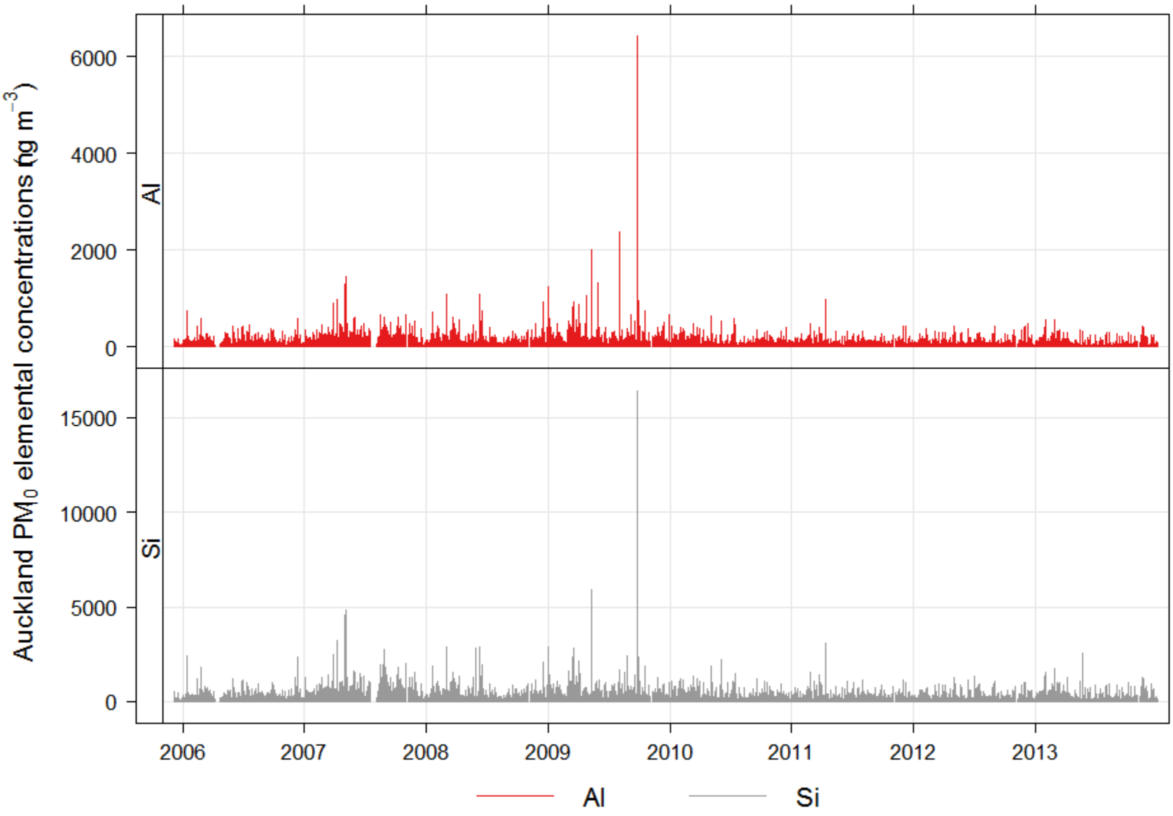

Figure 5.11 Time-series plots for aluminium and silicon in all Auckland PM_{10} samples

The trend analyses for crustal matter sources at the different monitoring sites presented in Section 4.2.5 show that crustal matter concentrations are largely affected by local dust generating activities. The temporal variation for both aluminium and silicon concentrations indicate that airborne concentrations are primarily from anthropogenic activities because of the day-of-the-week concentration dependence with weekend concentrations significantly lower than weekdays as presented in Figure 5.12.

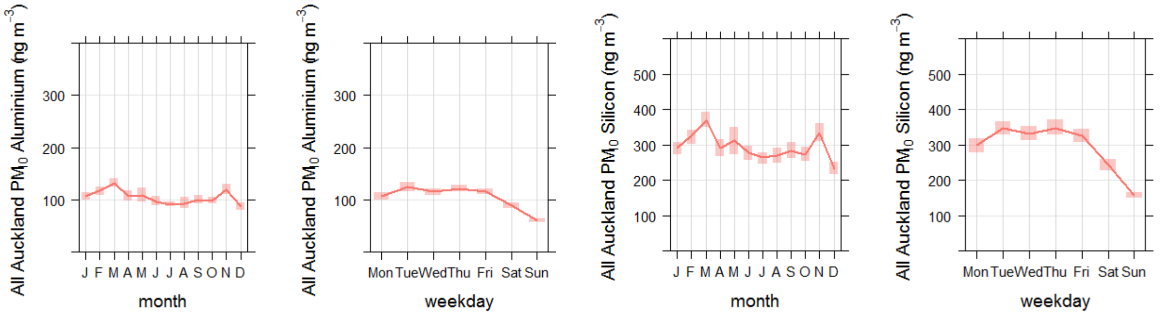

Figure 5.12 Temporal variations in aluminium (left) and silicon (right) in all Auckland PM$_{10}$ samples (the shaded bars are the 95 percentile confidence limits in the mean)

5.1.5 Trace element concentrations

A range of elements were present at trace concentrations in Auckland PM$_{2.5}$ and PM$_{10}$ and the following sections identify and describe the sources that these trace elements were mainly associated with.

5.1.5.1 Zinc

Zinc in particulate matter was relatively ubiquitous across the Auckland urban area and was significantly associated with biomass burning (an important trace element in plant material) and motor vehicle emissions (primarily due to the co-combustion of lubricant oils). Samples of particulate matter from the Penrose and Henderson sites showed that there were significant local industrial emissions of zinc.

5.1.5.2 Copper

Copper was more strongly associated with the coarse particle fraction (i.e. higher concentrations in PM$_{10}$ than PM$_{2.5}$) and mostly with the motor vehicle sources. Copper is a key indicator of brake wear due to brake pad composition containing significant amounts of the metal.

5.1.5.3 Vanadium and nickel

Concentrations of vanadium and nickel were found to be highest in particulate matter samples from the Queen Street site and were considered to be associated with combustion products from ships engines The major factor is the use of residual or bunker oil as fuel for ships which is generally of poor quality, high in sulphur, PAHs and heavy metals that can result in high sulphate containing particulate matter emissions contaminated with alkali earth and transition metals (V, Ni, Ca, Fe) (Fridell, Steen et al. 2008, Moldanová, Fridell et al. 2009).

Emissions of combustion products from ships engines can impact on local air quality in port areas, regional air quality and global climate (Huebert 1999, Endresen, Sørgård et al. 2003, Ault, Moore et al. 2009, Eyring, Isaksen et al. 2010, Hellebust, Allanic et al. 2010, Matthias, Bewersdorff et al. 2010). Species emitted to atmosphere from ships engines include usual combustion products (COx, NOx), gaseous sulphur oxides (SOx) that relate to fuel composition, volatile organic compounds (VOCs) from incomplete fuel combustion and particulate matter which includes trace heavy metals (e.g. vanadium and nickel) (Agrawal, Malloy et al. 2008, Agrawal, Welch et al. 2008, Fridell, Steen et al. 2008, Healy, O'Connor et al. 2009).

5.1.5.4 Arsenic and lead

The analysis of Henderson PM_{10} data shows that arsenic and lead concentrations were associated with Biomass burning sources. This was most likely due to copper chrome arsenate treated timber and old painted wood (for lead) finding its way into the fuel stream for solid fuel fires used for domestic space heating. Figure 5.13 presents the temporal variation for arsenic and lead showing a winter peak for both contaminants.

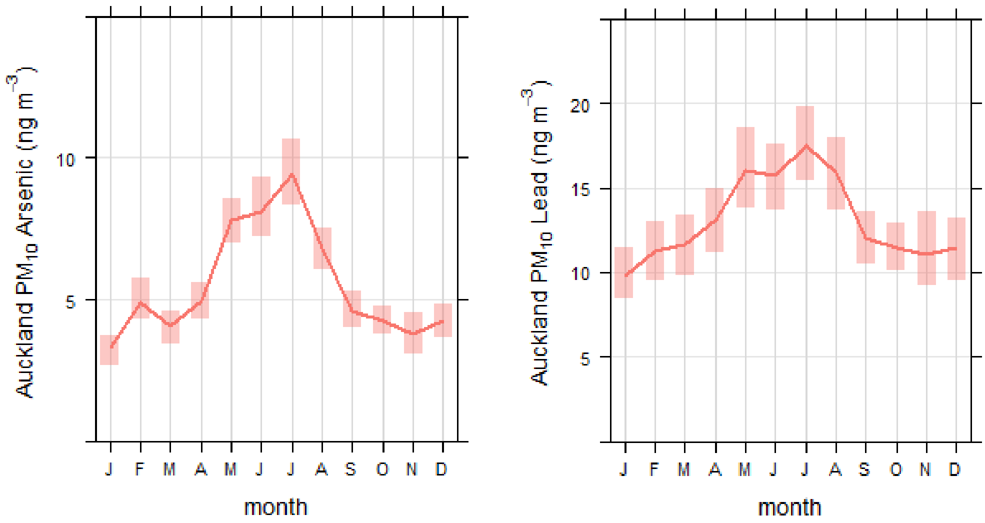

Figure 5.13 Temporal variation for arsenic (left); and lead (right) showing peak winter concentrations across Auckland (Shaded areas represent the 95% confidence intervals).

The New Zealand ambient air quality guidelines (AAQG) provide guideline values for arsenic (inorganic arsenic is 5.5 ng m^{-3} as an annual average) and lead (200 ng m^{-3} as a 3-month moving average, calculated monthly) in PM_{10} (MfE 2002). The calculation of an annual average for arsenic and a three-month running average from the Auckland data was not possible since the elemental analysis technique by IBA does not provide sufficient sensitivity (i.e. a low enough limit of detection). However, as a screening method it was considered adequate to provide an indication of the associated emission sources.

PART 2: ELEMENTAL CONCENTRATIONS, SOURCE APPORTIONMENT AND TREND ANALYSIS FOR INDIVIDUAL AUCKLAND COUNCIL MONITORING SITES

6.0 WESTLAKE GIRLS HIGH SCHOOL, TAKAPUNA

6.1 SITE DESCRIPTION

Samples of airborne particles were collected at an ambient air quality monitoring station located within the grounds of Westlake Girls High School, off Taharoto Road, Takapuna (Lat: -36.7803; Long: 174.7489). Figure 6.1 shows a map of the local area.

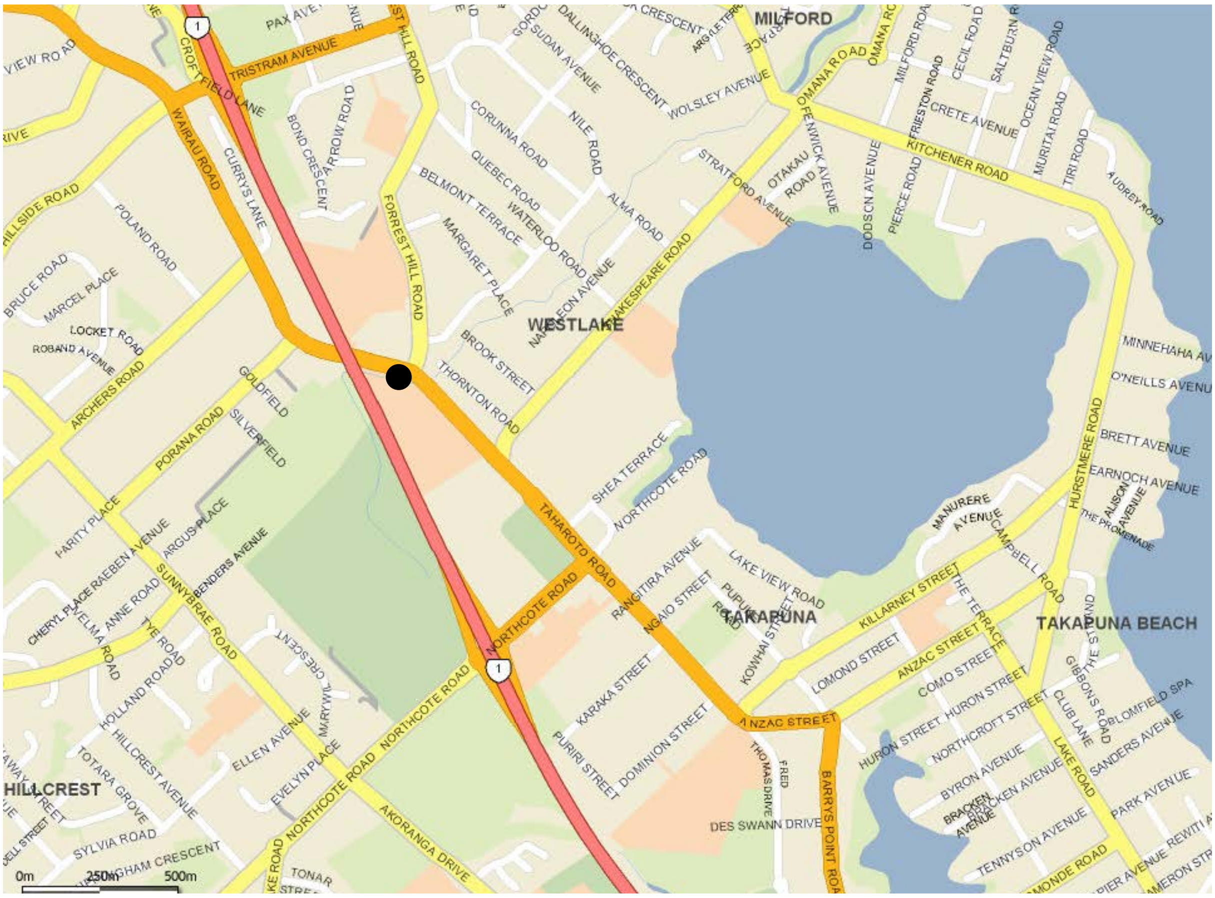

Figure 6.1 Map showing location of Takapuna monitoring site (●)

The Westlake Girls High School site is operated by WSL for AC as part of the AC ambient air quality monitoring programme. The site was established in mid-1995 and is classed as a residential – peak site. Pollutants monitored at the site include CO, NO_x, $PM_{2.5}$ (RAAS speciation sampler), PM_{10} (Beta Gauge and Partisol) as well as meteorological parameters on a 10 metre tower.

The Takapuna site is approximately 3.5 km northwest of the Takapuna shopping and commercial centre. Land use in the area is a mixture of residential and commercial activities with the Wairau industrial area (mainly warehousing and light industrial activities) 1 km to the northwest. The northern side of the monitoring station is near a 2 metre mesh fence next to Taharoto Road at the edge of the school fields. During 2011 the fields around the monitoring stations were substantially redeveloped to provide a major netball facility and artificial turf surfaces for hockey fields, the effect of which can be observed in the source contribution data (primarily the soil source) presented in this chapter.

To the west of the monitoring site (50 m) is State Highway 1, the main motorway into Auckland city to the south and to northern suburbs heading north, beyond the motorway is Takapuna Golf Course. The school buildings are 200 m immediately south of the monitoring station across the school grounds. 100 m southeast of the site is a concrete batching plant for producing ready-mix concrete. Beyond the immediate vicinity are residential properties. The land around the site at Westlake Girls High School is flat to rolling, and, 3 km east of the site is the coastline of the Hauraki Gulf. Figure 6.2a is an aerial view of the Takapuna site location taken during 2007. Substantial development of the environs around the speciation monitoring site has taken place over the years since the monitoring record began, including the redevelopment of the school playing fields mentioned previously as well as the installation of the bus-way along the northern motorway and the development of the Smales Farm precinct (bottom right) into a bus interchange hub completed in early 2008. The effects on these changes on air particulate matter concentrations and composition are observed in the Takapuna speciation data and source contributions.

E

Figure 6.2a Aerial view of Takapuna monitoring site and surrounds taken in 2007 (●) (Source: Google Maps 2007)

Figure 6.2 Aerial view of Takapuna monitoring site and surrounds taken in 2013 (●)(Source: Google Maps 2013)

6.2 AIR PARTICULATE MATTER SAMPLES AND MONITORING PERIOD

Filter samples from two instruments located at the Takapuna air quality monitoring station were supplied by AC for analysis:

1. 765 $PM_{2.5}$ samples from an Anderson RAAS speciation sampler on a one-day-in-three sampling regime for the period November 2006 – December 2013
2. 877 PM_{10} samples from a Partisol 2000 sampler on a one-day-in-three sampling regime for the period December 2005 – December 2013.

Separate receptor modelling studies were carried out for the $PM_{2.5}$ and PM_{10} sample sets are reported in Sections 6.6 and 6.7 respectively.

6.3 PM_{10} AND $PM_{2.5}$ CONCENTRATIONS AT THE TAKAPUNA SITE

The particulate matter results from the continuous $PM_{2.5}$ and PM_{10} B-gauge monitors (BAM) at Takapuna are presented in Figure 6.3. Note that the continuous $PM_{2.5}$ monitoring began in June 2007 while the PM_{10} began in February 2004 and the data have been put on the same time scale for comparative purposes. Figure 6.3 shows that $PM_{2.5}$ concentrations were highest during winter months (June - August), and while PM_{10} concentrations also peak in winter there are also other peaks evident at other times and the variations are explained by the relative contributions to ambient concentrations from different sources at different times of the year. Further discussion is provided in the following sections

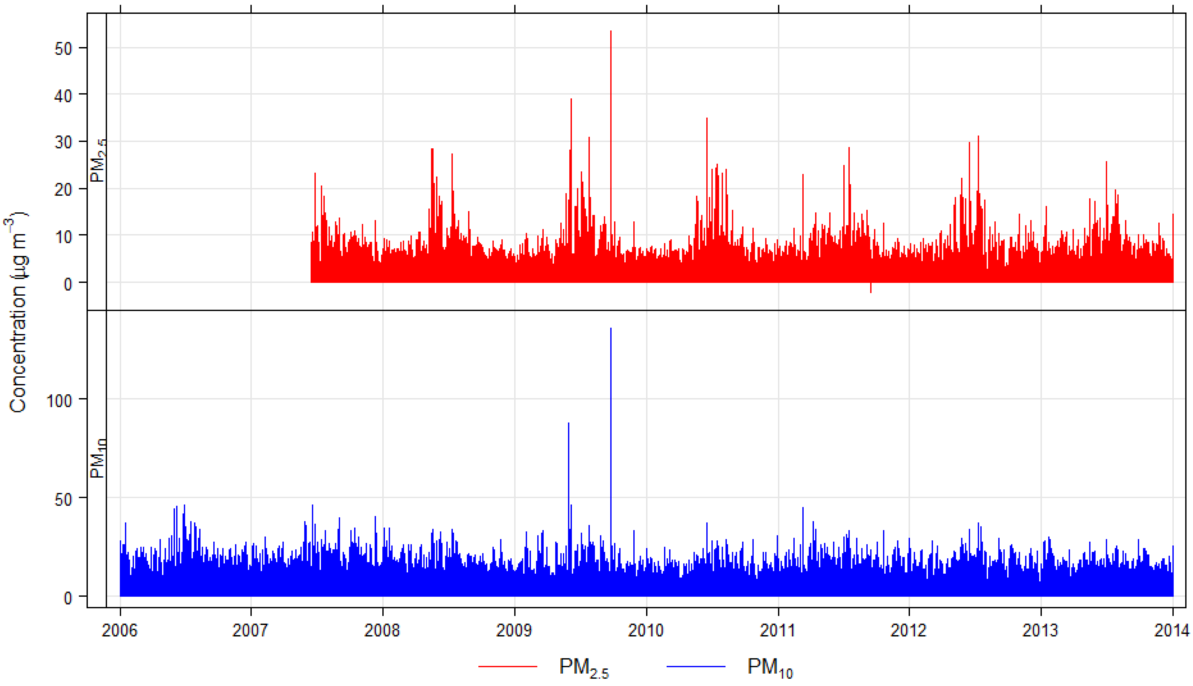

Figure 6.3 Results for 24-hour BAM PM$_{10}$ at the Takapuna site (note the differing scales)

Four exceedances of the NES for PM$_{10}$ (50 µg m^{-3}) have been recorded to date at Takapuna, one each of these were during winter 2004 and 2005 and two during 2009 (28 May and 25 September).

6.4 CONCEPTUAL RECEPTOR MODEL FOR PARTICULATE MATTER AT TAKAPUNA

The following initial conceptual model for Takapuna includes local emission sources:

- Domestic activities – likely to be dominated by emissions from solid fuel fires (biomass burning) used for domestic heating during the winter;
- Motor vehicles – all roads in the area act as line sources and roads with higher density traffic will dominate, particularly the motorway immediately to the west;
- Local wind-blown soil or road dust sources;
- Dust emissions from the nearby concrete batching plant,
- Katabatic wind flows down the Wairau Valley.

Longer range sources may also contribute to ambient particle loadings and these include:

- Marine aerosol;
- Secondary particulate matter resulting from atmospheric gas-to-particle conversion processes (sulphate and nitrate species, organic particle species resulting from photochemical reactions);
- Potential for long range transport of industrial emissions.

Another category of emission sources that may contribute are those considered as ‘one-off’ emission sources:

- Fireworks displays and other special events;

- Short-term road works and demolition/construction activities. For example, extension of the nearby motorway for a bus lane was underway during 2007, the Smales Farm bus interchange (both completed early 2008) and the WGHS playing fields were redeveloped during 2011.

The variety of sources described above can be recognised and accounted for by appropriate data analysis methods, such as examination of seasonal differences, temporal variations and receptor modelling itself.

6.5 LOCAL METEOROLOGY AT THE TAKAPUNA SITE

The predominant wind direction at the Takapuna site was from the southwesterly quarter as shown by the wind roses (2006-2014 data) in Figure 6.4 and Figure 6.5.

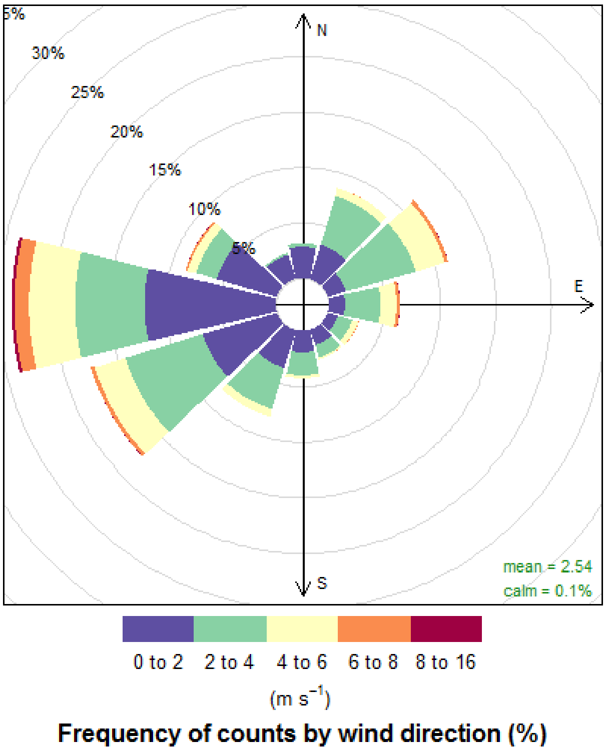

Figure 6.4 Takapuna wind rose for 2006-2014

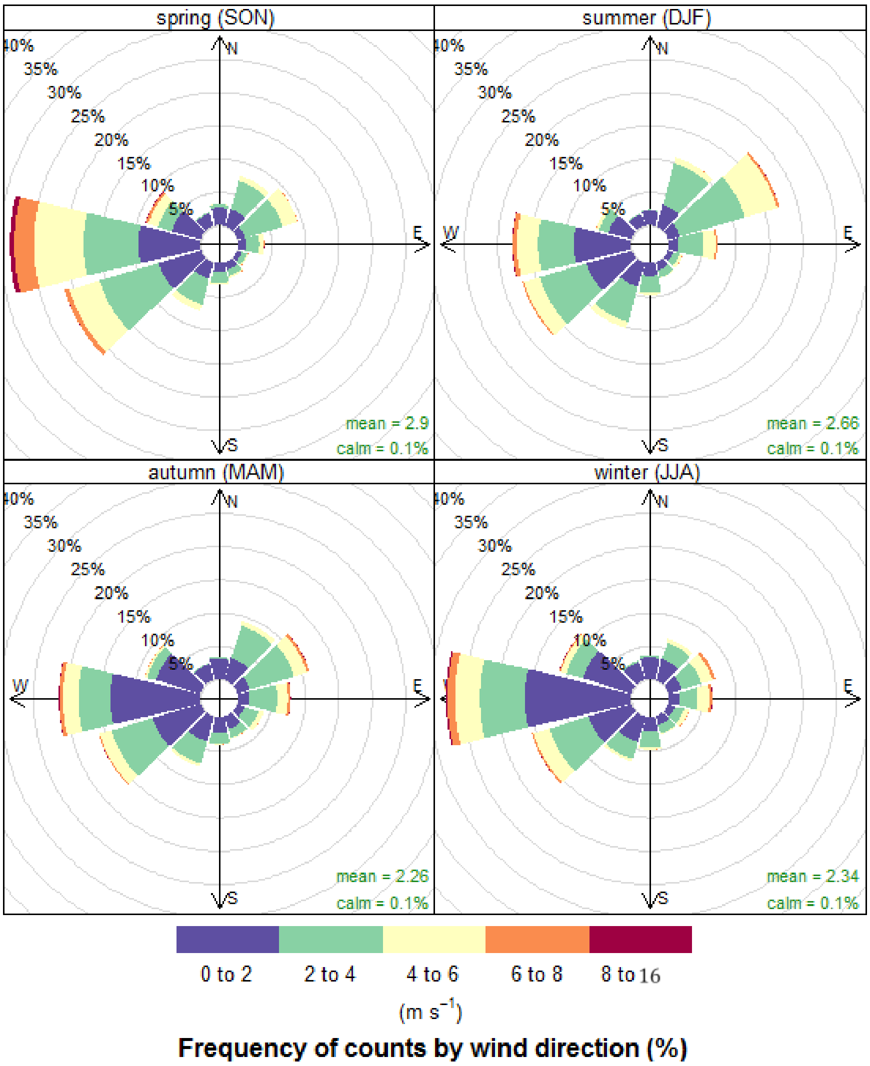

Figure 6.5 Takapuna seasonal wind roses for 2006 -2014

Meteorological differences between seasons at the Takapuna site can be seen in the wind roses presented in Figure 6.5. The predominance of stronger west to southwesterly winds was markedly more significant in winter and spring, while during the summer and autumn, a greater component of winds originate from the northeast.

6.6 ANALYSIS OF PM$_{2.5}$ SAMPLES FROM THE TAKAPUNA SITE

The Takapuna PM$_{2.5}$ samples from the Westlake Girls High School monitoring site refer to those PM$_{2.5}$ samples collected using a RAAS speciation sampler (Andersen Instruments Inc.) from November 2006 to December 2013. Gravimetric results for the PM$_{2.5}$ samples as presented in Figure 6.6 show distinct peaks in PM$_{2.5}$ concentrations during winter months (June – August). Note that gaps in the data are due to missed or excluded sample periods.

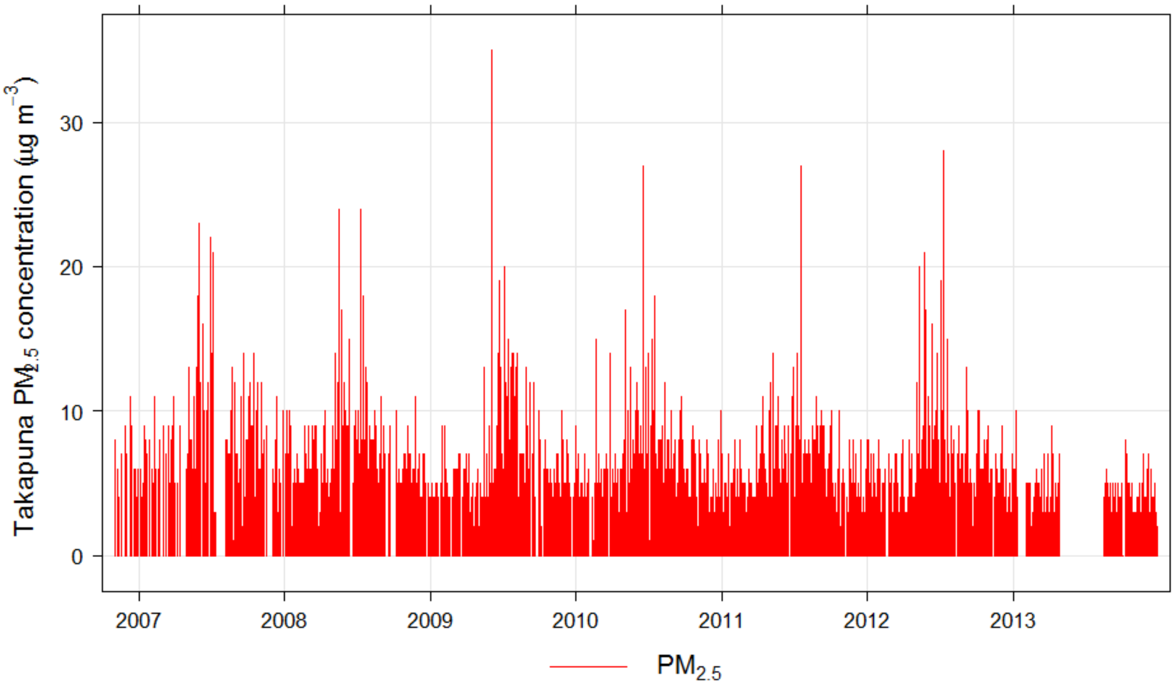

Figure 6.6 Gravimetric results for Speciation $PM_{2.5}$ at the Takapuna site

Peak concentrations in Speciation $PM_{2.5}$ correspond with peaks in BAM $PM_{2.5}$ concentrations (see Figure 6.3).

6.6.1 Composition of $PM_{2.5}$ at the Takapuna site

Elemental concentrations for Speciation $PM_{2.5}$ at the Takapuna site are listed in Table 6.1 with a box and whisker plot of the elemental concentrations shown in Figure 6.7.

Table 6.1 Elemental analysis results for Speciation $PM_{2.5}$ at the Takapuna site (765 samples)

Species	Average (ng/m^3)	Max (ng/m^3)	Min (ng/m^3)	Median (ng/m^3)	Std Dev (ng/m^3)	Av LOD (ng/m^3)	#>LOD
$PM_{2.5}$ (µg/m^3)	**7**	**35**	**0**	**6**	**4**		
H	103	983	0	80	96	47	579
BC	2870	16281	0	2346	2199	182	762
Na	845	4148	0	677	700	277	628
Mg	80	364	0	67	57	27	674
Al	22	432	0	18	24	13	543
Si	59	1267	17	48	58	9	765
P	4	32	0	1	6	15	88
S	232	1069	0	195	131	9	763
Cl	1106	5517	6	892	873	7	764
K	65	1458	0	47	75	7	760
Ca	47	730	6	42	35	7	764
Sc	2	17	0	1	2	8	37
Ti	3	31	0	2	4	8	130
V	1	12	0	0	2	8	31
Cr	2	44	0	0	3	7	55
Mn	2	14	0	1	2	7	95
Fe	70	351	0	62	50	5	747
Co	2	15	0	0	3	9	58
Ni	2	20	0	0	3	9	52
Cu	5	31	0	4	5	10	201
Zn	13	519	0	8	25	12	309
Ga	3	26	0	0	5	18	53
Ge	4	35	0	0	6	22	58
As	5	59	0	0	9	29	68
Se	8	71	0	0	12	35	77
Br	9	82	0	0	14	46	83
Rb	14	111	0	0	21	75	67
Sr	18	143	0	0	26	94	50
Mo	49	553	0	0	88	293	105
I	8	58	0	2	10	26	76
Ba	9	134	0	5	11	30	75
Hg	11	153	0	0	19	66	37
Pb	13	144	0	0	24	80	35

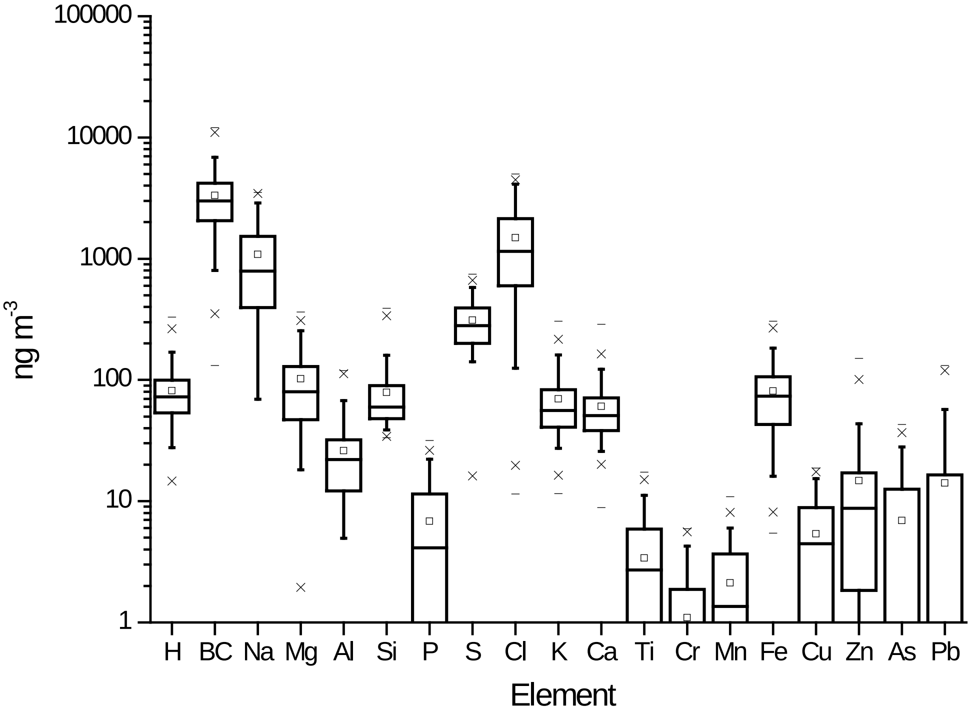

Figure 6.7 Box and whisker plot of $PM_{2.5}$ elemental concentrations at the Takapuna site (y- axis in logarithmic scale)

Table 6.1 shows a number of measured species being generally close to or below the limits of detection. Carbonaceous species (represented by BC), sodium and chlorine were found to dominate $PM_{2.5}$ elemental mass concentrations indicating that combustion processes and marine aerosol are important contributors to ambient $PM_{2.5}$ at Takapuna. A scatterplot matrix of the species in Table 6.1 is presented in Appendix 2.

6.6.2 Source contributions to $PM_{2.5}$ at Takapuna

Six primary source contributors were determined from the PMF receptor modelling analysis of speciation $PM_{2.5}$ elemental compositions at Takapuna. These are identified as presented in Table 6.2 along with the mass of $PM_{2.5}$ and elemental species associated with each source.

Table 6.2 Elemental composition of source profiles and contribution to $PM_{2.5}$ at the Takapuna site

	Factor 1	Factor 2	Factor 3	Factor 4	Factor 5	Factor 6
Species	**Biomass burning (ng/m^3)**	**Diesel vehicles (ng/m^3)**	**Petrol vehicles (ng/m^3)**	**Sulphate (ng/m^3)**	**Marine aerosol (ng/m^3)**	**Soil (ng/m^3)**
$PM_{2.5}$	1679	1489	177	800	2296	156
H	45	22	2	14	9	2
BC	1057	1326	142	171	76	22
Na	9	19	7	34	752	11
Mg	2	4	1	6	61	4
Al	1	1	1	2	3	15
Si	3	11	2	7	6	30
S	8	19	5	134	59	5
Cl	0	40	18	26	1008	16
K	30	6	0	1	21	2
Ca	2	8	2	3	22	8
Fe	13	46	2	3	0	6
Zn	1	1	9	0	0	0

Table 6.2 represents the summary results for a reiterative process that examines the effect of each species on the PMF receptor modelling process using the modelling diagnostics presented in Appendix 2. Species that were poorly modelled (slope, $r^2 < 0.6$) were removed from the analyses unless considered vital for source identification.

The source contributors identified in Table 6.2 were found, on average, to explain 94 % of $PM_{2.5}$ gravimetric mass. Figure 6.8 presents the source profiles extracted from the PMF analysis of Takapuna $PM_{2.5}$ data.

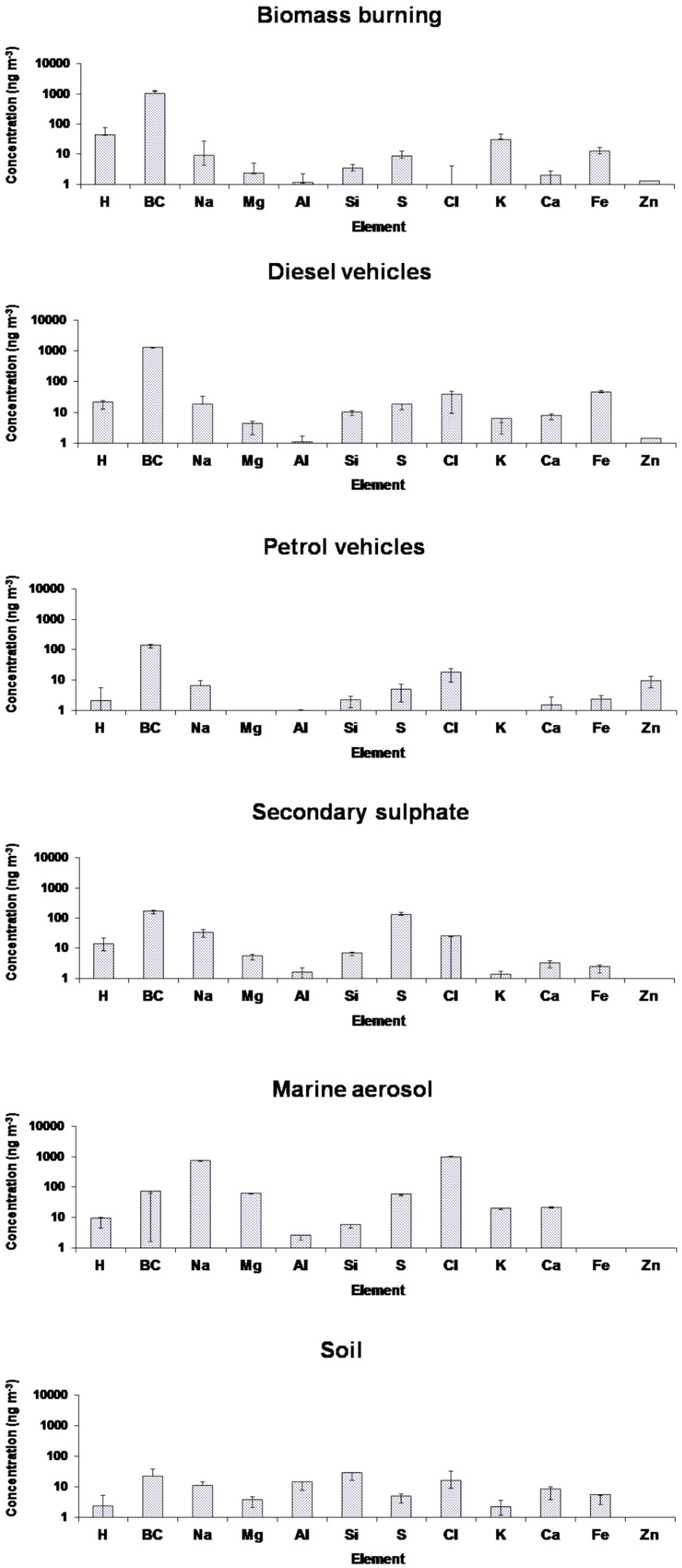

Figure 6.8 Source profiles and elemental concentrations for $PM_{2.5}$ at the Takapuna site (showing 5th and 95th confidence intervals in mean concentration derived from the receptor modelling)

- The first factor is due Biomass burning
- The second and third factors were attributed to motor vehicle emissions (diesel and petrol vehicles emissions respectively).
- The fourth factor has been identified as a secondary sulphate aerosol source due to the predominance of S.
- The fifth factor represents the contribution from marine aerosol due to the dominance of Na and Cl.
- The sixth source is from crustal matter (wind blown dust).

Figure 6.9 presents the average source contributions to $PM_{2.5}$ concentrations and includes standard deviations of average mass contributions from each of the sources indicating the variability in source strength.

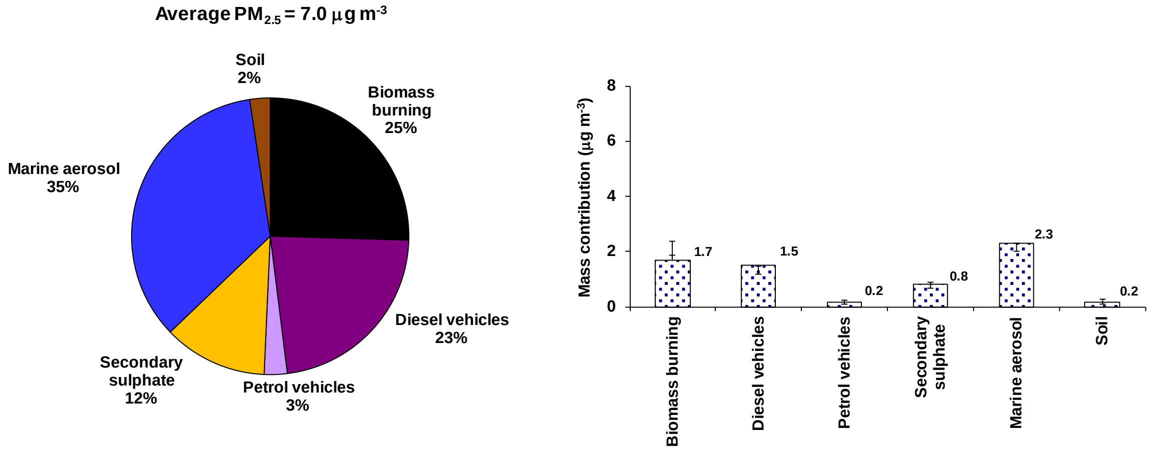

Figure 6.9 Average (2007-2013) source contributions to $PM_{2.5}$ at Takapuna site (showing 5th and 95th confidence intervals in mean concentration derived from the receptor modelling)

The average source contributions estimated by the receptor modelling shows that marine aerosol, biomass burning and motor vehicles were the most significant contributors (35 %, 25 % and 26 % respectively) to $PM_{2.5}$ concentrations at Takapuna, with lesser contributions from secondary sulphate particles (12 %) and trace crustal matter concentrations (2 %). Emissions from diesel vehicles were found to dominate the motor vehicle sources.

Figure 6.10 shows the mass contribution of sources to $PM_{2.5}$ mass for each sample collected at Takapuna (note that gaps in the data are from missed sampling periods). The temporal variation indicates that marine aerosol is an intermittent contributor throughout the year while biomass burning has peak contributions during winter months.

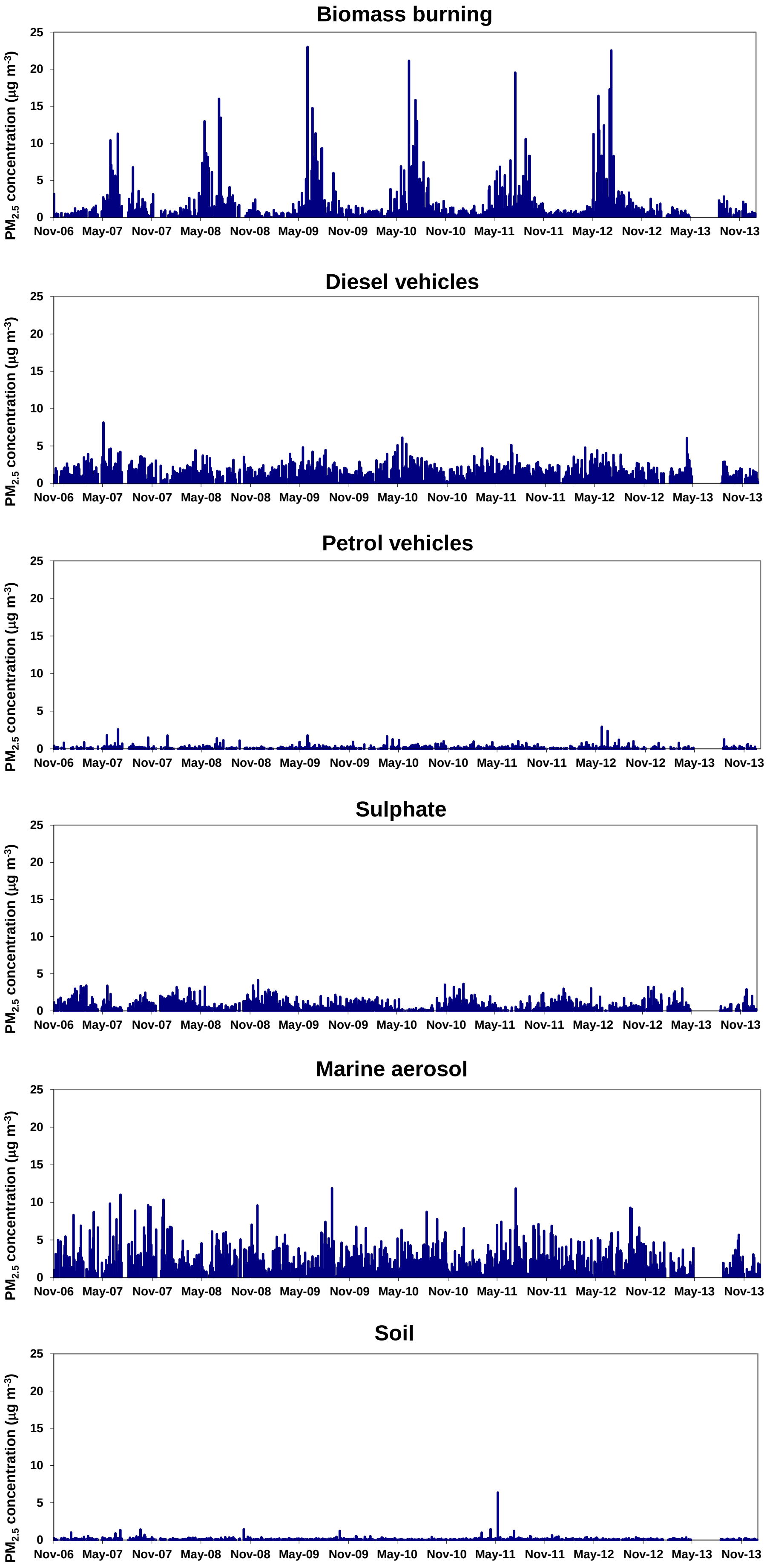

Figure 6.10 Time-series for source contributions to $PM_{2.5}$ samples at Takapuna

6.6.3 Temporal variations in $PM_{2.5}$ sources at the Takapuna site

The primary source of $PM_{2.5}$ during winter (June-August) at Takapuna was biomass burning attributed to emissions from solid fuel fires for domestic heating. Figure 6.11 presents the seasonal mass contributions at the Takapuna site. Average $PM_{2.5}$ concentrations were found to be higher in winter (10 $\mu g\ m^{-3}$) than in other seasons.

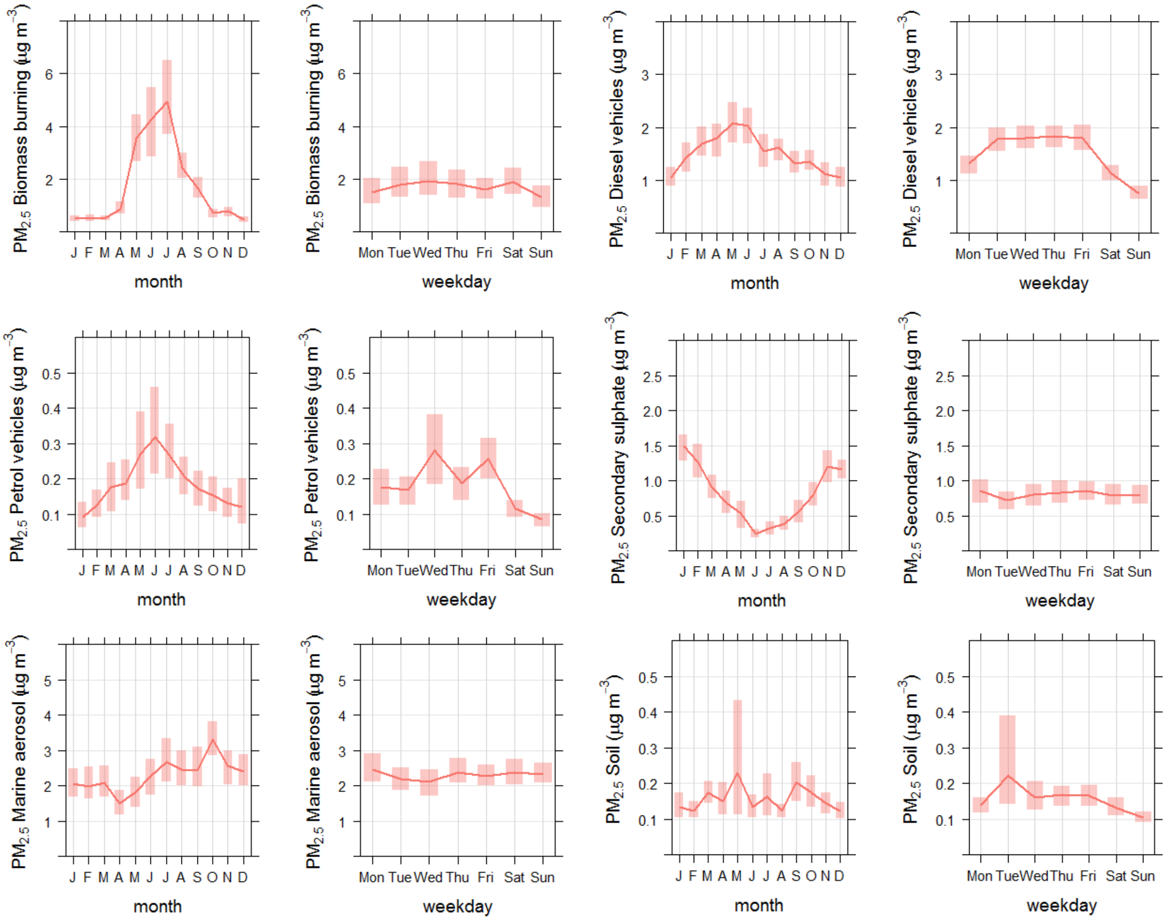

Figure 6.11 Temporal (2007-2013) variations in $PM_{2.5}$ source contributions at the Takapuna site (the shaded bars are the 95 percentile confidence limits in the mean)

Distinct seasonal patterns were observed for the biomass burning and motor vehicle sources with higher concentrations during the winter months (May, June, July, August) which were likely to be due to both activity (domestic fires for home heating) and meteorological factors such as cold and calm weather which restricts dispersion. The only sources to demonstrate significant temporal variation in day-of-the-week activity (with higher concentrations on weekdays), were the motor vehicle and crustal matter sources due to the behavioural patterns of higher weekday commercial (heavy duty diesel fuelled commercial vehicles) and commuter traffic.

6.6.4 Trends in $PM_{2.5}$ concentrations and source contributions at Takapuna

The temporal trends in $PM_{2.5}$ concentrations and $PM_{2.5}$ source contributions at Takapuna were explored using the Thielsen functionality available in *openair*. Figure 6.12 presents the trend in $PM_{2.5}$ concentrations showing that there was a significant decreasing trend (99.9 % CI) over the monitoring period.

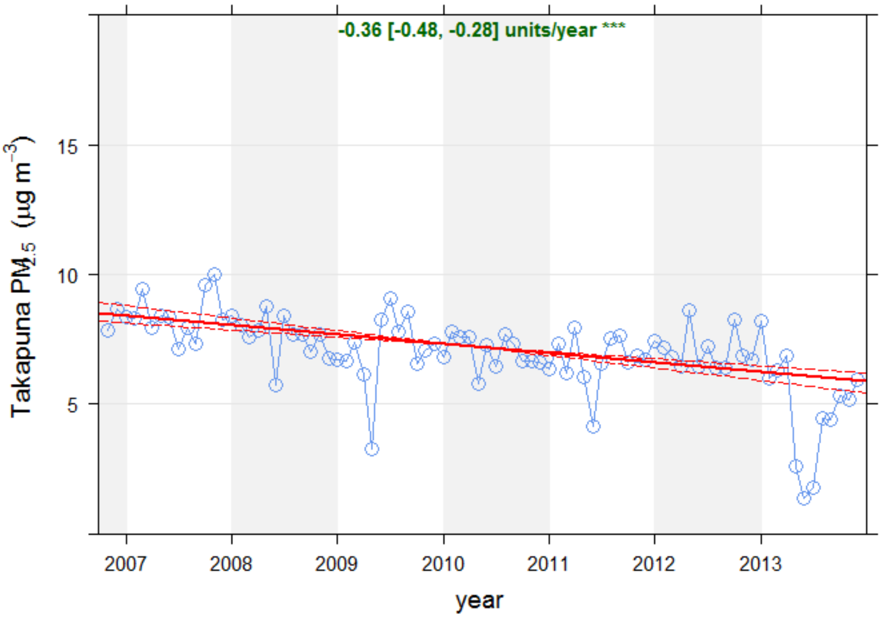

Figure 6.12 Trend in $PM_{2.5}$ concentrations for 2007-2013 at Takapuna (statistically significant at the 99.9 % confidence interval)

Figure 6.13 presents the trends in source contributions showing that there was no significant trend for the biomass burning motor vehicle and soil sources, but that there were significant decreasing trends for secondary sulphate (99.9% CI) and marine aerosol (99.9% CI). The primary influence for the decrease in secondary sulphate appears to the reduction in sulphur in automotive fuels as described in Chapter 5. However, the driver for the decrease in $PM_{2.5}$ marine aerosol is unclear but is likely to be associated with ocean-atmosphere interactions as discussed in Chapter 5.

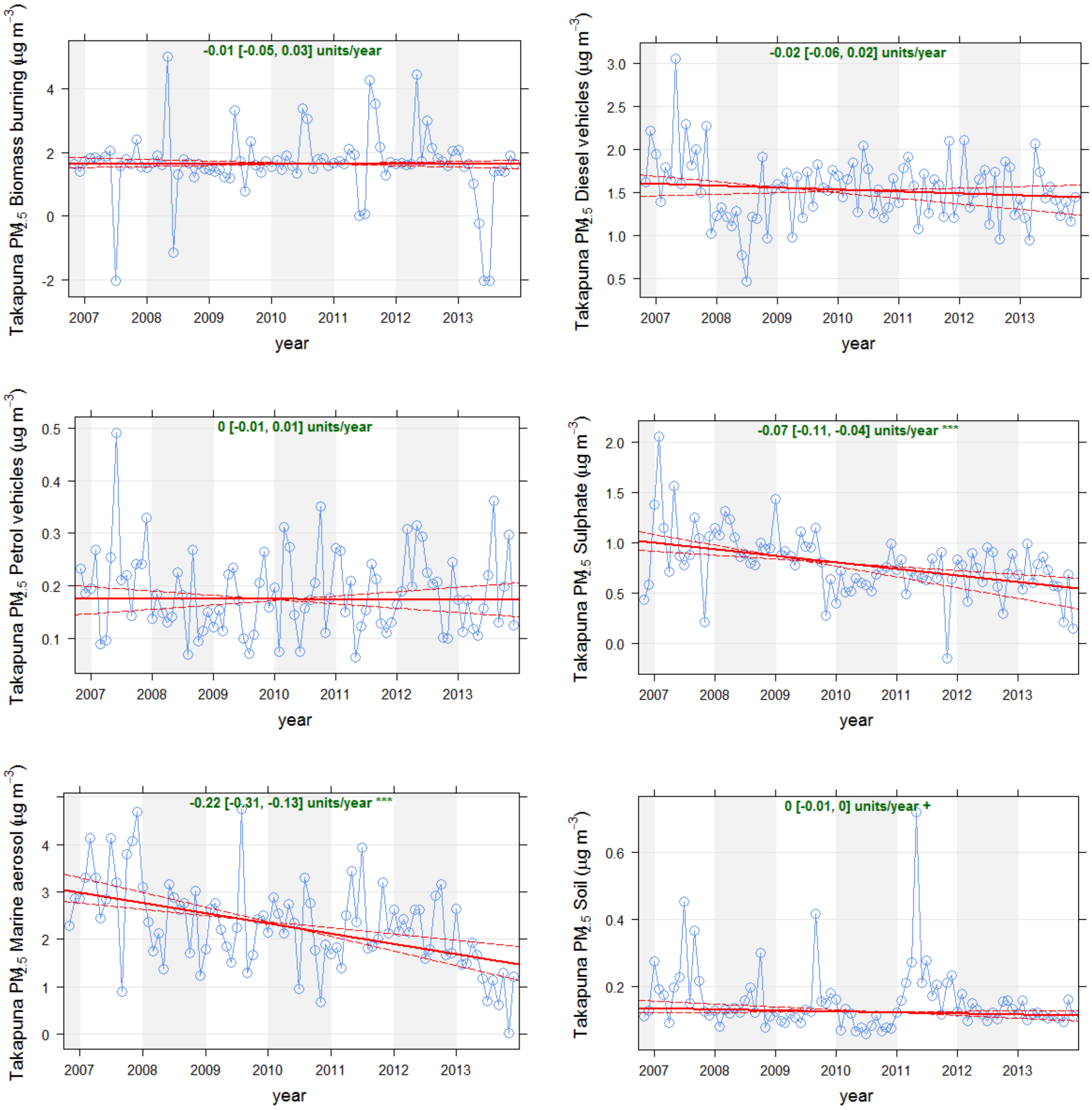

Figure 6.13 Trends in $PM_{2.5}$ source contributions for 2007-2013 at Takapuna

The decreasing trend in the marine aerosol and secondary sulphate were largely responsible for the observed decrease in $PM_{2.5}$ over the monitoring period.

6.6.5 Analysis of individual $PM_{2.5}$ events at the Takapuna site

Peak $PM_{2.5}$ events that exceeded the AAQG 'Alert' category (17 µg/m^3) during the sampling period at Takapuna have been chosen for further analysis. Figure 6.14 presents the relative source mass contributions for the days identified during the monitoring period. The primary source of peak $PM_{2.5}$ was found to be due to biomass burning except for one day (28/05/2007) which was dominated by marine aerosol (10 µg m^{-3}). Of the 6 days where $PM_{2.5}$ exceeded the AAQG, biomass burning was responsible for approximately 80 % of $PM_{2.5}$ mass.

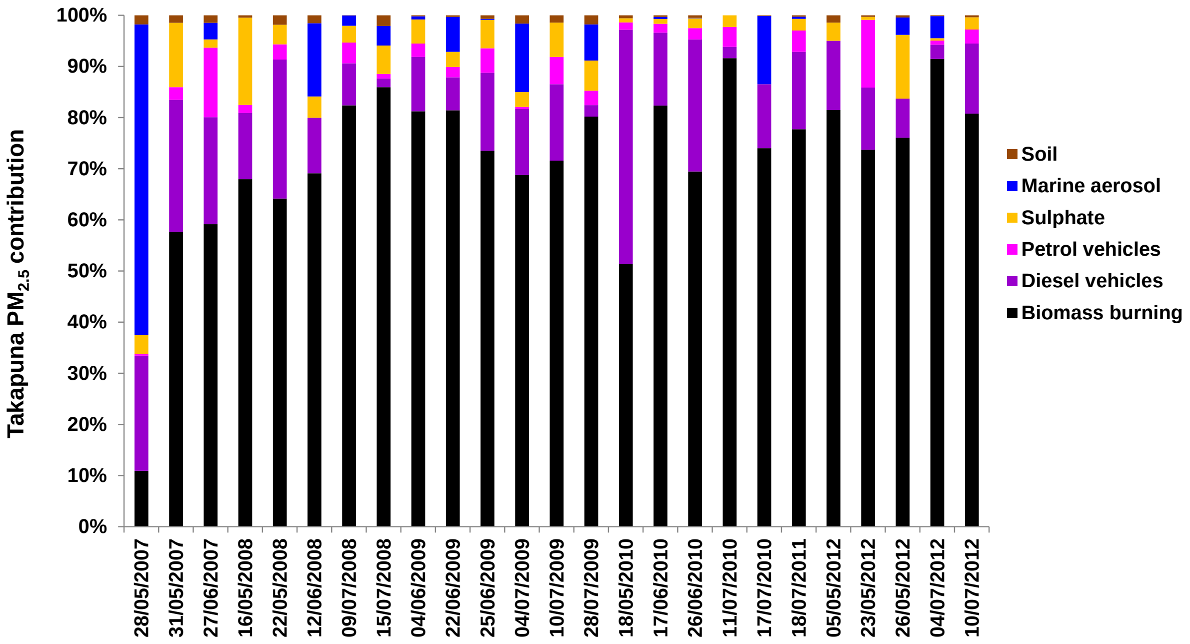

Figure 6.14 Source mass contributions to peak $PM_{2.5}$ concentrations (>17 μg m^{-3}) at Takapuna

6.6.6 Variation of $PM_{2.5}$ source contributions with wind direction at the Takapuna site

The CPF analysis of the relationship between the source contributions and wind direction is presented and discussed in the following sections.

6.6.6.1 Biomass Burning

Biomass burning source contributions to $PM_{2.5}$ at Takapuna are considered to be primarily due to emissions from domestic solid fuel fires during winter. Peak contributions are highest on cold, calm winter days under inversion conditions and local cold air drainage (katabatic) flows or with a light southerly wind, particularly for anticyclonic synoptic conditions. The CPF analysis for biomass burning presented in Figure 6.15 shows only a small westerly component likely to represent drainage flows down the Wairau Valley.

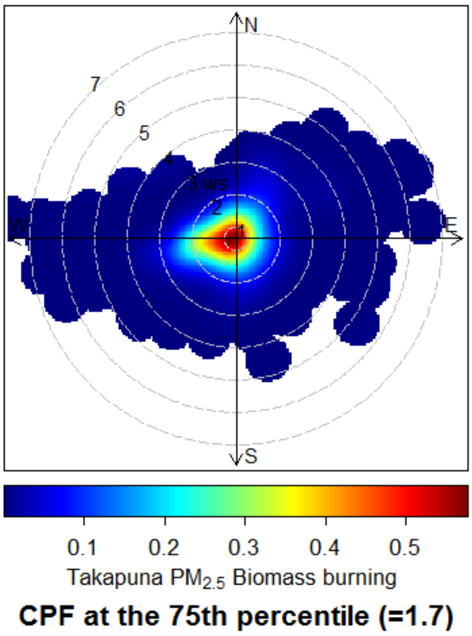

Figure 6.15 Takapuna $PM_{2.5}$ biomass burning CPF analysis

6.6.6.2 Diesel vehicles

The Diesel vehicle source for $PM_{2.5}$ shows a distinct west-southwest component as presented in Figure 6.16 and is aligned with the nearby motorway.

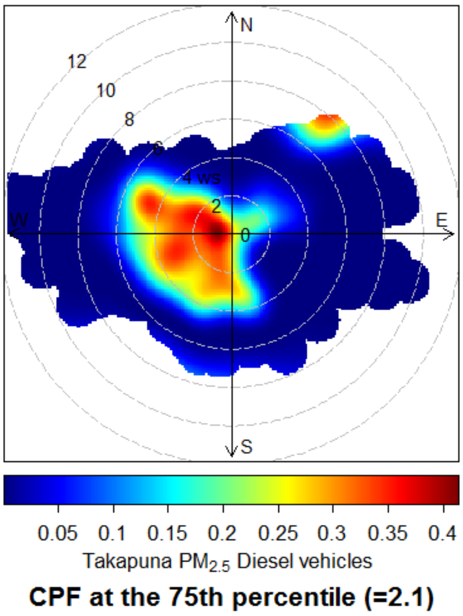

Figure 6.16 Takapuna $PM_{2.5}$ Diesel vehicle CPF analysis

6.6.6.3 Petrol vehicles

The petrol vehicle source for $PM_{2.5}$ shows a southwest and south to southeast component for peak concentrations as presented in Figure 6.17 and may be due to traffic on the motorway and nearby Taharoto Road (as a line source leading southeast) or associated with vehicle activity in WGHS carparks.

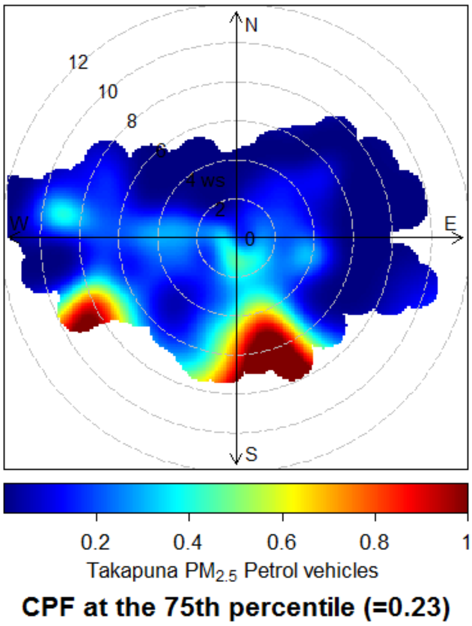

Figure 6.17 Takapuna $PM_{2.5}$ petrol vehicle CPF analysis

6.6.6.4 Secondary sulphate

The highest $PM_{2.5}$ secondary sulphate contributions were found to primarily originate from the easterly sector (Figure 6.18). This supports the case that the originating source was emissions from ships moving in and out of the Port of Auckland. Further discussion on the sources of secondary sulphate in the Auckland region is provided in Chapter 5.

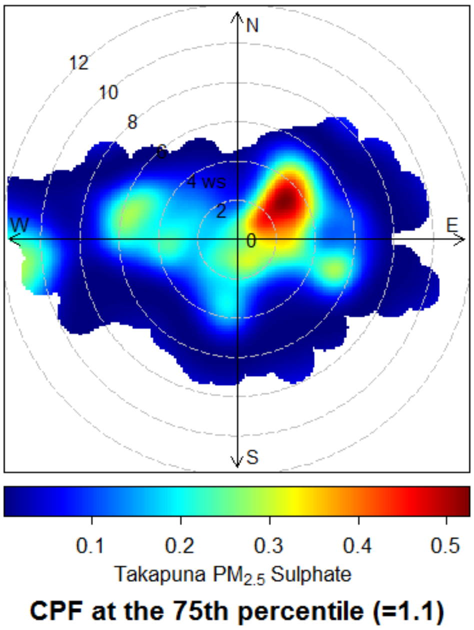

Figure 6.18 Takapuna $PM_{2.5}$ secondary sulphate CPF analysis

6.6.6.5 Marine aerosol

The Takapuna $PM_{2.5}$ marine aerosol contribution presented in Figure 6.19 originates from the southwest and northeast directions. The most likely source of the $PM_{2.5}$ marine aerosol is the Southern Ocean, Tasman Sea and Pacific Ocean.

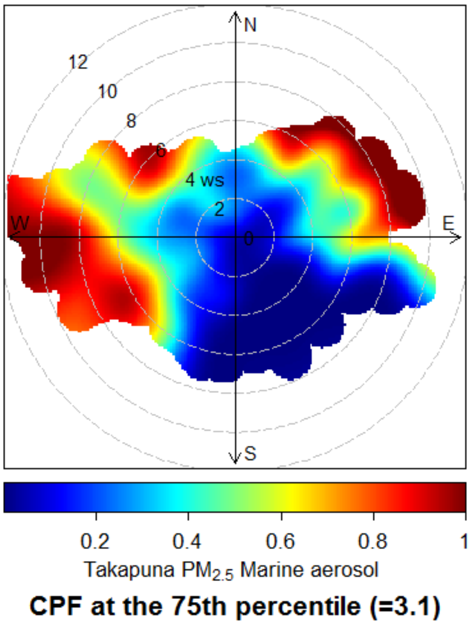

Figure 6.19 Takapuna $PM_{2.5}$ marine aerosol CPF analysis

6.6.6.6 Crustal matter

The crustal matter source for $PM_{2.5}$ shows a northwest-southeast component as presented in Figure 6.20 and is aligned with the nearby motorway although it is likely that some dust would originate from the school grounds in between the monitoring station and the motorway.

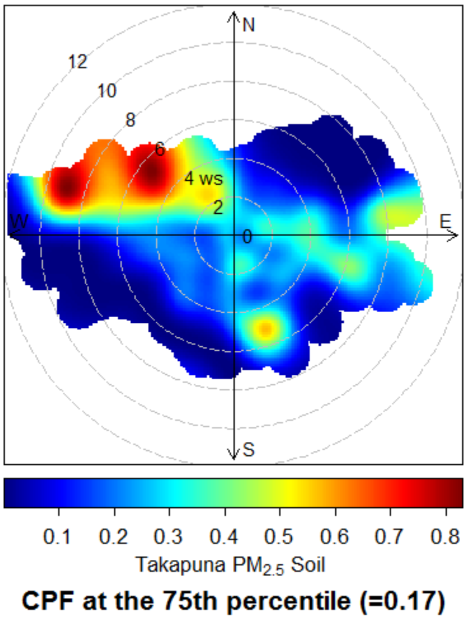

Figure 6.20 Takapuna $PM_{2.5}$ crustal matter CPF analysis

6.7 ANALYSIS OF PM_{10} SAMPLES FROM THE TAKAPUNA SITE

The Takapuna PM_{10} samples from the Westlake Girls High School monitoring site refer to those PM_{10} samples collected using a Partisol 2000 Sampler (Andersen Instruments Inc.) from December 2005 to December 2013. Gravimetric results for the Partisol PM_{10} samples as presented in Figure 6.21 show peaks (>33 μg m^{-3}) in PM_{10} concentrations at various times of the year, mainly during winter months (June – August) and occasionally during spring and summer. Gaps in the data are due to missed or excluded sample periods.

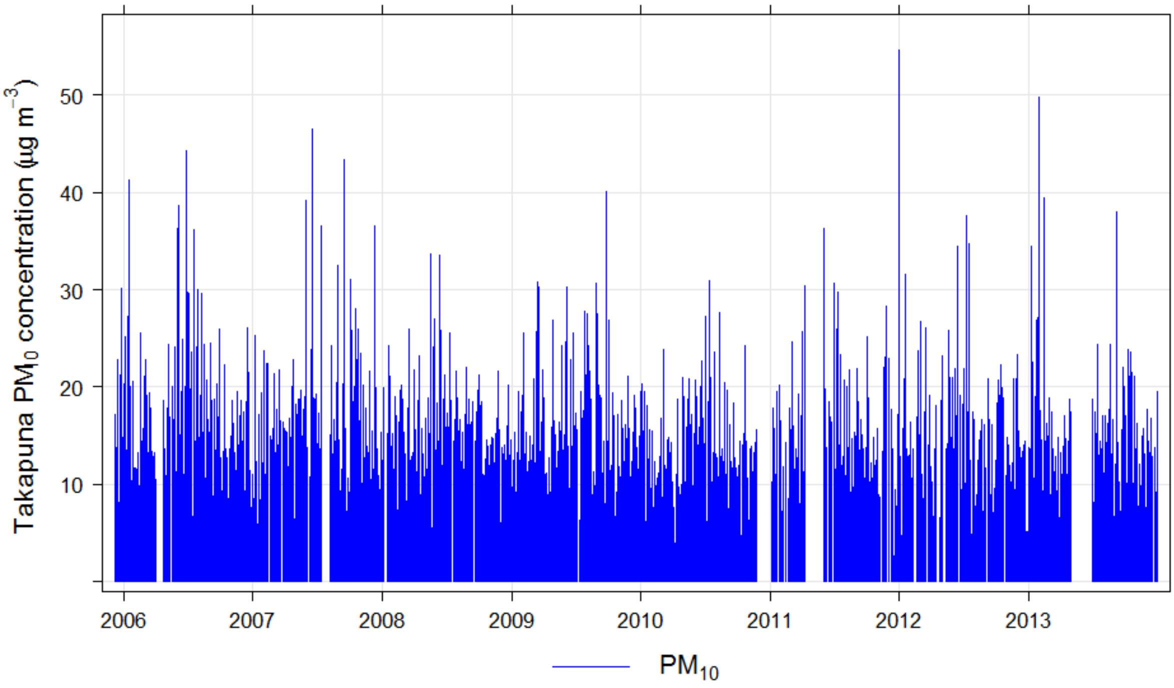

Figure 6.21 Gravimetric results for Partisol PM_{10} at the Takapuna site

Peak concentrations in Partisol PM_{10} correspond with peaks in BAM PM_{10} concentrations (see Figure 6.3).

6.7.1 Composition of PM_{10} at the Takapuna site

Elemental concentrations for Partisol PM_{10} at the Takapuna site are listed in Table 6.3 with a box and whisker plot of the elemental concentrations shown in Figure 6.22.

Table 6.3 Elemental analysis results for Partisol PM_{10} at the Takapuna site (877 samples)

Species	Average (ng/m^3)	Max (ng/m^3)	Min (ng/m^3)	Std Dev (ng/m^3)	Median (ng/m^3)	Av LOD (ng/m^3)	#>LOD
PM_{10} ($\mu g/m^3$)	**16**	**55**	**3**	**6**	**15**		
H	118	846	0	108	95	43	714
BC	2782	11610	105	1696	2402	165	876
Na	2024	9379	0	1338	1787	440	835
Mg	182	895	0	111	161	36	831
Al	108	2114	0	116	82	16	850
Si	316	5259	38	333	230	11	877
P	15	110	0	16	13	18	428
S	357	1424	58	170	331	13	877
Cl	3017	16774	35	2033	2617	9	877
K	132	1532	18	87	113	7	877
Ca	184	3381	5	171	159	7	876
Sc	4	31	0	5	2	10	121
Ti	17	822	0	31	12	8	595
V	1	17	0	2	0	10	32
Cr	1	16	0	2	0	9	58
Mn	5	31	0	5	4	7	331
Fe	257	1230	9	166	222	6	877
Co	4	46	0	6	2	11	163
Ni	2	13	0	3	0	9	78
Cu	12	97	0	10	11	9	536
Zn	18	298	0	23	12	11	483
Ga	3	25	0	5	0	18	52
Ge	3	31	0	6	0	23	52
As	6	83	0	11	0	29	94
Se	7	50	0	10	0	36	64
Br	11	95	0	15	5	45	111
Rb	14	130	0	21	0	78	68
Sr	20	262	0	30	0	99	79
Mo	44	429	0	78	0	214	88
I	12	78	0	16	4	31	143
Ba	25	331	0	23	22	31	347
Hg	12	126	0	18	0	63	45
Pb	13	159	0	23	0	81	50

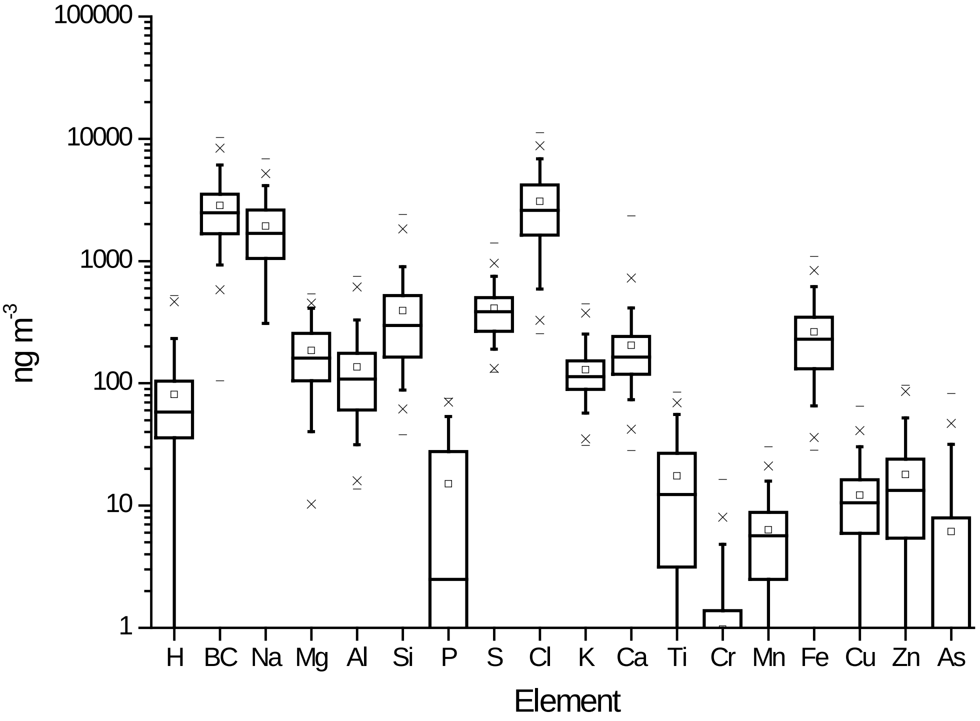

Figure 6.22 Box and whisker plot of PM_{10} elemental concentrations at the Takapuna site

Table 6.3 shows a number of measured species being generally close to or below the limits of detection. Carbonaceous species (represented by BC), sodium and chlorine were found to dominate PM_{10} elemental mass concentrations indicating that combustion processes and marine aerosol are important contributors to ambient PM_{10} at Takapuna. A scatterplot matrix of the key species in Table 6.3 is presented in Appendix 2.

6.7.2 Source contributions to PM_{10} at Takapuna

Seven primary source contributors were determined from the PMF receptor modelling analysis of the PM_{10} elemental composition at Takapuna. These are identified as presented in Table 6.4 along with the mass of PM_{10} and elemental species associated with each source.

Table 6.4 Elemental composition of source profiles and contribution to PM_{10} at the Takapuna site

	Factor 1	**Factor 2**	**Factor 3**	**Factor 4**	**Factor 5**	**Factor 6**	**Factor 7**
Species	**Biomass burning (ng/m^3)**	**Diesel vehicles (ng/m^3)**	**Petrol vehicles (ng/m^3)**	**Sulphate (ng/m^3)**	**Marine aerosol (ng/m^3)**	**Soil (ng/m^3)**	**Cement (ng/m^3)**
PM_{10}	**2128**	**3109**	**259**	**2152**	**6289**	**1016**	**453**
H	58	31	2	8	7	0	3
BC	756	1520	69	379	0	4	53
Na	40	35	12	183	1727	19	0
Mg	6	9	2	16	135	9	1
Al	1	17	2	15	7	59	5
Si	4	60	5	41	10	164	27
S	19	14	8	182	115	14	3
Cl	13	122	13	144	2671	35	15
K	37	17	2	8	47	10	4
Ca	5	31	2	10	56	9	71
Ti	0	8	0	0	0	5	2
Mn	0	2	0	1	1	1	0
Fe	19	147	9	19	7	41	12
Cu	1	8	1	1	1	0	0
Zn	2	3	12	0	0	0	0
Ba	2	11	1	4	7	1	0

Table 6.4 represents the summary results for a reiterative process that examines the effect of each species on the PMF receptor modelling process using the modelling diagnostics presented in Appendix 2. Species that were poorly modelled (slope, $r^2 < 0.6$) were removed from the analyses unless considered vital for source identification.

The source contributors identified in Table 6.4 were found on average to explain 95 % of PM_{10} gravimetric mass. Figure 6.23 presents the source profiles extracted from the PMF analysis of Takapuna PM_{10} data.

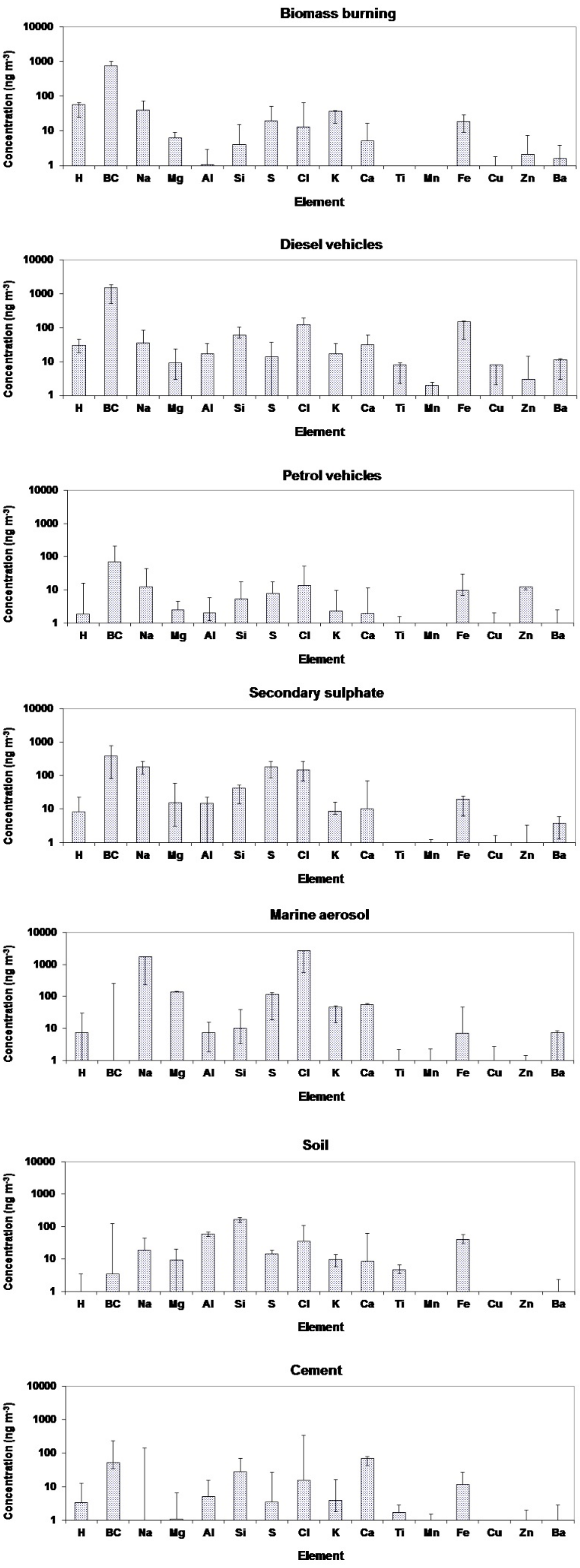

Figure 6.23 Source profiles and elemental concentrations for PM_{10} at the Takapuna site (showing 5th and 95th confidence intervals in mean concentration derived from the receptor modelling)

- The first factor is from Biomass burning primarily due to emissions from solid fuel fires for domestic heating.
- The second and third factors have been identified as originating from motor vehicle emissions. The second factor is due to the bulk of motor vehicle emissions (primarily diesel fuelled vehicles) coupled with some road dust (Al, Si content), while the third factor has been identified as originating from petrol vehicles due to the high zinc content with Fe and BC. Further discussion on the vehicle sources is provided in Chapter 5.
- The fourth source is a secondary sulphate aerosol source due to the predominance of S.
- The fifth factor represents the contribution from marine aerosol due to the dominance of Na and Cl.
- The sixth source is from crustal matter.
- The seventh source contribution, cement, has been identified as originating from concrete batching plant fugitive emissions as Ca is predominant in the profile.

Figure 6.24 presents the average source contributions to PM_{10} concentrations and includes standard deviations of average mass contributions from each of the sources indicating the variability in source strength.

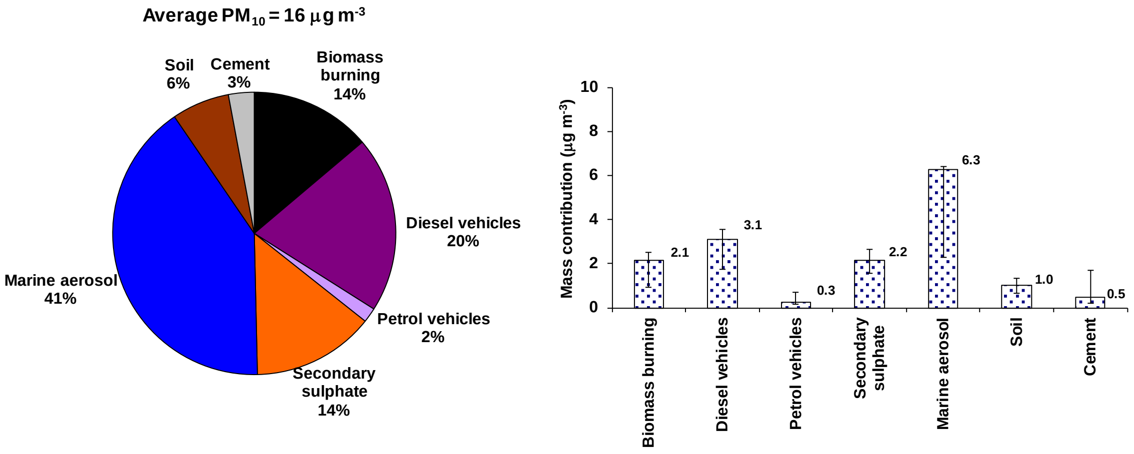

Figure 6.24 Average (2006-2013) source contributions to PM_{10} at Takapuna site (showing 5th and 95th confidence intervals in mean concentration derived from the receptor modelling)

The average source contributions estimated by the receptor modelling shows that marine aerosol and motor vehicle emissions (diesel and petrol) are the most significant contributors (43 % and 24 % respectively) to long-term PM_{10} concentrations at Takapuna, with lesser contributions from biomass burning emissions (14 %), secondary sulphate particles (14 %), crustal matter (6 %) and trace dust concentrations from the cement dust source (3 %). Figure 6.25 shows the mass contribution of sources to PM_{10} mass for each sample collected at Takapuna. The temporal variation indicates that marine aerosol is an important contributor throughout the year while biomass burning and motor vehicles have peak contributions during winter months. Other sources such as soil and cement show intermittent peaks that are associated with source activity and wind direction.

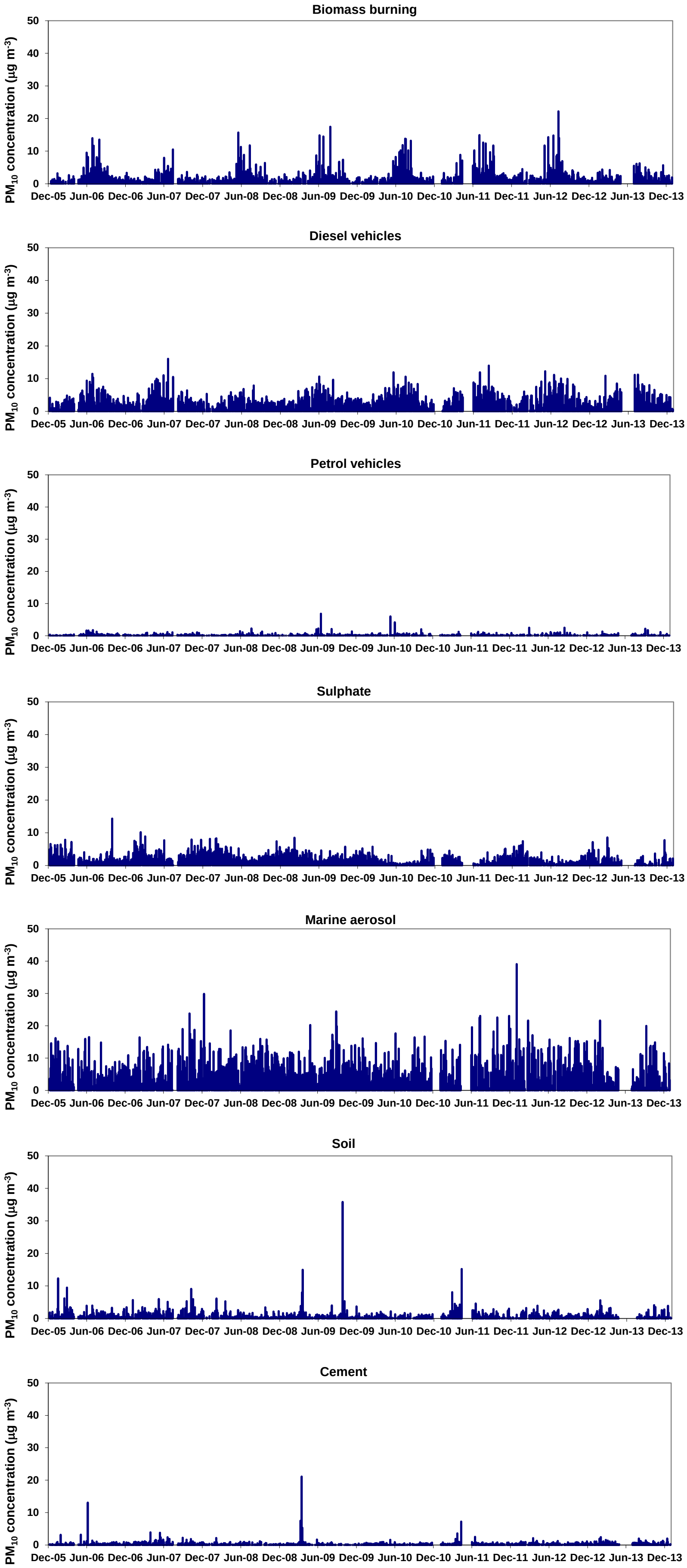

Figure 6.25 Time-series for source contributions to PM$_{10}$ mass at Takapuna

6.7.3 Temporal variations in PM_{10} sources at the Takapuna site

The primary sources of PM_{10} during winter (June-August) at Takapuna were marine aerosol, motor vehicles and biomass burning. Figure 6.26 presents the 2006-2013 temporal variations in mass contributions at the Takapuna site. PM_{10} contributions from the biomass burning and motor vehicle sources were found to be higher in winter than in other seasons, while secondary sulphate concentrations were at a maximum during summer months (December to February).

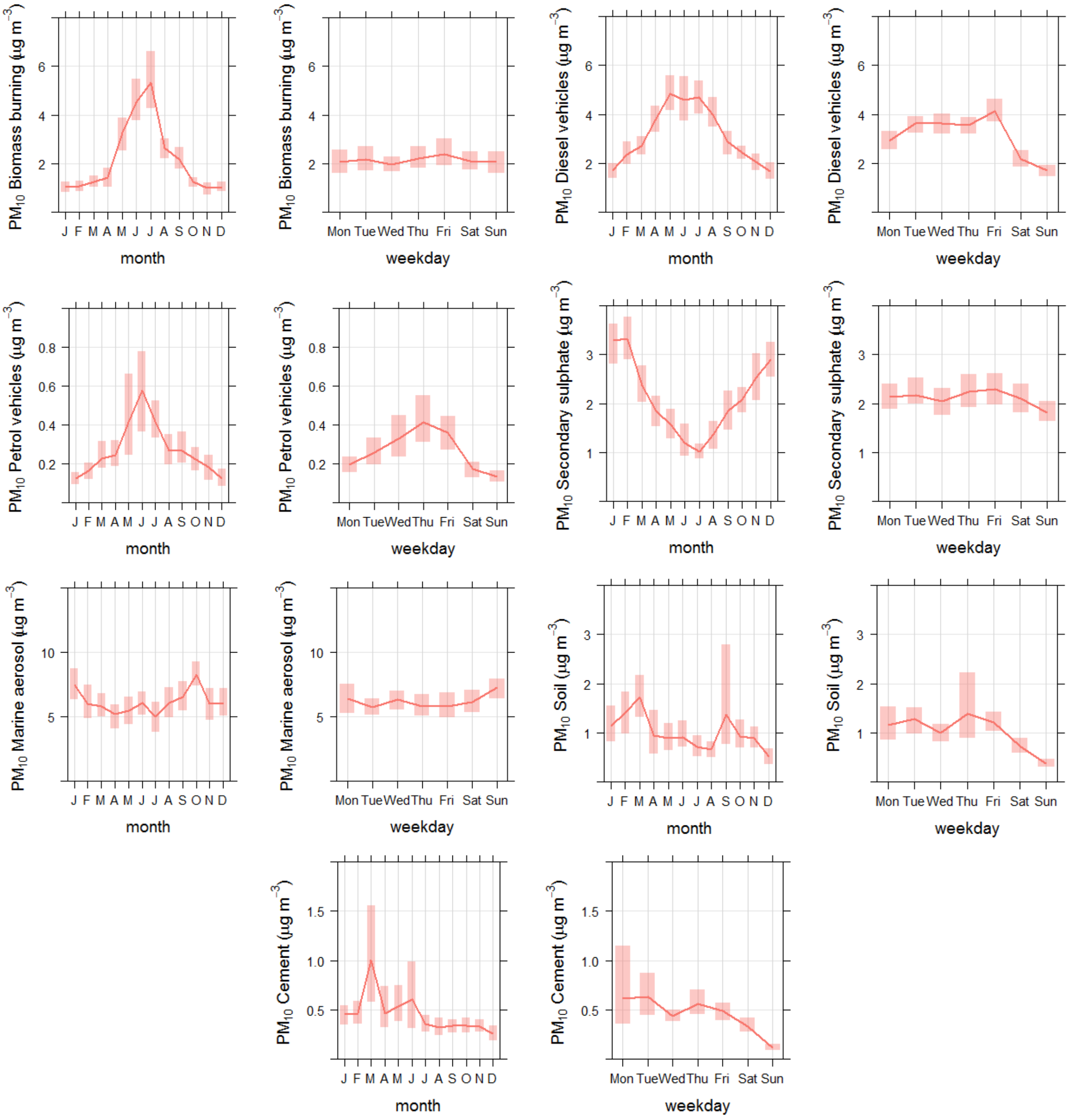

Figure 6.26 Temporal (2007-2013) variations in PM_{10} source contributions at the Takapuna site (the shaded bars are the 95 percentile confidence limits in the mean)

Average PM_{10} concentrations (15 - 16 $\mu g/m^3$) during autumn (March-May), spring (September-November) and summer (December-February) are relatively similar. Variations in PM_{10} concentrations during winter were largely driven by biomass burning and motor vehicle emissions. Marine aerosol was the predominant source during spring, summer and autumn. Motor vehicle emissions along with the soil and cement sources were found to have higher mass contributions during weekdays which is, for motor vehicle emissions, consistent with normal commuter behaviour and higher traffic volumes during weekdays. The soil source may be associated with weekday activities on the school fields and the cement source is associated with normal workday activities at the nearby concrete batching plant. No significant difference in mass contributions for the weekday/weekend categories was found for the biomass burning, secondary sulphate or marine aerosol sources.

6.7.4 Trends in PM_{10} concentrations and source contributions at Takapuna

Figure 6.27 presents the trend in PM_{10} concentrations at Takapuna showing that there was a significant decreasing trend (99.9 % CI) over the monitoring period.

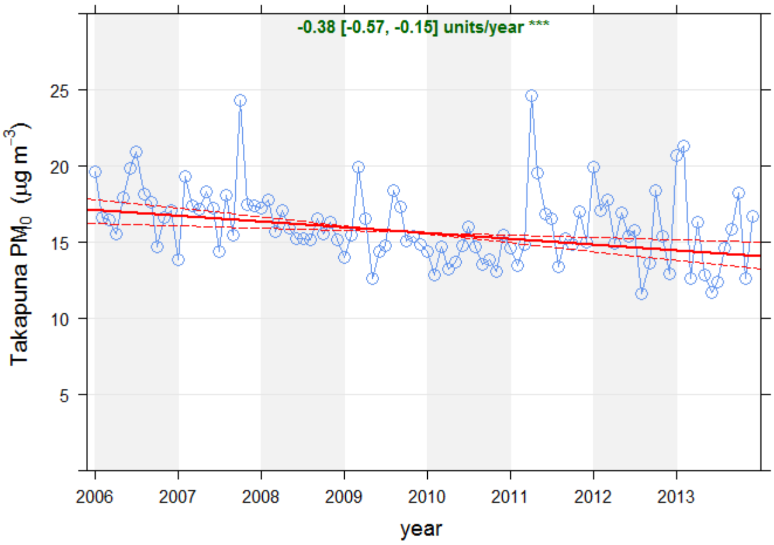

Figure 6.27 Trends in PM_{10} source contributions for 2006-2013 at the Takapuna site (statistically significant at the 99.9 % confidence interval)

Figure 6.28 presents the trends in source contributions showing that there was a significant increasing trend for the biomass burning and diesel vehicle sources (both at the 99.9% CI) along with a minor increase in cement source contributions (95% CI). No significant trend was observed for the petrol vehicle and marine aerosol sources. There were significant decreasing trends for secondary sulphate (99.9% CI) and soil (99.9% CI). The primary influence for the observed decrease trend in PM_{10} appears to the reduction in secondary sulphate related to sulphur in automotive fuels as described in Chapter 5.

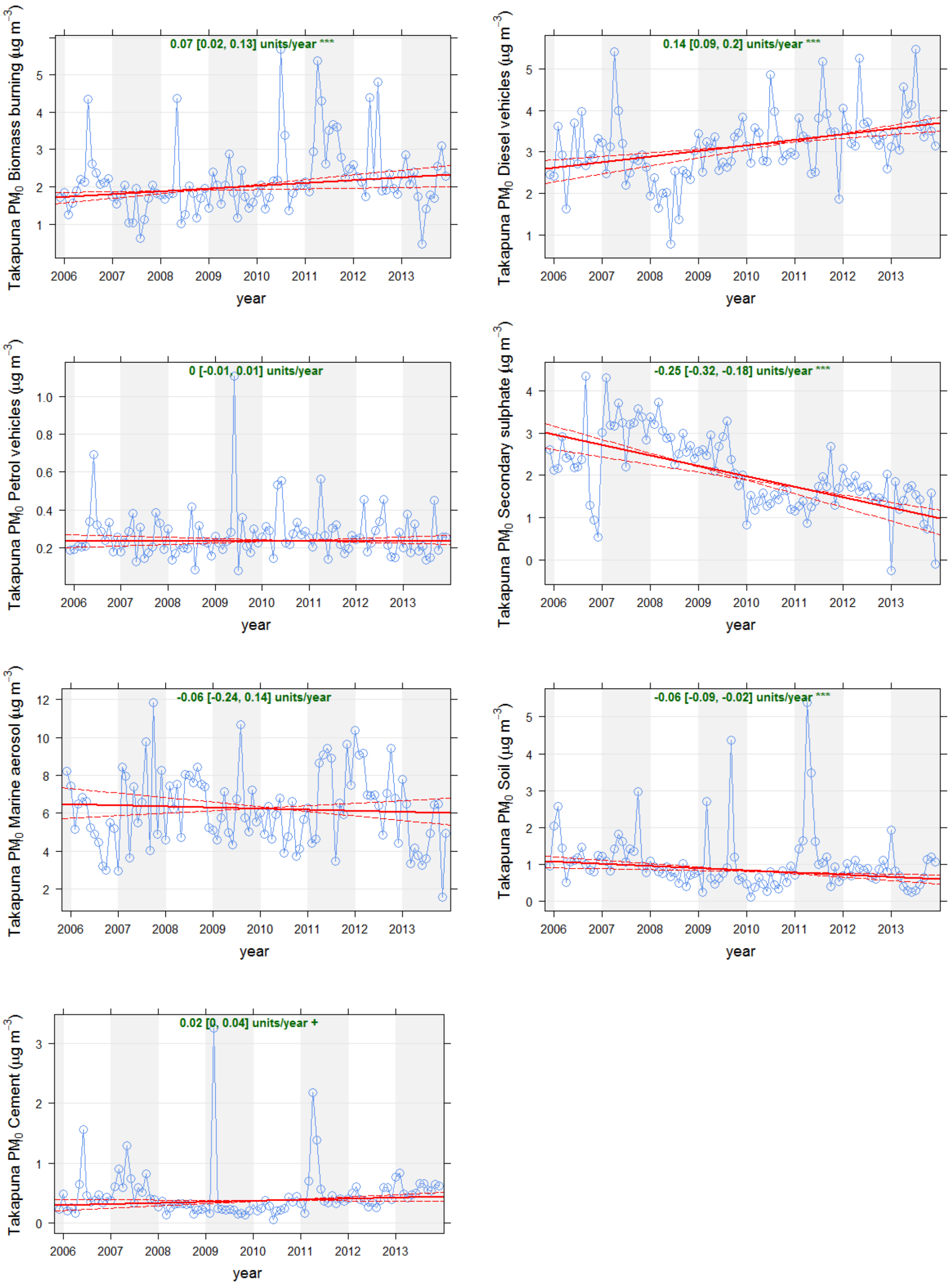

Figure 6.28 Trends in PM_{10} source contributions for 2006-2013 at the Takapuna site

6.7.5 Analysis of individual PM_{10} events at the Takapuna site

PM_{10} concentrations higher than 66 % (or 33 $\mu g\ m^{-3}$) of the NES during the sampling period at Takapuna have been chosen for further analysis. None of the sample days exceeded the NES (50 $\mu g\ m^{-3}$). As presented in Figure 6.29, the source apportionment results show that a variety of sources can be responsible for elevated PM_{10} concentrations at the Takapuna site. Biomass burning and motor vehicle emissions are the main sources but marine aerosol concentrations can be significant on occasion. The cement source (12 μg m^{-3}) was at least partially responsible for elevated PM_{10} on 6 June 2006. The soil source contributed 37 μg m^{-3} PM_{10} on 24 September 2009 and this event has been identified as originating from a significant Australian dust storm a few days earlier. A full analysis of this event is provided in (Davy, Trompetter et al. 2011).

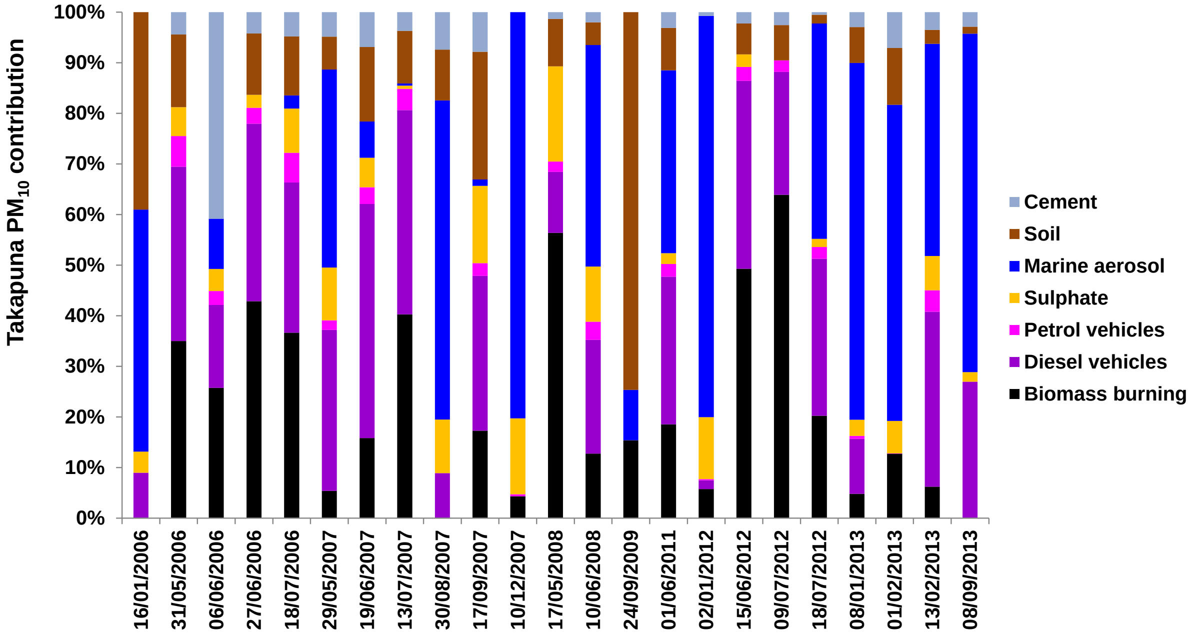

Figure 6.29 Source mass contributions to peak PM_{10} concentrations (>33 μg m^{-3}) at Takapuna

6.7.6 Variation of PM_{10} source contributions with wind direction at the Takapuna site

The CPF analysis of the relationship between the source contributions and wind direction is presented and discussed in the following sections.

6.7.6.1 Biomass Burning

As for $PM_{2.5}$ biomass burning source contributions to PM_{10} at Takapuna are considered to be primarily due to emissions from domestic solid fuel fires during winter. Peak contributions are highest on cold, calm winter days under inversion conditions or light winds, particularly for anticyclonic synoptic conditions. The CPF analysis for biomass burning presented in Figure 6.30 confirms this.

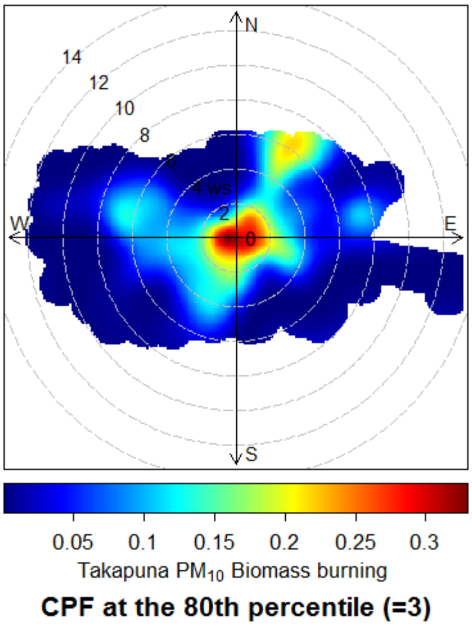

Figure 6.30 Takapuna PM_{10} biomass burning CPF analysis

6.7.6.2 Diesel vehicles

The motor vehicle source for PM_{10} shows a northwest-southwest component as presented in Figure 6.31 and is aligned with the nearby motorway.

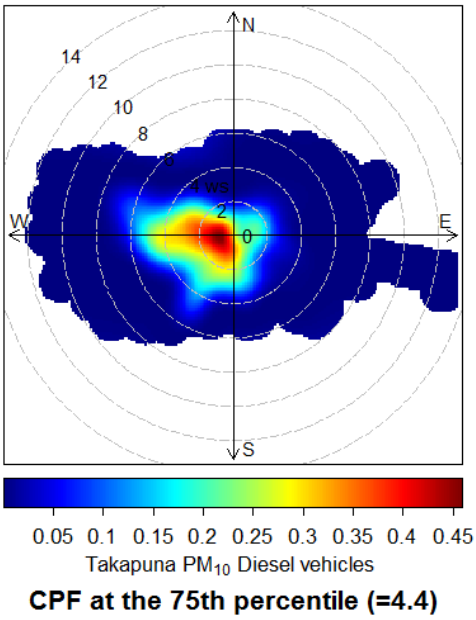

Figure 6.31 Takapuna PM_{10} diesel vehicle CPF analysis

6.7.6.3 Petrol Vehicles

The petrol vehicle source for PM_{10} shows a south to southeast component for peak concentrations as presented in Figure 6.32 and, similar to the result for $PM_{2.5}$, may be due to traffic on Taharoto Road (as a line source) or associated with vehicle activity in WGHS carparks.

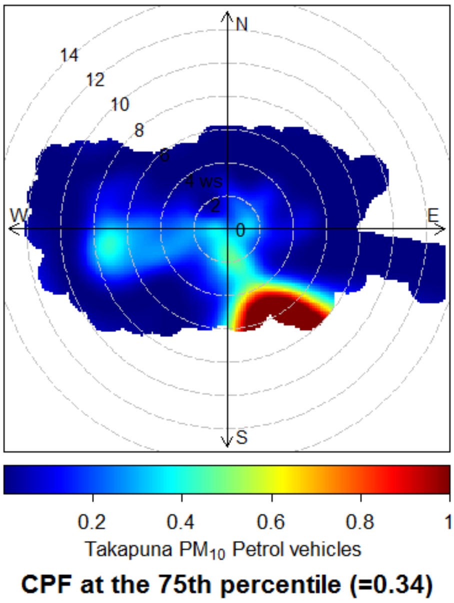

Figure 6.32 Takapuna PM_{10} petrol vehicle CPF analysis

6.7.6.4 Secondary sulphate

The PM_{10} secondary sulphate contribution was found to primarily originate from the easterly sector (Figure 6.33). The originating source of peak sulphate contributions (the CPF analysis only includes the upper 25% of concentrations) is likely to be emissions from ships moving in and out of the Port of Auckland as suggested for the Takapuna $PM_{2.5}$ analysis.

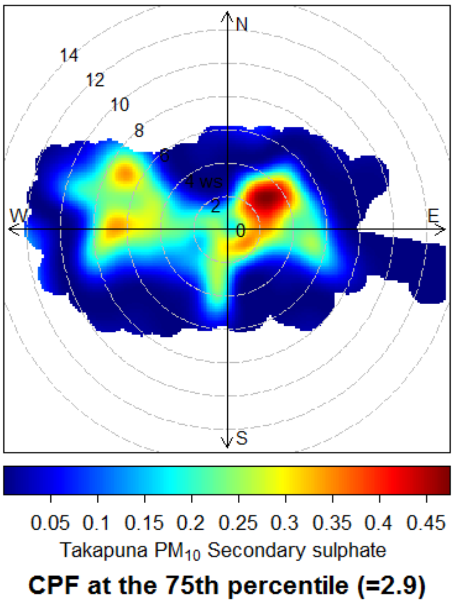

Figure 6.33 Takapuna PM_{10} secondary sulphate CPF analysis

6.7.6.5 Marine aerosol

The peak Takapuna PM_{10} marine aerosol contributions presented in Figure 6.34 originates from the west-southwest and east-northeast directions at higher wind speeds. The most likely source of the PM_{10} marine aerosol is the Tasman Sea and Pacific Ocean.

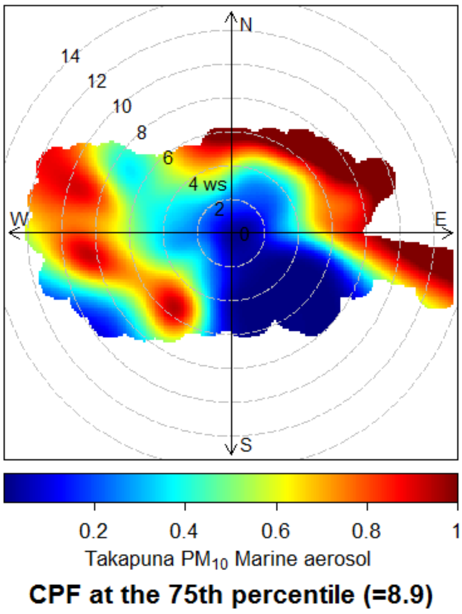

Figure 6.34 Takapuna PM_{10} marine aerosol CPF analysis

6.7.6.6 Crustal matter

The crustal matter source for PM_{10} shows a northwest and southeast components as presented in Figure 6.35 and is likely to have originated from the nearby motorway (road dust) and from the school grounds immediately south of the monitoring station, particularly during the school field conversion process undertaken in 2011.

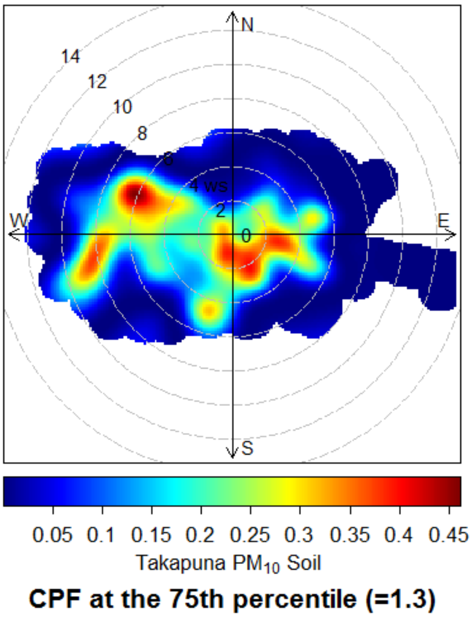

Figure 6.35 Takapuna PM_{10} crustal matter CPF analysis

6.7.6.7 Cement

The Takapuna PM_{10} CPF analysis for the Cement source presented in Figure 6.36 shows that peak concentrations originate during moderate to strong winds from the southeast in the direction of the concrete batching plant 100 m away.

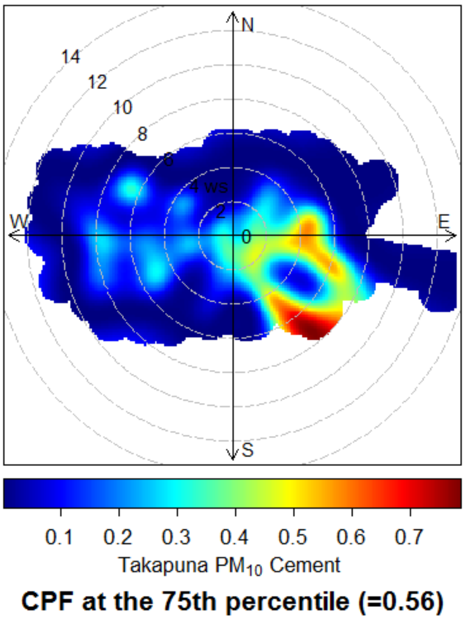

Figure 6.36 Takapuna PM_{10} Cement source matter CPF analysis

6.8 SUMMARY OF TAKAPUNA RECEPTOR MODELLING ANALYSIS

The receptor modelling analysis of $PM_{2.5}$ and PM_{10} at Takapuna found that peak $PM_{2.5}$ and PM_{10} concentrations occurred mainly during winter due to biomass burning (solid fuel fires for home heating), motor vehicles and marine aerosol. During summer, peak PM_{10} concentrations are most likely due to marine aerosol with minor contributions from crustal matter. Fugitive dust emissions from a nearby concrete batching plant were found to contribute to PM_{10} at low levels but with the occasional ‘spike’ in concentrations probably due to specific activities occurring on site such as during the filling of cement silos.

The analysis of source strength with wind direction and wind speed suggests that biomass burning source contributions are carried to the monitoring site by cold air drainage down the Wairau Valley, motor vehicle emissions were primarily from the nearby Northern Motorway and secondary sulphate concentrations are likely to be significantly influenced by emissions from ships in the Hauraki Gulf and Port of Auckland area. Marine aerosol was likely to be from the Tasman Sea and Pacific Ocean, while crustal matter was probably generated the fields immediately adjacent the monitoring station and/or road dust from the nearby motorway and roads.

6.8.1 Comparison between $PM_{2.5}$ and PM_{10} sources at Takapuna

This section presents a comparison between the results from the receptor modelling analyses of the $PM_{2.5}$ and PM_{10} datasets from the Takapuna site (2006 - 2014). Note that the $PM_{2.5}$ and PM_{10} samples were collected on different days at Takapuna therefore a direct sample-on-sample comparison cannot be made. However, general comparisons on average contributions can be examined. Table 6.5 lists the average source contributions determined for each of the sample sets and Figure 6.37 presents the corresponding pie graphs.

Table 6.5 Average source mass contributions (± modelled standard deviation) derived for the two Takapuna particulate matter size fraction datasets

Species	Biomass burning ($\mu g\ m^{-3}$)	Diesel vehicles ($\mu g\ m^{-3}$)	Petrol vehicles ($\mu g\ m^{-3}$)	Sulphate ($\mu g\ m^{-3}$)	Marine aerosol ($\mu g\ m^{-3}$)	Soil ($\mu g\ m^{-3}$)	Cement ($\mu g\ m^{-3}$)
$PM_{2.5}$	2.0±0.2	1.5±0.3	0.18±0.04	0.8±0.06	2.3±0.09	0.2±0.05	~
PM_{10}	2.1±0.4	3.1±0.5	0.3±0.2	2.2±0.4	6.3±1.5	1.0±0.2	0.5±0.4

Immediately evident from Table 6.5 are the higher mass contribution to PM_{10} (compared to $PM_{2.5}$) from marine aerosol and soil as they are mainly coarse particle ($PM_{10-2.5}$) sources. The biomass burning is primarily a $PM_{2.5}$ source with a similar $PM_{2.5}$ and PM_{10} mass. Secondary sulphate is also a fine particle but some of the sulphate particle size range does extend into the coarse fraction (Anlauf, Li et al. 2006), particularly where heterogeneous atmospheric chemistry takes place on the surface of particles (such as marine aerosol) or in aerosol droplets during the reaction of sulphur gaseous species to form secondary sulphate particle species (Gard, Kleeman et al. 1998, O'Dowd, Lowe et al. 2000, George and Abbatt 2010).

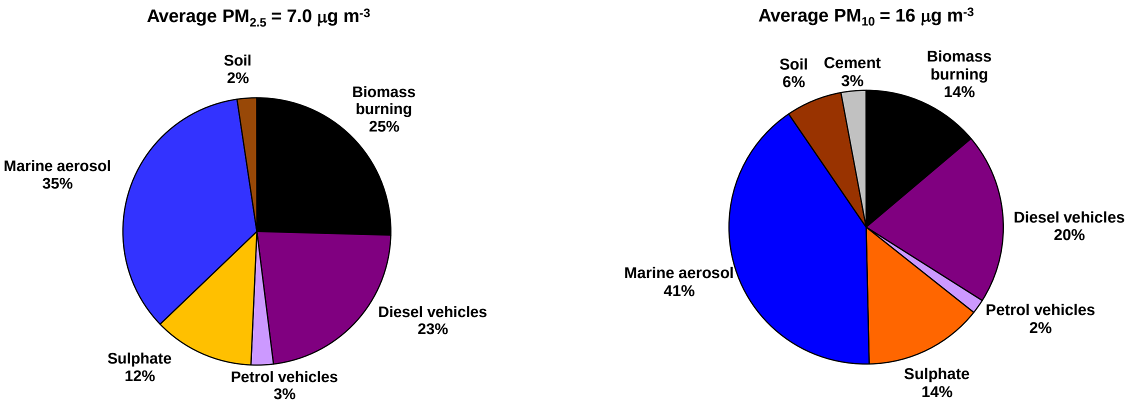

Figure 6.37 Average source contributions for (left) $PM_{2.5}$ and; (right) PM_{10} results

The motor vehicle source has higher mass contributions to PM_{10} than $PM_{2.5}$ and this is due to a coarse particle road dust component covariant with tailpipe emissions. The PM_{10} source profile for the motor vehicle sources shows this with a much higher crustal matter component (Al, Si, Ca, Ti, Fe) than the corresponding $PM_{2.5}$ motor vehicle source profiles (see Figure 6.9 and Figure 6.23 for the $PM_{2.5}$ and PM_{10} source profiles respectively). No $PM_{2.5}$ 'cement' source was extracted from the $PM_{2.5}$ data, most likely due to the associated particle size being mostly in the coarse ($PM_{10-2.5}$) fraction because of the nature of the emission source.

7.0 QUEEN STREET, AUCKLAND CITY

7.1 SITE DESCRIPTION

Samples of airborne particulate matter were collected at an ambient air quality monitoring station located on the veranda over the footpath 4 m above Queen Street (Lat: -36.8476; Long. 174.7655). Figure 7.1 shows a map of the local area.

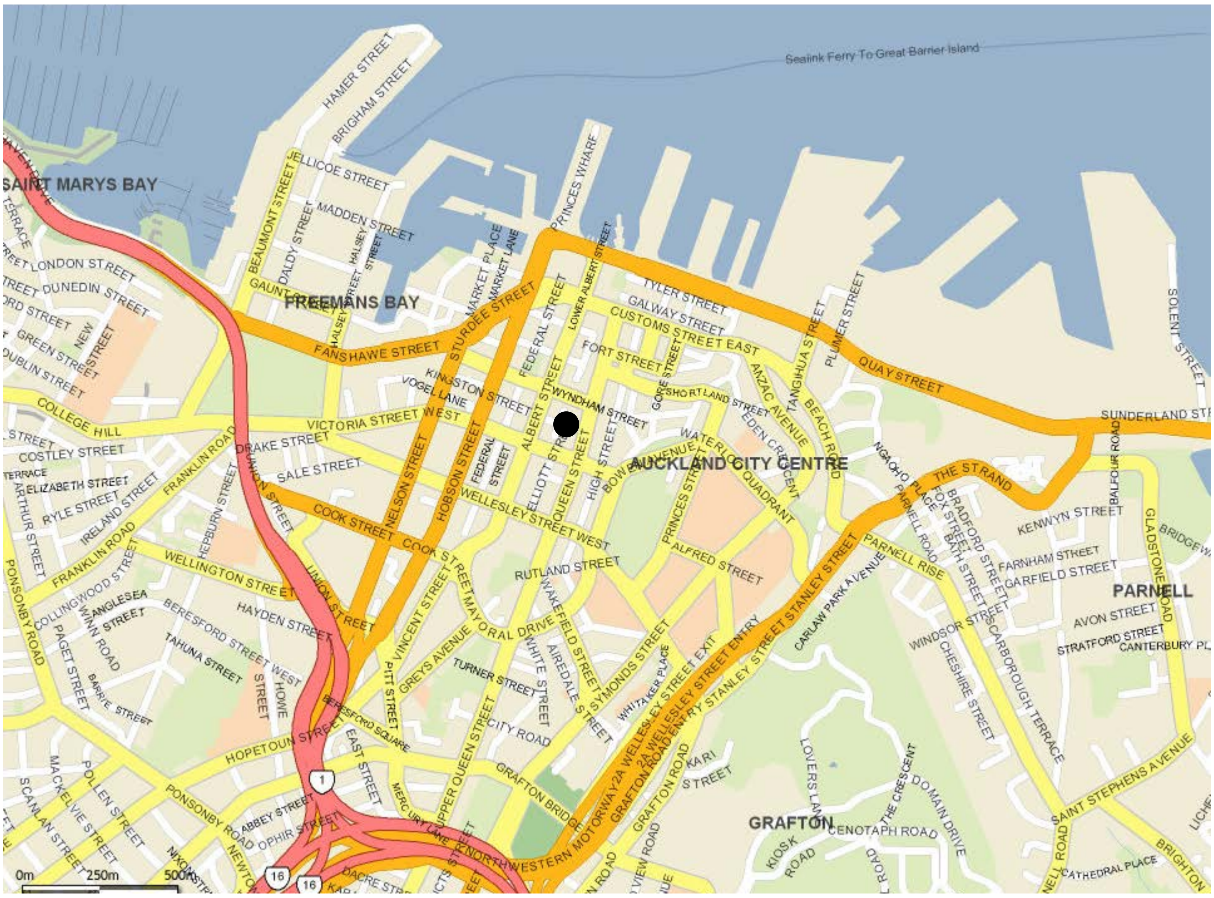

Figure 7.1 Map showing location of Queen Street monitoring site (●)

The Queen Street site is operated by WSL for AC for its ambient air quality monitoring programme. The site was established in mid-1995 and is classed as a traffic–peak site. Pollutants monitored at the site include CO, NO_x, PM_{10} (Sequential Partisol) and $PM_{2.5}$ (Partisol).

The Queen Street site is located in the heart of Auckland City CBD above the main commercial shopping thoroughfare. Land use in the area is a mixture of residential apartments, hotels, corporate office complexes and commercial activities with the Port of Auckland nearby. The monitoring station is essentially located in a street canyon which is aligned northeast-southwest. Figure 7.2 is an aerial view of the Queen Street site location and Figure 7.3 is a photo showing the set-up of monitors on the roof above the footpath. A series of changes and upgrades to Queen Street roadway and pedestrian areas has occurred throughout the monitoring period and these have been tracked through particle composition and source contributions remarked upon in previous iterations of the source apportionment reporting. A significant change has been the changing of bus routes on Queen Street with fewer buses using the roadway since 2011 due to rerouting of the public transport system.

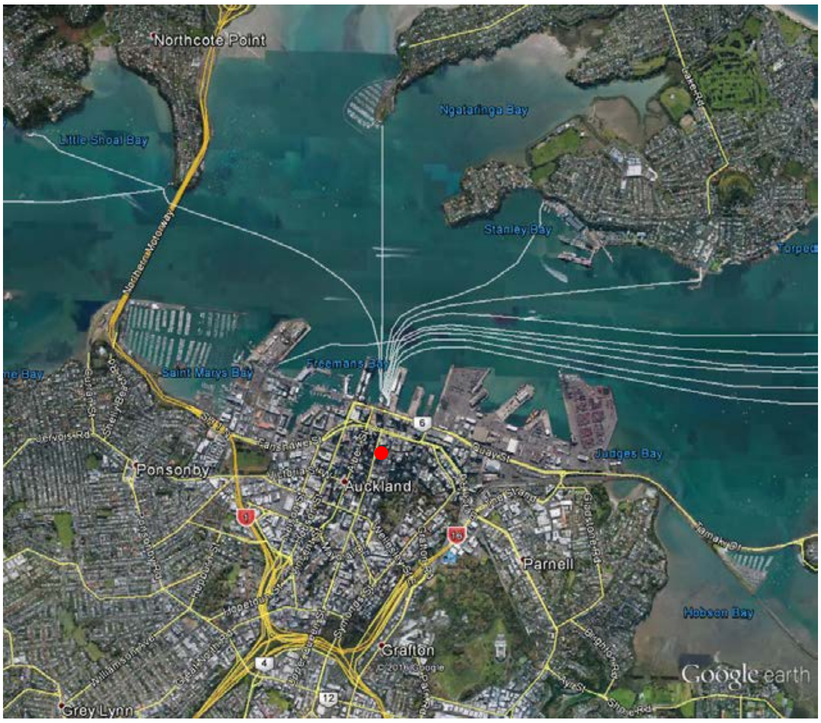

Figure 7.2 Aerial view of Queen Street monitoring site and surrounds (●) (Source: Google Earth 2016)

Figure 7.3 Photo of Queen Street monitoring site with sampling inlets circled in red

7.2 AIR PARTICULATE MATTER SAMPLES AND MONITORING PERIOD

Filter samples from two instruments located at the Queen St monitoring site air quality monitoring station was supplied by AC for analysis:

1. 908 $PM_{2.5}$ samples from a Partisol sampler on a one-day-in-three sampling regime for the period December 2005 – December 2013.
2. 2622 PM_{10} samples from a Partisol Sequential (daily) sampler for the period December 2005 – December 2013.

Receptor modelling studies were carried out for both the $PM_{2.5}$ and PM_{10} sample sets and are reported in Sections 7.5 and 7.6 respectively.

7.3 CONCEPTUAL RECEPTOR MODEL FOR PARTICULATE MATTER AT QUEEN STREET

The following initial conceptual model for Queen Street includes local emission sources:

- Motor vehicles – all roads in the area act as line sources and tall buildings lining the roads serve to confine local dispersion of vehicle emissions;
- Local wind-blown soil or road dust sources;
- Dust emissions from road works, construction activities such as new office blocks, apartments and building refurbishments. Major road works and footpath widening/refurbishment were carried out on Queen Street near the sampling location during 2007;
- Domestic activities – likely to be dominated by biomass burning such as emissions in surrounding suburbs from solid fuel fires used for domestic heating during the winter;
- Port activities – emissions from shipping traffic to and from the Port of Auckland.

Longer range sources may also contribute to ambient particle loadings and these include:

- Marine aerosol;
- Secondary particulate matter resulting from atmospheric gas-to-particle conversion processes (sulphate and nitrate species, organic particle species resulting from photochemical smog events);
- Potential for long range transport of industrial emissions.

Another category of emission sources that may contribute are those considered as ‘one-off’ emission sources:

- Fireworks displays and other special events;
- Short-term road works and demolition/construction activities.

The variety of sources described above can be recognised and accounted for by appropriate data analysis methods, such as examination of seasonal differences, temporal variations and receptor modelling itself.

7.4 LOCAL METEOROLOGY AT QUEEN STREET

Meteorology at the Queen Street site is likely to be dominated by the street canyons of the Auckland CBD and wind direction will be primarily aligned with the Queen Street coupled with significant eddies and turbulences around the tall buildings. Note that no meteorological instruments were located at the site and general meteorological conditions are inferred from other monitoring sites such as Khyber Pass Road.

7.5 ANALYSIS OF $PM_{2.5}$ SAMPLES FROM QUEEN STREET

The Queen Street $PM_{2.5}$ samples refer to those $PM_{2.5}$ samples collected using a Partisol 2000 Sampler (Andersen Instruments Inc.) from December 2005 to December 2013. Gravimetric results for the $PM_{2.5}$ samples as presented in Figure 7.4 show peak concentrations during 2007.

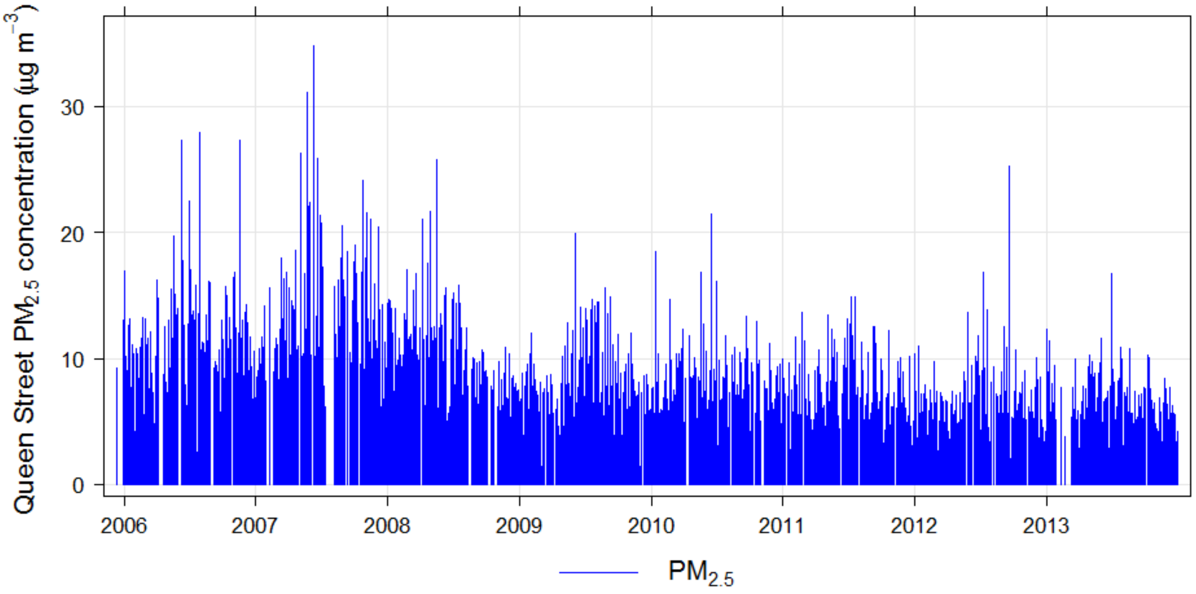

Figure 7.4 Gravimetric results for $PM_{2.5}$ at Queen Street

7.5.1 Composition of $PM_{2.5}$ at Queen Street

Elemental concentrations for $PM_{2.5}$ at Queen Street are presented in Table 7.1 with a box and whisker plot of the elemental concentrations shown in Figure 7.5.

Table 7.1 Elemental analysis results for Partisol $PM_{2.5}$ at Queen Street (908) samples)

Species	Average (ng/m^3)	Max (ng/m^3)	Min (ng/m^3)	Median (ng/m^3)	StdDev (ng/m^3)	Av LOD (ng/m^3)	#>LOD
$PM_{2.5}$ ($\mu g/m^3$)	**9**	**35**	**1**	**8**	**4**		
H	121	724	0	111	82	45	768
BC	3294	7923	432	3120	1380	177	908
Na	696	3532	0	561	601	259	705
Mg	74	567	0	62	57	25	780
Al	37	2895	0	21	110	13	717
Si	78	1831	15	53	94	9	908
P	6	63	0	3	8	14	161
S	276	1273	37	231	185	9	908
Cl	929	7042	1	694	856	7	907
K	63	1990	12	53	79	7	908
Ca	69	1196	2	52	78	6	906
Sc	2	19	0	1	2	8	55
Ti	2	51	0	1	4	7	112
V	4	80	0	1	7	7	215
Cr	2	11	0	0	2	6	73
Mn	2	15	0	1	2	6	136
Fe	66	441	3	55	45	5	904
Co	2	12	0	0	2	8	62
Ni	3	30	0	1	4	8	134
Cu	5	45	0	4	5	10	217
Zn	14	187	0	9	19	11	426
Ga	3	25	0	0	5	17	66
Ge	4	42	0	0	6	22	59
As	4	45	0	0	8	29	72
Se	7	57	0	0	10	34	81
Br	8	71	0	0	12	44	76
Rb	13	109	0	0	20	72	76
Sr	18	123	0	0	27	90	91
Mo	41	393	0	0	72	166	93
I	8	54	0	3	10	25	81
Ba	9	217	0	5	13	27	89
Hg	10	119	0	0	17	63	30
Pb	12	148	0	0	23	77	51

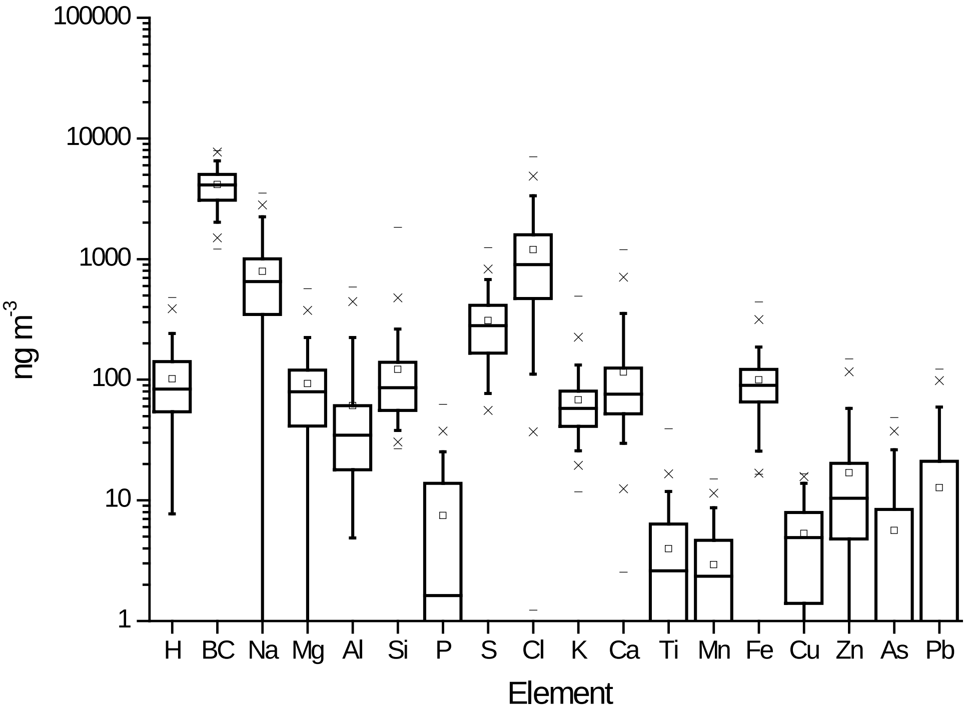

Figure 7.5 Box and whisker plot of $PM_{2.5}$ elemental concentrations at Queen Street (logarithmic scale)

Table 7.1 shows some of the measured species being generally close to or below the limits of detection over all samples. Carbonaceous species (represented by BC) were found to dominate $PM_{2.5}$ elemental mass concentrations indicating that combustion processes are significant contributors to ambient $PM_{2.5}$ at Queen Street. Sodium and chlorine were also present in relatively high concentrations indicating that marine aerosol was likely to be an important source of $PM_{2.5}$. At times both calcium and potassium had high concentrations and are likely to be explained by contributions from specific sources. A scatterplot matrix of the species in Table 7.1 is presented in Appendix 3.

7.5.2 Source contributions to $PM_{2.5}$ at Queen Street

Eight primary source contributors were determined from the PMF receptor modelling analysis of speciation $PM_{2.5}$ elemental compositions at Queen Street. These are identified as presented in Table 7.2 along with the mass of $PM_{2.5}$ and elemental species associated with each source.

Table 7.2 Elemental composition of source profiles and contribution to $PM_{2.5}$ at Queen Street

	Factor 1	**Factor 2**	**Factor 3**	**Factor 4**	**Factor 5**	**Factor 6**	**Factor 7**	**Factor 8**
Species	**Biomass burning (ng/m^3)**	**Diesel vehicles (ng/m^3)**	**Petrol vehicles (ng/m^3)**	**Secondary sulphate (ng/m^3)**	**Ship Emissions (ng/m^3)**	**Marine aerosol (ng/m^3)**	**Soil (ng/m^3)**	**Construction (ng/m^3)**
$PM_{2.5}$	**810**	**3290**	**290**	**940**	**410**	**2070**	**140**	**580**
H	50	35	11	10	4	8	1	0
BC	206	2323	112	196	351	169	32	100
Na	19	39	8	0	60	565	0	0
Mg	2	10	0	1	7	49	2	1
Al	1	5	1	0	4	3	14	2
Si	2	19	5	2	9	5	33	5
S	14	28	13	47	147	45	1	1
Cl	0	75	4	23	0	799	0	32
K	18	15	5	0	3	16	1	2
Ca	2	12	0	0	5	19	3	26
V	0	0	0	4	0	0	0	0
Fe	5	34	8	0	6	2	8	4
Ni	0.2	0.7	0	2	0	0	0	0
Zn	2	2	14	0	0	0	1	0

Table 7.2 lists the summary results for a reiterative process that examines the effect of each species on the PMF receptor modelling process using the modelling diagnostics presented in Appendix 3. Species that were poorly modelled (slope, $r^2 < 0.6$) have been removed from the analyses unless considered vital for source identification. The source contributors identified in Table 7.2 were found on average to explain 92 % of $PM_{2.5}$ gravimetric mass. Figure 7.6 presents the source profiles extracted from the PMF analysis of Queen Street $PM_{2.5}$ data.

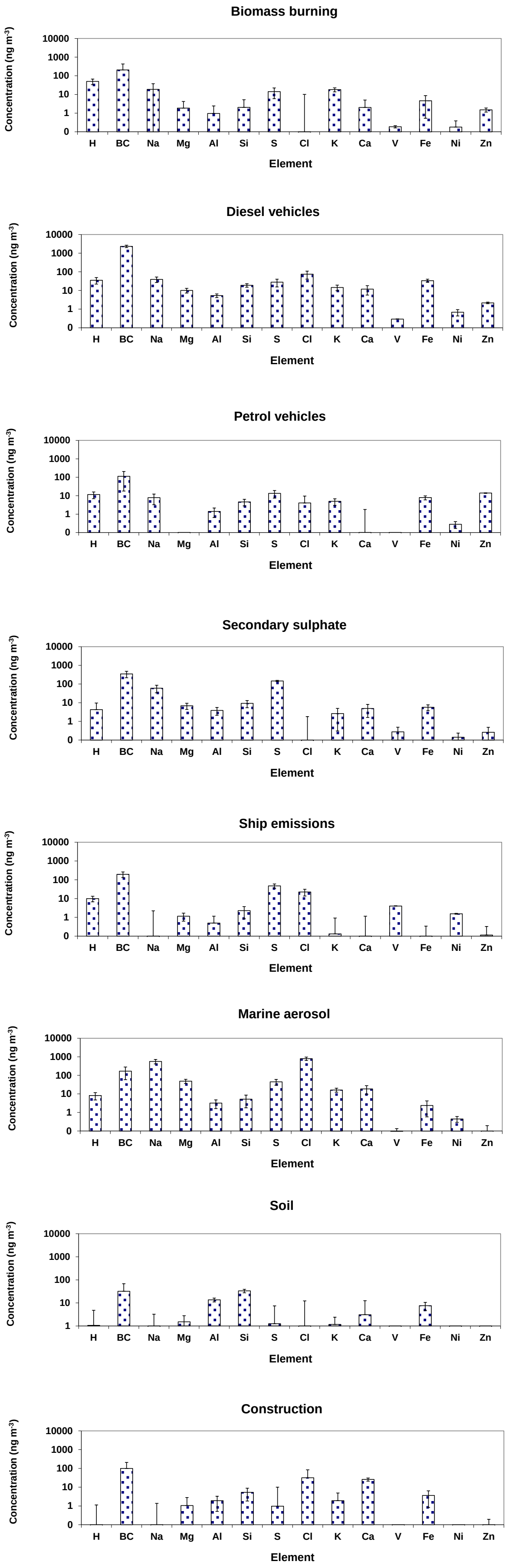

Figure 7.6 Source profiles and elemental concentrations for $PM_{2.5}$ at Queen Street site (showing 5th and 95th confidence intervals in mean concentration derived from the receptor modelling)

- The first source was attributed to biomass burning;
- The second and third factors represent the contribution from diesel and petrol powered motor vehicle emissions respectively;
- The fourth source contributor was identified as secondary sulphate;
- The fifth source contribution is due to primary shipping emissions with a characteristic vanadium and nickel content;
- The sixth source is the contribution from marine aerosol;
- The seventh factor represents the crustal matter component;
- The eighth source, construction, with a high Ca loading is due to dust from construction (cement/concrete) activities in the area. Note that this may include road works or work on foot paths where concrete cutting and use of cement was taking place.

Figure 7.7 presents the 2006-2013 average source contributions to PM$_{2.5}$ concentrations and includes the standard deviations of the average mass contributions from each of the sources indicating the variability in source strength.

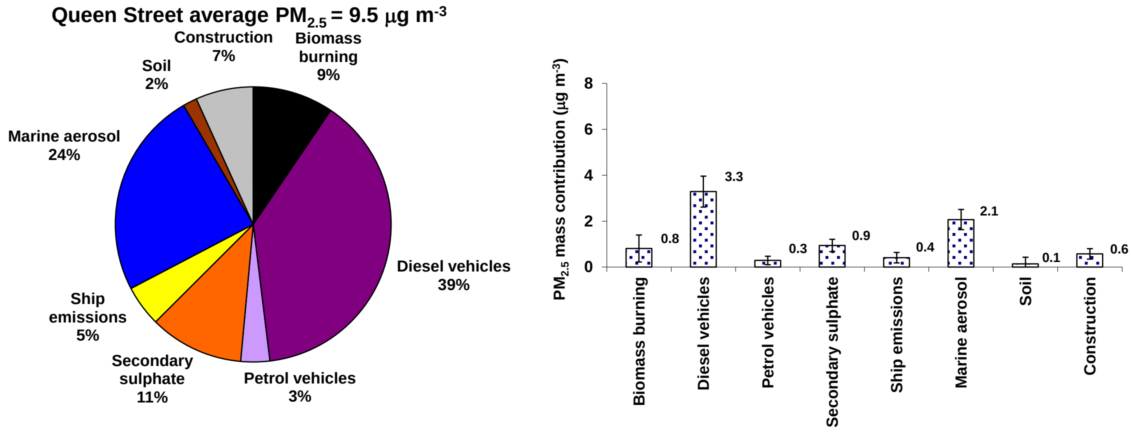

Figure 7.7 Average (2006-2013) source contributions to PM$_{2.5}$ at Queen Street site (showing 5th and 95th confidence intervals in mean concentration derived from the receptor modelling)

The average source contributions estimated by the receptor modelling indicate that motor vehicle emissions and marine aerosol are the most significant contributors (42% and 24 % respectively) to PM$_{2.5}$ concentrations at Queen Street, with lesser contributions from secondary sulphate sources (11 %), particles from shipping emissions (5 %), construction dusts (7 %), biomass burning (9 %) and crustal matter (2 %).

Figure 7.8 shows the mass contribution of sources to PM$_{2.5}$ mass for each sample collected at Queen Street. The temporal variation indicates that PM$_{2.5}$ mass is dominated by the motor vehicle and marine aerosol sources.

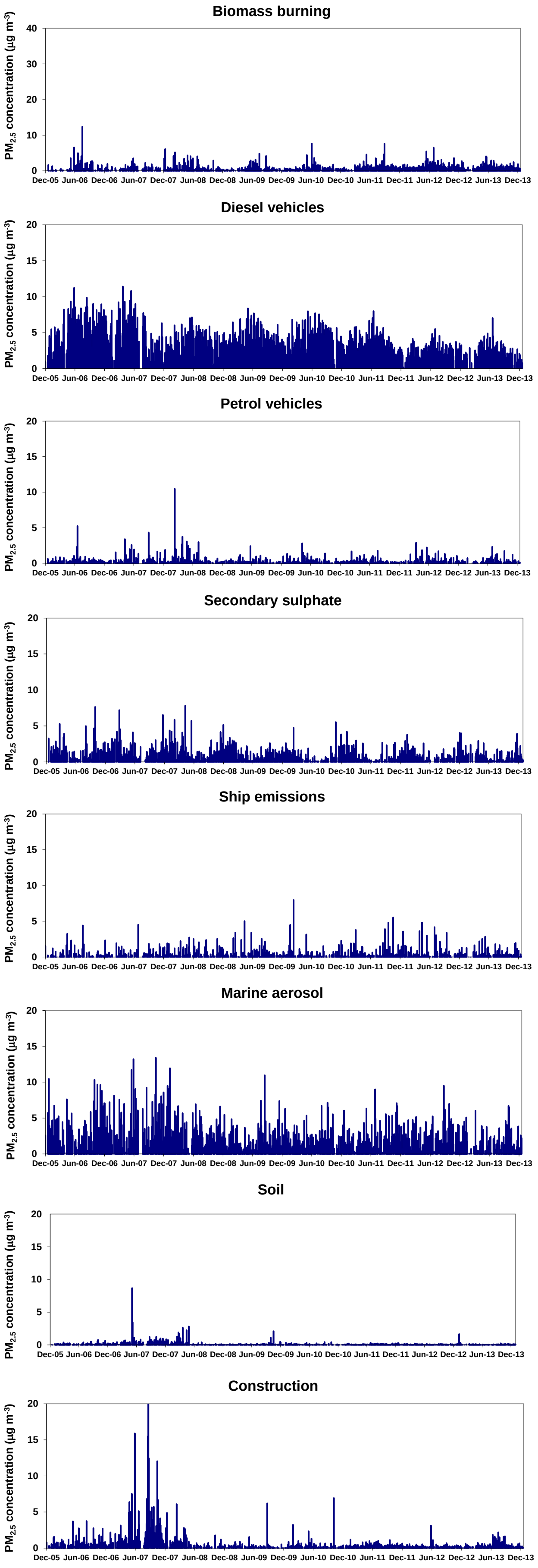

Figure 7.8 Time-series for source contributions to PM$_{2.5}$ mass at Queen Street

It is clear from the temporal variation in source contributions shown in Figure 7.8 that construction sources were responsible for some of the highest $PM_{2.5}$ concentrations during 2007 (see Section 7.5.6). Interestingly, the motor vehicle source showed a decrease in contributions after the construction work ended (August 2007). This may be due to a change in traffic volumes, vehicle type or traffic congestion on Queen Street.

7.5.3 Temporal variations in source contributions to $PM_{2.5}$ at Queen Street

Figure 7.9 presents the 2006-2013 $PM_{2.5}$ temporal variation mass contributions at Queen Street. The primary source of $PM_{2.5}$ during all seasons at Queen Street was motor vehicle emissions, with both the diesel and petrol vehicle contributions lower on the weekends in line with commuter behaviour and commercial activities. Average $PM_{2.5}$ concentrations were slightly higher in winter (12 $\mu g/m^3$) than in other seasons due to higher motor vehicle and biomass burning contributions.

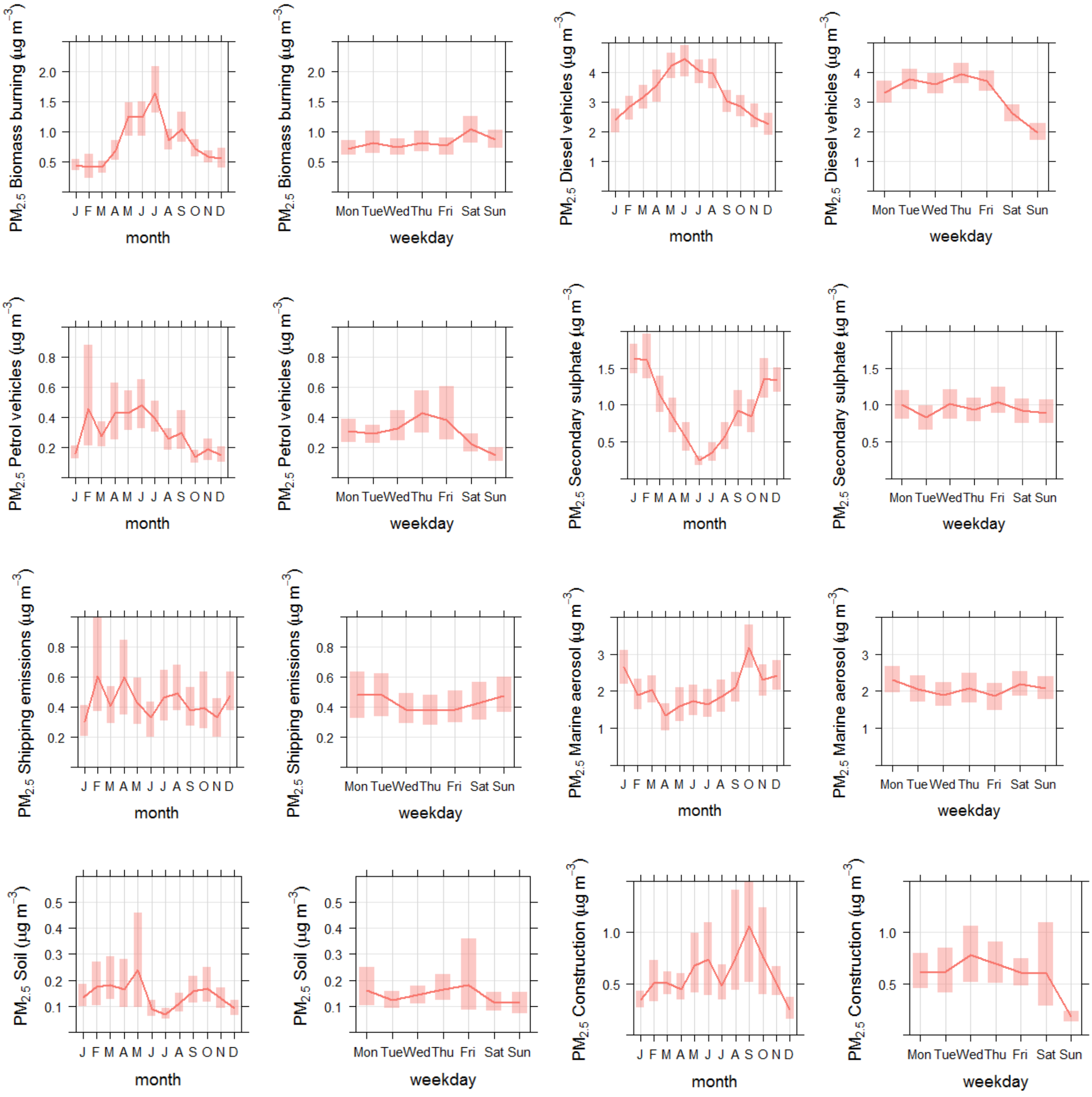

Figure 7.9 Temporal variations (2006-2013) in $PM_{2.5}$ source contributions at Queen Street (the shaded bars are the 95 percentile confidence limits in the mean)

Secondary sulphate aerosol demonstrated a winter minimum, while $PM_{2.5}$ contributions from shipping emissions, soil or construction did not show any significant seasonality and are likely to be dependent on local activity. Mass contributions from marine aerosol were higher during spring probably due to the higher spring equinox winds. The construction source showed a bias towards lower concentrations on Sunday and is likely to reflect a lower activity on that day associated with construction practices (i.e. most sites do not operate on a Sunday).

7.5.4 Trends in $PM_{2.5}$ concentrations and source contributions at Queen Street

The temporal trends in $PM_{2.5}$ source contributions at Queen Street were explored using the Thielsen functionality available in *openair*. Figure 7.10 presents the trend in $PM_{2.5}$ concentrations showing that there was a significant decreasing trend (99.9 % CI) over the monitoring period.

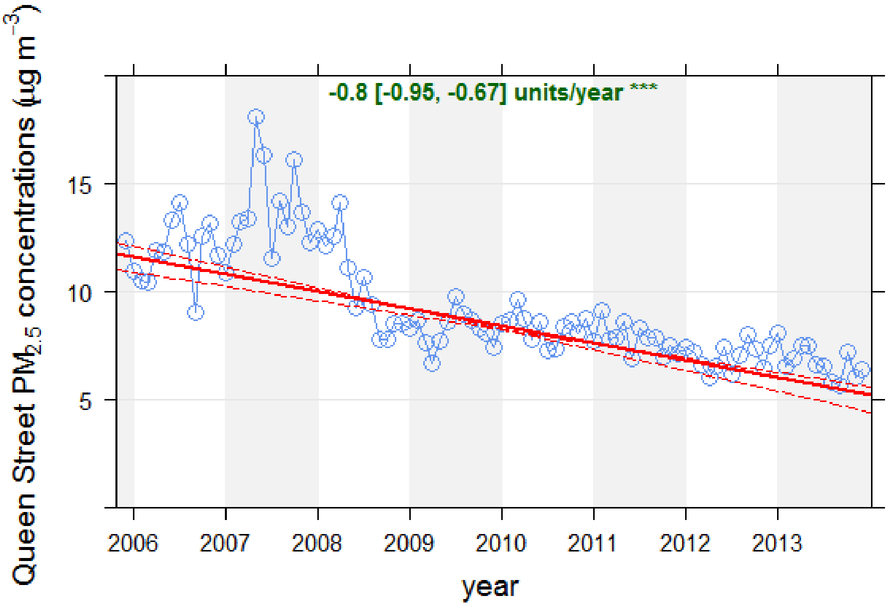

Figure 7.10 Trend in $PM_{2.5}$ concentrations at Queen Street (statistically significant at the 99.9 % confidence interval)

The trends in $PM_{2.5}$ source contributions are presented in Figure 7.11 and show that the decrease in $PM_{2.5}$ was largely driven by a commensurate decrease in diesel vehicle and marine aerosol contributions. Interestingly the Queen Street $PM_{2.5}$ marine aerosol trend is exactly the same as that for the Takapuna $PM_{2.5}$ marine aerosol. There were also significant decreasing trends for the secondary sulphate, soil and construction sources (all at the 99.9% CI). The trends in soil and construction source contributions are clearly influenced by the impact of significant activity during 2007-2008 and much less since then. No significant trend was observed for ship emissions. The primary influence for the decrease in secondary sulphate appears to the reduction in sulphur in automotive fuels as described in Chapter 5. The biomass source shows a steady increase (99.9% CI).

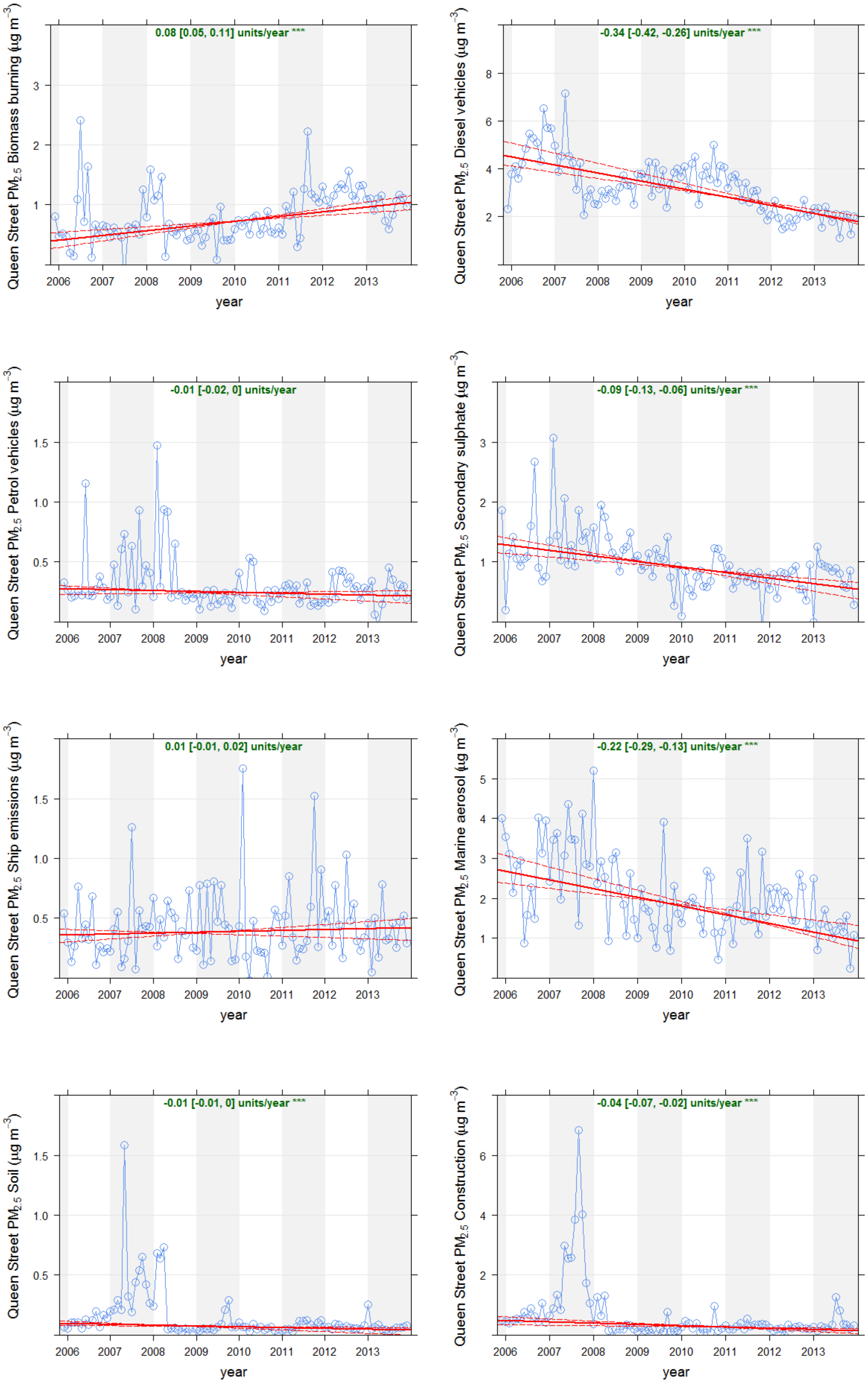

Figure 7.11 Trends in $PM_{2.5}$ source contributions at Queen Street

7.5.5 Analysis of individual $PM_{2.5}$ events at Queen Street

Peak $PM_{2.5}$ events during the sampling period at Queen Street have been chosen for further analysis. Peak $PM_{2.5}$ events are defined as those that were higher than 66 % (17 μg/m^3) of the AAQG (25 μg m^{-3} 24-hour average). It was found that there were 47 days where $PM_{2.5}$ concentrations were higher than 66 % of the AAQG and of those, 8 days exceeded the AAQG monitoring guideline.

Figure 7.12 presents the mass contributions of individual sources to each of the peak $PM_{2.5}$ days (> 17 μg m^{-3}).

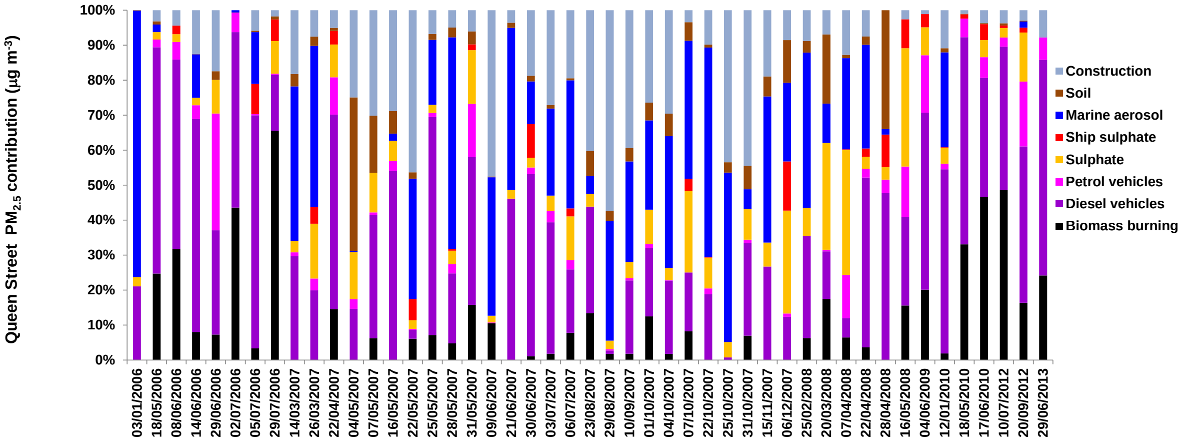

Figure 7.12 Source contributions to peak $PM_{2.5}$ concentrations at Queen Street

It is clear from Figure 7.12 that motor vehicle emission sources were primarily responsible for elevated $PM_{2.5}$ concentrations at Queen Street, but that local construction and/or road work activities had a significant impact during 2007. Marine aerosol and biomass burning sources were also significant contributors on a few occasions.

7.6 ANALYSIS OF PM$_{10}$ SAMPLES FROM QUEEN STREET

The Queen Street PM$_{10}$ samples refer to those PM$_{10}$ samples collected using a Partisol Sequential Sampler (Andersen Instruments Inc.) from January 2006 to December 2013. The PM$_{10}$ gravimetric results are presented in Figure 7.13 and show the highest PM$_{10}$ concentrations during winter months (June – August) and lesser maximums at other times of the year. Three exceedances of the NES at Queen Street were recorded during the monitoring period, two in 2007 (02/05/2007 and 04/05/2007) and the other in 2009 (25/092009). Further discussion on the NES exceedances is provided in Section 7.6.6. The variations in peak PM$_{10}$ concentrations are likely to be explained by source emissions activity and the relative contribution to PM$_{10}$ mass. Note that gaps in the data are due to missed sample days.

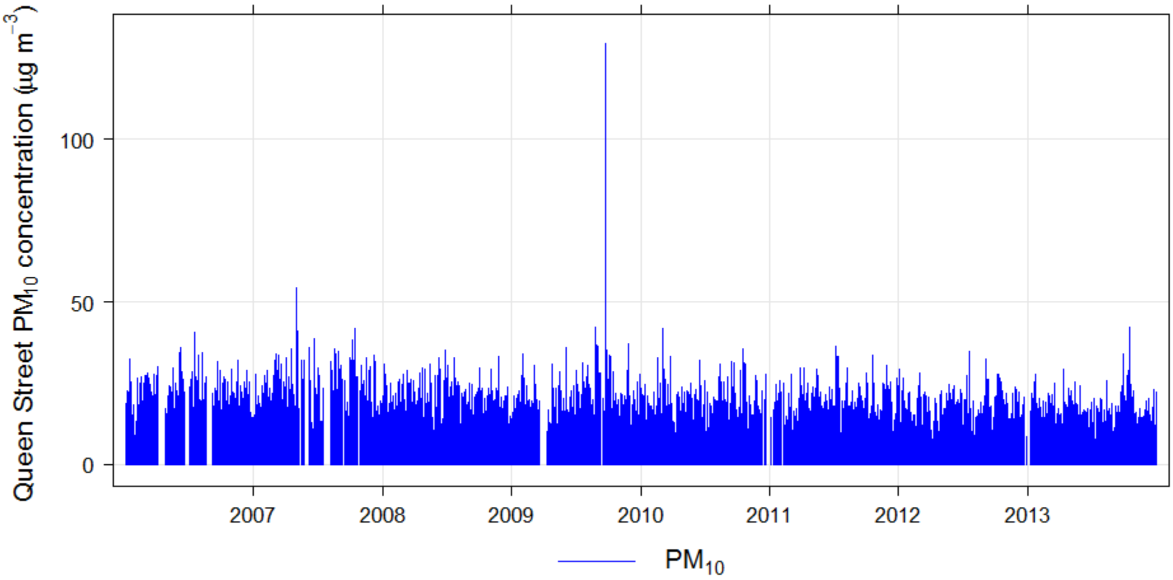

Figure 7.13 Gravimetric results for PM$_{10}$ at Queen Street

7.6.1 Composition of PM_{10} at Queen Street

Elemental concentrations for PM_{10} at Queen Street are presented in Table 7.3 with a box and whisker plot of the elemental concentrations shown in Figure 7.14. Table 7.3 also shows some measured species being close to or below the limits of detection over all samples.

Table 7.3 Elemental analysis results for Partisol PM_{10} at Queen Street (2622 samples)

Species	Average (ng/m^3)	Max (ng/m^3)	Min (ng/m^3)	Median (ng/m^3)	Std Dev (ng/m^3)	Av LOD (ng/m^3)	#>LOD
PM_{10} (μg m^{-3})	**18**	**130**	**2**	**17**	**6**		
H	78	893	0	137	92	45	2396
BC	4270	12651	232	3928	2101	191	2621
Na	2251	8623	0	2072	1298	480	2558
Mg	207	1002	0	193	110	36	2589
Al	98	6415	0	77	152	16	2584
Si	274	16439	26	211	413	11	2621
P	18	1393	0	15	31	16	1428
S	437	2471	5	399	219	13	2620
Cl	3288	13229	7	2944	1996	6	2620
K	130	1617	1	119	74	7	2620
Ca	262	4949	7	212	259	7	2621
Sc	3	46	0	2	4	10	217
Ti	11	395	0	9	13	8	1546
V	4	87	0	0	7	10	466
Cr	1	20	0	0	2	9	199
Mn	5	99	0	4	5	7	855
Fe	264	4254	5	254	145	6	2621
Co	3	62	0	2	4	11	302
Ni	3	33	0	2	4	9	369
Cu	11	170	0	10	8	9	1527
Zn	19	192	0	15	19	12	1658
Ga	3	36	0	0	5	18	189
Ge	4	51	0	0	6	23	157
As	4	61	0	0	8	30	191
Se	7	74	0	0	11	36	234
Br	12	106	0	5	16	44	382
Rb	14	144	0	0	20	73	225
Sr	20	166	0	0	28	90	281
Mo	41	455	0	0	72	167	249
I	14	211	0	7	18	32	478
Ba	22	143	0	19	19	32	914
Hg	11	157	0	0	18	65	132
Pb	12	147	0	0	22	79	127

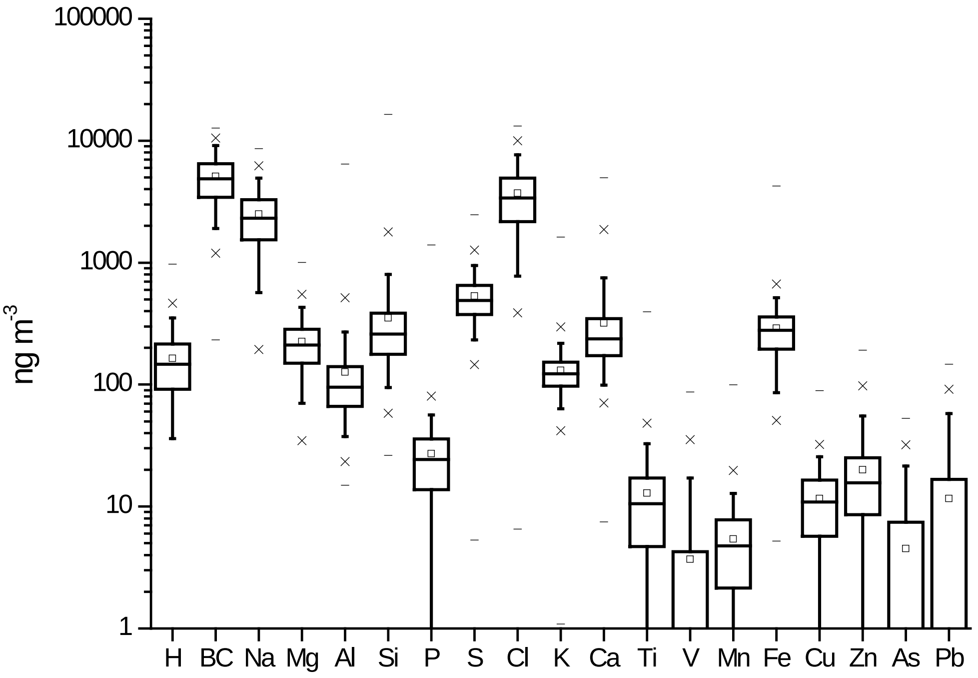

Figure 7.14 Box and whisker plot of PM_{10} elemental concentrations at Queen Street (logarithmic scale)

Carbonaceous species (represented by BC), sodium and chlorine were found to dominate PM_{10} elemental mass concentrations indicating that combustion processes and marine aerosol are important contributors to ambient PM_{10} at Queen Street. A scatterplot matrix of the species in Table 7.3 is presented in Appendix 3.

7.6.2 Source contributions to PM_{10} at Queen Street

Eight primary source contributors were determined from the PMF receptor modelling analysis of speciation PM_{10} elemental compositions at Queen Street. These are identified as presented in Table 7.4 along with the mass of PM_{10} and elemental species associated with each source.

Table 7.4 Elemental composition of source profiles and contribution to PM_{10} at Queen Street

	Factor 1	Factor 2	Factor 3	Factor 4	Factor 5	Factor 6	Factor 7	Factor 8
Species	Biomass burning (ng/m^3)	Diesel vehicles (ng/m^3)	Petrol vehicles (ng/m^3)	Sulphate (ng/m^3)	Ship Emissions (ng/m^3)	Marine aerosol (ng/m^3)	Soil (ng/m^3)	Construction (ng/m^3)
PM_{10}	**1242**	**5300**	**507**	**968**	**728**	**6869**	**1037**	**193**
H	60	6	0	3	0	0	0	0
BC	213	3486	155	44	216	0	0	159
Na	39	129	8	92	14	1929	25	8
Mg	5	23	1	5	2	156	12	2
Al	0	11	0	3	0	16	65	2
Si	4	37	4	8	2	29	156	30
S	5	29	11	200	39	133	2	16
Cl	21	265	0	5	34	2867	36	34
K	23	22	3	0	3	59	11	4
Ca	7	34	10	6	5	70	10	123
Ti	0	3	1	0	1	0	5	0
V	0	0	0	0	4	0	0	0
Mn	0	1	1	0	0	1	1	0
Fe	3	175	13	0	5	19	42	6
Ni	0	1	0	0	2	1	0	0
Cu	0	8.6	0	0	0	1	0	0
Zn	1	2	15	0	0	1	0	0
Ba	0	11	0	1	0	9	0	1

Table 7.4 represents the summary results for a reiterative process that examines the effect of each species on the PMF receptor modelling process using the modelling diagnostics presented in Appendix 3. Species that were poorly modelled (slope, $r^2 < 0.6$) have been removed from the analyses unless considered vital for source identification. The source contributors identified in Table 7.4 were found on average to explain 95 % of PM_{10} gravimetric mass. Figure 7.15 presents the source profiles extracted from the PMF analysis of Queen Street PM_{10} data.

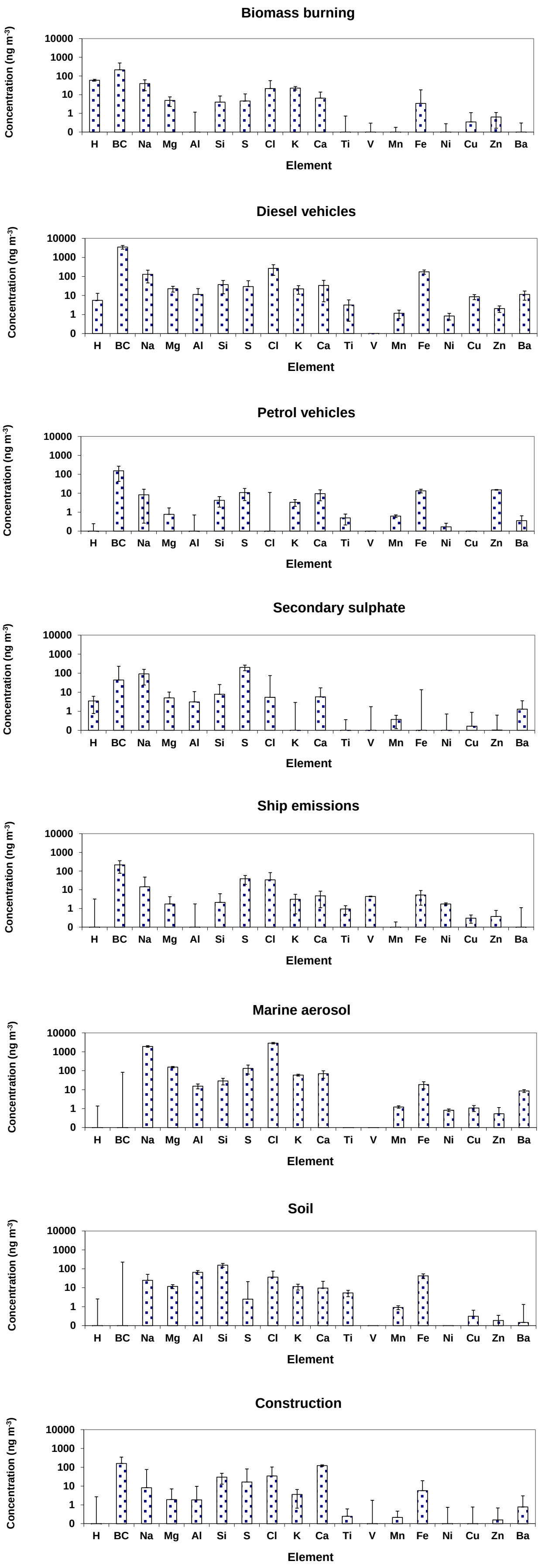

Figure 7.15 Source profiles and elemental concentrations for PM_{10} at Queen Street site (showing 5th and 95th confidence intervals in mean concentration derived from the receptor modelling)

Similar sources were identified for PM_{10} as for the $PM_{2.5}$ analysis in Section 7.5.

- The first was attributed to biomass burning;
- The second and third sources were from diesel and petrol fuelled motor vehicle emissions respectively;
- The fourth source was from secondary sulphate sources;
- The fifth source was attributed to particulate matter originating from ship emissions due to the BC, S, V and Ni content;
- The sixth source is the contribution from marine aerosol;
- The seventh source is from crustal matter, probably associated with dusts from local excavation work and road dust;
- The eighth source, Construction, with a high Ca loading has been attributed to cementitious dusts from construction activities in the area such as roadwork, footpath improvements and work on buildings (i.e. concrete cutting, cement mixing and suchlike).

Figure 7.16 presents the 2006-2013 average source contributions to PM_{10} concentrations and includes the standard deviation of the average mass contributions from each of the sources indicating the variability in source strength.

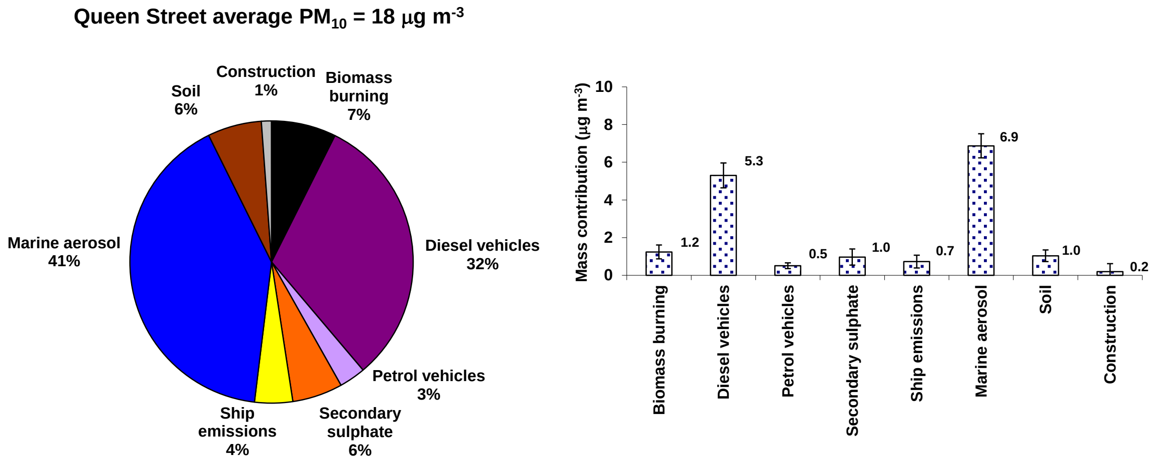

Figure 7.16 Average 2006-2013 source contributions to PM_{10} at Queen Street site (showing 5th and 95th confidence intervals in mean concentration derived from the receptor modelling)

The average source contributions estimated by the receptor modelling indicate that motor vehicle emissions and marine aerosol are the most significant contributors (35 % and 41 % respectively) to PM_{10} concentrations at Queen Street, with lesser contributions from biomass burning (7 %), the construction dusts (1 %), secondary sulphate particles (6 %) and crustal matter (6 %). Figure 7.17 shows the mass contribution of sources to PM_{10} mass for each sample collected at Queen Street. The temporal variation indicates that PM_{10} mass is generally dominated by marine aerosol and motor vehicle emissions, but that mass contributions from biomass burning sources during winter and intermittent crustal matter or construction dusts can lead to elevated PM_{10} concentrations.

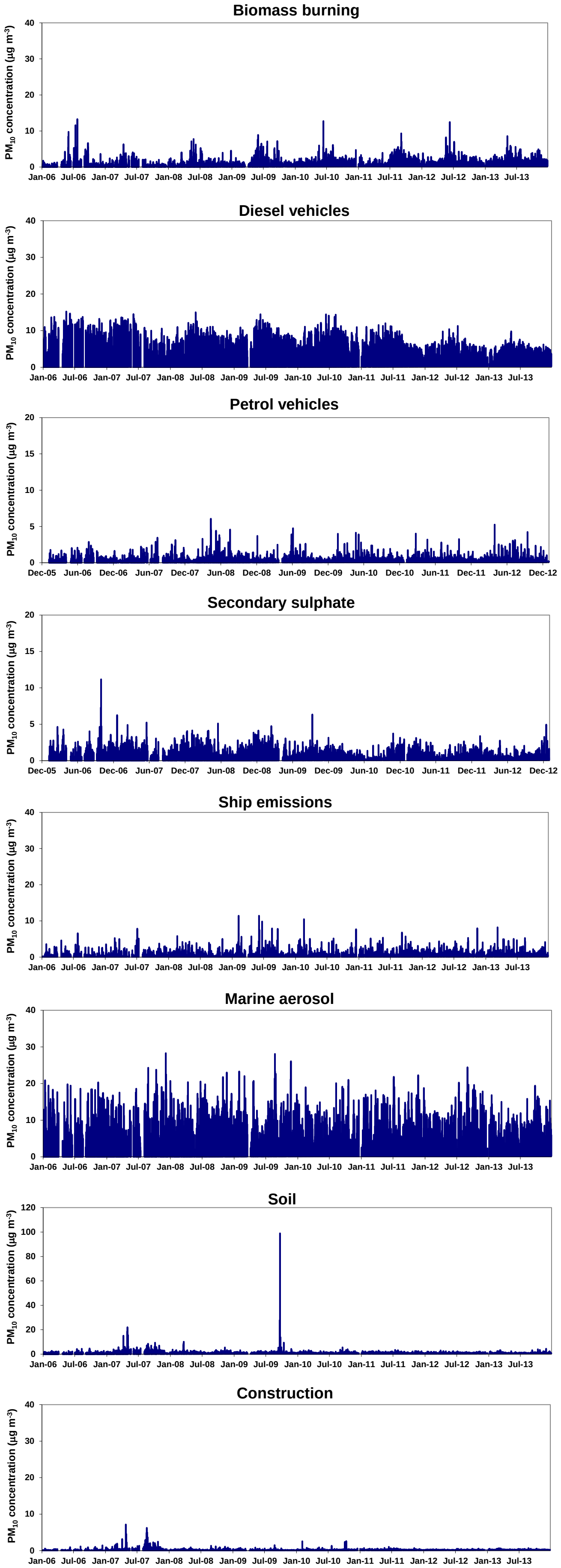

Figure 7.17 Time-series for source contributions to PM$_{10}$ mass at Queen Street

The temporal variations in the PM_{10} sources are similar to those for $PM_{2.5}$. Increased activity in the soil and construction sources was evident for 2007 and the soil source, most likely from roadworks on Queen Street was responsible for high PM_{10} concentrations in May 2007. The soil event in September 2009 (peak at 115 µg m^{-3}) is due to an Australian dust storm and further discussion is provided in (Davy, Trompetter et al. 2011).

7.6.3 Temporal variations in source contributions to PM_{10} at Queen Street

Figure 7.18 presents the 2006-2013 PM_{10} temporal variation mass contributions at Queen Street. The primary source of $PM_{2.5}$ during all seasons at Queen Street was motor vehicle emissions, with both the diesel and petrol vehicle contributions lower on the weekends in line with commuter behaviour and commercial activities. Average PM_{10} concentrations were slightly higher in winter (12 µg/m^3) than in other seasons due to higher motor vehicle and biomass burning contributions.

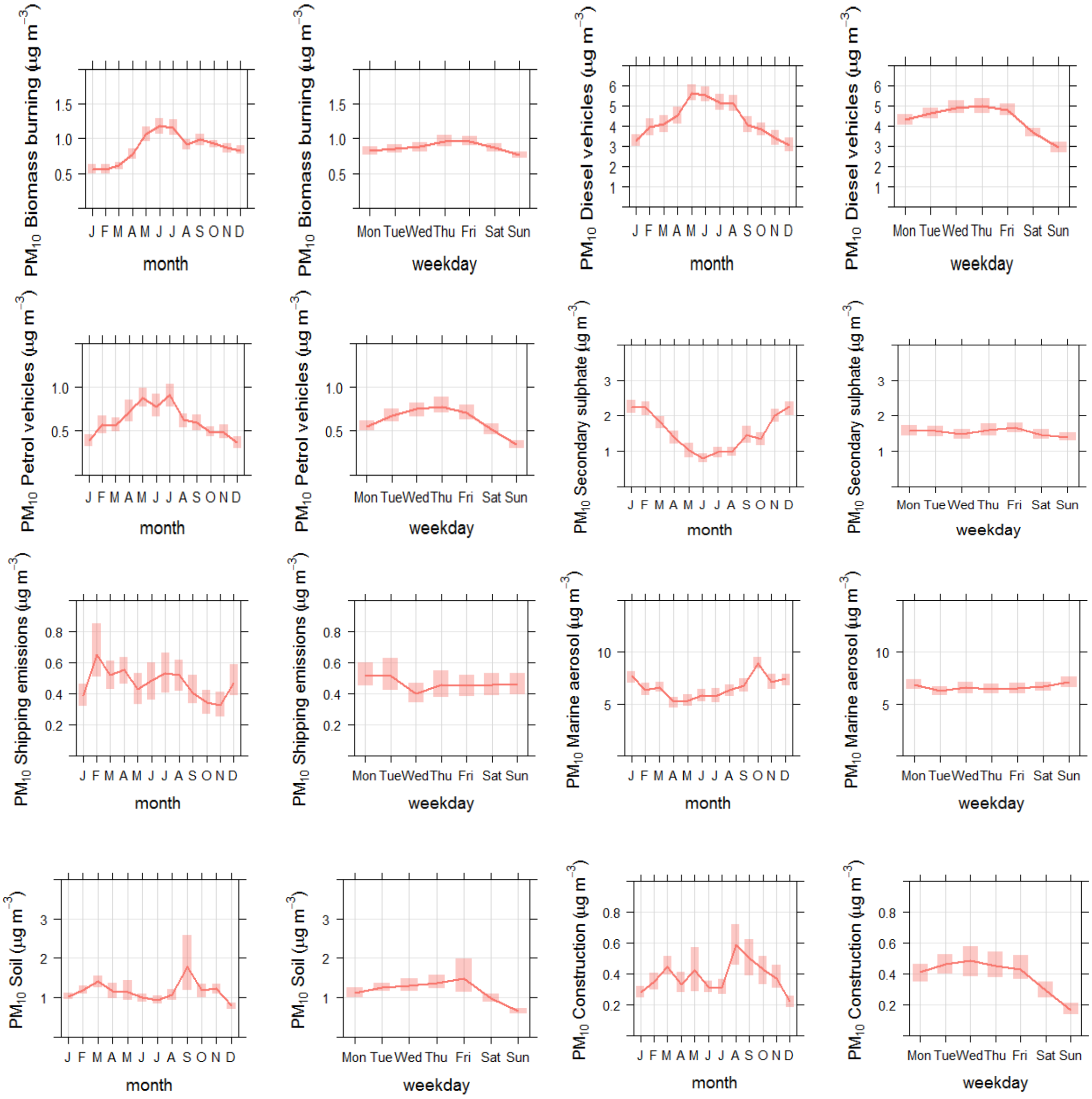

Figure 7.18 Temporal (2006-2013) variations in PM_{10} source contributions at Queen Street (the shaded bars are the 95 percentile confidence limits in the mean)

Average PM_{10} concentrations (18 - 21 µg m^{-3}) during autumn (March-May), spring (September-November) and summer (December-February) were relatively similar.

Contributions from marine aerosol and secondary sulphate were higher during summer but shipping emissions were more variable which may be a consequence of local meteorology and shipping activity at the Port. The motor vehicle, soil and construction sources all demonstrated a weekday-weekend difference in source contributions indicating they were all most likely generated by anthropogenic sources reflecting normal working week activities.

7.6.4 Trends in PM_{10} concentrations and source contributions at Queen Street

The temporal trends in PM_{10} source contributions at Queen Street were explored using the Thielsen functionality available in *openair*. Figure 7.19 presents the de-seasonailsed trend in PM_{10} concentrations showing that there was a significant decreasing trend (99.9 % CI) over the monitoring period.

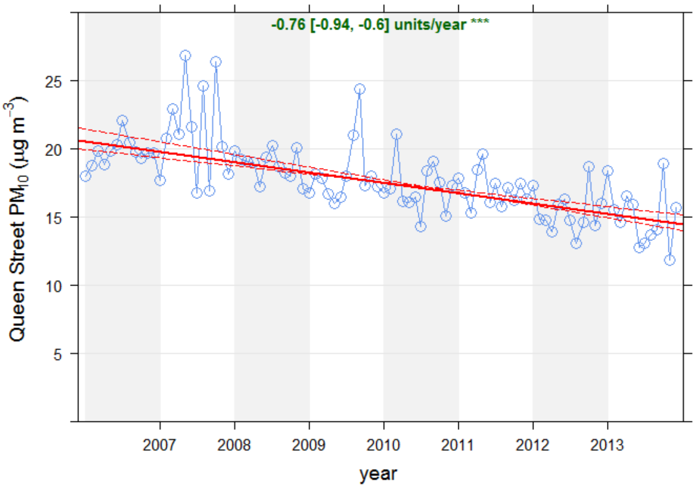

Figure 7.19 Trend in PM10 concentrations at Queen Street (statistically significant at the 99.9 % confidence interval)

The trends in PM_{10} source contributions are presented in Figure 7.20 and show that the decrease in PM_{10} was largely driven by a commensurate decrease in diesel vehicle, secondary sulphate and marine aerosol contributions. It is likely that the change in road layout, light phasing and a reduction in bus routing along Queen Street has had an influence on diesel emissions concentrations, while for secondary sulphate it would appear that the decrease was consistent with a reduction in the sulphur content of fuels as discussed in Chapter 5. The Queen Street PM_{10} marine aerosol trend was probably due to the underlying decrease in $PM_{2.5}$ marine aerosol as presented in Figure 7.11. There were also decreasing trends for the soil and construction sources (both at the 99.9% CI). The trends in soil and construction source contributions are clearly influenced by the impact of significant activity during 2007-2008 and much less since then. No significant trend was observed for ship emissions. The primary influence for the decrease in secondary sulphate appears to the reduction in sulphur in automotive fuels as described in Chapter 5. Particulate matter from biomass burning and shipping emissions sources showed a steady increase (99 % CI and 95 % CI respectively) over the monitoring period but no trend was evident for petrol vehicle emissions.

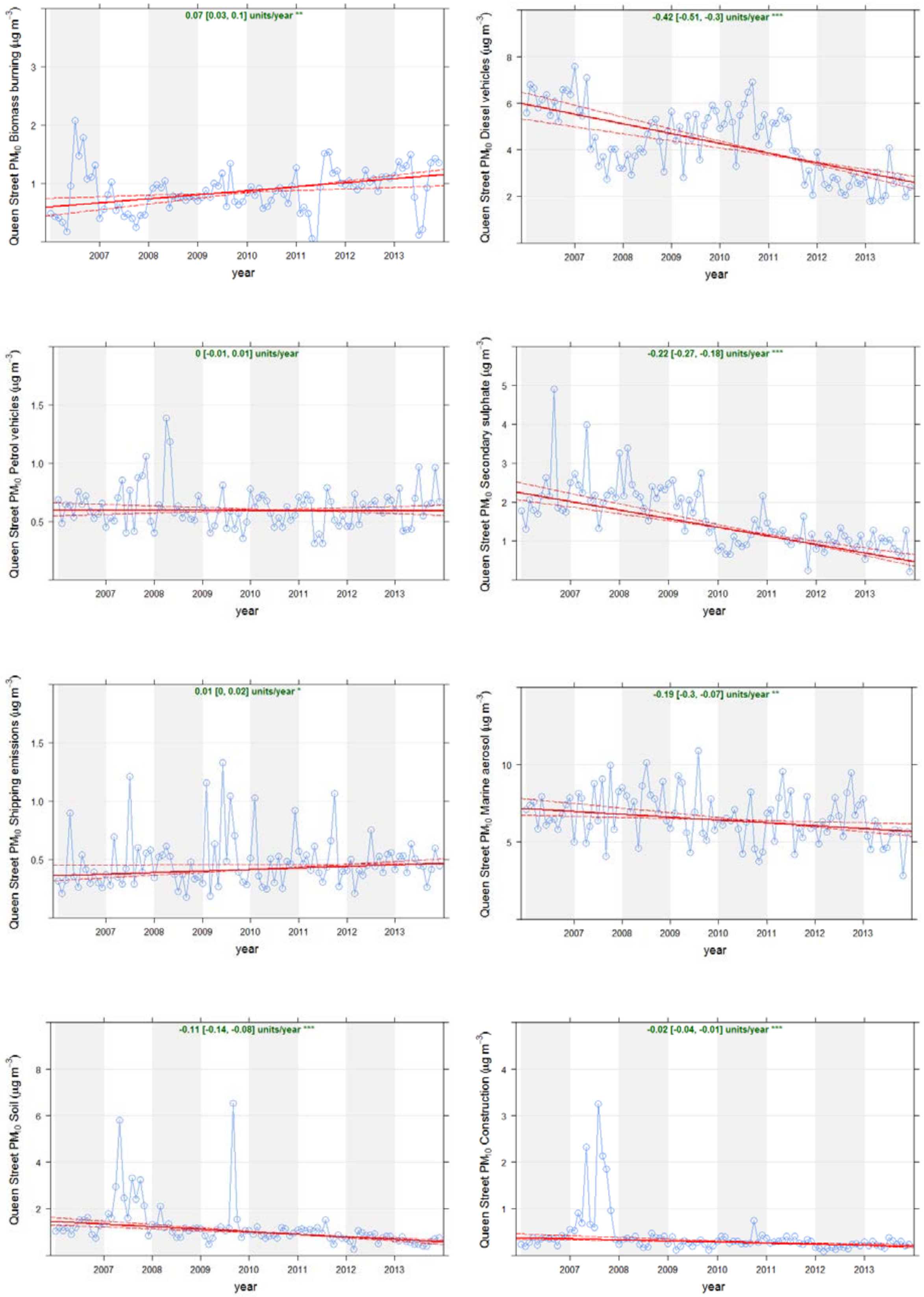

Figure 7.20 Trends in PM$_{2.5}$ source contributions at Queen Street

7.6.5 Analysis of individual PM_{10} events at Queen Street

Peak PM_{10} events during the sampling period at Queen Street have been chosen for further analysis. Peak PM_{10} events are defined as those that were higher than 66 % (33 μg/m^3) of the NES (50 μg m^{-3} 24-hour average). It was found that there were 53 days where PM_{10} concentrations were higher than 66 % of the NES and of those, 3 days exceeded the NES (02/05/2007, 04/05/2007 and 25/09/2009). Crustal matter (Soil) was the major contributor to PM_{10} on those days with the first two likely to be associated with local earthworks/construction activities during the Queen Street upgrade but the September 2009 exceedance (130 μg m^{-3}) was due to an Australian dust storm and has been reported previously (Davy, Trompetter et al. 2011).

Figure 7.21 presents the mass contributions of individual sources to each of the peak $PM_{2.5}$ days (> 33 μg m^{-3}).

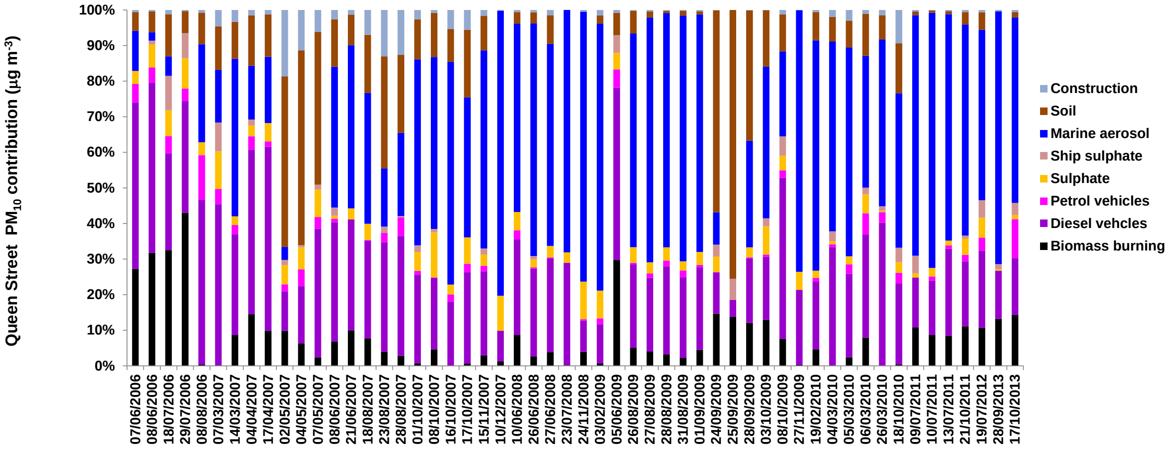

Figure 7.21 Source contributions to peak PM_{10} concentrations at Queen Street

It is clear from Figure 7.21 that motor vehicle emission and marine aerosol sources were primarily responsible for elevated PM_{10} concentrations at Queen Street, but that local construction and/or road work activities had a significant impact during 2007.

7.7 SUMMARY OF QUEEN STREET RECEPTOR MODELLING ANALYSIS

Source apportionment results for Queen Street show that combustion sources are the main contributor to $PM_{2.5}$, predominantly from motor vehicle emissions. Marine aerosol was also found to contribute significantly to $PM_{2.5}$ at Queen Street, probably due to the proximity of the monitoring site to the Waitemata Harbour.

PM_{10} sources were found to be similar to $PM_{2.5}$ sources at Queen Street with combustion sources and marine aerosol responsible for peak PM_{10} concentrations. Motor vehicle emissions were the primary source of PM_{10} all year but on occasion during summer marine aerosol dominates and during winter there can be significant contributions from biomass burning sources. Interestingly it was found that there was an increase in soil and construction source activity during 2007 (associated with local road works and building construction) and on two occasions, contributions from the soil source raised PM_{10} concentrations above the NES (50 μg m^{-3}).

7.7.1 Comparison between $PM_{2.5}$ and PM_{10} sources at Queen Street

This section presents a comparison between the results from the receptor modelling analyses of the $PM_{2.5}$ and PM_{10} datasets from the Queen Street site (2006 - 2014). Note that only the coincident $PM_{2.5}$ and PM_{10} samples collected at Queen Street have been considered here since PM_{10} sampling was daily but $PM_{2.5}$ was 1-day-in-3. There were a total of 753 coincident PM_{10} and $PM_{2.5}$ samples over the monitoring period which provides sufficient data for a robust analysis. Table 6.3 lists the average source contributions determined for each of the sample sets and Figure 7.22 presents the corresponding pie graphs which are essentially the same as for the contributions over the entire $PM_{2.5}$ and PM_{10} datasets respectively.

Table 7.5 Average source mass contributions (± modelled standard deviation) derived for the two Queen Street particulate matter size fraction datasets

Source	Biomass burning (µg m^{-3})	Diesel vehicles (µg m^{-3})	Petrol vehicles (µg m^{-3})	Secondary sulphate (µg m^{-3})	Shipping emissions (µg m^{-3})	Marine aerosol (µg m^{-3})	Soil (µg m^{-3})	Construction (µg m^{-3})
$PM_{2.5}$	0.8±0.6	3.2±0.7	0.3±0.02	0.9±0.3	0.4±0.2	2.3±0.4	0.1±0.3	0.5±0.2
PM_{10}	1.3±0.4	5.3±0.7	0.5±0.2	1.0 ±0.4	0.8±0.3	6.3±0.6	1.0±0.3	0.2±0.4

Immediately evident from Table 7.5 are the higher mass contribution to PM_{10} (compared to $PM_{2.5}$) from marine aerosol and soil as they are mainly coarse particle ($PM_{10-2.5}$) sources. The biomass burning is primarily a $PM_{2.5}$ source with a similar $PM_{2.5}$ and PM_{10} mass. Secondary sulphate is also a fine particle but some of the sulphate particle size range does extend into the coarse fraction (Anlauf, Li et al. 2006), particularly where heterogeneous atmospheric chemistry takes place on the surface of particles (such as for shipping emissions) or in aerosol droplets during the reaction of sulphur gaseous species to form secondary sulphate particle species (Gard, Kleeman et al. 1998, O'Dowd, Lowe et al. 2000, George and Abbatt 2010).

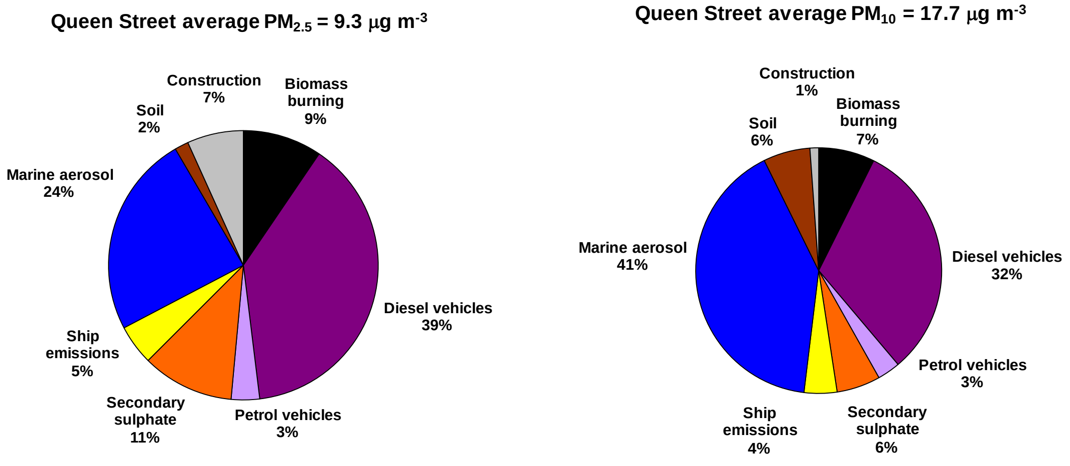
Queen Street average $PM_{2.5}$ = 9.3 µg m^{-3}

Queen Street average PM_{10} = 17.7 µg m^{-3}

Figure 7.22 Average source contributions for coincident monitoring results (left) $PM_{2.5}$ and; (right) PM_{10} results

The motor vehicle source has higher mass contributions to PM_{10} than $PM_{2.5}$ and this is due to a coarse particle road dust component covariant with tailpipe emissions. The PM_{10} source profile for the motor vehicle sources shows this with a much higher crustal matter component (Al, Si, Ca, Ti, Fe) than the corresponding $PM_{2.5}$ motor vehicle source profiles (see Figure 6.9 and Figure 6.23 for the $PM_{2.5}$ and PM_{10} source profiles respectively). Figure 7.23 presents a correlation matrix plot for the $PM_{2.5}$ and PM_{10} source contributors showing that the same sources are highly correlated between the two independent datasets indicating the robustness of the receptor modelling results.

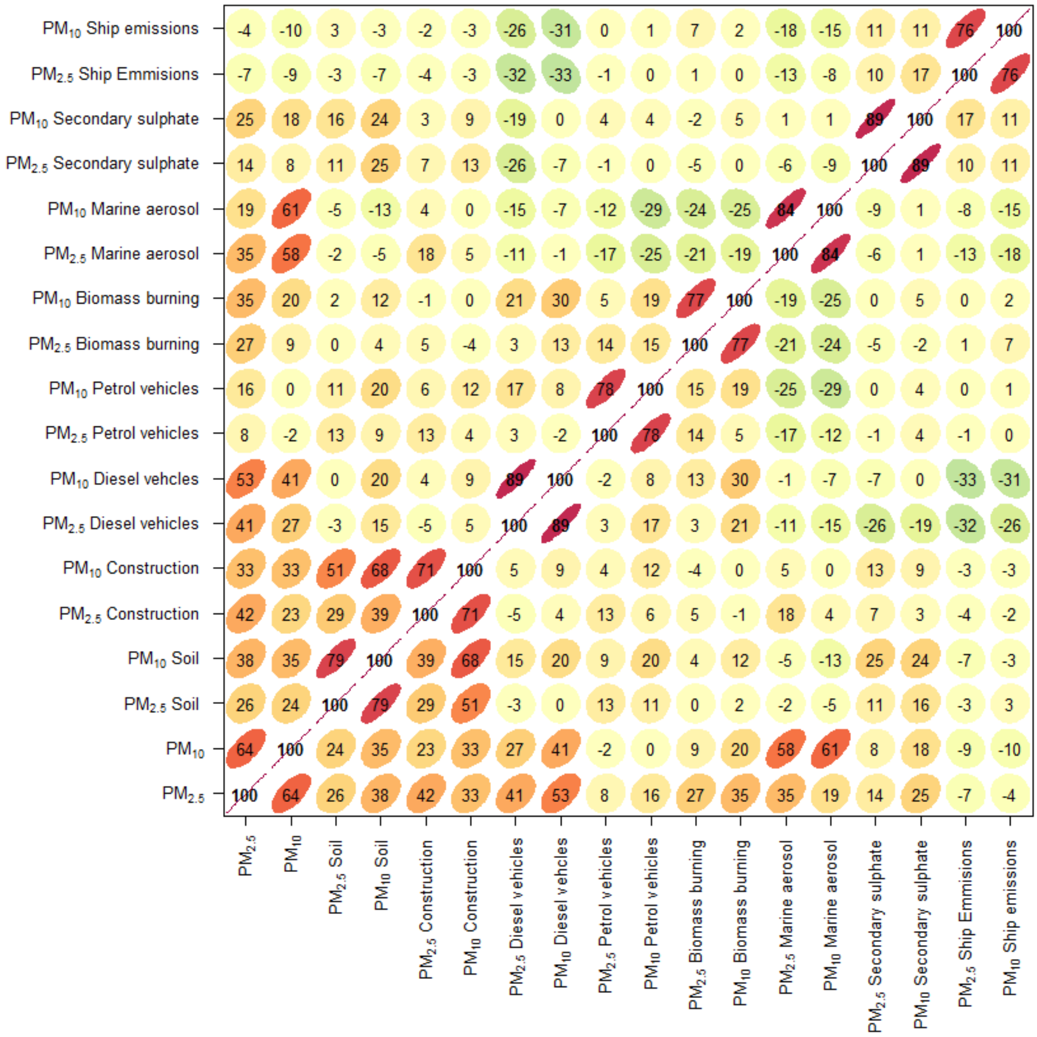

	$PM_{2.5}$	PM_{10}	$PM_{2.5}$ Soil	PM_{10} Soil	$PM_{2.5}$ Construction	PM_{10} Construction	$PM_{2.5}$ Diesel vehicles	PM_{10} Diesel vehcles	$PM_{2.5}$ Petrol vehicles	PM_{10} Petrol vehicles	$PM_{2.5}$ Biomass burning	PM_{10} Biomass burning	$PM_{2.5}$ Marine aerosol	PM_{10} Marine aerosol	$PM_{2.5}$ Secondary sulphate	PM_{10} Secondary sulphate	$PM_{2.5}$ Ship Emmisions	PM_{10} Ship emissions
PM_{10} Ship emissions	-4	-10	3	-3	-2	-3	-26	-31	0	1	7	2	-18	-15	11	11	76	100
$PM_{2.5}$ Ship Emmisions	-7	-9	-3	-7	-4	-3	-32	-33	-1	0	1	0	-13	-8	10	17	100	76
PM_{10} Secondary sulphate	25	18	16	24	3	9	-19	0	4	4	-2	5	1	1	89	100	17	11
$PM_{2.5}$ Secondary sulphate	14	8	11	25	7	13	-26	-7	-1	0	-5	0	-6	-9	100	89	10	11
PM_{10} Marine aerosol	19	61	-5	-13	4	0	-15	-7	-12	-29	-24	-25	84	100	-9	1	-8	-15
$PM_{2.5}$ Marine aerosol	35	58	-2	-5	18	5	-11	-1	-17	-25	-21	-19	100	84	-6	1	-13	-18
PM_{10} Biomass burning	35	20	2	12	-1	0	21	30	5	19	77	100	-19	-25	0	5	0	2
$PM_{2.5}$ Biomass burning	27	9	0	4	5	-4	3	13	14	15	100	77	-21	-24	-5	-2	1	7
PM_{10} Petrol vehicles	16	0	11	20	6	12	17	8	78	100	15	19	-25	-29	0	4	0	1
$PM_{2.5}$ Petrol vehicles	8	-2	13	9	13	4	3	-2	100	78	14	5	-17	-12	-1	4	-1	0
PM_{10} Diesel vehcles	53	41	0	20	4	9	89	100	-2	8	13	30	-1	-7	-7	0	-33	-31
$PM_{2.5}$ Diesel vehicles	41	27	-3	15	-5	5	100	89	3	17	3	21	-11	-15	-26	-19	-32	-26
PM_{10} Construction	33	33	51	68	71	100	5	9	4	12	-4	0	5	0	13	9	-3	-3
$PM_{2.5}$ Construction	42	23	29	39	100	71	-5	4	13	6	5	-1	18	4	7	3	-4	-2
PM_{10} Soil	38	35	79	100	39	68	15	20	9	20	4	12	-5	-13	25	24	-7	-3
$PM_{2.5}$ Soil	26	24	100	79	29	51	-3	0	13	11	0	2	-2	-5	11	16	-3	3
PM_{10}	64	100	24	35	23	33	27	41	-2	0	9	20	58	61	8	18	-9	-10
$PM_{2.5}$	100	64	26	38	42	33	41	53	8	16	27	35	35	19	14	25	-7	-4

Figure 7.23 Correlation matrix plot for the Queen Street $PM_{2.5}$ and PM_{10} source contributors

8.0 KHYBER PASS ROAD, NEWMARKET

8.1 SITE DESCRIPTION

Samples of airborne particles were collected at an ambient air quality monitoring station on the corner of Khyber Pass Road and Mountain Road, Newmarket (Lat: -36.8662E; Long: 174.7705). Figure 8.1 shows a map of the local area.

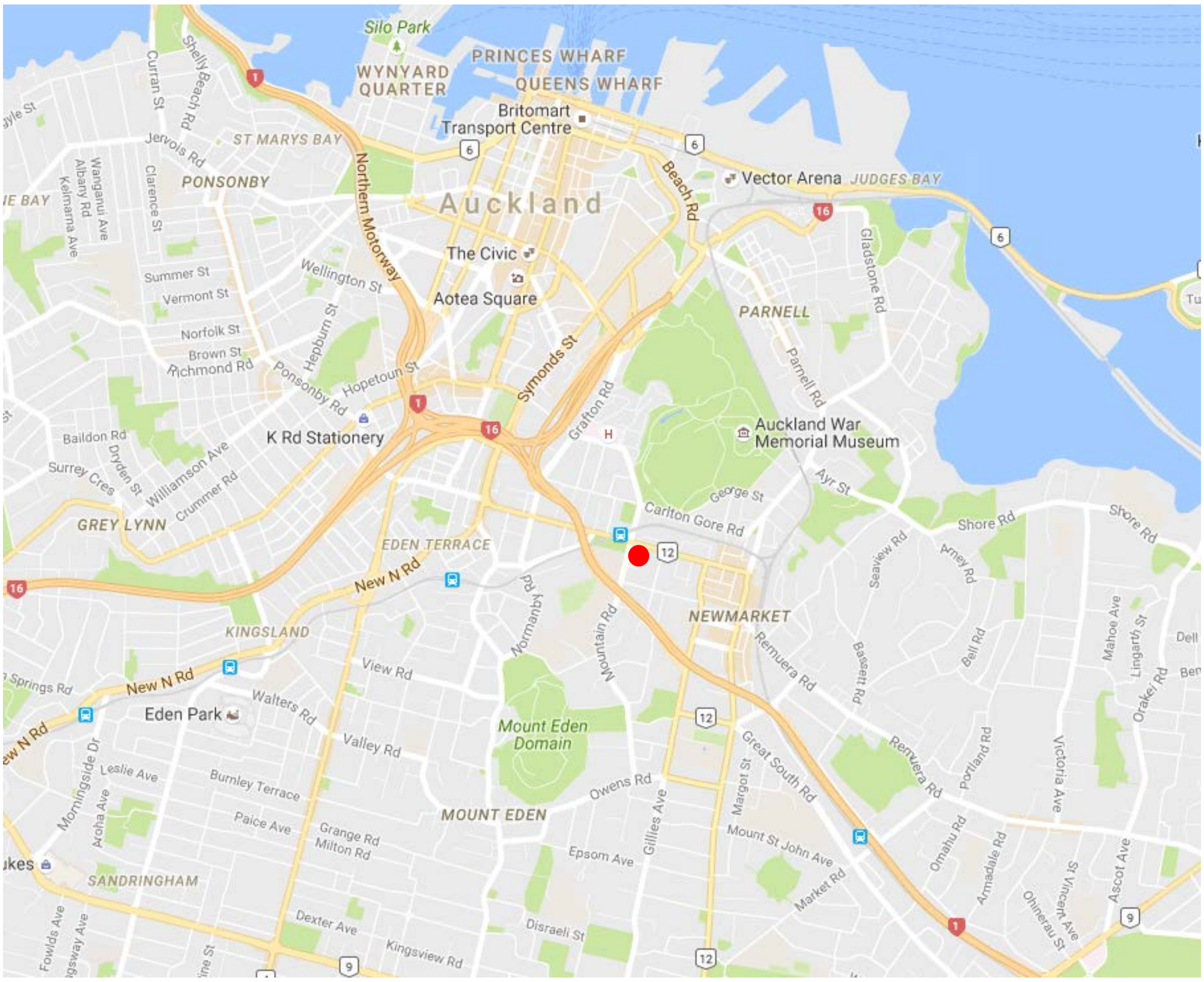

Figure 8.1 Map showing location of Khyber Pass Road monitoring site (●) Source Google Maps

The Khyber Pass Road site is operated by WSL (Partisol samples) and NIWA (BAM, gases and meteorological data) on behalf of AC for its ambient air quality monitoring programme. The site was established in late 1996 and is classed as a peak (traffic) site. Pollutants monitored include CO, NO_x, VOCs (all until 2012), PM_{10} (BAM and Partisol) and $PM_{2.5}$ (Partisol) and meteorological parameters.

The Khyber Pass Road site is immediately adjacent to Khyber Pass Road (arterial, aligned WNW-ESE); and 8 m west of Mountain Road (arterial, aligned NNW-SSE). Further west (250 m) is the Southern Motorway (aligned NW-SE). The Partisol sampler that was used to collect PM_{10} and $PM_{2.5}$ samples for the receptor modelling study was approximately 3 m from the roadside (on Mountain Road) at the intersection of Khyber Pass Road and Mountain Roads. Khyber Pass Road slopes toward the east and the Newmarket shopping centre (700 m E). Figure 8.2 provides an aerial view of the Khyber Pass Road site location.

Figure 8.2 Aerial view of Khyber Pass Road monitoring site and surrounds (●) (source Google Maps 2016)

8.2 AIR PARTICULATE MATTER SAMPLES AND MONITORING PERIOD

Filter samples from one instrument (Partisol Satellite and Hub system) located at the Khyber Pass Road air quality monitoring station were supplied by AC for analysis:

1. 921 $PM_{2.5}$ samples from a Partisol 2000 sampler on a one-day-in-three sampling regime for the period December 2005 – December 2013.
2. 892 PM_{10} samples from a Partisol 2000 sampler on a one-day-in-three sampling regime or the period December 2005 – December 2013.

The Partisol sampler was set up as a satellite and hub system, therefore $PM_{2.5}$ and PM_{10} samples were collected on an alternating one-day-in-three sampling regime. Receptor modelling studies were carried out for the $PM_{2.5}$ and PM_{10} sample sets and are reported in Sections 8.5 and 8.6 respectively.

8.3 CONCEPTUAL RECEPTOR MODEL FOR PARTICULATE MATTER AT KHYBER PASS ROAD

The following initial conceptual model for Khyber Pass Road includes local emission sources:

- Motor vehicles – all roads in the area act as line sources and roads with higher density traffic will dominate particularly the motorway nearby with Khyber Pass Road and Mountain Roads immediately adjacent;
- Local wind-blown soil or road dust sources;
- Domestic activities – likely to be dominated by biomass burning such as emissions from solid fuel fires used for domestic heating during the winter.
- Local commercial/industrial activities – there are a range of light commercial activities in the area with a large brewery located across Khyber Pass Road from the monitoring site.

Longer range sources may also contribute to ambient particle loadings and these include:

- Marine aerosol;
- Secondary particulate matter resulting from atmospheric gas-to-particle conversion processes (sulphate and nitrate species, organic particle species resulting from photochemical smog events);
- Potential for long range transport of industrial emissions.

Another category of emission sources that may contribute are those considered as 'one-off' emission sources:

- Fireworks displays and other special events (Auckland Domain is 1 km northeast of the site);
- Short-term road works and demolition/construction activities. Such activities have been carried out intermittently over the monitoring period near the monitoring site and include the rebuild of the Newmarket viaduct, realignment of the motorway lanes, construction works on the adjacent railway line, rail underpass and rail station, construction of a multi-storey block at the adjacent Mt Eden Prison complex

The variety of sources described above can be recognised and accounted for by appropriate data analysis methods, such as examination of seasonal differences, temporal variations and receptor modelling itself.

8.4 LOCAL METEOROLOGY AT KHYBER PASS ROAD

The predominant wind direction at Khyber Pass Road is from the southwesterly quarter as shown by the wind roses in Figure 8.3 (2006-2013 data). The meteorological station for Khyber Pass Road is located on top of a three storey building next to the samplers and therefore wind speed and direction data is likely to be influenced by building wake and turbulence effects. There is also likely to be a topographical influence as the land to the south-southwest rises rapidly towards Mt Eden.

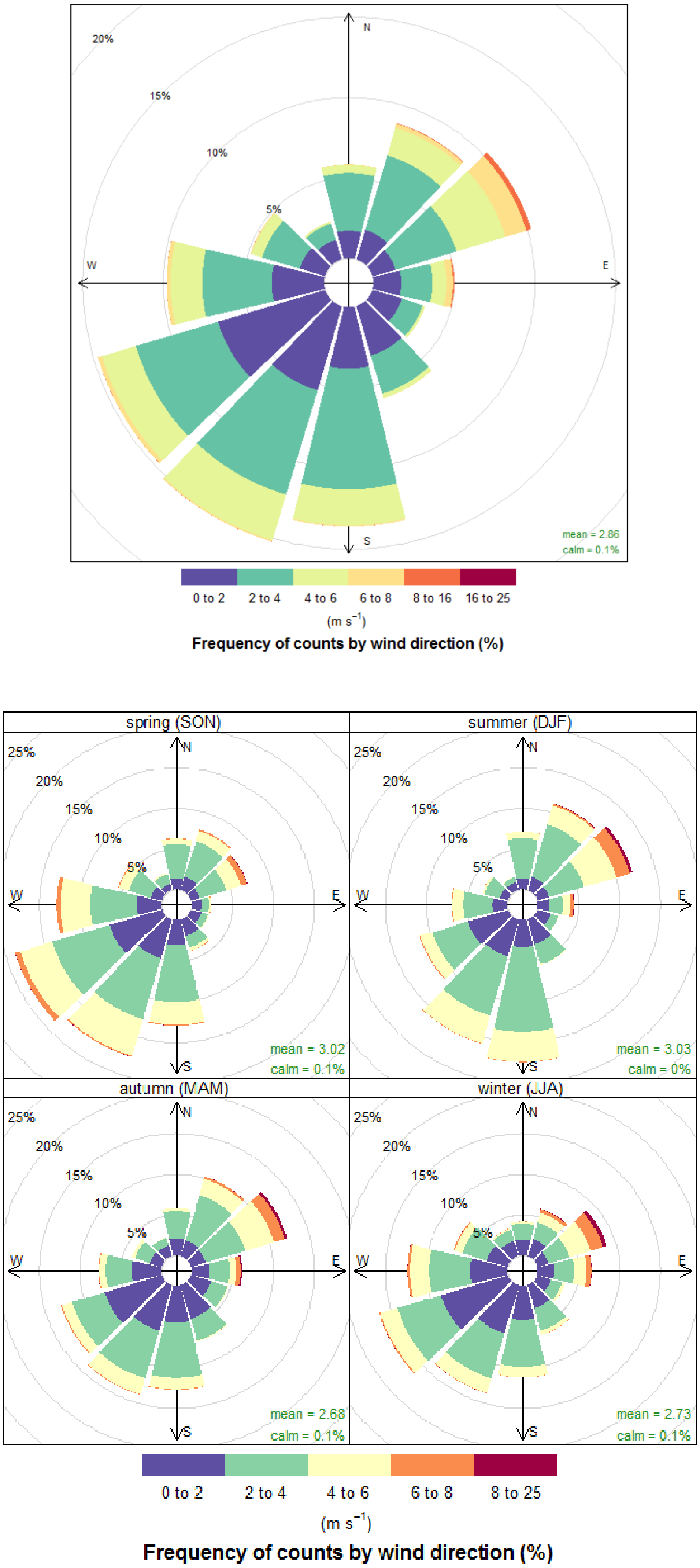

Figure 8.3 (Top) Wind rose for 2006-2011 at Khyber Pass Road; (Bottom) Seasonal wind roses at Khyber Pass Road

Meteorological differences between winter and summer at Khyber Pass Road can be seen in the wind roses presented in Figure 8.3 respectively. The predominance of southwesterly winds was markedly more in winter, with a corresponding decrease in winds from the northeasterly quarter. During the summer, there is a greater component of winds from the northeasterly sector and a significant component from directly south.

8.5 ANALYSIS OF $PM_{2.5}$ SAMPLES FROM KHYBER PASS ROAD

The Khyber Pass Road $PM_{2.5}$ samples from the monitoring site refer to those $PM_{2.5}$ samples collected using a Partisol 2000 Sampler (Andersen Instruments Inc.) from December 2005 to December 2013. Gravimetric results for the Partisol $PM_{2.5}$ samples as presented in Figure 8.4 shows distinct peaks in $PM_{2.5}$ concentrations during winter months (June – August).

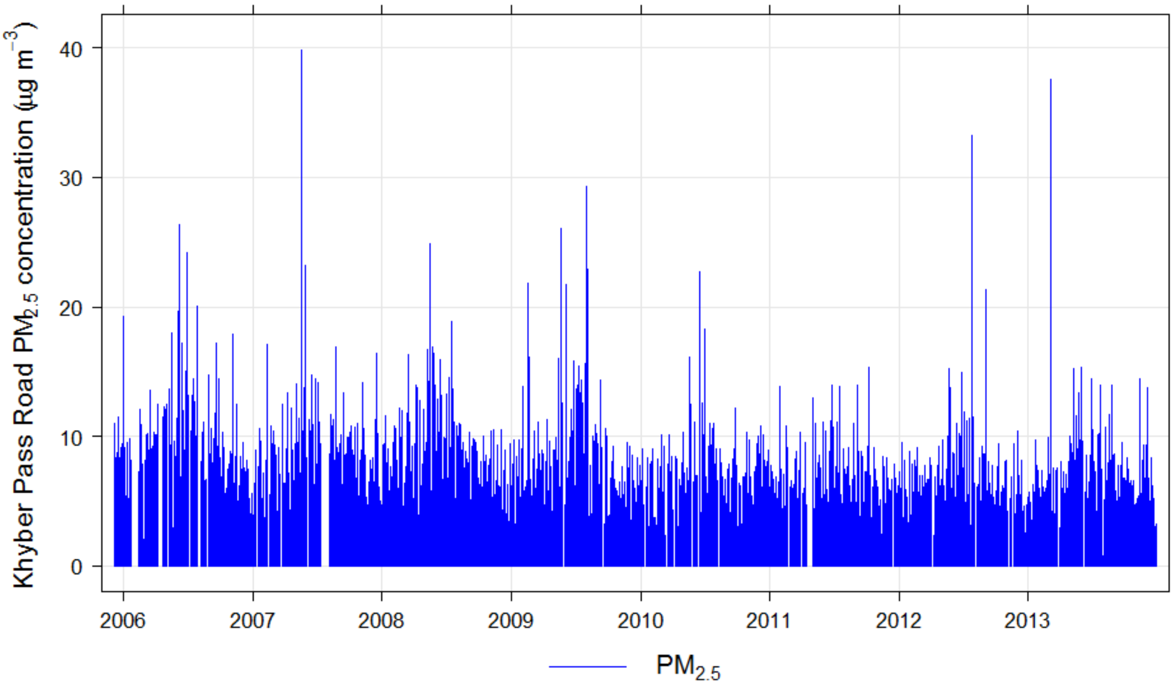

Figure 8.4 Gravimetric results for Partisol $PM_{2.5}$ at Khyber Pass Road

8.5.1 Composition of $PM_{2.5}$ at Khyber Pass Road

Elemental concentrations for Partisol $PM_{2.5}$ samples at Khyber Pass Road are presented in Table 8.1 with a box and whisker plot of the elemental concentrations shown in Figure 8.5.

Table 8.1 Elemental analysis results for Partisol $PM_{2.5}$ at Khyber Pass Road (921 samples)

Species	Average (ng/m^3)	Max (ng/m^3)	Min (ng/m^3)	Std Dev (ng/m^3)	Median (ng/m^3)	Av LOD (ng/m^3)	#>LOD
$PM_{2.5}$ (μg/m^3)	**8**	**40**	**1**	**4**	**8**		
H	97	1238	0	81	83	44	710
BC	3862	9152	0	1594	3728	183	920
Na	510	4605	0	526	379	263	580
Mg	56	643	0	51	46	25	697
Al	24	1603	0	58	18	13	660
Si	66	4435	13	186	48	9	921
P	5	144	0	8	3	15	172
S	234	2897	33	176	191	9	921
Cl	666	6040	1	660	488	7	917
K	58	8100	1	285	36	7	920
Ca	46	3224	2	108	36	6	920
Sc	2	26	0	2	1	8	47
Ti	2	125	0	5	1	7	105
V	2	28	0	3	0	7	111
Cr	1	20	0	2	1	6	71
Mn	2	26	0	2	1	6	117
Fe	79	952	4	62	68	5	920
Co	2	18	0	3	1	8	63
Ni	2	18	0	3	0	8	67
Cu	5	235	0	9	4	9	275
Zn	15	140	0	18	10	11	462
Ga	3	31	0	5	0	17	77
Ge	4	35	0	6	0	22	56
As	5	51	0	8	0	29	72
Se	7	67	0	10	0	35	90
Br	7	83	0	13	0	46	68
Rb	12	114	0	20	0	73	73
Sr	19	238	0	28	0	90	90
Mo	48	488	0	79	0	273	111
I	7	71	0	10	2	25	75
Ba	9	364	0	18	4	27	80
Hg	10	159	0	18	0	63	45
Pb	12	140	0	23	0	77	47

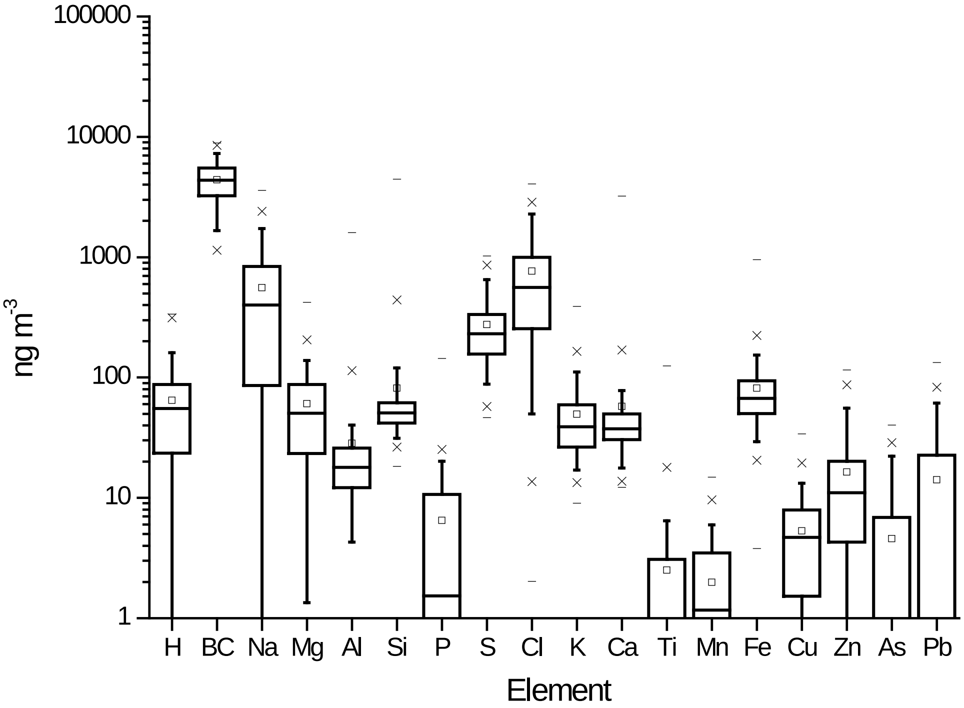

Figure 8.5 Box and whisker plot of $PM_{2.5}$ elemental concentrations at Khyber Pass Road (logarithmic scale)

Carbonaceous species (represented by BC), sodium, sulphur and chlorine were found to dominate $PM_{2.5}$ elemental mass concentrations indicating that combustion processes, secondary sulphate and marine aerosol are important contributors to ambient $PM_{2.5}$ at Khyber Pass Road. A scatterplot matrix of the species in Table 8.1 shows that that a number of measured species were generally close to or below the limits of detection over all samples.

8.5.2 Source contributions to $PM_{2.5}$ at Khyber Pass Road

Six primary source contributors were determined from the PMF receptor modelling analysis of speciation $PM_{2.5}$ elemental compositions at Khyber Pass Road. These are identified as presented in Table 8.2 along with the mass of $PM_{2.5}$ and elemental species associated with each source.

Table 8.2 Elemental composition of source profiles and contribution to $PM_{2.5}$ at Khyber Pass Road

	Factor 1	**Factor 2**	**Factor 3**	**Factor 4**	**Factor 5**	**Factor 6**
Species	**Biomass burning (ng/m^3)**	**Diesel vehicles (ng/m^3)**	**Petrol vehicles (ng/m^3)**	**Sulphate (ng/m^3)**	**Marine aerosol (ng/m^3)**	**Soil (ng/m^3)**
$PM_{2.5}$	**1289**	**3205**	**853**	**1245**	**944**	**28**
H	29.8	33.9	7.0	11.0	1.1	3.1
BC	330.5	2556.8	465.9	473.2	0.0	20.0
Na	13.0	0.0	4.1	49.8	433.4	1.7
Mg	3.3	2.6	0.0	5.2	37.0	4.3
Al	0.4	0.7	1.0	2.1	2.3	15.7
Si	2.4	9.8	4.1	6.3	5.4	31.2
S	3.7	36.3	5.6	144.1	35.7	3.4
Cl	0.0	72.1	0.2	0.0	587.8	0.0
K	20.9	4.0	2.1	1.2	11.3	3.6
Ca	2.8	9.0	3.3	3.3	13.2	8.8
Ti	0.2	0.6	0.2	0.2	0.4	1.2
Fe	10.0	30.0	13.4	2.5	0.0	19.9
Cu	0.8	2.6	0.7	0.7	0.5	0.2
Zn	1.2	1.4	11.6	0.4	0.1	0.2

Table 8.2 represents the summary results for a reiterative process that examines the effect of each species on the PMF receptor modelling process using the modelling diagnostics presented in Appendix 4. Species that were poorly modelled (slope, $r^2 < 0.6$) have been removed from the analyses unless considered vital for source identification. The source contributors identified in Table 8.2 were found on average to explain 91 % of $PM_{2.5}$ gravimetric mass. Figure 8.6 presents the source profiles extracted from the PMF analysis of Khyber Pass Road $PM_{2.5}$ data.

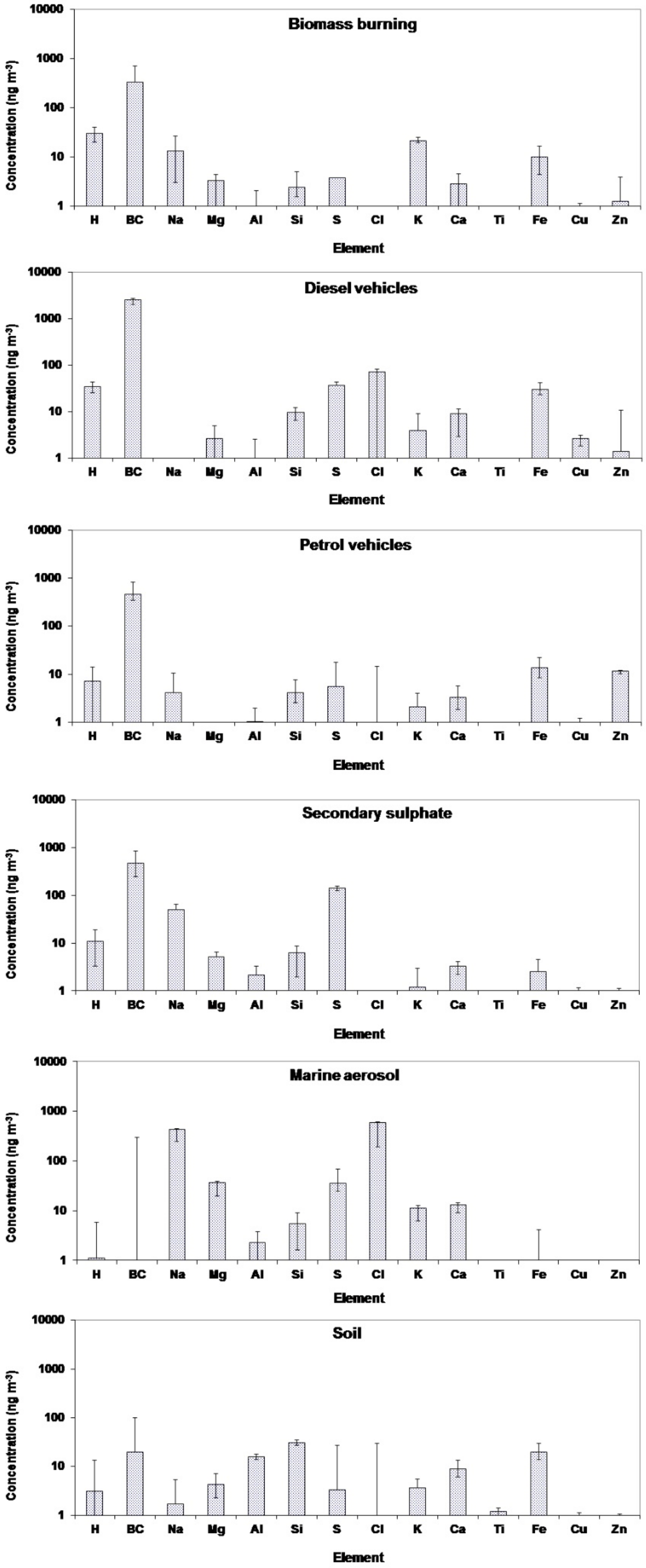

Figure 8.6 Source profiles and elemental concentrations for $PM_{2.5}$ at Khyber Pass Road site (showing 5th and 95th confidence intervals in mean concentration derived from the receptor modelling)

- The first factor is from biomass burning due to the association between H, BC and K.
- The second source contribution, Diesel vehicles, has been identified as originating from diesel powered motor vehicle emissions and is largely composed of BC along with S, Cl, Ca and Fe.
- The third factor, Petrol vehicles, is the contribution from petrol powered motor vehicles because of the grouping of H, BC, Ca, Fe and most of the Zn.
- The fourth factor has been identified as a secondary sulphate aerosol source due to the predominance of S.
- The fifth source profile is dominated by Na and Cl and represents the contribution from marine aerosol.
- The sixth source is due to crustal matter, construction activities and/or road dust.

Figure 8.7 presents the average source contributions to $PM_{2.5}$ concentrations and includes the standard deviation of the average mass contributions from each of the sources indicating the variability in source strength.

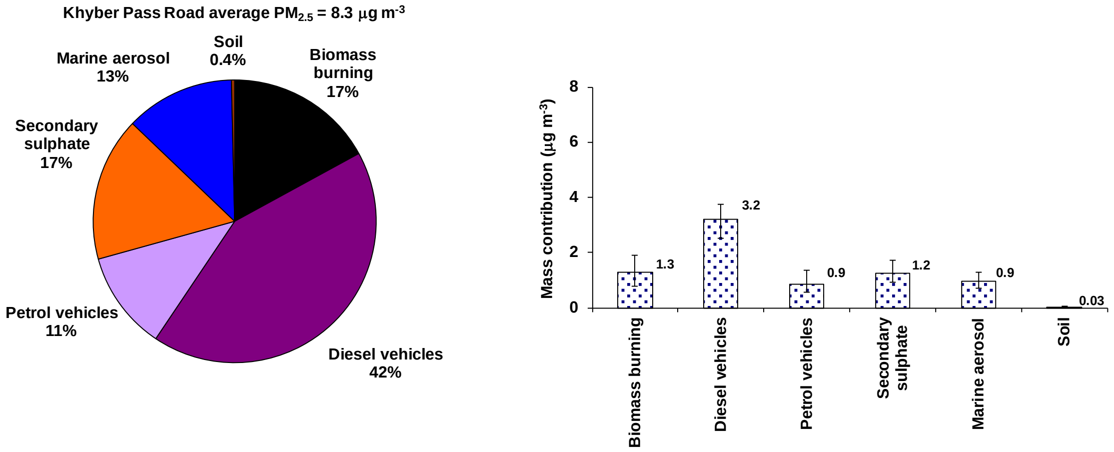

Figure 8.7 Average source contributions to $PM_{2.5}$ (2006 – 2013) at Khyber Pass Road site (showing 5th and 95th confidence intervals in mean concentration derived from the receptor modelling)

The average source contributions estimated by the receptor modelling indicate that motor vehicle emissions are the most significant contributors (combined motor vehicle contribution 53 %) to $PM_{2.5}$ concentrations at Khyber Pass Road, with lesser contributions from biomass burning (17 %), marine aerosol (13 %), secondary sulphate particles (17 %), and a minor crustal matter contribution (>1 %).

Figure 8.8 shows the mass contribution of sources to $PM_{2.5}$ mass for each sample collected at Khyber Pass Road.

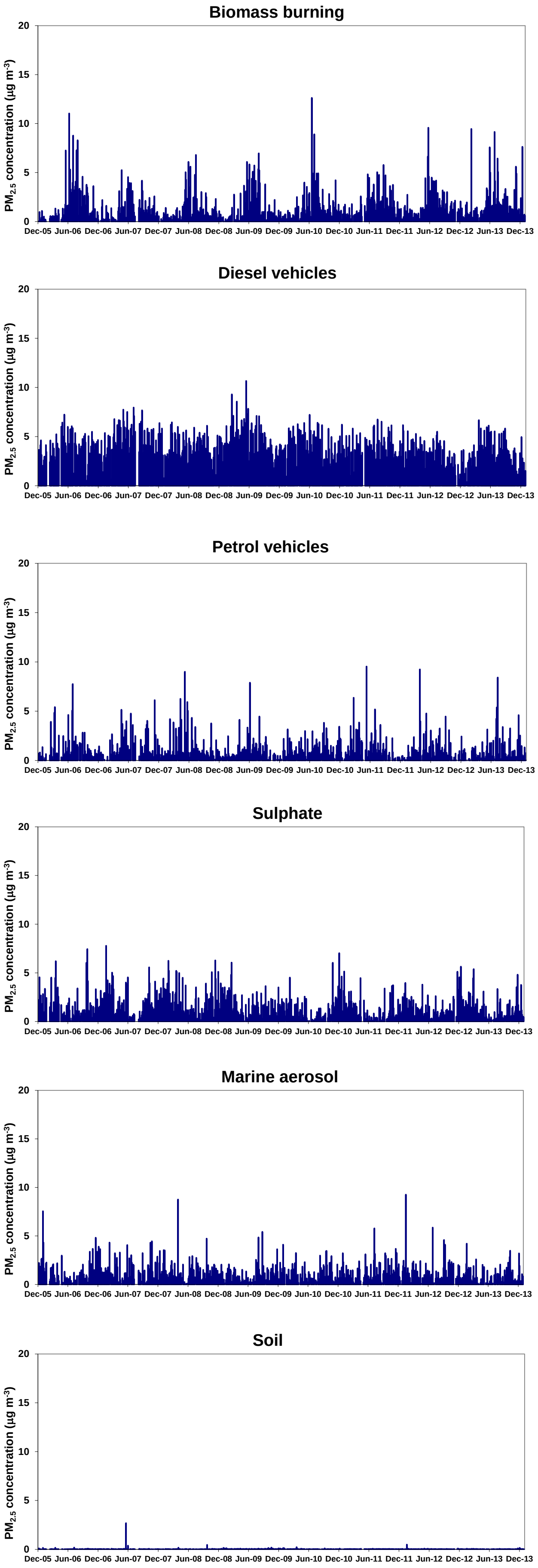

Figure 8.8 Time-series in source contributions to PM$_{2.5}$ mass at Khyber Pass Road

Figure 8.8 shows that peak biomass burning contributions occur during winter and that there was a distinct temporal pattern of peak contributions during winter for the Petrol vehicle source whereas the diesel vehicles source is more constant throughout the year with a slight rise during winter. The source profiles presented in Figure 8.6 indicate that most of the Zn is associated with the Petrol vehicle source and is indicative of the combustion of crankcase lubrication oil along with fuel i.e. a signature for petrol powered vehicles related to engine design. The higher motor vehicle emissions in winter is consistent with colder conditions and less efficient combustion (cold-start engine emissions). The soil source shows a significant peak on 19 May 2007 and is likely to be associated with some local road work or other excavation or disturbance of crustal matter.

8.5.3 Temporal variations in $PM_{2.5}$ source contributions at the Khyber Pass Road site

Figure 8.9 presents the temporal variations in mass contributions at Khyber Pass Road. The primary sources of $PM_{2.5}$ during winter (June-August) at Khyber Pass Road were motor vehicle emissions and biomass burning. Average $PM_{2.5}$ concentrations during winter (11 $\mu g\ m^{-3}$) were higher in winter than spring and summer (7 to 8 $\mu g\ m^{-3}$). Motor vehicle emissions were the primary source of $PM_{2.5}$ during all seasons at Khyber Pass Road, with both the diesel and petrol vehicle contributions lower on the weekends in line with commuter behaviour and commercial activities.

The secondary sulphate and marine aerosol sources showed a winter minimum, while $PM_{2.5}$ contributions from soil did not show any significant seasonality but concentrations were lower on Sunday most likely reflecting lower source contributions on that day associated with anthropogenic activities.

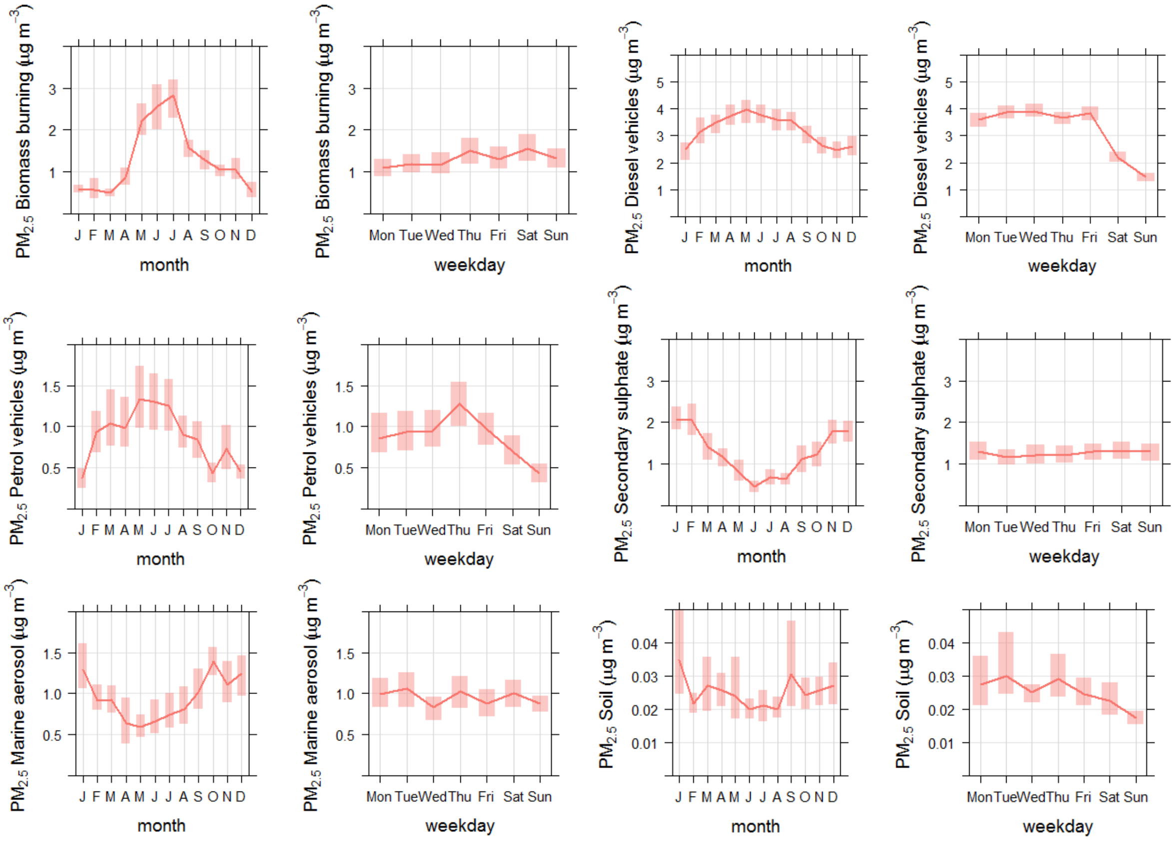

Figure 8.9 Temporal variations (2006-2013) in $PM_{2.5}$ source contributions at Khyber Pass Road (the shaded bars are the 95 percentile confidence limits in the mean)

8.5.4 Trends in $PM_{2.5}$ concentrations and source contributions at Khyber Pass Road

The temporal trends in $PM_{2.5}$ source contributions at Khyber Pass Road were explored using the Thielsen functionality available in *openair*. Figure 8.10 presents the deseasonailsed trend in $PM_{2.5}$ concentrations showing that there was a significant decreasing trend (99.9 % CI) over the monitoring period.

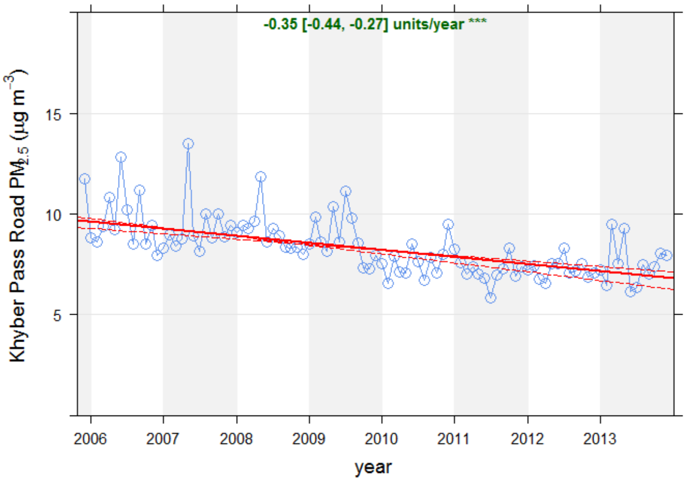

Figure 8.10 Trend in $PM_{2.5}$ concentrations at Khyber Pass Road (statistically significant at the 99.9 % confidence interval)

The trends in $PM_{2.5}$ source contributions are presented in Figure 8.11 and show that the decrease in $PM_{2.5}$ was largely driven by a commensurate decrease in contributions from diesel vehicles along with decreases in secondary sulphate and marine aerosol contributions. It is likely that the fuel formulation and engine emissions has had an influence on diesel emissions concentrations, similarly for secondary sulphate it would appear that the decrease was consistent with a reduction in the sulphur content of fuels as discussed in Chapter 5. There were no significant trends for the soil and petrol vehicle sources. Particulate matter from biomass burning sources showed a steady increase (99.9 % CI) over the monitoring period.

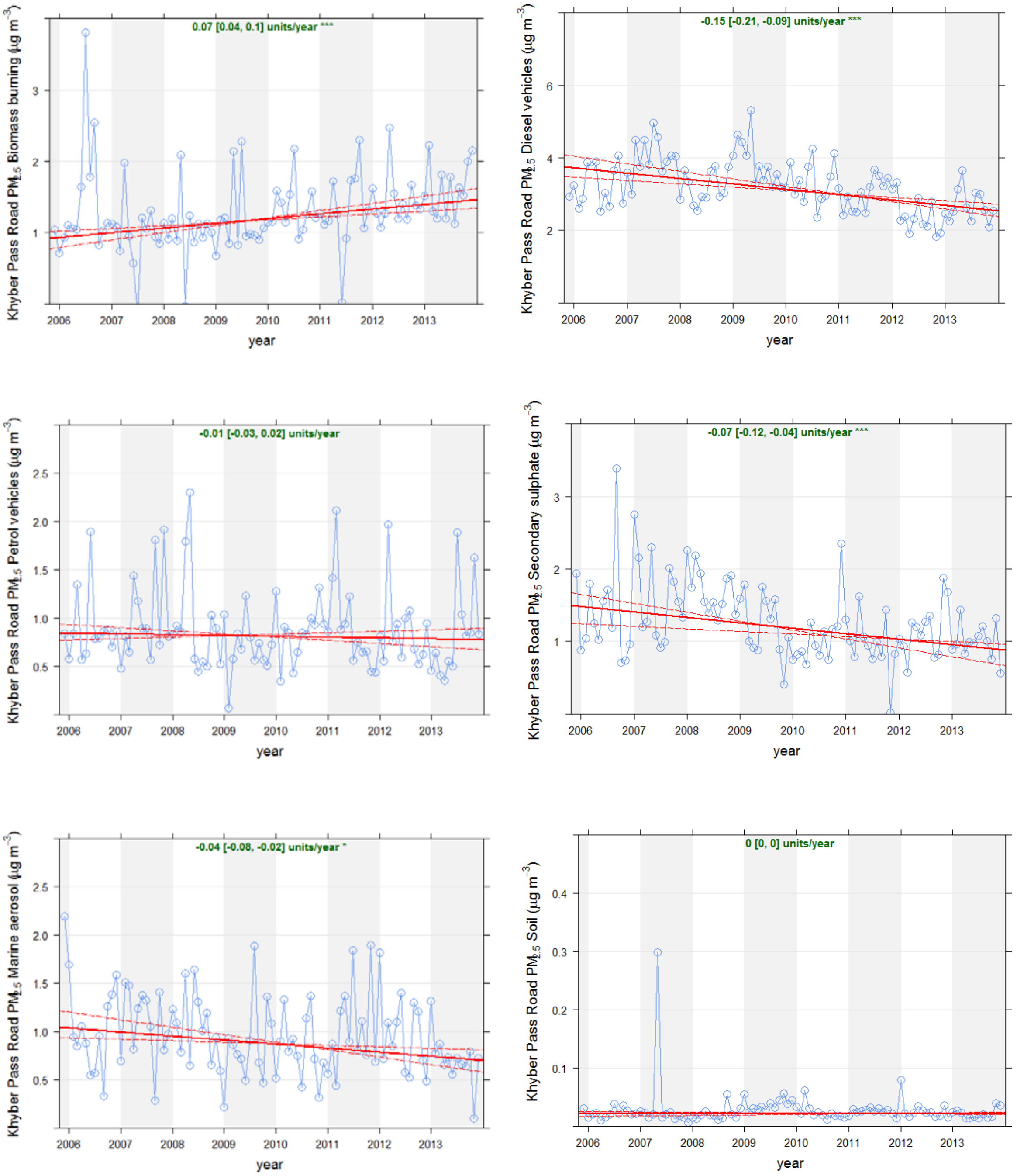

Figure 8.11 Trends in $PM_{2.5}$ source contributions at Khyber Pass Road

8.5.5 Analysis of individual $PM_{2.5}$ events at Khyber Pass Road

Peak $PM_{2.5}$ events during the sampling period at Khyber Pass Road have been chosen for further analysis. Peak $PM_{2.5}$ events are defined as those that were higher than 66 % (17 µg m^{3}) of the AAQG (25 µg m^{-3} 24-hour average). It was found that there were 26 days where $PM_{2.5}$ concentrations were higher than 66 % of the AAQG.

Figure 8.12 presents the mass contributions of individual sources to each of the peak $PM_{2.5}$ days (> 17 µg m^{-3}).

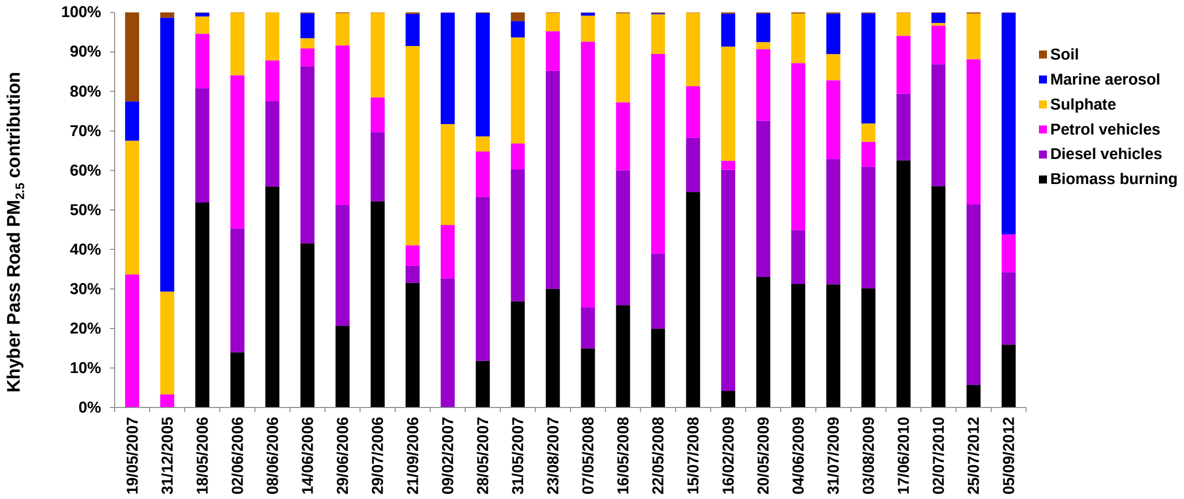

Figure 8.12 Source contributions to peak $PM_{2.5}$ concentrations at Khyber Pass Road

Figure 8.12 shows that motor vehicle emissions and biomass burning sources (during winter) were primarily responsible for elevated $PM_{2.5}$ concentrations at Khyber Pass Road, but that occasional incursions of marine aerosol could also cause elevated concentrations.

8.5.6 Variation of $PM_{2.5}$ source contributions with wind direction at the Khyber Pass Road site

The CPF analysis of the relationship between the source contributions and wind direction is presented and discussed in the following sections.

8.5.6.1 Biomass Burning

Biomass burning source contributions to $PM_{2.5}$ at Khyber Pass Road are considered to be primarily due to emissions from domestic solid fuel fires during winter. Peak contributions are highest on cold, calm winter days under inversion conditions and local cold air drainage (katabatic) flows or with a light southerly wind, particularly for anticyclonic synoptic conditions.

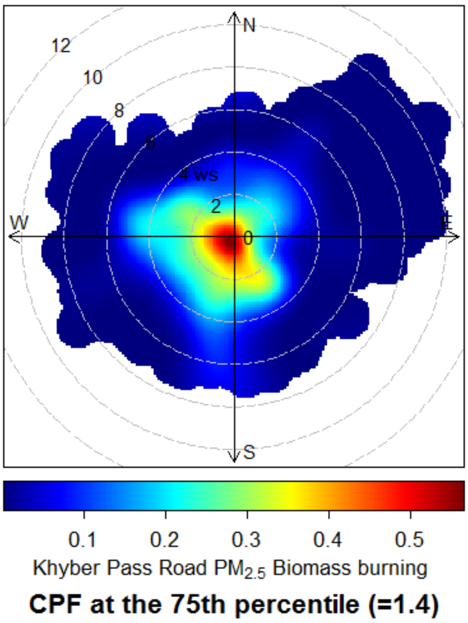

Figure 8.13 Khyber Pass Road $PM_{2.5}$ biomass burning CPF analysis

8.5.6.2 Diesel vehicles

The CPF polar plot for diesel vehicle source contributions to $PM_{2.5}$ shows a distinct south-east component as presented in Figure 8.14 and was most likely aligned with the nearby motorway (SH1) as the major line source.

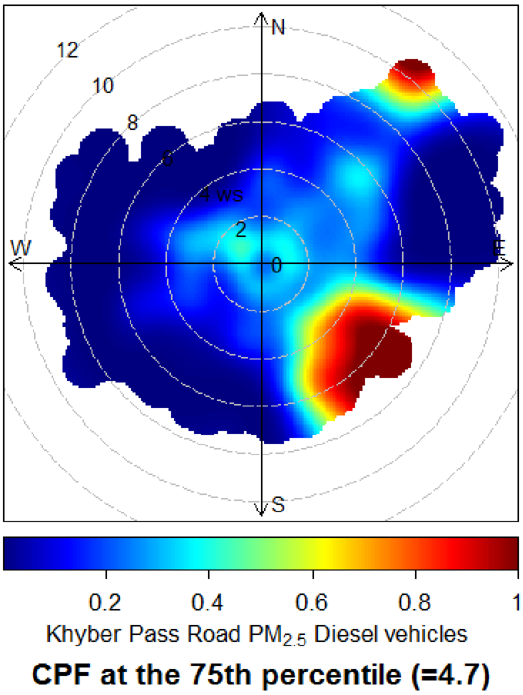

Figure 8.14 Khyber Pass Road $PM_{2.5}$ Diesel vehicle CPF analysis

8.5.6.3 Petrol vehicles

The petrol vehicle source for $PM_{2.5}$ shows a distinct south-southeast component as presented in Figure 8.15 and is most likely aligned with the nearby motorway.

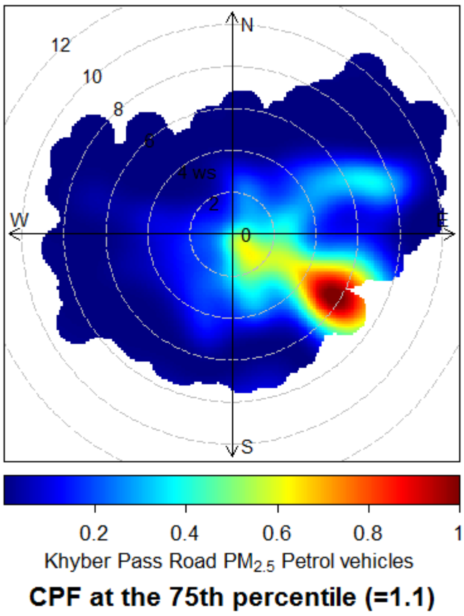

Figure 8.15 Khyber Pass Road $PM_{2.5}$ petrol vehicle CPF analysis

8.5.6.4 Secondary sulphate

The highest 25 percent of $PM_{2.5}$ secondary sulphate contributions were found to primarily originate from the northerly sector (Figure 8.16). It is likely that the primary originating source was emissions from ships moving in and out of the Port of Auckland. Further discussion on the sources of secondary sulphate in the Auckland region is provided in Chapter 5.

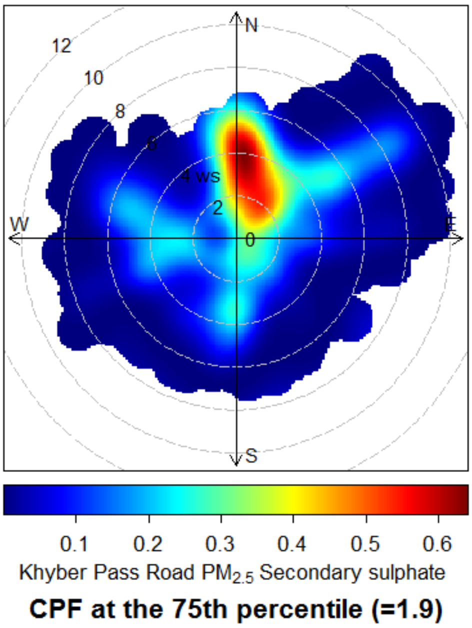

Figure 8.16 Khyber Pass Road $PM_{2.5}$ secondary sulphate CPF analysis

8.5.6.5 Marine aerosol

The Khyber Pass Road $PM_{2.5}$ marine aerosol contribution presented in Figure 8.17 originates from the west-southwest and northeast directions. The most likely source of the $PM_{2.5}$ marine aerosol is the Tasman Sea and Pacific Ocean.

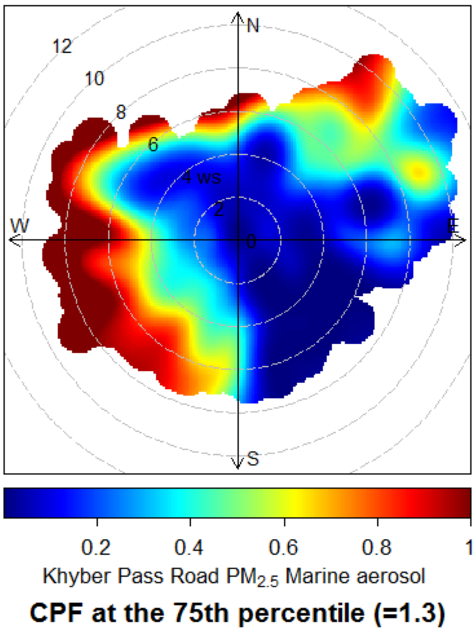

Figure 8.17 Khyber Pass Road $PM_{2.5}$ marine aerosol CPF analysis

8.5.6.6 Crustal matter

The highest crustal matter source contributions to $PM_{2.5}$ were from the northwest sector as presented in Figure 8.18 and was likely that dusts originated from nearby construction and excavation activities.

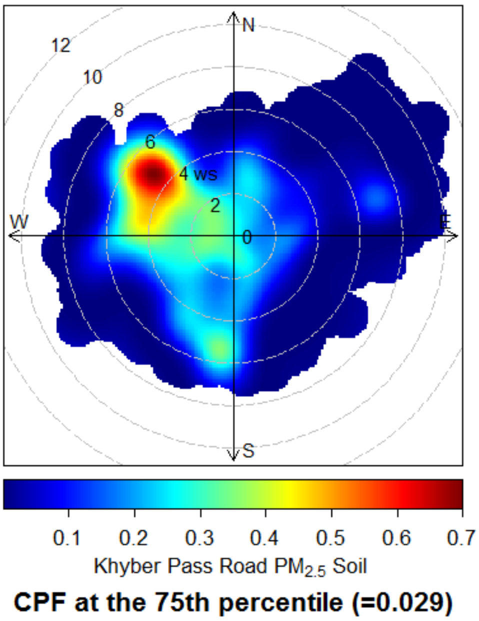

Figure 8.18 Khyber Pass Road PM$_{2.5}$ crustal matter CPF analysis

8.6 ANALYSIS OF PM_{10} SAMPLES FROM KHYBER PASS ROAD

The Khyber Pass Road PM_{10} samples from the Khyber Pass Road monitoring site refer to those PM_{10} samples collected using a Partisol 2000 Sampler (Andersen Instruments Inc.) from December 2005 to December 2013. Gravimetric results for the Partisol PM_{10} samples as presented in Figure 8.19 shows distinct peaks in PM_{10} concentrations during winter months (June – August) but that peak concentrations also occurred at other times throughout the year. The temporal variations in peak PM_{10} concentrations are likely to be explained by variations in source emissions activity. Partisol PM_{10} concentrations exceeded the NES on one occasion at Khyber Pass Road with the concentrations reaching 53 μg m^{-3} on 12 May 2009.

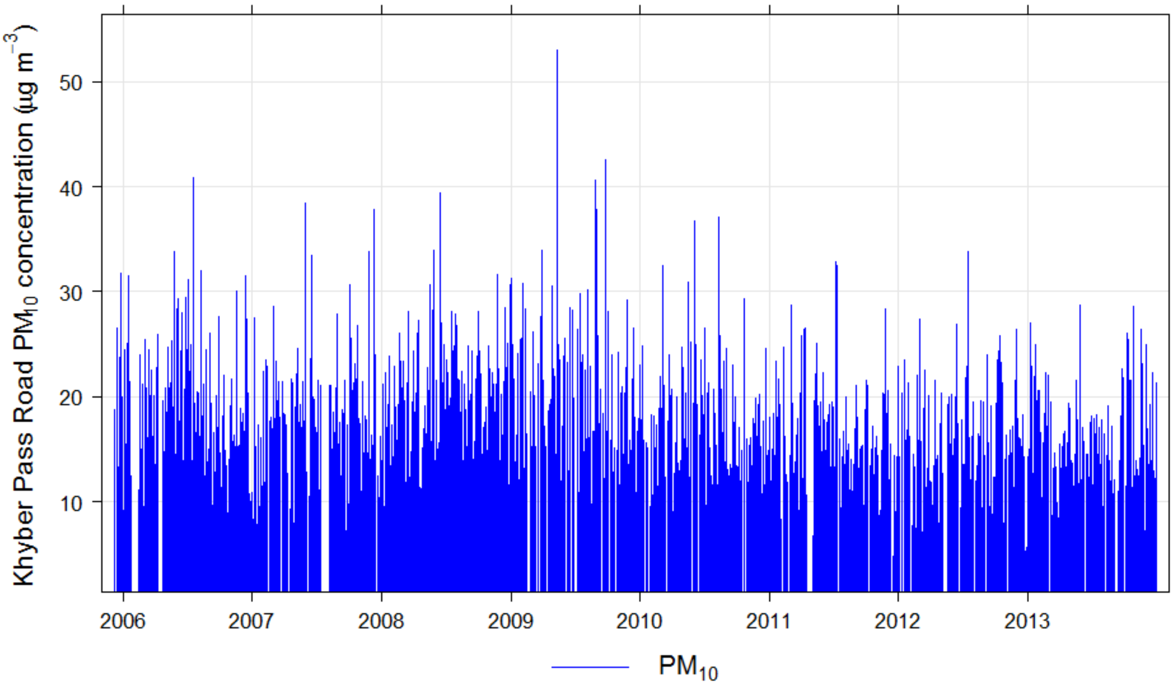

Figure 8.19 Gravimetric results for Partisol PM_{10} at Khyber Pass Road

8.6.1 Composition of PM_{10} at Khyber Pass Road

Elemental concentrations for PM_{10} at Khyber Pass Road are presented in Table 8.3 with a box and whisker plot of the elemental concentrations shown in Figure 8.20.

Table 8.3 Elemental analysis results for Partisol PM_{10} at Khyber Pass Road (892samples)

Species	Average (ng/m^3)	Max (ng/m^3)	Min (ng/m^3)	StdDev (ng/m^3)	Median (ng/m^3)	Av LOD (ng/m^3)	#>LOD
PM_{10} ($\mu g/m^3$)	**18**	**53**	**5**	**6**	**17**		
H	143	823	0	99	127	45	765
BC	4802	14964	0	2232	4520	193	891
Na	2071	7900	0	1258	1899	445	854
Mg	198	864	0	108	182	36	877
Al	122	2003	0	155	85	16	877
Si	317	5924	35	382	230	11	892
P	19	136	0	19	15	17	504
S	393	1946	7	177	363	13	892
Cl	3097	12127	1	1988	2780	7	891
K	119	690	4	58	111	7	891
Ca	203	3922	6	178	174	7	891
Sc	3	49	0	4	2	10	64
Ti	15	208	0	17	12	8	617
V	2	36	0	3	0	10	64
Cr	2	24	0	3	0	8	110
Mn	6	35	0	5	5	7	403
Fe	420	1713	6	227	378	6	892
Co	6	54	0	7	3	13	164
Ni	2	56	0	3	1	9	94
Cu	17	69	0	11	16	9	682
Zn	24	297	0	28	17	11	612
Ga	3	30	0	5	0	18	54
Ge	4	37	0	6	0	23	60
As	5	53	0	8	0	29	66
Se	7	64	0	11	0	36	76
Br	11	74	0	15	5	44	106
Rb	14	169	0	21	0	73	73
Sr	19	200	0	29	0	93	86
Mo	45	529	0	79	0	150	91
I	12	105	0	16	4	31	145
Ba	23	89	0	18	22	32	339
Hg	11	114	0	18	0	66	35
Pb	12	111	0	21	0	80	36

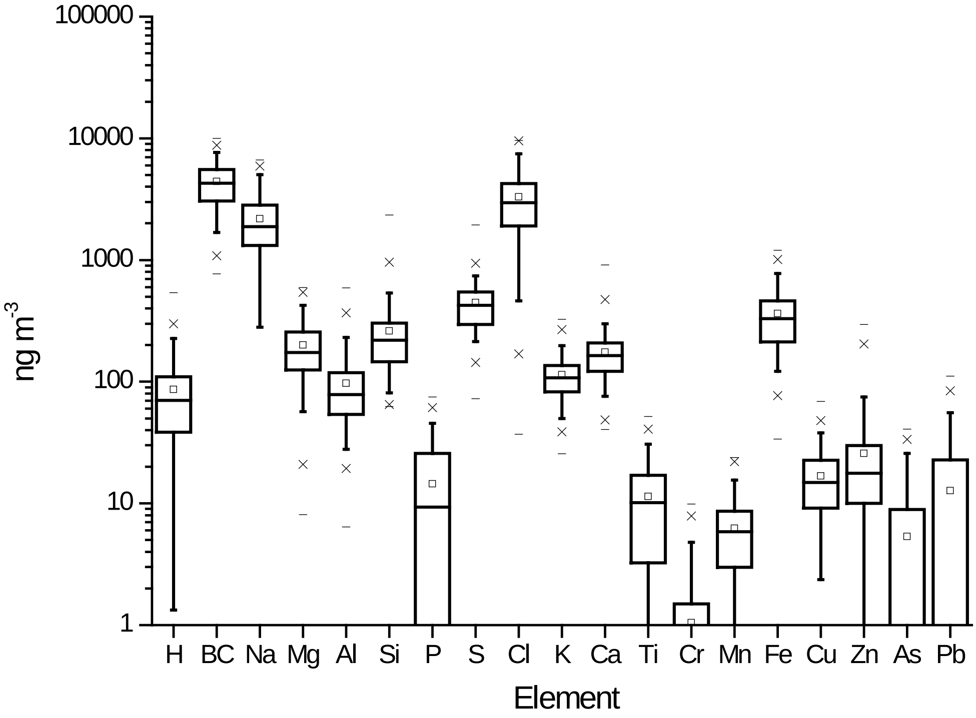

Figure 8.20 Box and whisker plot of PM_{10} elemental concentrations at Khyber Pass Road (logarithmic scale)

Table 8.3 shows that that a number of measured species were generally close to or below the limits of detection over all samples. Carbonaceous species (represented by BC), sodium and chlorine were found to dominate PM_{10} elemental mass concentrations indicating that combustion processes and marine aerosol are important contributors to ambient PM_{10} at Khyber Pass Road. A scatterplot matrix of the species in Table 8.3 is presented in Appendix 4.

8.6.2 Source contributions to PM_{10} at Khyber Pass Road

Six primary source contributors were determined from the PMF receptor modelling analysis of PM_{10} elemental composition at Khyber Pass Road. These are identified as presented in Table 8.4 along with the mass of PM_{10} and elemental species associated with each source.

Table 8.4 Elemental composition of source profiles and contribution to PM_{10} at Khyber Pass Road

	Factor 1	Factor 2	Factor 3	Factor 4	Factor 5	Factor 6
Species	**Biomass burning (ng/m^3)**	**Diesel vehicles (ng/m^3)**	**Petrol vehicles (ng/m^3)**	**Sulphate (ng/m^3)**	**Marine aerosol (ng/m^3)**	**Soil (ng/m^3)**
PM_{10}	**1430**	**4330**	**580**	**1700**	**7570**	**1440**
H	93	23	0	0	14	8
BC	639	2941	103	349	433	198
Na	92	17	19	98	1777	60
Mg	11	9	1	11	147	16
Al	2	11	4	9	15	76
Si	0	59	12	23	33	182
S	26	29	6	168	150	12
Cl	24	124	23	99	2723	81
K	16	17	3	4	59	14
Ca	6	48	7	6	69	52
Ti	1	4	1	0	0	8
Mn	0	2	1	0	1	2
Fe	59	226	15	6	35	76
Cu	2	11	1	1	1	0
Zn	2	5	16	0	1	1
Ba	1	12	0	2	9	1

Table 8.4 represents the summary results for a reiterative process that examines the effect of each species on the PMF receptor modelling process using the modelling diagnostics presented in Appendix 4. Species that were poorly modelled (slope, $r^2 < 0.6$) have been removed from the analyses unless considered vital for source identification. The source contributors identified in Table 8.4 were found on average to explain 94 % of PM_{10} gravimetric mass. Figure 8.21 presents the source profiles extracted from the PMF analysis of Khyber Pass Road PM_{10} data.

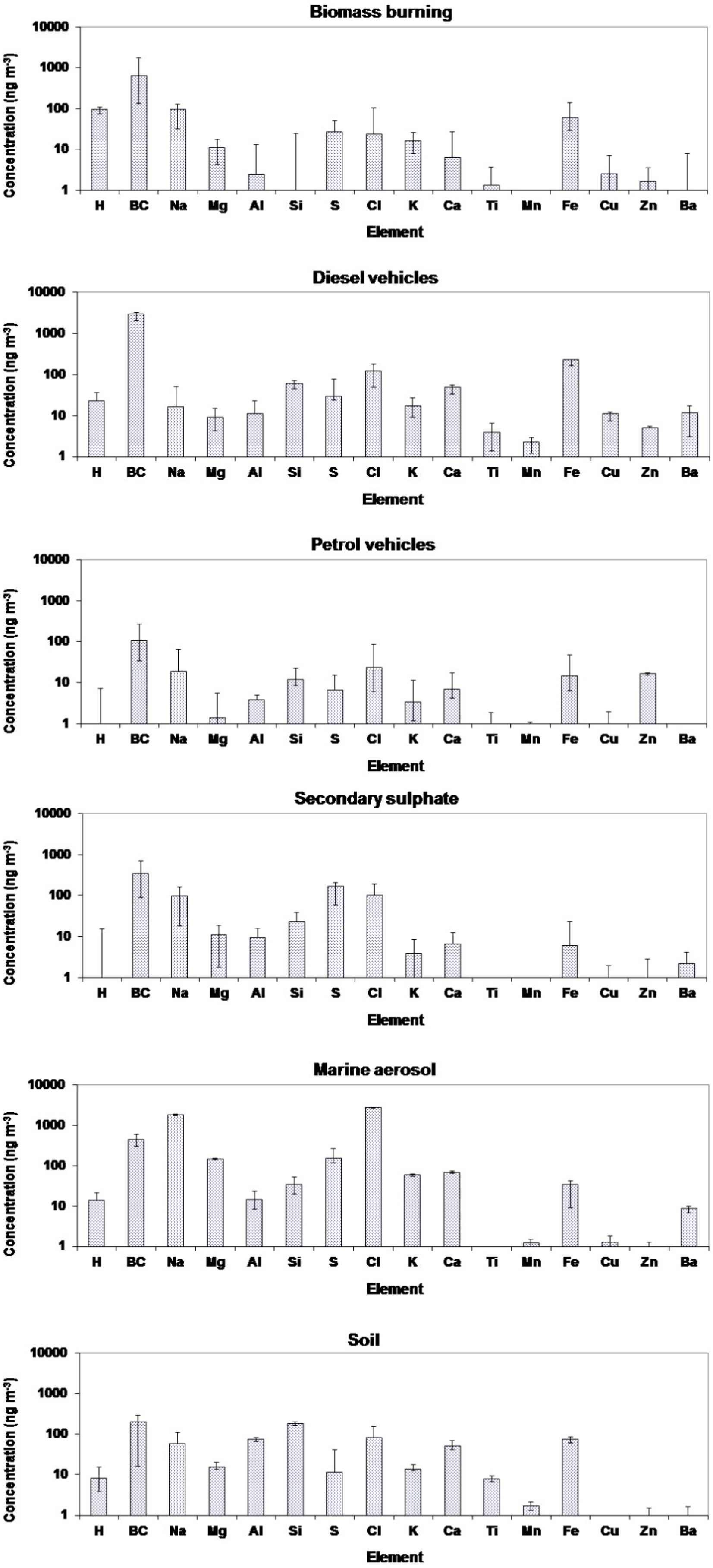

Figure 8.21 Source profiles and elemental concentrations for PM_{10} at Khyber Pass Road site (showing 5th and 95th confidence intervals in mean concentration derived from the receptor modelling)

- The first source is from biomass burning due to the association between H, BC and K.
- The second factor has been identified as originating from diesel vehicle emissions and is largely composed of H, BC, Ca, Fe, most of the Cu and Ba with some of the Zn
- The third source contribution, Petrol vehicles, has identified as another motor vehicle source emission due to the grouping of BC, Ca, Fe and most of the Zn.
- The fourth factor, Sulphate, has been identified as a secondary aerosol source due to the predominance of S.
- The fifth source profile is dominated by Na and Cl and represents the contribution from marine aerosol.
- The sixth factor, Soil is from crustal matter and/or road dust.

The sources identified for PM_{10} are similar to those extracted for $PM_{2.5}$ at Khyber Pass Road. With respect to the two motor vehicle sources it would appear that the diesel vehicle source has a significant road and brake dust component associated (Al, Si, Ca, Fe, Cu and Ba) and therefore represents the general contribution of motor vehicle emissions in the Khyber Pass Road area, whereas the petrol vehicles is thought to represent tailpipe emissions from petroleum fuelled vehicles that are burning a considerable amount of lubrication oil (high Zn content). Figure 8.22 presents the average source contributions (2006-2013) to PM_{10} concentrations and includes the standard deviations of the average mass contributions from each of the sources indicating the variability in source strength.

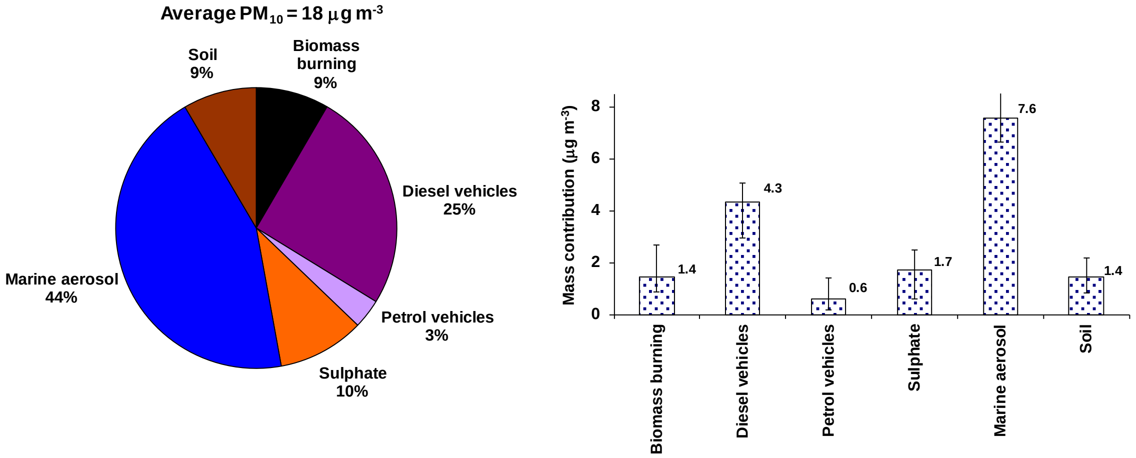

Figure 8.22 Average source contributions to PM_{10} (2006-2009) at Khyber Pass Road site (showing 5th and 95th confidence intervals in mean concentration derived from the receptor modelling)

The average source contributions estimated by the receptor modelling indicate that motor vehicle emissions and marine aerosol are the most significant contributors (28 % and 44 % respectively) to PM_{10} concentrations at Khyber Pass Road, with lesser contributions from biomass burning (9 %), secondary sulphate particles (10 %), and crustal matter (9 %). Figure 6.11 shows the mass contribution of sources to PM_{10} mass for each sample collected at Khyber Pass Road. The temporal variation indicates that PM_{10} mass is dominated by motor vehicle sources during winter, and the marine aerosol source can contribute significantly all year. There were significant contributions from the soil (crustal matter) source at times from mid-2008 to mid-2010 and this was likely to be related to local demolition and construction activities. For example major road works and replacement of the Newmarket viaduct, construction of a new rail station nearby and construction on the Mt Eden Prison site occurred during that time period. Also later in 2013 there was major demolition work undertaken at the Lion Breweries site across Khyber road from the monitoring station.

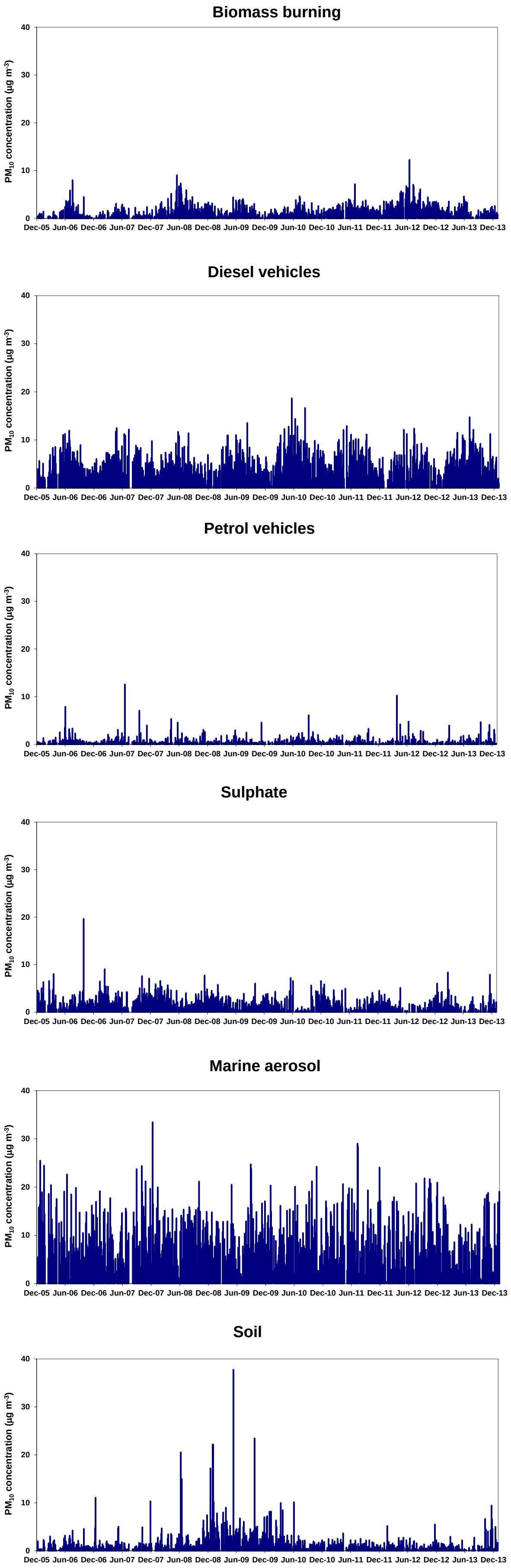

Figure 8.23 Time-series of source contributions to PM_{10} mass at Khyber Pass Road

8.6.3 Temporal variations in PM_{10} source contributions at the Khyber Pass Road site

Figure 8.24 presents the temporal variations in mass contributions at Khyber Pass Road. The primary sources of $PM_{2.5}$ during winter (June-August) at Khyber Pass Road were motor vehicle emissions and biomass burning. Average PM_{10} concentrations during winter (20 μg m^{-3}) were higher in winter than spring and summer (17 - 18 μg m^{-3}). Motor vehicle emissions and marine aerosol were the primary sources of PM_{10} during all seasons at Khyber Pass Road, with both the diesel and petrol vehicle contributions lower on the weekends in line with commuter behaviour and commercial activities.

The secondary sulphate and marine aerosol sources showed a winter minimum, while $PM_{2.5}$ contributions from soil did not show any significant seasonality but concentrations were lower on Sunday most likely reflecting lower source emissions on that day indicative that the crustal matter source was primarily generated by anthropogenic activities (construction, excavation).

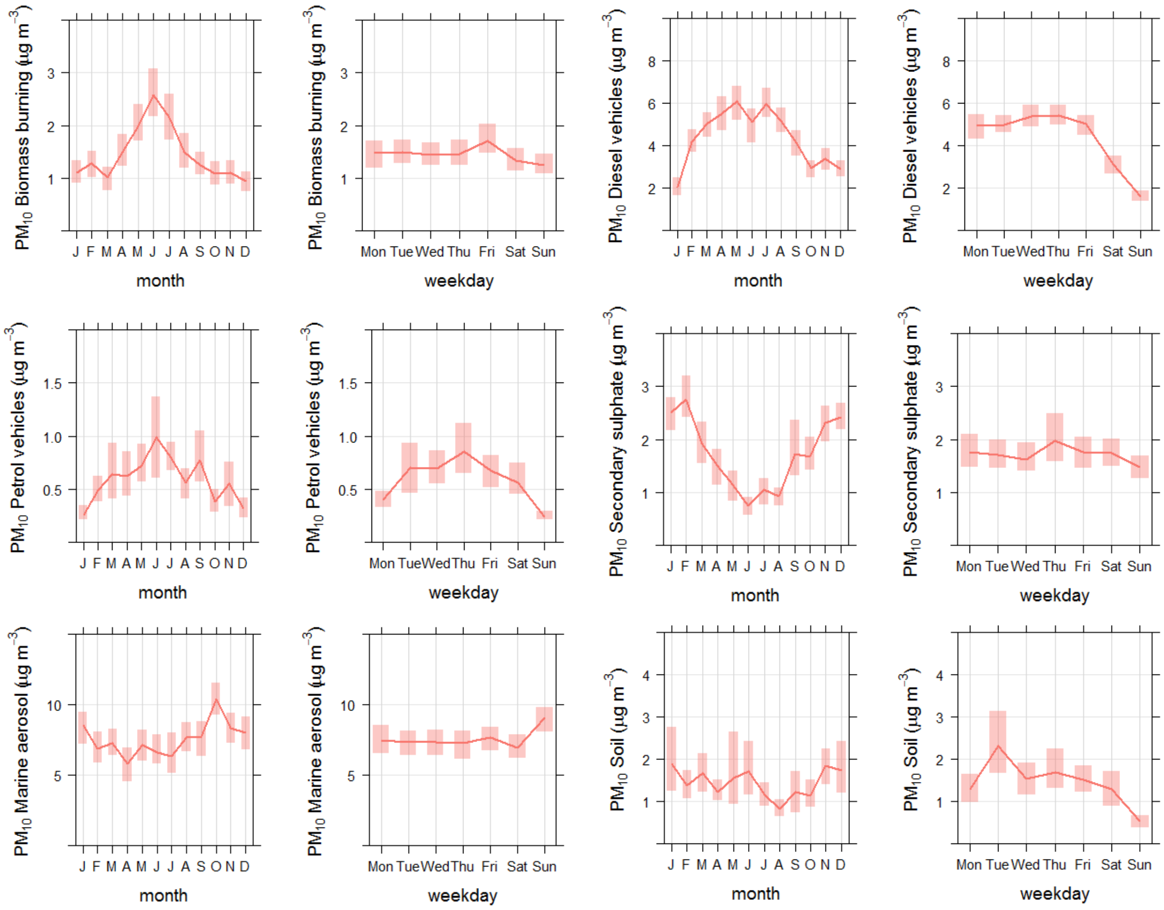

Figure 8.24 Temporal variations (2006-2013) in PM_{10} source contributions at Khyber Pass Road (the shaded bars are the 95 percentile confidence limits in the mean)

8.6.4 Trends in PM_{10} concentrations and source contributions at Khyber Pass Road

The temporal trends in PM_{10} source contributions at Khyber Pass Road were explored using the Thielsen functionality available in *openair*. Figure 8.6.7 presents the deseasonailsed trend in PM_{10} concentrations showing that there was a significant decreasing trend (99.9 % CI) over the monitoring period.

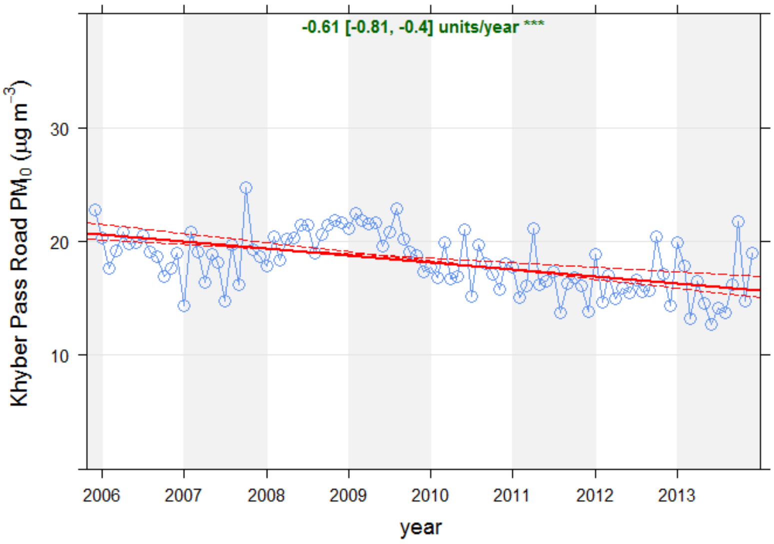

Figure 8.25 Trend in PM_{10} concentrations at Khyber Pass Road (statistically significant at the 99.9 % confidence interval)

The trends in PM_{10} source contributions are presented in Figure 8.26 and show that the decrease in PM_{10} was primarily due to decreases in contributions from marine aerosol and secondary sulphate contributions. The latter was consistent with a reduction in the sulphur content of fuels as discussed in Chapter 5. While it is likely that the fuel formulation and engine (tailpipe) emissions has had an influence on (decreasing as for $PM_{2.5}$ diesel vehicle source contributions), interestingly contributions from this source to PM_{10} appear to have a small but statistically significant (95 % CL). This increase may related to increases in the road dust component (coarse particles) There were no significant trends evident for the soil and petrol vehicle sources. Particulate matter from biomass burning sources showed a steady increase (99.9 % CI) over the monitoring period.

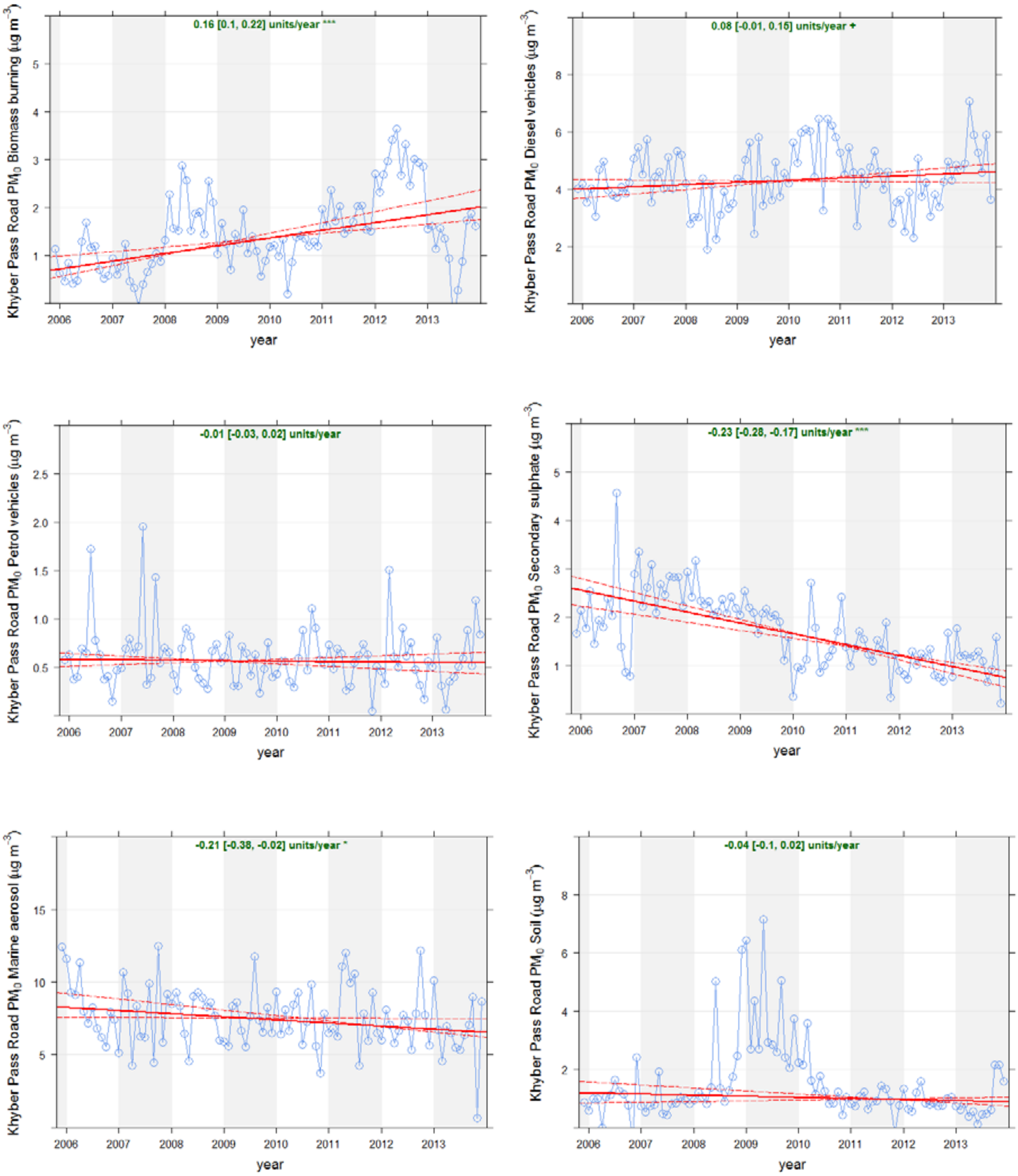

Figure 8.26 Trends in PM$_{10}$ source contributions at Khyber Pass Road

8.6.5 Analysis of individual PM$_{10}$ events at Khyber Pass Road

Peak PM$_{10}$ events during the sampling period at Khyber Pass Road have been chosen for further analysis. Peak PM$_{10}$ events are defined as those that were higher than 66 % (33 µg m^{-3}) of the NES (50 µg m^{-3} 24-hour average). It was found that there were 19 days where PM$_{10}$ concentrations were higher than 66 % of the NES.

Figure 8.27 presents the mass contributions of individual sources to each of the peak PM$_{10}$ days (> 33 µg m^{-3}).

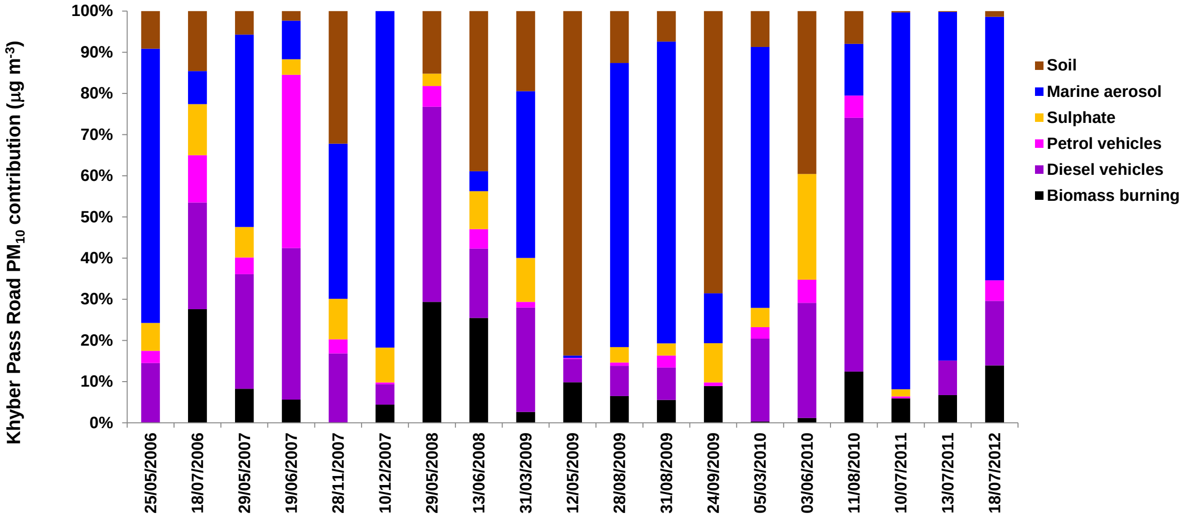

Figure 8.27 Source contributions to peak PM_{10} concentrations at Khyber Pass Road

Figure 8.27 shows that contributions from the coarse particle sources, marine aerosol and crustal matter have a significant influence on peak PM_{10} although at times motor vehicle emissions and biomass burning sources (during winter) were primarily responsible for elevated PM_{10} concentrations at Khyber Pass Road.

8.6.6 Variation of PM_{10} source contributions with wind direction at the Khyber Pass Road site

The CPF analysis of the relationship between the source contributions and wind direction is presented and discussed in the following sections.

8.6.6.1 Biomass Burning

As with $PM_{2.5}$, biomass burning source contributions to PM_{10} at Khyber Pass Road were primarily due to emissions from domestic solid fuel fires during winter. Peak contributions are highest on cold, calm winter days under inversion conditions and local cold air drainage (katabatic) flows or with a light southerly wind, particularly for anticyclonic synoptic conditions.

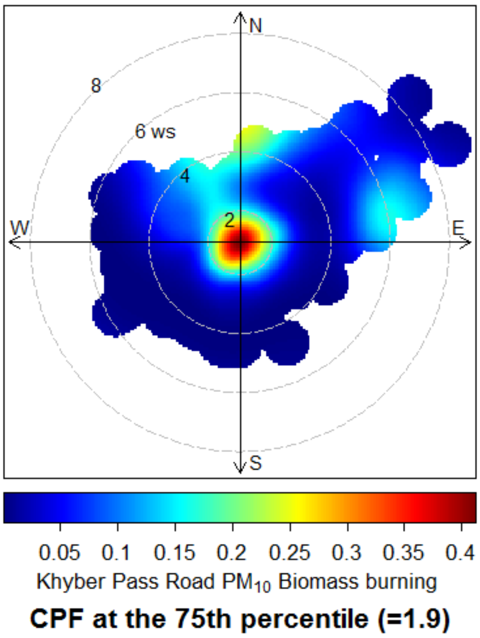

Figure 8.28 Khyber Pass Road PM_{10} biomass burning CPF analysis

8.6.6.2 Diesel vehicles

The CPF polar plot for diesel vehicle source contributions to PM_{10} shows a distinct south-east component as presented in Figure 8.29 and was most likely aligned with the nearby motorway (SH1) as the major line source.

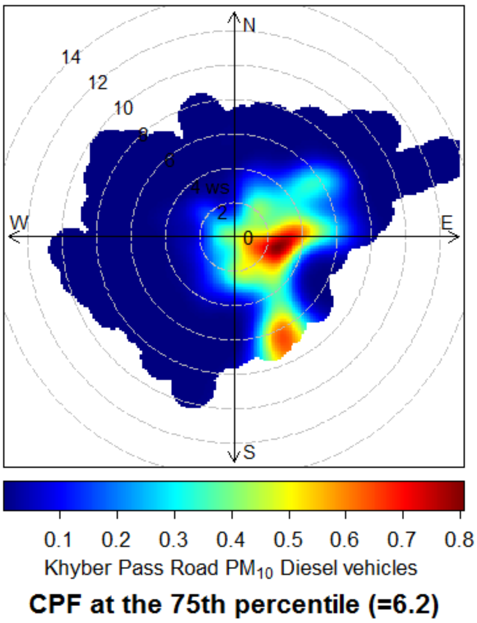

Figure 8.29 Khyber Pass Road PM_{10} Diesel vehicle CPF analysis

8.6.6.3 Petrol vehicles

The petrol vehicle source for PM_{10} shows a distinct south-southeast component as presented in Figure 8.30 and is most likely aligned with the nearby motorway.

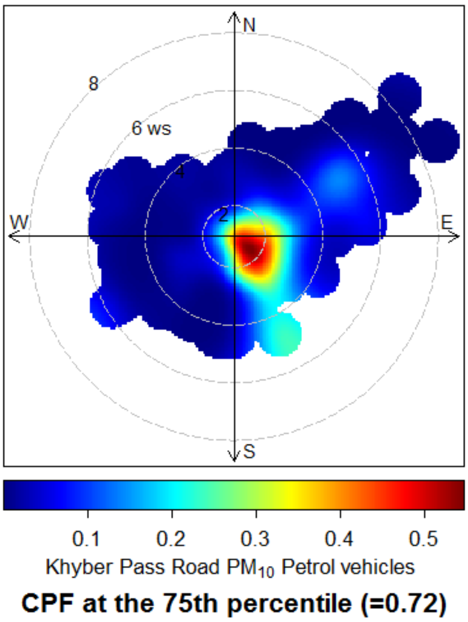

Figure 8.30 Khyber Pass Road PM_{10} petrol vehicle CPF analysis

8.6.6.4 Secondary sulphate

The highest 25-percentile of PM_{10} secondary sulphate contributions were found to primarily originate from the northerly sector (Figure 8.31). It is likely that the primary originating source was emissions from ships moving in and out of the Port of Auckland. Further discussion on the sources of secondary sulphate in the Auckland region is provided in Chapter 5.

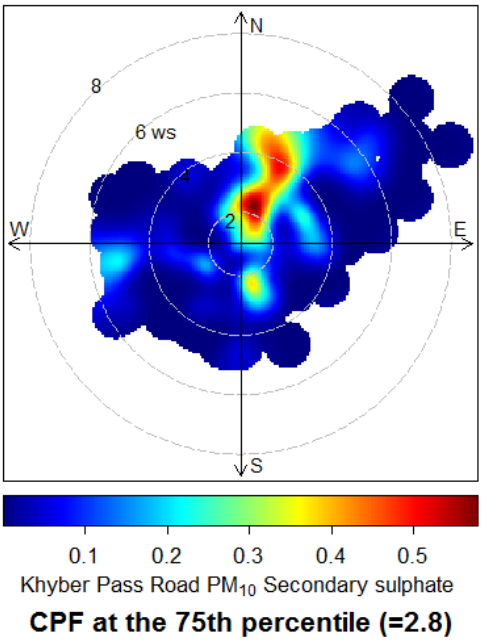

Figure 8.31 Khyber Pass Road PM_{10} secondary sulphate CPF analysis

8.6.6.5 Marine aerosol

The Khyber Pass Road PM_{10} marine aerosol contribution presented in Figure 8.32 originates from the west-southwest and northeast directions. The most likely source of the PM_{10} marine aerosol is the Tasman Sea and Pacific Ocean.

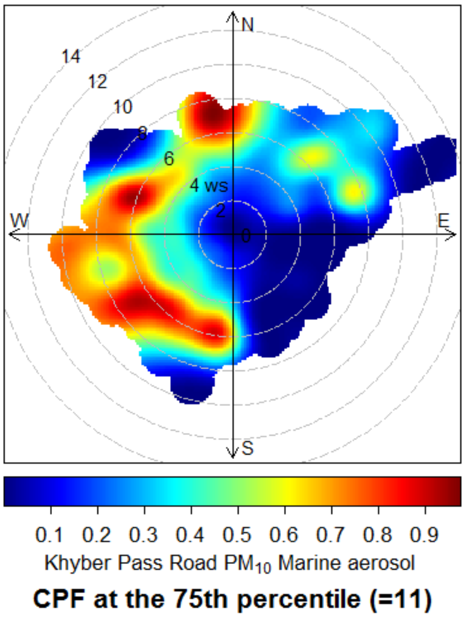

Figure 8.32 Khyber Pass Road PM_{10} marine aerosol CPF analysis

8.6.6.6 Crustal matter

The highest crustal matter source contributions to PM_{10} were from the northwest sector as presented in Figure 8.33 and was likely that dusts originated from nearby construction and excavation activities.

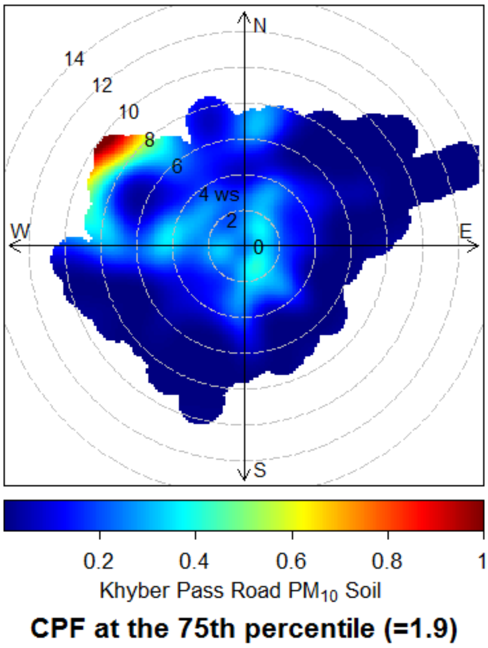

Figure 8.33 Khyber Pass Road PM_{10} crustal matter CPF analysis

8.7 SUMMARY OF KHYBER PASS ROAD $PM_{2.5}$ AND PM_{10} RECEPTOR MODELLING RESULTS

Since the $PM_{2.5}$ and PM_{10} Partisol samplers at Khyber Pass Road were working on a satellite-and-hub system, samples were collected on an alternating one-day-in-three sampling regime. Therefore no direct comparison can be made between $PM_{2.5}$ and PM_{10} samples. Instead a comparison of average mass contributions and source profiles is presented and discussed. Table 8.5 shows the average source contributions to $PM_{2.5}$ and PM_{10} at Khyber Pass Road and Figure 8.34 presents the corresponding pie graphs.

Table 8.5 Average source mass contributions (± modelled standard deviation) derived for $PM_{2.5}$ and PM_{10} at Khyber Pass Road

	Biomass burning $\mu g/m^3$	**Diesel vehicles $\mu g/m^3$**	**Petrol vehicles $\mu g/m^3$**	**Sulphate $\mu g/m^3$**	**Marine aerosol $\mu g/m^3$**	**Soil $\mu g/m^3$**
$PM_{2.5}$	1.3±0.3	3.2±0.3	0.9±0.3	1.3±0.3	0.9±0.2	0.03±0.02
PM_{10}	1.4±0.4	4.3±0.4	0.6±0.4	1.7±0.5	7.6±0.5	1.4±0.4

Average mass concentrations of particles from biomass burning were found to be similar for $PM_{2.5}$ and PM_{10} which is the expected result for the predominantly fine particle combustion source.

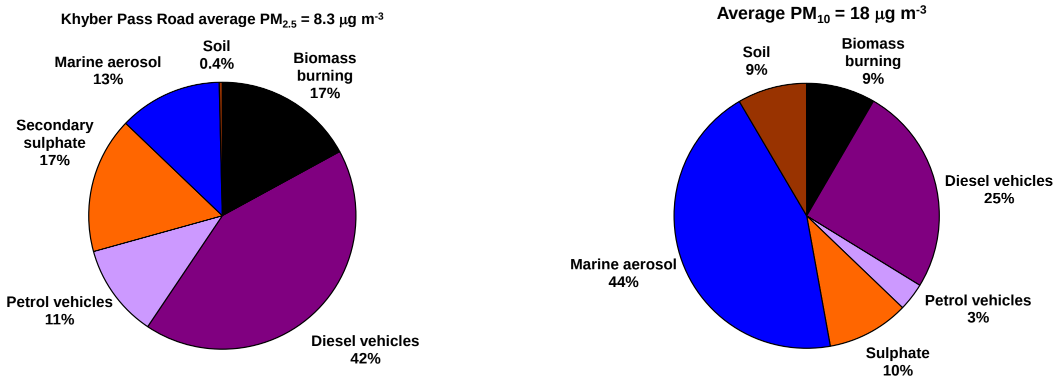

Figure 8.34 Average source contributions at Khyber Pass Road for (left) $PM_{2.5}$ and; (right) PM_{10} results

Mass concentrations for the PM_{10} diesel vehicles source were higher than that for the corresponding $PM_{2.5}$ diesel vehicles source indicating that some coarse particle ($PM_{10-2.5}$) mass is associated with the PM_{10} diesel vehicles source. A probable explanation is the covariant inclusion of coarse particle road dust with the motor vehicle fine particle exhaust emissions and this is supported in part by the presence of Cu and Ba (wear of brake linings) in the PM_{10} diesel vehicles source elemental profile. The PM_{10} and $PM_{2.5}$ petrol vehicle source mass contributions were similar which implies the source is primarily composed of $PM_{2.5}$ and therefore directly related to tailpipe emissions associated with the combustion of lubricating oil (hence the zinc content).

Both the marine aerosol and soil sources are clearly dominated by the coarse particle fraction and therefore the relative contributions to PM_{10} are significantly higher than for $PM_{2.5}$.The difference between the average PM_{10} and $PM_{2.5}$ concentrations at Khyber Pass Road is largely explained by the coarse particle contribution from the road dust component of the motor vehicle source along with marine aerosol and crustal matter. The mass concentrations for secondary sulphate were slightly higher for PM$_{10}$ than PM$_{2.5}$ samples, probably for the same reasons described for the Takapuna and Queen Street results.

8.8 ANALYSIS OF PM$_{10}$ EXCEEDENCE EVENT AT KHYBER PASS ROAD

Air quality monitoring recorded an exceedence of NES for PM$_{10}$ (50 μg m^{-3}) at the Khyber Pass Road air quality monitoring site on 7 March 2013. The exceedence coincided with the Auckland Arts Festival event 'Breath of the Volcano' at Auckland Domain (approximately 1 km from the Khyber Pass Road site) that was a large pyrotechnics (fireworks) display. Fireworks events are a regular feature of public displays and celebrations with at least biannual events in Auckland (Guy Fawkes and New Year Eve) plus others as such as large sports fixtures.

Continuous PM$_{10}$ (BAM) monitoring data from the Auckland Council Khyber Pass air quality monitoring site shows that the PM10 peak occurred during the evening and was transient over approximately 2 hours (8pm – 10pm) as shown in Figure 8.35. The data showed that the PM$_{10}$ concentration for 7 March 2013 was 77 mg m^{-3} (24-hour average) while the corresponding PM$_{2.5}$ concentration was 38 mg m^{-3} (24-hour average).

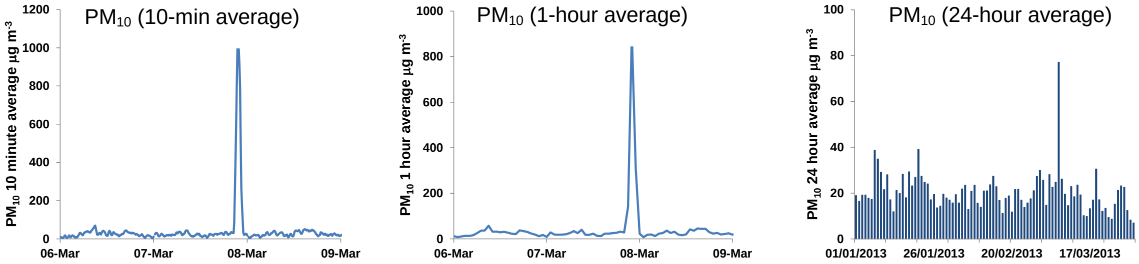

Figure 8.35 Time series plot of PM$_{10}$ (BAM) at the Khyber Pass Road site

For the analysis of likely sources contributing to the PM$_{10}$ exceedence on 7 March 2013, the PM$_{2.5}$ elemental data from the Khyber Pass Road site has been used as only a PM$_{2.5}$ sample was collected at the Khyber Pass Road site on the day in question. Pyrotechnic displays use a variety of chemical compounds to achieve the desired effects for light, colour and sound (detonation). These chemicals have distinct elemental signatures and particulate matter emissions to the atmosphere associated with pyrotechnical displays are distinguishable from other sources by the combination of elements present i.e. there is a distinct chemical 'fingerprint'. Potassium is a primary elemental constituent of fireworks along with sulphur. The presence of other elemental species depends on the nature of the fireworks, with the colours of a pyrotechnic display being the main determinant of composition.

The effects of pyrotechnic displays on the elemental composition of particulate matter collected at the various monitoring sites have been identified as shown in Figure 8.36, which presents a time-series plot for PM$_{2.5}$ potassium concentrations at all Auckland sites.

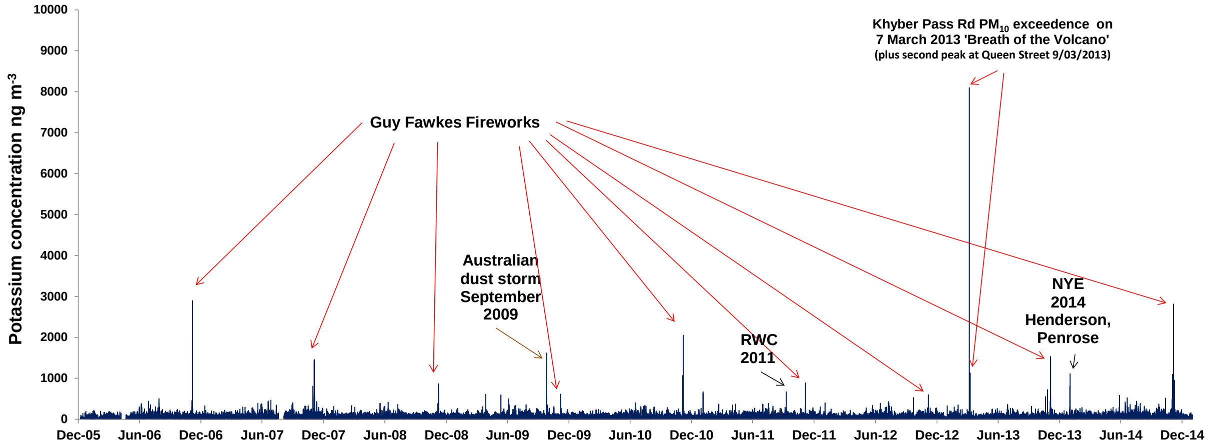

Figure 8.36 Time series plot of $PM_{2.5}$ potassium at all Auckland sites (RWC = Rugby World Cup)

The time-series plot in Figure 8.36 shows that on or around 5 November each year there are significant peaks (note the logarithmic scale) in potassium concentrations due to fireworks associated with Guy Fawkes celebrations. Occasionally New Year's Eve celebrations can also impact on a monitoring site, and for the Kingsland site, activities at Mt Eden Stadium may also feature.

The elemental composition record for Khyber Pass Road is no exception and demonstrates the influence of fireworks-related particulate matter that occasionally impacts on the monitoring site. The extent of the impact is dependent on the location of the fireworks event and the prevailing wind speed and direction at the time, which may or may not carry fireworks emissions across an air quality monitoring site. Fireworks emissions at height are likely to disperse significantly before reaching ground level and impacting at a receptor (air quality monitoring) site. Most of these events occur on or around November 5 as demonstrated in the concentration time series presented in Figure 8.37 for potassium in $PM_{2.5}$ particles collected at the Khyber Pass Road air quality monitoring site.

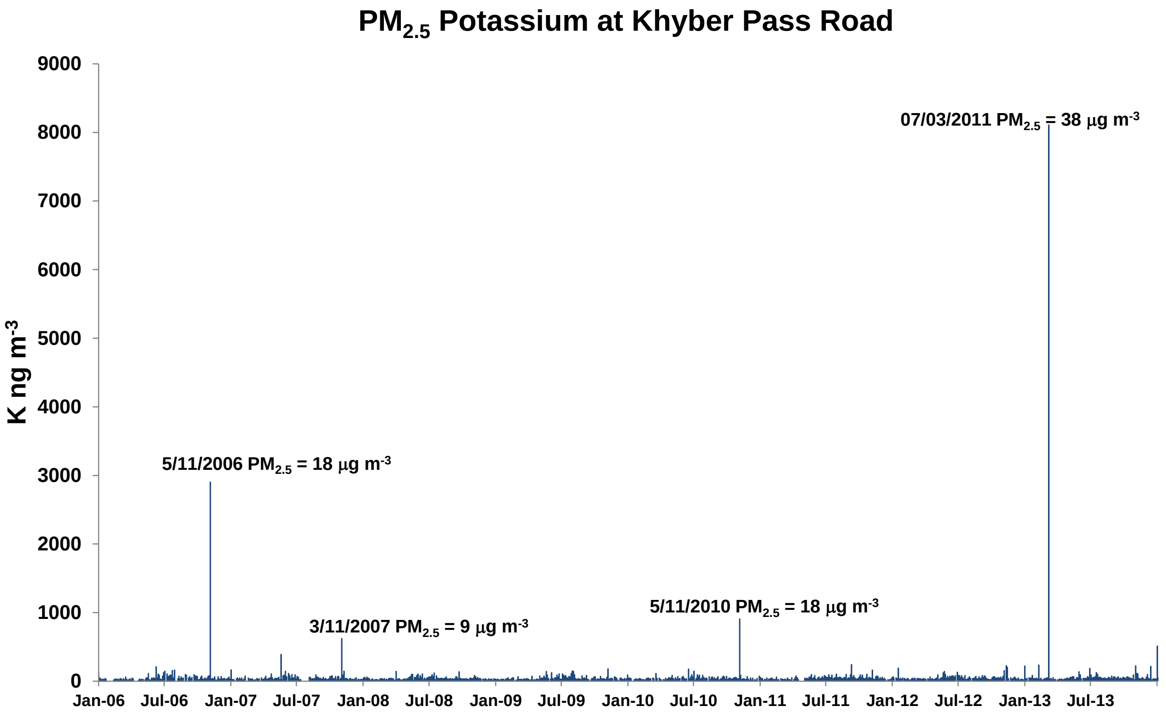

Figure 8.37 Time series plot of $PM_{2.5}$ potassium concentrations at Khyber Pass Road

The potassium concentration data suggests that there was a significant event on 7 March 2013 that resulted in the highest potassium concentration recorded at the site to date. Data for other elements are presented in Figure 8.38 which shows that there were significant concurrent concentration spikes on 7 March 2013 for other elemental species. For example, elemental species used as chemical colorants in fireworks displays are presented in Table 8.6.

Table 8.6 Metals responsible for different colours in pyrotechnics displays[2]:

Metal	Strontium	Copper	Barium	Sodium	Calcium	Iron
Colour	Red	Blue	Green	Yellow/Orange	Orange	Gold

---

[2] Conkling, J. A. 2000. Pyrotechnics. Kirk-Othmer Encyclopedia of Chemical Technology

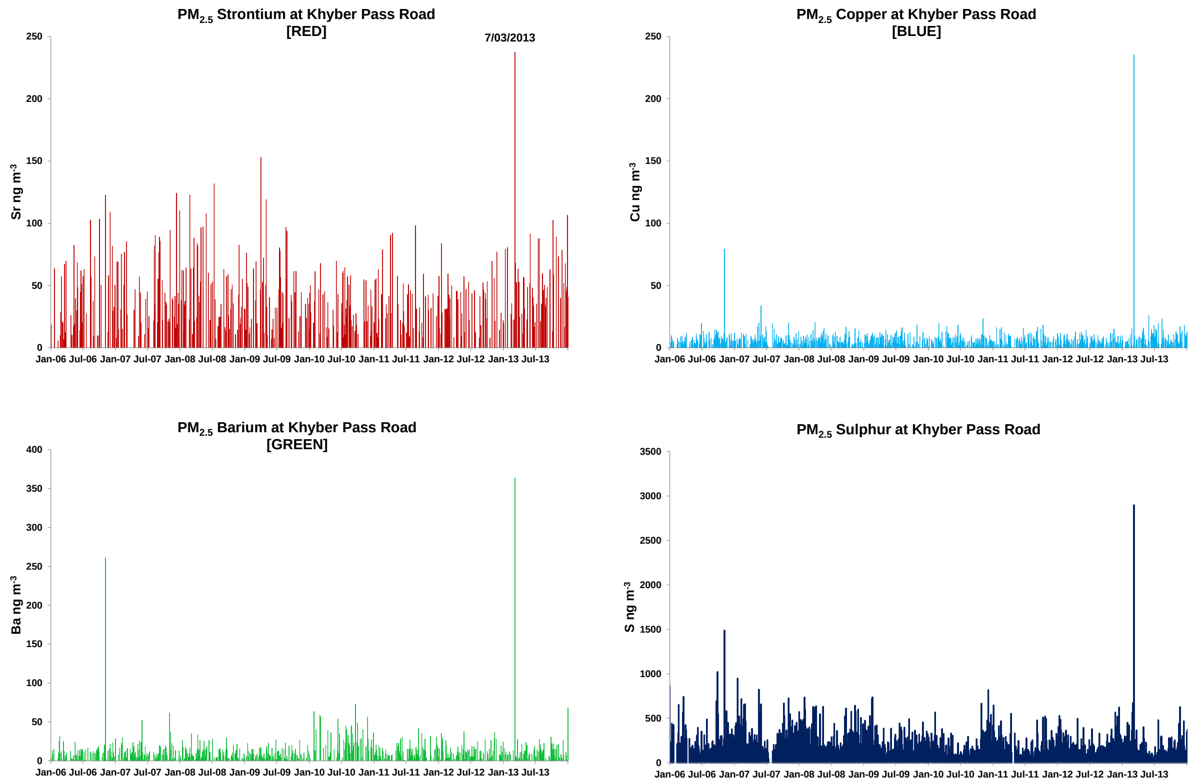

Figure 8.38 Time series plot of various $PM_{2.5}$ elemental species at the Khyber Pass Road site (indicating fireworks colours associated with each element)

The full record of elements which had concentration spikes on the 7 March 2013 include K, Al, Sr, Ba, Cu, Ti, Mg, and S, all of which are known components of pyrotechnics. It was calculated that these elements (as their respective oxides) alone account for 90% of the 24-hour average $PM_{2.5}$ mass recorded at the Khyber Pass Road site on 7 March 2013. Coupled with the carbonaceous content associated with fireworks smoke, the evidence indicates that a pyrotechnics event was the primary contributor to $PM_{2.5}$ at Khyber Pass Road site on that day. The transient nature of the PM_{10} (a two hour ‘spike’ to a maximum of around 1000 μg m^{-3} (10-minute average)), suggests that the relative contribution of the fireworks source was very much higher (>95%) during that short time period. The pyrotechnics display ‘Breath of the Volcano’ at Auckland Domain was largely at ground level and therefore the local impact of the resulting particulate matter was much greater.

9.0 GAVIN STREET, PENROSE

9.1 SITE DESCRIPTION

Samples of particulate matter were collected at an ambient air quality monitoring station located at the Gavin Street electricity substation, Penrose (Lat: -36.9045; Long: 174.8156). Figure 9.1 shows a map of the local area.

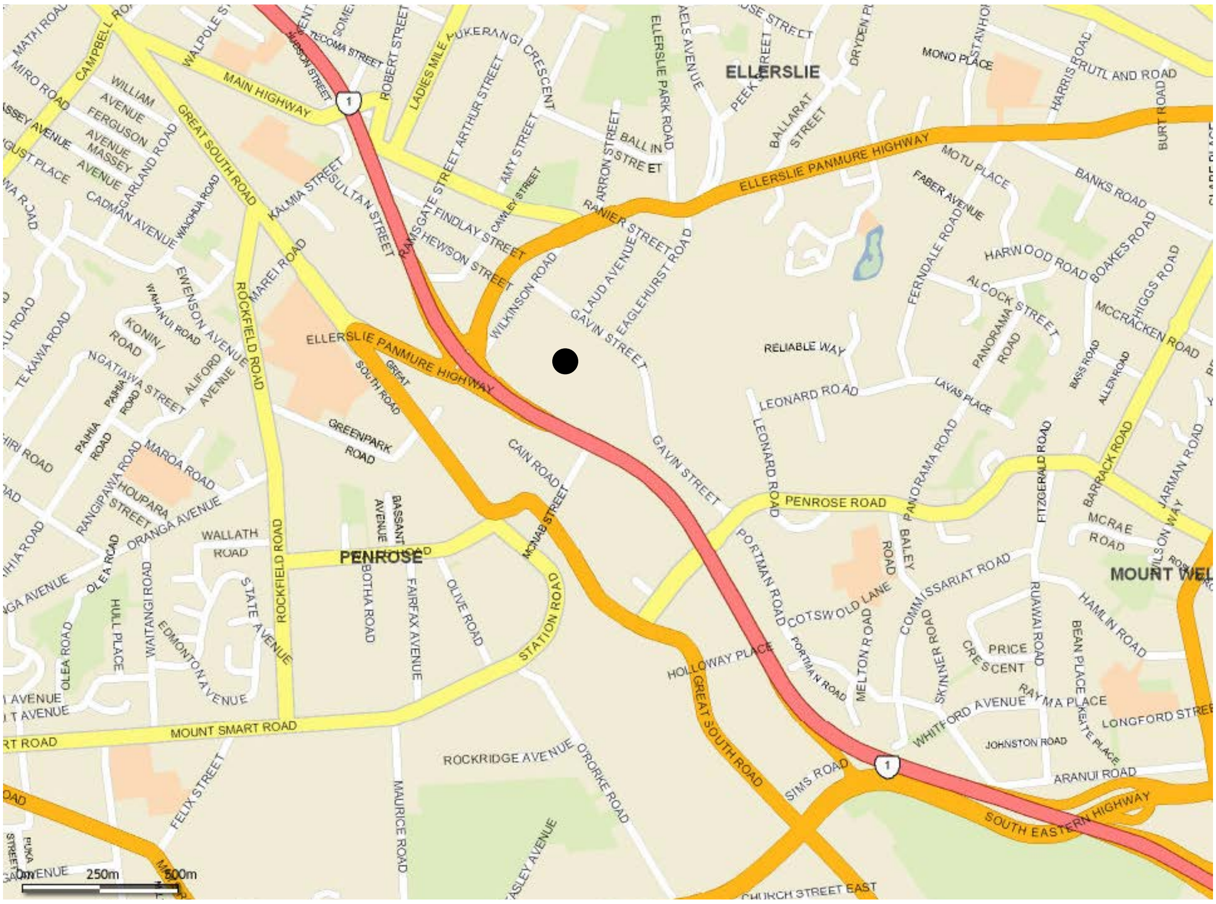

Figure 9.1 Map showing location of Penrose monitoring site (●)

The Penrose site is operated by WSL for AC for its ambient air quality monitoring programme. The site was established at the end of 2000 and is classed as a peak-residential site. Pollutants monitored include NO_x, PM_{10} (BAM, HiVol), SO_2, TSP/Lead (HD MedVol), Partisol Speciation Sampling and meteorological parameters.

The Penrose site is immediately adjacent to the Southern Motorway (100 m southwest) with the Penrose/Otahuhu industrial area further southwest across the motorway. Northeast of the site are more industrial activities with a concrete batching plant and quarrying operations. Immediately to the west is a printing operation and to the north are residential properties. Figure 9.2 provides an aerial view of the Penrose site location.

Figure 9.2 Aerial view of Penrose monitoring site and surrounds (●) (Source: Google Maps 2014)

9.2 AIR PARTICULATE MATTER SAMPLES AND MONITORING PERIOD

Filter samples from a Partisol 2300 Speciation Sampler and a Partisol 2000 PM_{10} Sampler located at the Penrose air quality monitoring station were supplied by AC for analysis:

1. 810 $PM_{2.5}$ samples from a Partisol 2300 sampler collected on a one-day-in-three basis for the period January 2006 – December 2013.
2. 790 PM_{10} samples from a Partisol 2300 sampler collected on a one-day-in-three basis for the period May 2006 – December 2013.
3. 800 PM_{10} samples from a Partisol 2000 sampler collected on a one-day-in-three basis for the period January 2007 – December 2013.

Receptor modelling studies were carried out for the $PM_{2.5}$ and combined PM_{10} sample sets and are reported in Sections 9.6 and 9.7 respectively.

9.3 $PM_{2.5}$ AND PM_{10} CONCENTRATIONS AT PENROSE

The particulate matter results from continuous $PM_{2.5}$ and PM_{10} β-gauge monitors (BAM) at Penrose presented in Figure 9.3 show that $PM_{2.5}$ concentrations tended to be highest during winter months (June - August) with PM_{10} maxima occasionally featuring at other times of the year. The peak during September 2009 was due to the Australian dust storm event described in (Davy, Trompetter et al. 2011).

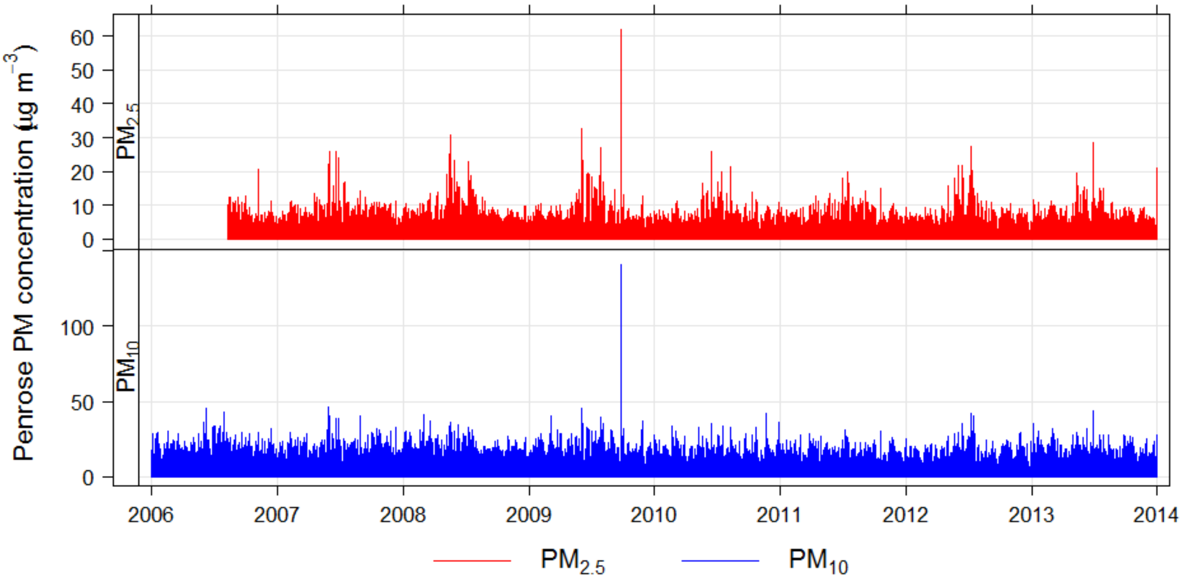

Figure 9.3 Time-series for continuous (BAM) $PM_{2.5}$ and PM_{10} (24-hour averages) at Penrose

9.4 CONCEPTUAL RECEPTOR MODEL FOR PARTICULATE MATTER AT PENROSE

The initial conceptual model for Penrose identifies the following local emission sources:

- Motor vehicles – all roads in the area act as line sources and roads with higher density traffic will dominate particularly the motorway immediately adjacent, also there is a large car auction business (500 m southeast);
- Local wind blown soil or road dust sources;
- Domestic activities – likely to be dominated by biomass burning such as emissions from solid fuel fires used for domestic heating during the winter;
- Industrial activities – industries in the immediate vicinity include a concrete batching plant, quarry and printing with many more industrial sites across the motorway to the southwest

Longer range sources may also contribute to ambient particle loadings and these include:

- Marine aerosol;
- Secondary particulate matter resulting from atmospheric gas-to-particle conversion processes (sulphate and nitrate species, organic particle species resulting from photochemical smog events);
- Trans-boundary events such as bush fires or dust storms in Australia
- Potential for long range transport of industrial emissions from the southwest of the monitoring site;

Another category of emission sources that may contribute are those considered as ‘one-off’ emission sources:

- Fireworks displays and other special events (Mt Smart Stadium is 3 km west of the site);
- Short-term road works and demolition/construction activities.

The variety of sources described above can be recognised and accounted for by appropriate data analysis methods, such as examination of seasonal differences, temporal variations and receptor modelling itself.

9.5 LOCAL METEOROLOGY AT PENROSE

The predominant wind direction at Penrose is from the southwesterly quarter as shown by the windroses in Figure 9.4. The windrose for summer months shows a predominant southwest wind component and a lesser northeast wind component. The winter period has lower wind speeds and a greater spread of wind directions from other sectors. The windroses also suggest some sheltering effect from the southeast, probably due to the proximity of the electricity substation building in that direction.

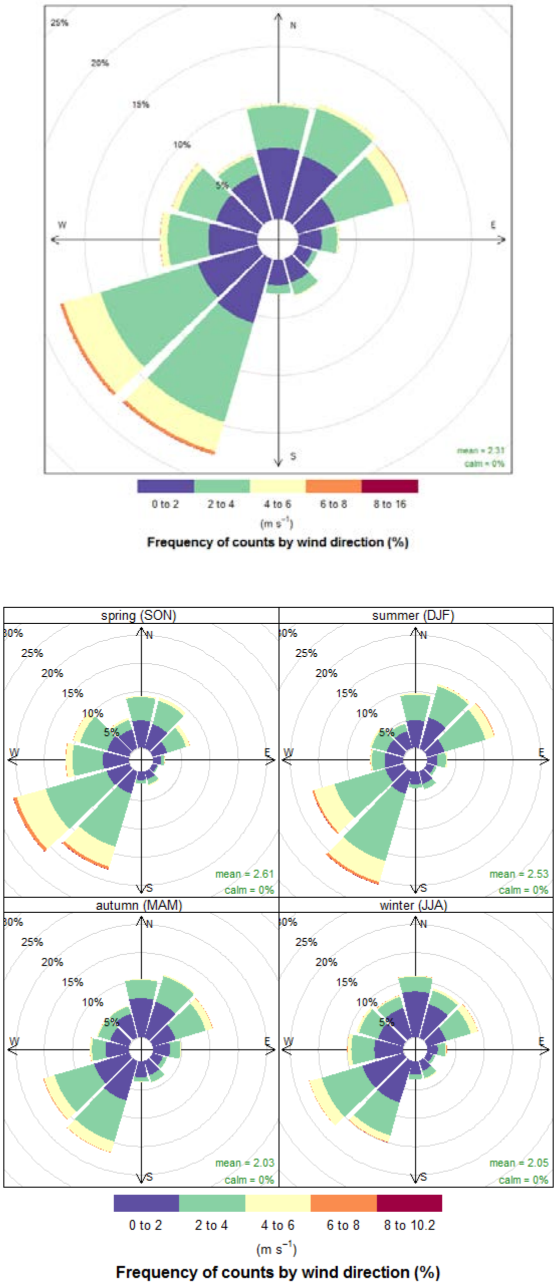

Figure 9.4 (Top) Wind rose for 2006-2013; (Bottom) Seasonal wind roses for 2006-2013.

9.6 ANALYSIS OF PM$_{2.5}$ SAMPLES FROM PENROSE

The Penrose PM$_{2.5}$ samples from the monitoring site refer to those PM$_{2.5}$ samples collected using a Partisol 2300 Speciation Sampler (Andersen Instruments Inc.) from January 2006 to December 2013. Gravimetric results for the Partisol PM$_{2.5}$ samples as presented in Figure 9.5 shows peak PM$_{2.5}$ concentrations during winter months (June – August). Note that the initial sampling regime was one-day-in-six then switched to one-day-in-three in May 2006. Gaps in the data are due to missed sampling periods.

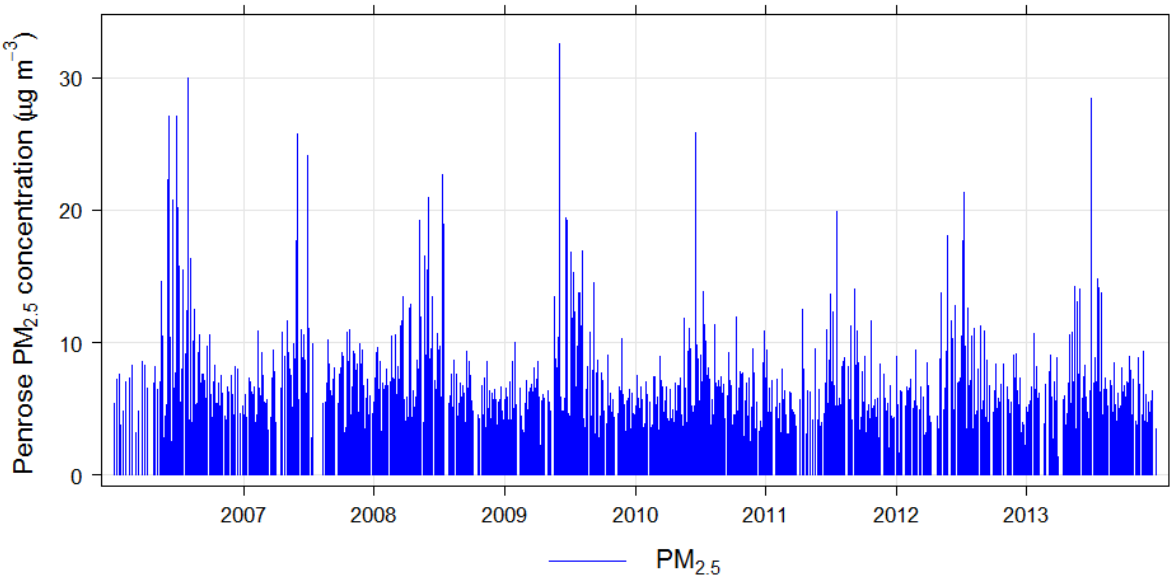

Figure 9.5 Gravimetric results for $PM_{2.5}$ concentrations (24-hour time integrated samples) at Penrose.

9.6.1 Composition of $PM_{2.5}$ at Penrose

Elemental concentrations for $PM_{2.5}$ at Penrose are presented in Table 9.1 with a box and whisker plot of the elemental concentrations shown in Figure 9.6.

Table 9.1 Elemental analysis results for $PM_{2.5}$ at Penrose (810 samples)

Species	Average (ng/m^3)	Max (ng/m^3)	Min (ng/m^3)	Median (ng/m^3)	Std Dev (ng/m^3)	Av LOD (ng/m^3)	#>LOD
$PM_{2.5}$ ($\mu g/m^3$)	**7**	**40**	**0**	**6**	**5**		
H	100	909	0	74	102	41	574
BC	2389	9092	0	2157	1514	176	804
Na	267	4175	0	134	409	247	337
Mg	30	427	0	23	34	25	391
Al	19	152	0	16	16	12	523
Si	52	1271	0	42	53	9	806
P	3	28	0	0	5	16	70
S	208	1058	0	166	148	8	804
Cl	361	6968	0	206	533	7	790
K	44	627	0	27	58	7	769
Ca	28	272	0	23	24	6	771
Sc	2	14	0	1	2	8	51
Ti	2	48	0	0	3	8	77
V	1	12	0	0	2	7	33
Cr	2	16	0	1	2	6	86
Mn	2	37	0	1	3	6	130
Fe	37	274	0	25	37	5	749
Co	2	13	0	1	2	8	48
Ni	2	13	0	1	2	8	66
Cu	3	87	0	2	5	10	116
Zn	29	521	0	12	51	11	457
Ga	4	41	0	0	5	17	72
Ge	4	33	0	0	6	22	52
As	6	69	0	0	10	29	75
Se	7	50	0	0	10	35	78
Br	9	103	0	0	14	44	94
Rb	15	113	0	0	22	71	92
Sr	19	193	0	0	29	92	87
Mo	43	449	0	0	75	137	84
I	7	64	0	2	9	24	72
Ba	6	72	0	1	10	28	47
Hg	10	120	0	0	18	65	34
Pb	16	214	0	0	27	79	62

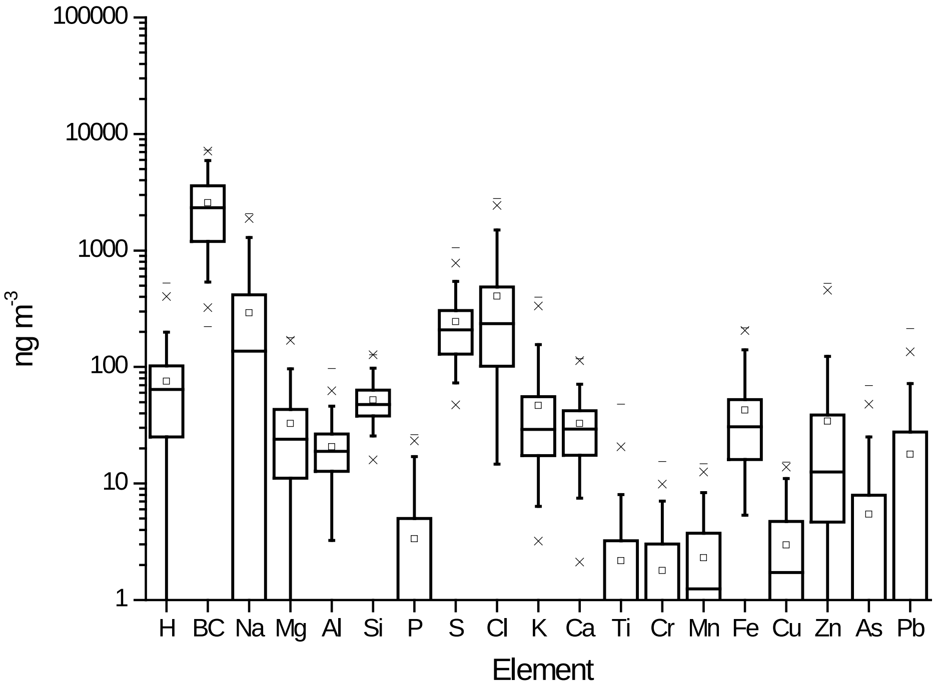

Figure 9.6 Box and whisker plot of $PM_{2.5}$ elemental concentrations at Penrose (logarithmic scale)

Carbonaceous species (represented by BC) dominates $PM_{2.5}$ elemental mass concentrations indicating that combustion processes are important contributors to ambient $PM_{2.5}$ at Penrose. A scatterplot matrix of the species in Table 9.1 is presented in Appendix 5. Table 9.1 also shows that that a number of measured species were generally close to or below the limits of detection over all samples.

9.6.2 Source contributions to $PM_{2.5}$ at Penrose

Eight primary source contributors were determined from the PMF receptor modelling analysis of speciation $PM_{2.5}$ elemental composition at Penrose. These are identified as presented in Table 9.2 along with the mass of $PM_{2.5}$ and elemental species associated with each source.

Table 9.2 Elemental composition of source profiles and contribution to $PM_{2.5}$ at Penrose

	Factor 1	**Factor 2**	**Factor 3**	**Factor 4**	**Factor 5**	**Factor 6**	**Factor 7**	**Factor 8**
Species	**Biomass burning (ng/m^3)**	**Motor vehicles (ng/m^3)**	**Sulphate (ng/m^3)**	**Marine aerosol (ng/m^3)**	**Soil (ng/m^3)**	**Cement (ng/m^3)**	**Industry (ng/m^3)**	**Galvanising (ng/m^3)**
$PM_{2.5}$	**1500**	**2500**	**1030**	**500**	**350**	**5**	**250**	**200**
H	38.7	19.8	12.2	1.2	9.4	0.0	7.8	1.7
BC	439.0	1422.2	99.0	0.0	0.0	2.4	373.2	51.5
Na	0.2	0.0	29.0	217.0	0.0	1.8	17.4	4.3
Mg	0.9	3.1	2.7	18.2	3.6	0.0	0.7	0.0
Al	0.2	2.7	1.4	1.6	8.9	0.7	1.8	0.4
Si	1.6	9.5	5.0	3.6	19.5	3.8	5.2	1.1
S	8.6	23.9	134.3	16.7	11.1	0.0	8.3	4.4
Cl	3.6	13.2	0.0	311.3	25.0	4.8	0.0	7.8
K	26.8	2.7	0.8	6.3	2.3	1.4	1.5	0.3
Ca	0.3	3.1	2.0	6.8	1.5	10.9	3.6	0.2
Mn	0.2	0.6	0.4	0.1	0.2	0.1	0.6	0.2
Fe	3.0	4.3	1.2	1.1	0.5	0.8	26.0	0.5
Cu	0.4	1.5	0.6	0.3	0.5	0.0	0.4	0.2
Zn	1.5	3.0	0.7	0.0	0.0	0.0	1.7	22.9

Table 9.2 represents the summary results for a reiterative process that examines the effect of each species on the PMF receptor modelling process using the modelling diagnostics presented in Appendix 5. Species that were poorly modelled (slope, $r^2 < 0.6$) have been removed from the analyses unless considered vital for source identification. The source contributors identified in Table 9.2 were found on average to explain 89 % of Partisol $PM_{2.5}$ gravimetric mass. Figure 9.7 presents the source profiles extracted from the PMF analysis of Penrose $PM_{2.5}$ data.

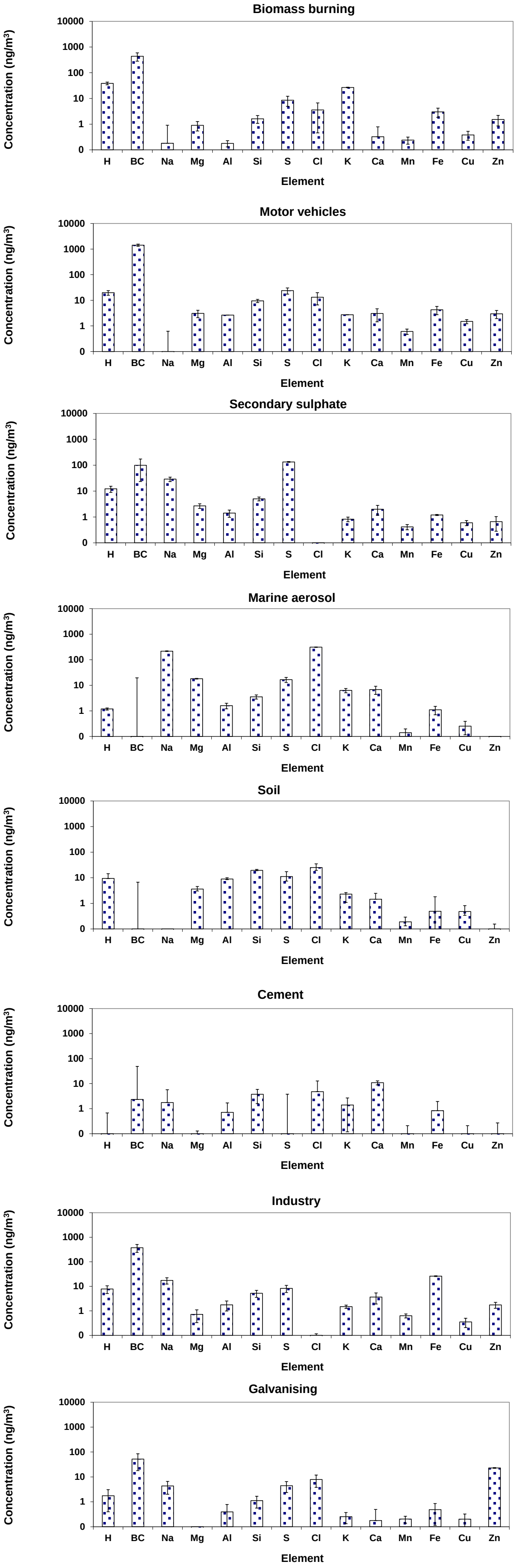

Figure 9.7 Source profiles and elemental concentrations for $PM_{2.5}$ at Penrose site (showing 5th and 95th confidence intervals in mean concentration derived from the receptor modelling)

- The first factor is from biomass burning due to the association between H, BC and K.
- The second factor, Motor vehicles, represents a source profile for motor vehicle emissions due to the grouping of H, BC, Ca, Fe and Cu.
- The third factor has been identified as a secondary sulphate aerosol source due to the predominance of S.
- The fourth source profile is dominated by Na and Cl and represents the contribution from marine aerosol.
- The fifth source, Soil is from crustal matter due to the combination of Al, Si, Ca and Fe. It may be that the soil.
- The sixth source has been attributed to a cement component due to the high Ca concentration,
- The seventh source has been identified as originating from industrial emissions.
- The eighth source profile is primarily composed of zinc and is considered to be due to emissions from hot-dip galvanising activities.

Figure 9.8 presents the 2006-2013 average source contributions to PM$_{2.5}$ concentrations and includes the standard deviations of the average mass contributions from each of the sources indicating the variability in source strength.

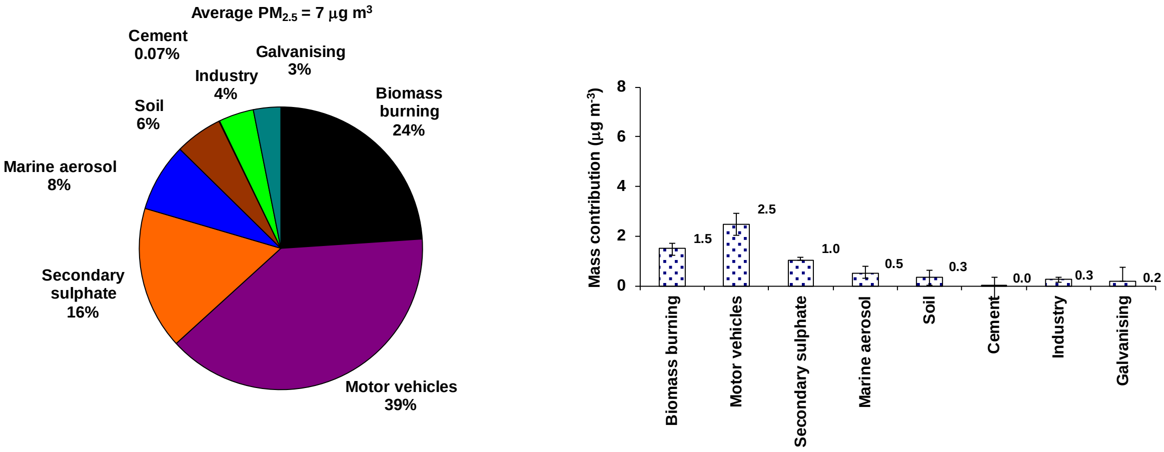

Figure 9.8 Average 2006-2013 source contributions to PM$_{2.5}$ at Penrose site (showing 5th and 95th confidence intervals in mean concentration derived from the receptor modelling)

The average source contributions estimated by the receptor modelling indicate that motor vehicle emissions and biomass burning are the most significant contributors (motor vehicle contribution 39 % and biomass burning 24 % respectively) to PM$_{2.5}$ concentrations at Penrose, with lesser contributions from, secondary sulphate particles 16 %), marine aerosol (8 %), soil (6 %), a trace contribution from concrete batching activities (0.07 %), the industrial source (4 %) and emissions from galvanising activities (3 %).

Figure 9.9 shows the mass contribution of sources to PM$_{2.5}$ mass for each sample collected at Penrose.

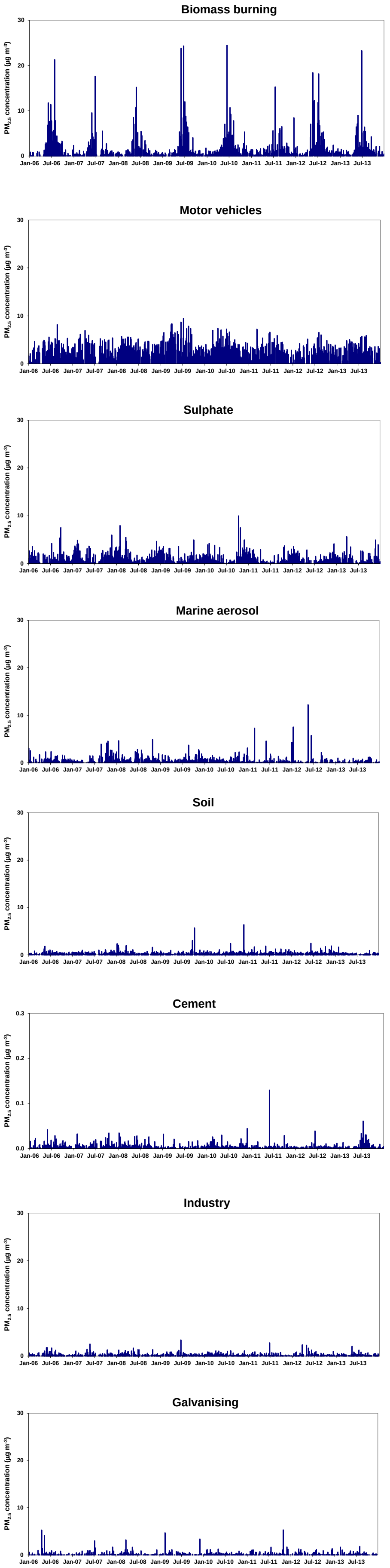

Figure 9.9 Time-series of source contributions to PM$_{2.5}$ mass at Penrose

9.6.3 Temporal variations in $PM_{2.5}$ source contributions at the Penrose site

Figure 9.10 presents the temporal variations in mass contributions at Penrose. The primary sources of $PM_{2.5}$ during winter (June-August) at Penrose were motor vehicle emissions and biomass burning. Average $PM_{2.5}$ concentrations during winter (11 µg m^{-3}) were higher in winter than spring and summer (7 to 8 µg m^{-3}). Motor vehicle emissions were the primary source of $PM_{2.5}$ during all seasons at Penrose, with contributions lower on the weekends in line with commuter behaviour and commercial activities.

The secondary sulphate source showed a winter minimum, while $PM_{2.5}$ contributions from marine aerosol and soil sources did not show any significant seasonality. $PM_{2.5}$ contributions from both the Industry and Galvanising sources were lower on Sunday whereas no weekday/weekend difference was evident or the Cement source.

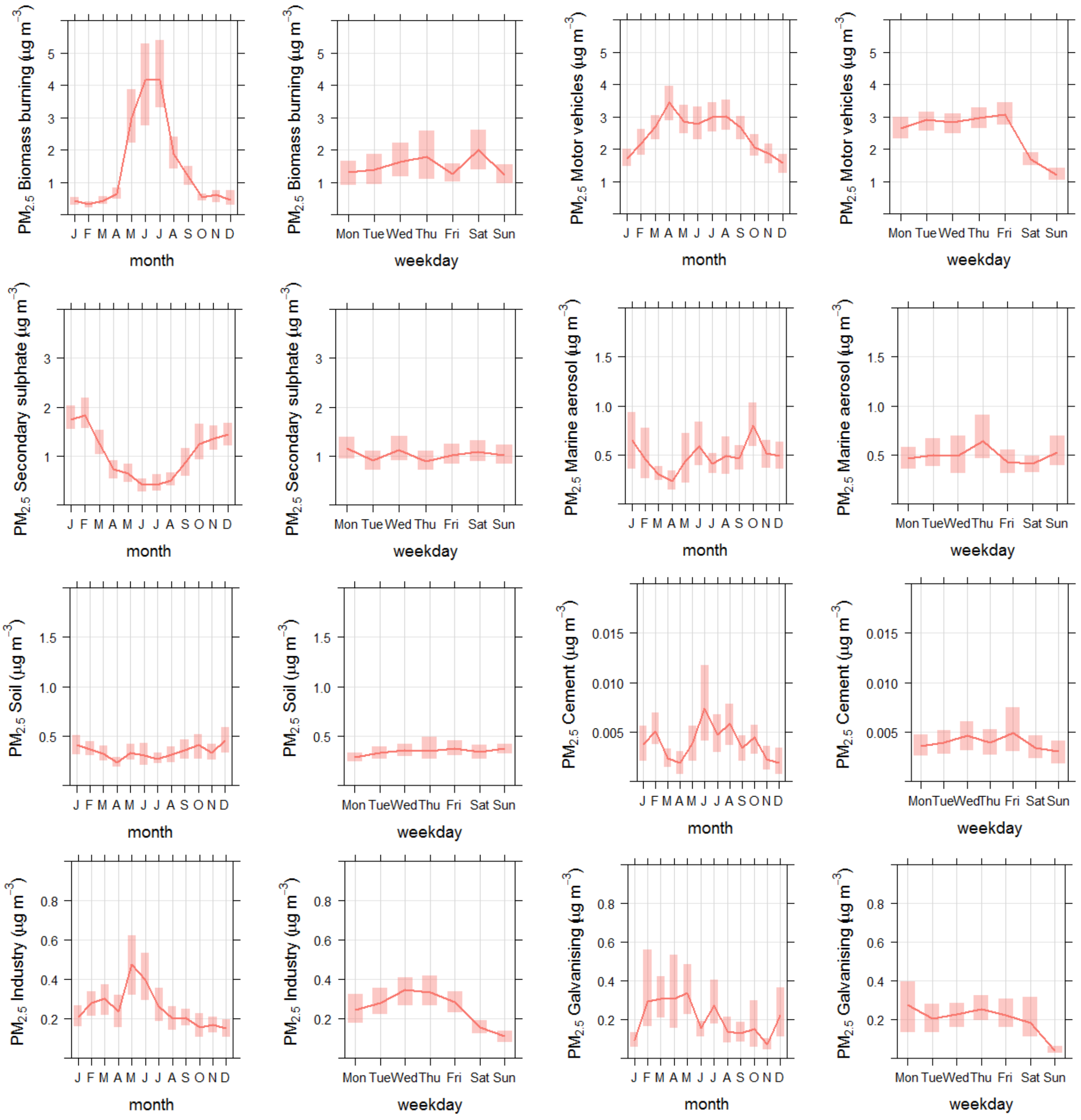

Figure 9.10 Temporal variations (2006-2013) in $PM_{2.5}$ source contributions at Penrose (the shaded bars are the 95 percentile confidence limits in the mean)

9.6.4 Trends in PM$_{2.5}$ concentrations and source contributions at Penrose

The temporal trends in PM$_{2.5}$ source contributions at Penrose were explored using the Thielsen functionality available in *openair*. Figure 9.11 presents the deseasonailsed trend in PM$_{2.5}$ concentrations showing that there was a significant decreasing trend (99.9 % CI) over the monitoring period.

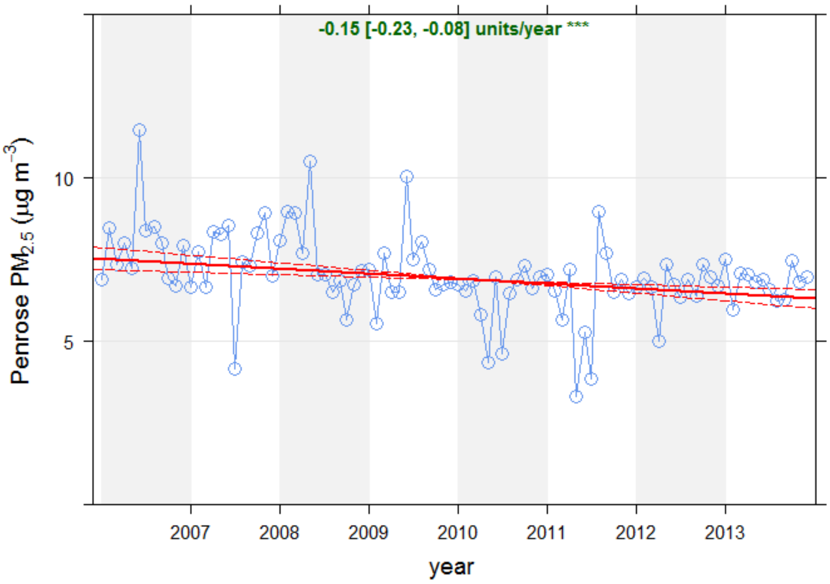

Figure 9.11 Trend in PM$_{2.5}$ concentrations at Penrose (statistically significant at the 99.9 % confidence interval)

The trends in PM$_{2.5}$ source contributions are presented in Figure 9.12 and show that the decrease in PM$_{2.5}$ was largely driven by a commensurate decrease in contributions from motor vehicles (95 % CI) along with decreases in secondary sulphate and marine aerosol contributions (both at the 99.9 % CI). It is likely that the fuel formulation and engine emissions has had an influence on motor vehicle emissions concentrations, similarly for secondary sulphate it would appear that the decrease was consistent with a reduction in the sulphur content of fuels as discussed in Chapter 5. There were no statistically significant trends for the PM$_{2.5}$ soil or biomass burning sources. Of the sources identified as originating from industrial emissions, both the Cement and Industry sources showed a decrease over the monitoring period whereas there was no trend evident for the Galvanising source.

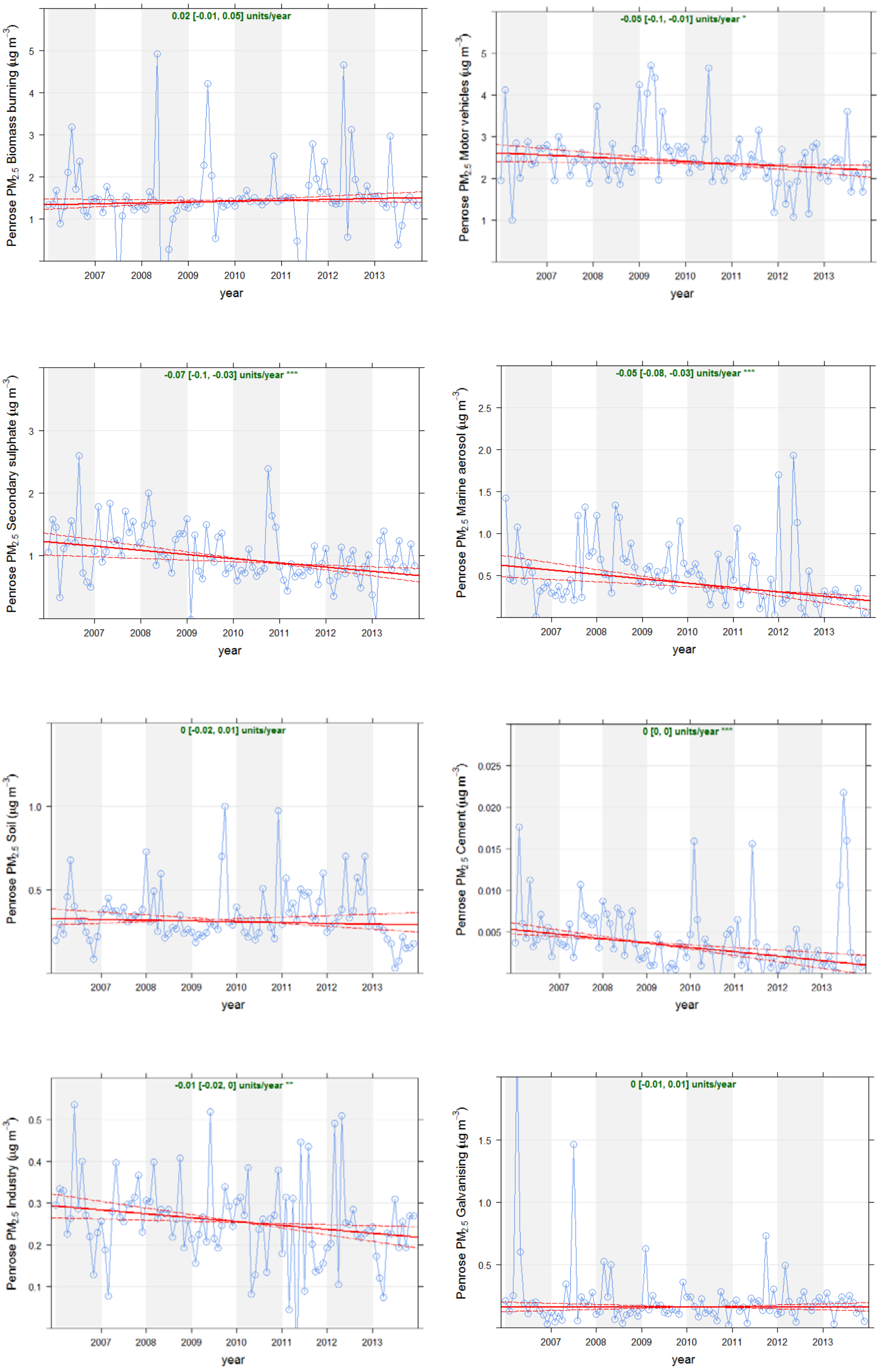

Figure 9.12 Trends in $PM_{2.5}$ source contributions at Penrose

9.6.5 Analysis of individual $PM_{2.5}$ events at Penrose

Peak $PM_{2.5}$ events during the sampling period at Penrose have been chosen for further analysis. Peak $PM_{2.5}$ events are defined as those that were higher than 66 % (17 µg m^{-3}) of the AAQG (25 µg m^{-3} 24-hour average). It was found that there were 26 days over the monitoring period where $PM_{2.5}$ concentrations were higher than 66 % of the AAQG.

Figure 9.13 presents the mass contributions of individual sources to each of the peak $PM_{2.5}$ days (> 17 µg m^{-3}).

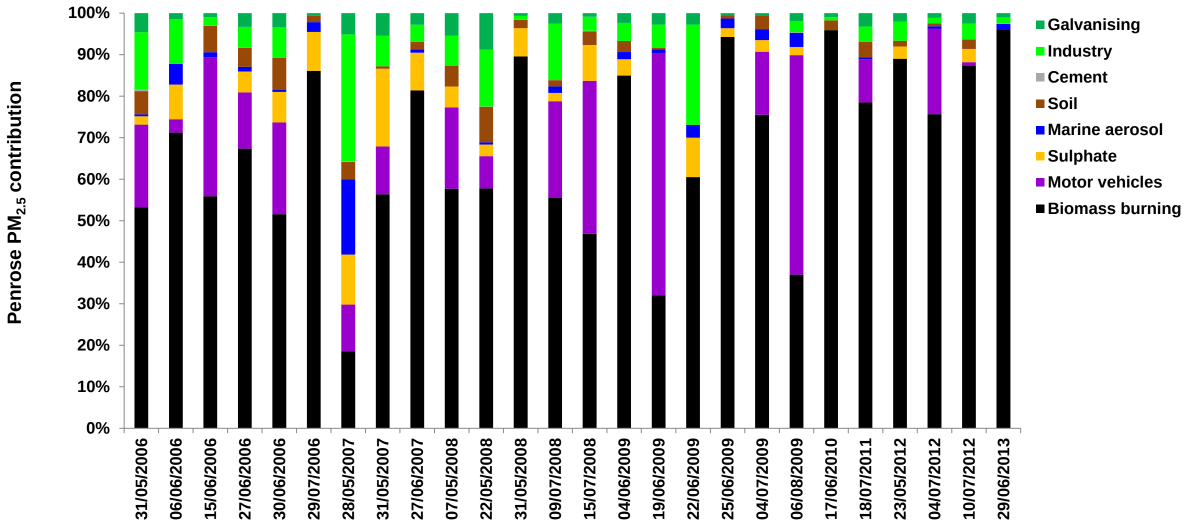

Figure 9.13 Source contributions to peak $PM_{2.5}$ concentrations at Penrose

Figure 9.13 shows that biomass burning and motor vehicle emission sources (during winter) were primarily responsible for elevated $PM_{2.5}$ concentrations at Penrose.

9.6.6 Variation of $PM_{2.5}$ source contributions with wind direction

The CPF analysis of the relationship between the source contributions and wind direction is presented and discussed in the following sections. Note that the sheltering effect of the building to the southeast of the monitoring station (see wind roses in Section 7.5) may have affected the CPF analysis and as such most sources show a southeast component that may not be real. The CPF figures are presented in polar coordinates with north as 0 degrees and the axes are in relative probability units (i.e. maximum = 1.0).

9.6.6.1 Biomass Burning

Biomass burning source contributions to $PM_{2.5}$ are considered to be primarily due to emissions from domestic solid fuel fires. Peak contributions are highest on cold calm winter days under inversion conditions or with a light southerly wind, particularly for anticyclonic synoptic conditions. The CPF analysis for biomass burning as presented in Figure 9.14 shows northerly and southerly components. The closest residential dwellings are immediately north of the monitoring site across Gavin Street and emissions from domestic fires from these homes accounts for the northerly component.

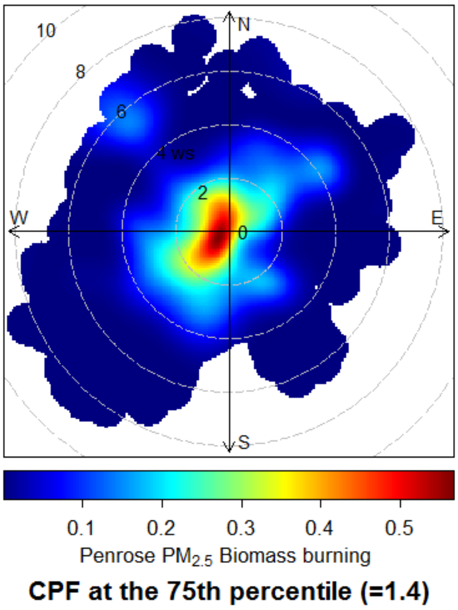

Figure 9.14 Penrose $PM_{2.5}$ biomass burning CPF analysis

9.6.6.2 Motor vehicles

Peak contributions to $PM_{2.5}$ from the Motor vehicles source occurred during light to moderate winds from the southwest as presented in Figure 9.15 and is aligned with the southern motorway.

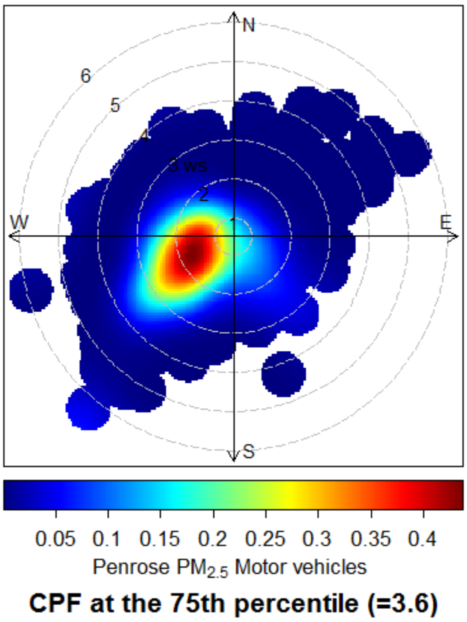

Figure 9.15 Penrose $PM_{2.5}$ Motor vehicle CPF analysis

9.6.6.3 Sulphate

The $PM_{2.5}$ secondary sulphate contribution was found to primarily originate from the southeast sector as shown in Figure 9.16. This result differs to the other sites in this study as they all indicate a peak source in the Port of Auckland or Waitemata Harbour area. It is likely that the southern sulphate source at Penrose is due to industrial emissions of SO_2 in the Penrose – Otahuhu area or potentially further away.

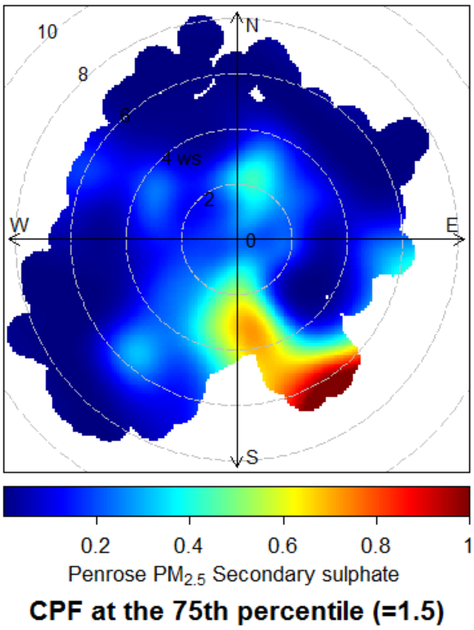

Figure 9.16 Penrose $PM_{2.5}$ secondary sulphate CPF analysis

9.6.6.4 Marine aerosol

The $PM_{2.5}$ marine aerosol contribution presented in Figure 9.17 primarily originates from the west-southwest and north-northeast directions at higher wind speeds. The most likely source of the $PM_{2.5}$ marine aerosol is the Pacific Ocean, Tasman Sea and Southern Ocean.

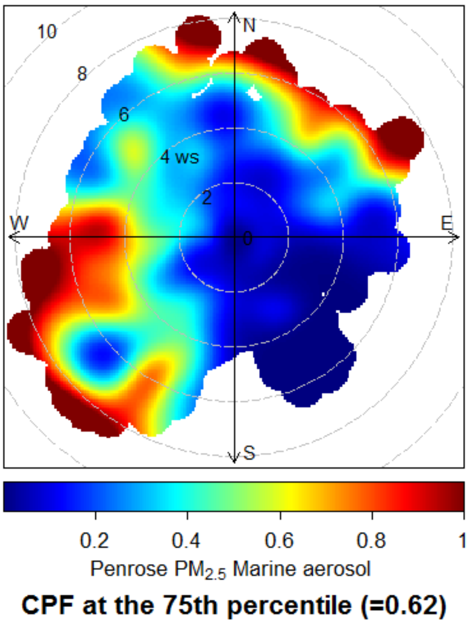

Figure 9.17 Penrose $PM_{2.5}$ marine aerosol CPF analysis

9.6.6.5 Soil

The Soil source shows an easterly component as presented in Figure 9.18 and is probably due to dusts from vehicle movements on unsealed yards in the vicinity. Significant works have been undertaken at the electrical substation where the AC monitoring site was located during the monitoring period. There is also an aggregate and landscape garden supply operation immediately east of the monitoring site along with cement batching and asphalt production facilities further east across Gavin Street, all of which involve the movement, processing and storing of crustal matter aggregates.

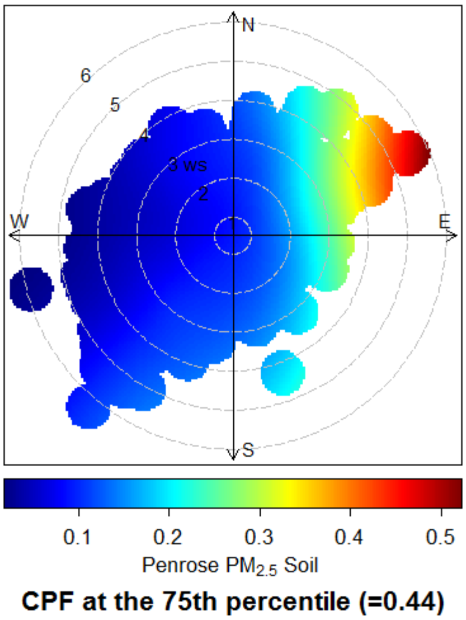

Figure 9.18 Penrose $PM_{2.5}$ Soil CPF analysis

9.6.6.6 Cement

The CPF polar plot for the Cement source shows a southeasterly component at higher wind speeds for peak contributions as presented in Figure 9.19. While there was a nearby concrete batching plant more to the east of the site, it may be that concrete work (cutting/grinding) in the immediate vicinity of the monitoring station had the greatest influence on peak concentrations.

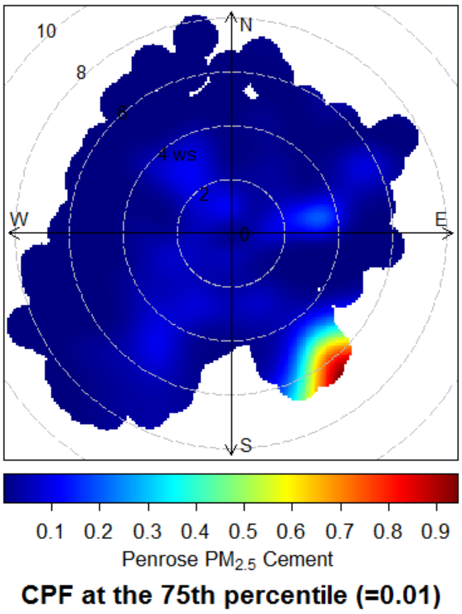

Figure 9.19 Penrose $PM_{2.5}$ Cement CPF analysis

9.6.6.7 Industry

The Industry source shows a southerly component as presented in Figure 9.20 and is thought be due to point source emissions from an industrial site(s) across the motorway.

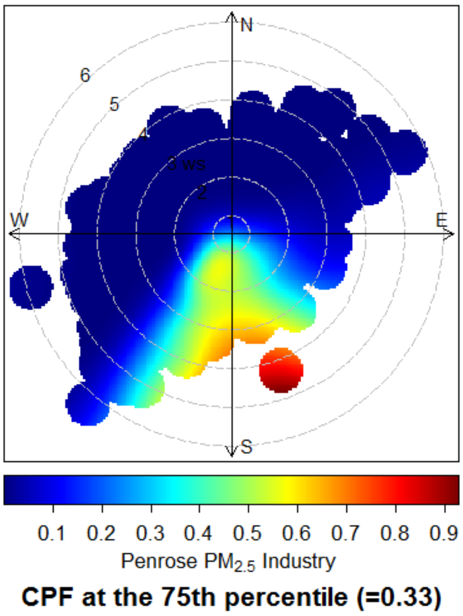

Figure 9.20 Penrose $PM_{2.5}$ Industry CPF analysis

9.6.6.8 Galvanising

The Galvanising source profile is dominated by zinc and has been identified as likely to originate from local hot-dip galvanising activities. There are two hot-dip galvanising operations south of the monitoring site in the industrial area on the other side of the Southern Motorway and another hot-dip galvanising facility to the east across Gavin Street. The CPF analysis presented in Figure 9.21 indicates that the galvanising source originates from the southerly and easterly sectors.

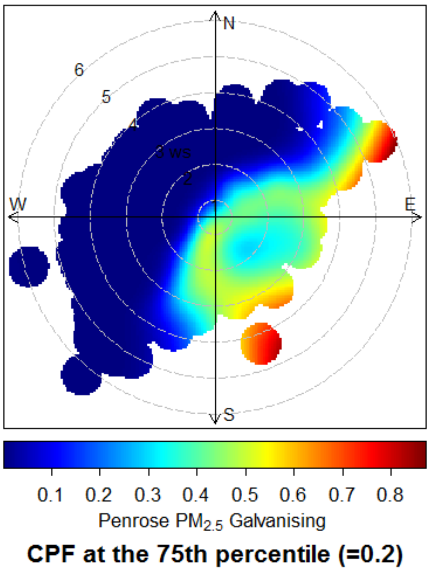

Figure 9.21 Penrose $PM_{2.5}$ Galvanising CPF analysis

9.7 ANALYSIS OF SPECIATION AND PARTISOL PM$_{10}$ SAMPLES FROM PENROSE

The Penrose Speciation and Partisol PM$_{10}$ samples from the Gavin Street monitoring site refer to those PM$_{10}$ samples collected using a Partisol 2300 Speciation Sampler and a separate set of samples on alternate days collected using a Partisol 2000 sampler (Andersen Instruments Inc.) from May 2006 to December 2013. Separate source apportionment analyses were carried out for both sets and were found to produce equivalent results therefore the data sets were combined to produce one analysis with a total sample set of 1590 filters. Only the combined analysis has been reported here for brevity.

Gravimetric results for the Penrose PM$_{10}$ samples as presented in Figure 9.22 shows peaks in PM$_{10}$ concentrations during winter months (June – August).

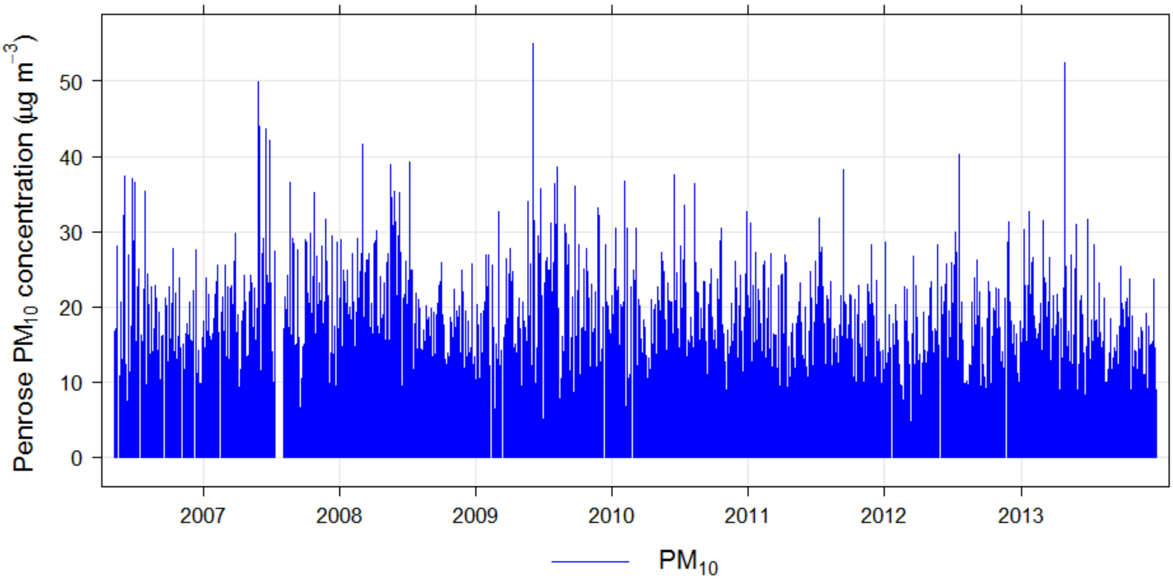

Figure 9.22 Gravimetric results for PM$_{10}$ (24-hour averages) at Penrose

9.7.1 Composition of PM_{10} at Penrose

Elemental concentrations for PM_{10} at Penrose are presented in Table 9.3 with a box and whisker plot of the elemental concentrations shown in Figure 9.23.

Table 9.3 Elemental analysis results for PM_{10} at Penrose (1590 samples)

Species	Average (ng/m^3)	Max (ng/m^3)	Min (ng/m^3)	Median (ng/m^3)	Std Dev (ng/m^3)	Av LOD (ng/m^3)	#>LOD
PM_{10} (μg/m^3)	**17**	**55**	**3**	**17**	**7**		
H	141	1416	0	121	130	41	1356
BC	2406	9474	0	2255	1524	181	1558
Na	2017	7529	0	1913	1282	459	1495
Mg	187	632	0	188	113	37	1527
Al	126	1921	0	96	115	16	1501
Si	359	4692	0	240	317	11	1569
P	15	123	0	11	18	17	613
S	384	1459	0	378	212	13	1567
Cl	3068	12736	0	2782	2234	8	1567
K	127	1431	0	122	81	7	1566
Ca	230	2325	0	194	149	7	1567
Sc	3	27	0	2	4	10	157
Ti	19	211	0	11	20	8	1027
V	1	13	0	0	2	11	58
Cr	4	401	0	0	16	9	294
Mn	7	40	0	5	7	7	655
Fe	247	1501	0	181	210	6	1563
Co	4	41	0	2	5	11	221
Ni	2	107	0	1	5	10	117
Cu	8	945	0	7	8	10	562
Zn	45	754	0	18	71	12	993
Ga	4	35	0	0	5	18	124
Ge	4	38	0	0	6	23	94
As	6	72	0	0	11	30	156
Se	8	69	0	0	11	36	154
Br	12	100	0	4	15	45	178
Rb	14	123	0	0	22	74	133
Sr	21	183	0	0	29	92	161
Mo	32	470	0	0	78	184	115
I	8	100	0	3	17	33	142
Ba	17	130	0	16	20	35	345
Hg	13	161	0	0	19	67	84
Pb	14	257	0	0	26	82	91

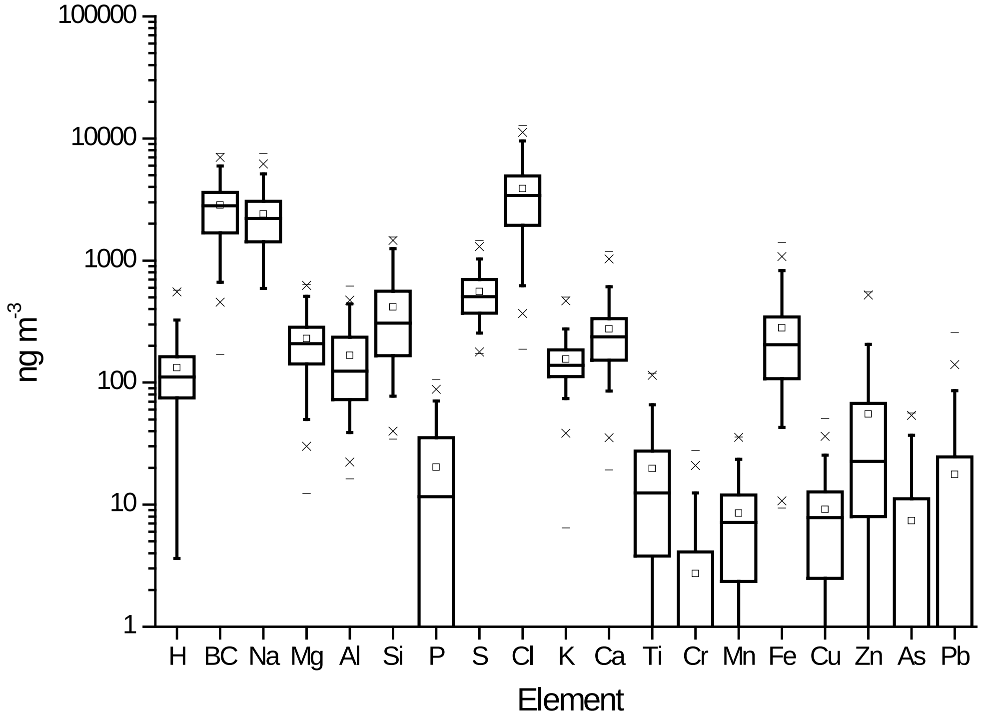

Figure 9.23 Box and whisker plot of PM_{10} elemental concentrations at Penrose (logarithmic scale)

Carbonaceous species (represented by BC), sodium and chlorine were found to dominate PM_{10} elemental mass concentrations indicating that combustion processes and marine aerosol are important contributors to ambient PM_{10} at Penrose. A scatterplot matrix of the species in Table 9.3 is presented in Appendix 5.

Table 9.3 also shows that some measured species were generally close to or below the limits of detection over all samples.

9.7.2 Source contributions to PM_{10} at Penrose

Six primary source contributors were determined from the PMF receptor modelling analysis of PM_{10} elemental composition at Penrose. These are identified as presented in Table 9.4 along with the mass of PM_{10} and elemental species associated with each source.

Table 9.4 Elemental composition of source profiles and contribution to PM_{10} at Penrose

	Factor 1	**Factor 2**	**Factor 3**	**Factor 4**	**Factor 5**	**Factor 8**
Species	**Biomass burning (ng/m^3)**	**Motor vehicles (ng/m^3)**	**Sulphate (ng/m^3)**	**Marine aerosol (ng/m^3)**	**Soil (ng/m^3)**	**Galvanising (ng/m^3)**
PM_{10}	**2048**	**3872**	**1390**	**6782**	**1693**	**74**
H	91	33	4	4	1	1
BC	233	1862	153	65	91	0
Na	5	81	129	1733	32	30
Mg	3	11	12	142	16	0
Al	0	7	24	9	80	1
Si	9	29	46	18	247	4
S	9	26	178	140	24	3
Cl	4	177	54	2746	22	42
K	32	18	6	51	15	0
Ca	1	38	10	66	100	7
Ti	0	4	0	0	13	1
Mn	0	2	0	1	3	0
Fe	4	105	0	10	117	3
Cu	1	5	0	1	1	0
Zn	1	6	1	0	1	36

Table 9.4 represents the summary results for a reiterative process that examines the effect of each species on the PMF receptor modelling using the modelling diagnostics presented in Appendix 5. Species that were poorly modelled (slope, $r^2 < 0.6$) have been removed from the analyses unless considered vital for source identification. The source contributors identified in Table 9.4 were found on average to explain 94 % of PM_{10} gravimetric mass. Figure 9.24 presents the source profiles extracted from the PMF analysis of Penrose PM_{10} data.

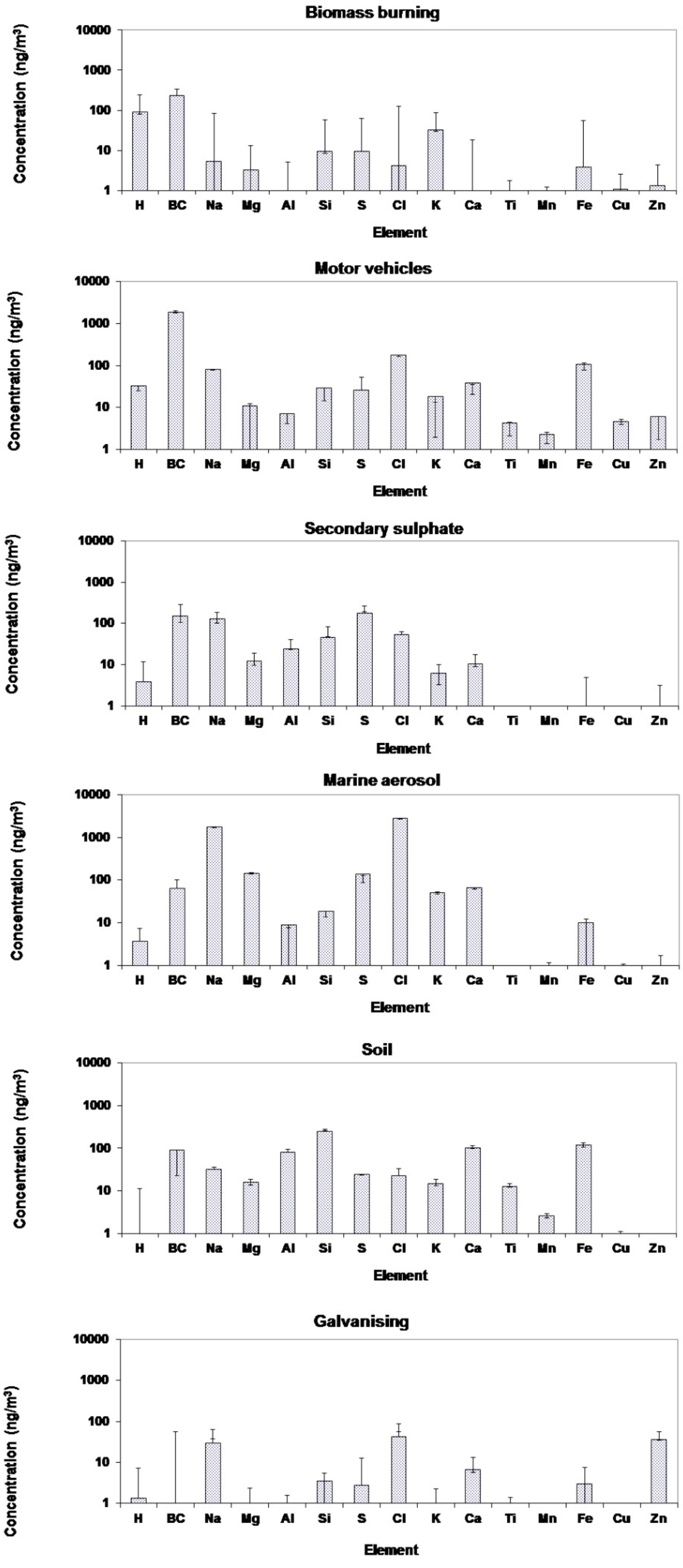

Figure 9.24 Source profiles and elemental concentrations for PM_{10} at Penrose site (showing 5th and 95th confidence intervals in mean concentration derived from the receptor modelling)

- The first factor is from biomass burning due to the association between H, BC and K.
- The second factor, Motor vehicles, represents a source profile for motor vehicle emissions due to the grouping of H, BC, Ca, Fe and Zn.
- The third factor has been identified as a secondary sulphate aerosol source due to the predominance of S.
- The fourth source profile is dominated by Na and Cl and represents the contribution from marine aerosol.
- The fifth source, Soil is from crustal matter due to the combination of Al, Si, Ca and Fe.
- The sixth source profile had a high zinc content and is considered to be due to emissions from hot-dip galvanising activities.

Interestingly, some of the trace $PM_{2.5}$ sources that relate to industrial activity (i.e. the Cement and Industry sources) were not resolved for the PM_{10} analyses. This is likely to be due to covariance of key elements with other sources particularly with the Marine aerosol and Soil contributions dominating PM_{10} composition as shown in Figure 9.25 (including the standard deviations of the average mass contributions from each of the sources indicating the variability in source strength).

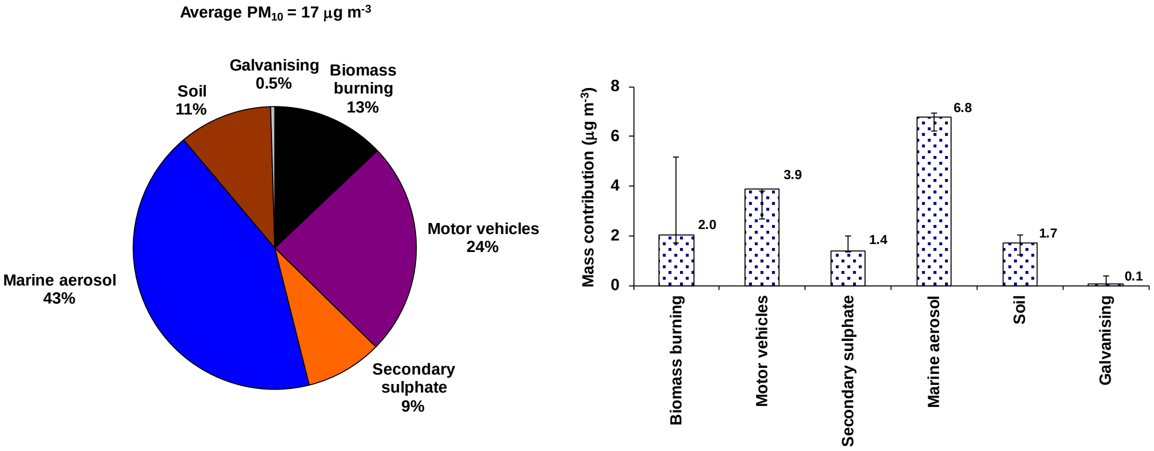

Figure 9.25 Average 2006-2013 source contributions to PM_{10} at Penrose site (showing 5th and 95th confidence intervals in mean concentration derived from the receptor modelling)

The average source contributions estimated by the receptor modelling indicate that motor vehicle emissions and marine aerosol are the most significant contributors (motor vehicle contribution (24 % and 43 % respectively) to PM_{10} concentrations at Penrose, with lesser contributions from biomass burning (13 %), secondary sulphate particles (9 %), soil (11 %), emissions from galvanising activities (<1 %).

Figure 9.26 shows the mass contribution of sources to PM_{10} mass for each sample collected at Penrose.

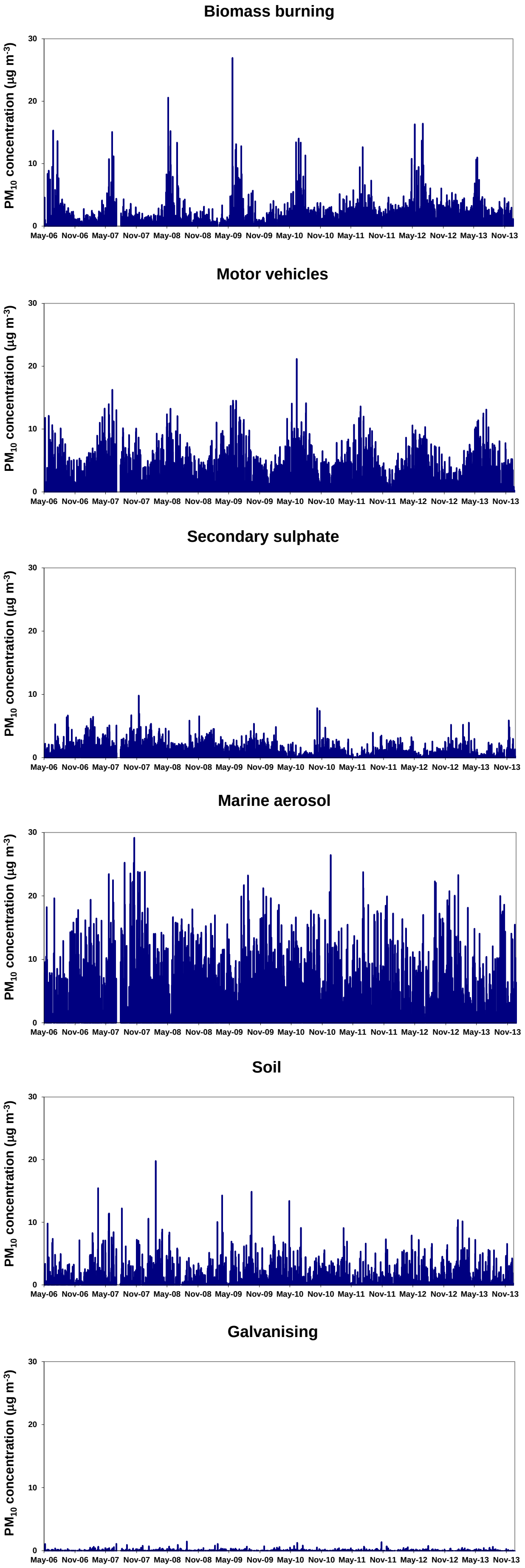

Figure 9.26 Time-series for source contributions to PM$_{10}$ mass at Penrose

9.7.3 Temporal variations in PM_{10} source contributions at the Penrose site

Figure 9.27 presents the temporal variations in mass contributions at Penrose. The primary sources of PM_{10} during winter (June-August) at Penrose were motor vehicle emissions and biomass burning. Marine aerosol was a significant contributor to PM_{10} during all seasons at Penrose. Motor vehicle emissions, crustal matter and galvanising contributions were all lower on the weekends in line with commuter behaviour and local industrial activities.

The secondary sulphate source showed a winter minimum, while PM_{10} contributions from marine aerosol and soil sources did not show any significant seasonality. PM_{10} contributions from both the Industry and Galvanising sources were lower on Sunday whereas no weekday/weekend difference was evident or the Cement source.

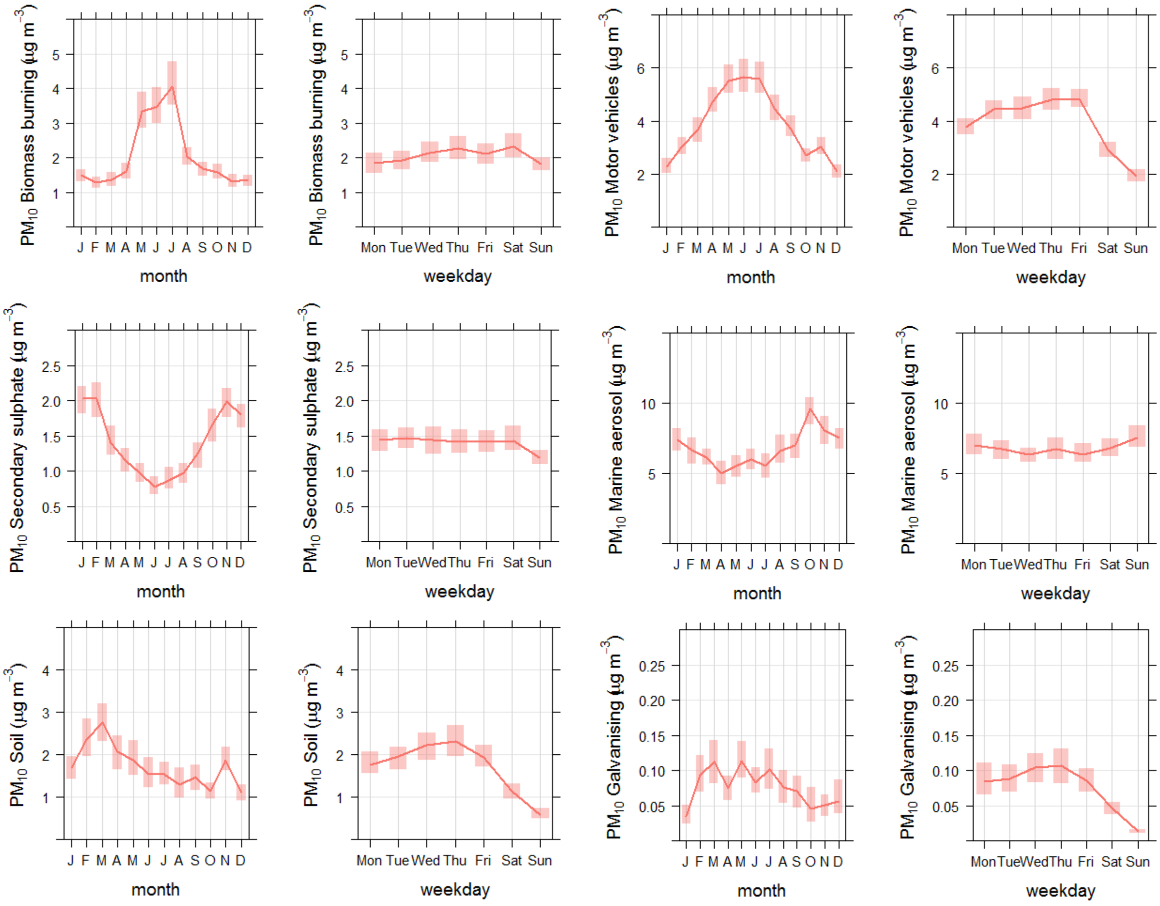

Figure 9.27 Temporal variations (2006-2013) in PM_{10} source contributions at Penrose (the shaded bars are the 95 percentile confidence limits in the mean)

9.7.4 Trends in PM_{10} concentrations and source contributions at Penrose

The temporal trends in PM_{10} source contributions at Penrose were explored using the Thielsen functionality available in *openair*. Figure 9.28 presents the deseasonailsed trend in PM_{10} concentrations showing that there was a significant decreasing trend (99.9 % CI) over the monitoring period.

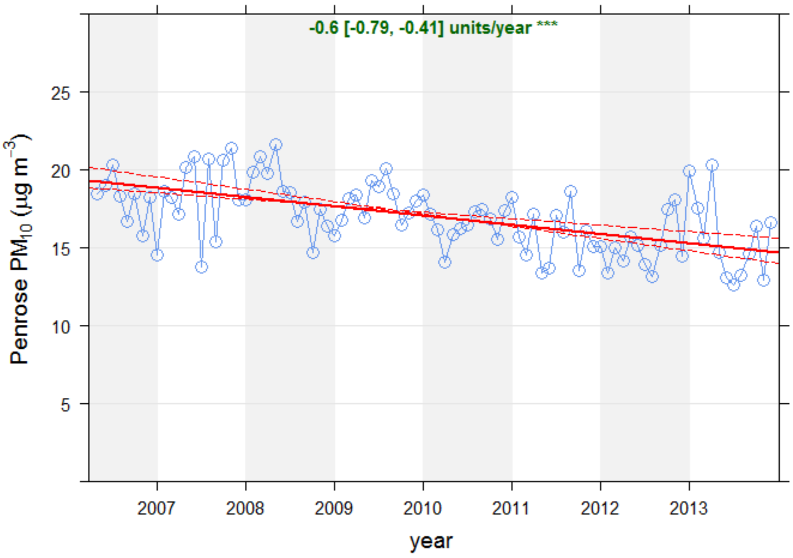

Figure 9.28 Trend in PM_{10} concentrations at Penrose (statistically significant at the 99.9 % confidence interval)

The trends in PM_{10} source contributions are presented in Figure 9.29 and show that the decrease in PM_{10} was largely driven by a commensurate decrease in contributions from motor vehicles (99.9 % CI) along with decreases in secondary sulphate (99.9 % CI) and marine aerosol contributions (99 % CI). It is likely that the fuel formulation and engine emissions has had an influence on motor vehicle emissions concentrations, similarly for secondary sulphate it would appear that the decrease was consistent with a reduction in the sulphur content of fuels as discussed in Chapter 5. There were also statistically significant decreasing trends for the PM_{10} soil and Galvanising sources (90 % CI) probably linked to local activities such as a decrease in production throughput for the galvanising operations or alternatively an improvement in emissions abatement. The decrease in re-suspension of crustal matter may be due to a change in activity on the substation site where the AQMS is located. Biomass burning emissions was the only source that showed an increasing trend (99.9 % CI) over the monitoring period.

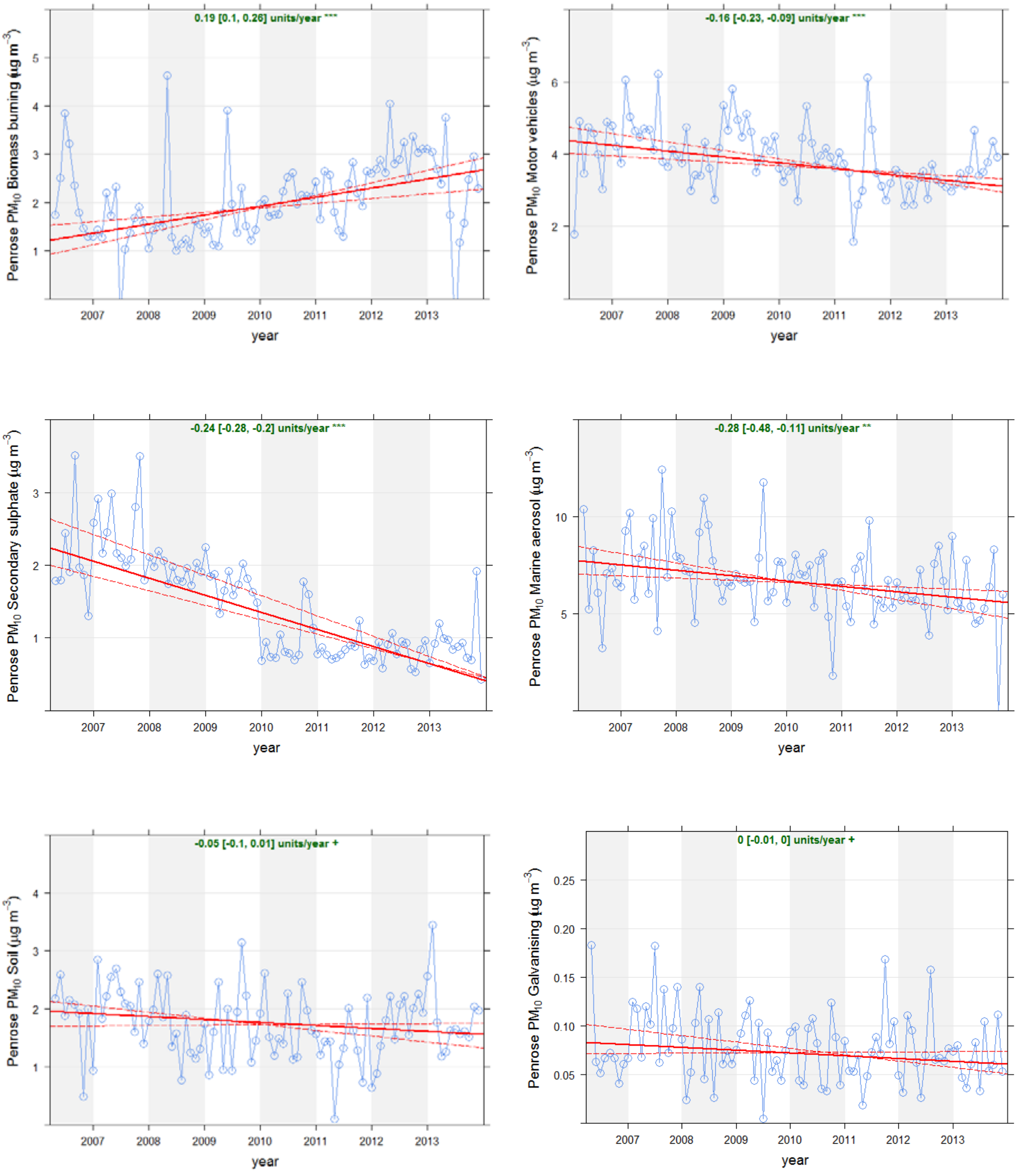

Figure 9.29 Trends in PM_{10} source contributions at Penrose

9.7.5 Analysis of individual PM_{10} events at Penrose

Peak PM_{10} events during the sampling period at Penrose have been chosen for further analysis. Peak PM_{10} events are defined as those that were higher than 66 % (33 µg m^{-3}) of the NES (50 µg m^{-3} 24-hour average). It was found that there were 33 days over the monitoring period where PM_{10} concentrations were higher than 66 % of the NES.

Figure 9.30 presents the mass contributions of individual sources to each of the peak PM_{10} days (> 33 µg m^{-3}).

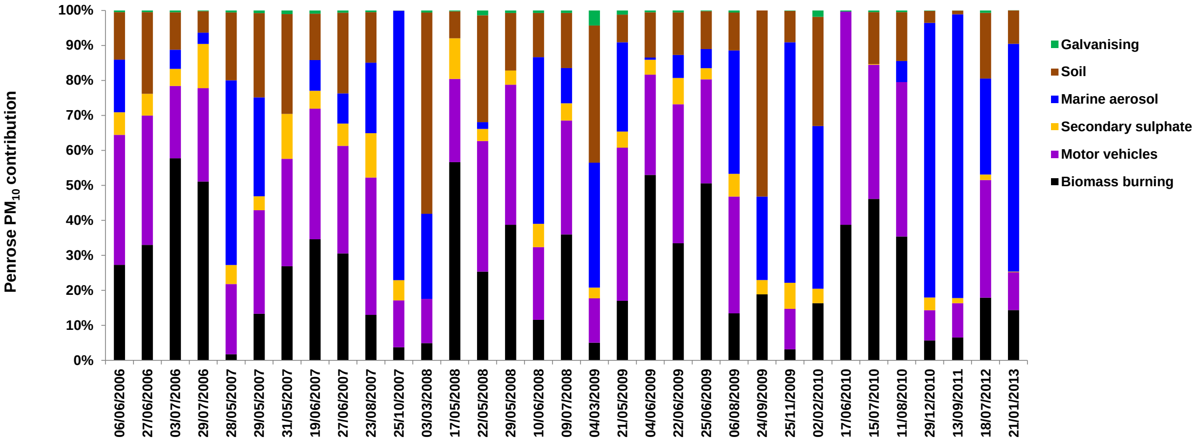

Figure 9.30 Source contributions to peak PM$_{10}$ concentrations at Penrose

Figure 9.13 shows that biomass burning and motor vehicle emission sources (during winter) were primarily responsible for elevated PM$_{10}$ concentrations at Penrose, while at other times coarse particle sources (marine aerosol, crustal matter) dominated peak concentrations.

9.7.6 Variation of PM$_{210}$ source contributions with wind direction

The CPF analysis of the relationship between the source contributions and wind direction is presented and discussed in the following sections. Note that the sheltering effect of the building to the southeast of the monitoring station (see wind roses in Section 9.5) may have affected the CPF analysis and as such most sources show a southeast component that may not be real. The CPF figures are presented in polar coordinates with north as 0 degrees and the axes are in relative probability units (i.e. maximum = 1.0).

9.7.6.1 Biomass Burning

Biomass burning source contributions to PM$_{2.5}$ are considered to be primarily due to emissions from domestic solid fuel fires. Peak contributions are highest on cold calm winter days under inversion conditions or with a light southerly wind, particularly for anticyclonic synoptic conditions. The CPF analysis for biomass burning as presented in Figure 9.31 shows northerly and southerly components. The closest residential dwellings are immediately north of the monitoring site across Gavin Street and emissions from domestic fires from these homes accounts for the northerly component.

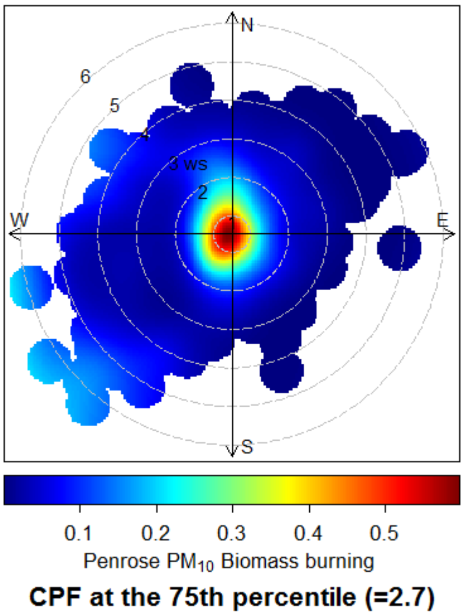

Figure 9.31 Penrose PM_{10} biomass burning CPF analysis

9.7.6.2 Motor vehicles

Peak contributions to PM_{10} from the Motor vehicles source occurred during light to moderate winds from the southwest as presented in Figure 9.32 and is aligned with the southern motorway.

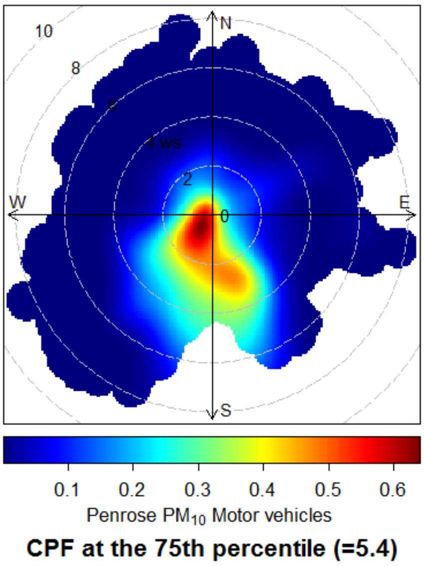

Figure 9.32 Penrose PM_{10} Motor vehicle CPF analysis

9.7.6.3 Secondary sulphate

The PM_{10} secondary sulphate contribution was found to primarily originate from the southeast sector as shown in Figure 9.33. This result differs to the other sites in this study as they all indicate a peak source in the Port of Auckland or Waitemata Harbour area. It is likely that the southern sulphate source at Penrose is due to industrial emissions of SO_2 in the Penrose – Otahuhu area or potentially further away.

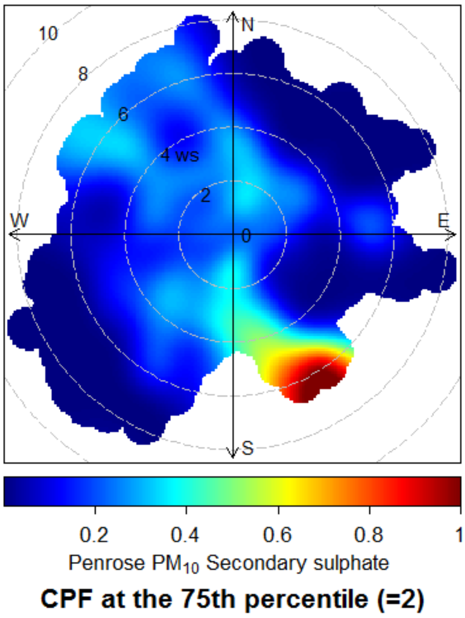

Figure 9.33 Penrose PM_{10} secondary sulphate CPF analysis

9.7.6.4 Marine aerosol

The CPF polar plot for PM_{10} marine aerosol contribution presented in Figure 9.34 shows that the highest concentrations primarily originate from a west-southwest direction under higher wind speeds with smaller northerly and easterly components. The most likely source of the PM_{10} marine aerosol is the Pacific Ocean, Tasman Sea and Southern Ocean.

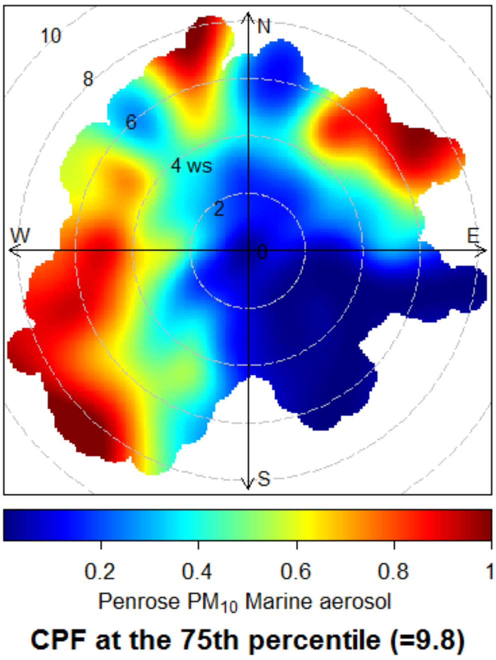

Figure 9.34 Penrose PM_{10} marine aerosol CPF analysis

9.7.6.5 Soil

The Soil source shows a small easterly component as presented in Figure 9.35 and is probably due to dusts from vehicle movements on unsealed yards in the vicinity. There was also a significant southerly component which suggests that this may be due to road dust, a conclusion supported by the significantly lower weekend contributions compared to weekdays, similar to the motor vehicle source as shown in Figure 9.27.

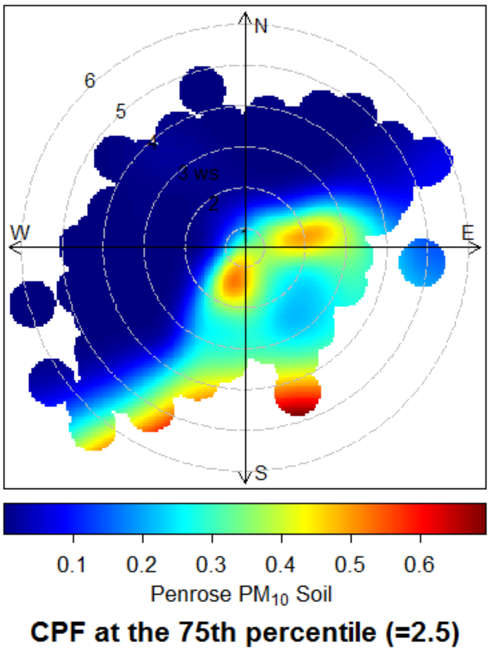

Figure 9.35 Penrose PM$_{2.5}$ Soil CPF analysis

9.7.6.6 Galvanising

The Galvanising source profile is dominated by zinc and has been identified as likely to originate from local hot-dip galvanising activities. There are two hot-dip galvanising operations south of the monitoring site in the industrial area on the other side of the Southern Motorway and another hot-dip galvanising facility to the east across Gavin Street. The CPF analysis presented in Figure 9.36 indicates that the galvanising source originates from the southerly and easterly sectors.

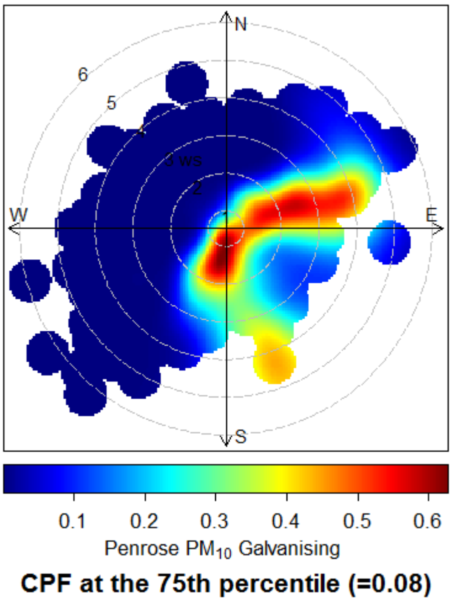

Figure 9.36 Penrose PM$_{10}$ Galvanising CPF analysis

9.8 SUMMARY OF PENROSE RECEPTOR MODELLING ANALYSES

The receptor modelling of $PM_{2.5}$ at Penrose has shown that motor vehicle and biomass burning sources are the major contributors to $PM_{2.5}$ mass and dominate source contributions during peak $PM_{2.5}$ events. Biomass burning, most likely due to emissions from domestic solid fuel fires, was found to be largely responsible for exceedances of the AAQG for $PM_{2.5}$. PM_{10} mass was also found to be dominated by $PM_{2.5}$ during peak PM_{10} events although only one exceedence (on 4 June 2009) of the NES was recorded during the speciation sampling, primarily due to biomass burning and motor vehicle emission sources. Seasonal analysis of source contributions shows that biomass burning is significantly higher during winter while motor vehicle emissions are the primary source of $PM_{2.5}$ during all other seasons. The mass apportioned to each source for $PM_{2.5}$ and PM_{10} is presented in Table 9.5.

Table 9.5 Mass apportioned to $PM_{2.5}$ and PM_{10} (± modelled standard deviation) sources at Penrose

Species	Biomass burning (µg m^{-3})	Motor vehicles 1 (µg m^{-3})	Sulphate (µg m^{-3})	Marine aerosol (µg m^{-3})	Soil (µg m^{-3})	Cement (µg m^{-3})	Industry (µg m^{-3})	Galvanising (µg m^{-3})
$PM_{2.5}$	1.5±0.3	2.5±0.3	1.0±0.1	1.0±0.1	0.5±0.1	0.005±0.17	0.3±0.06	0.2±0.06
PM_{10}	2.0±0.5	3.9±0.4	1.4±0.3	6.8±0.2	1.7±0.2	~	~	0.1±0.1

Figure 9.37 reproduces the $PM_{2.5}$ and PM_{10} pie graphs of source contributions at Penrose.

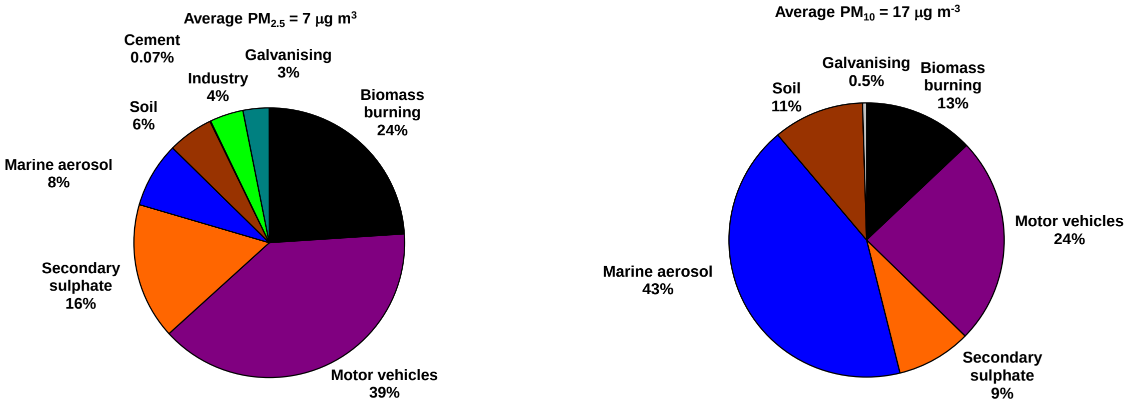

Figure 9.37 (left) Speciation $PM_{2.5}$; and (right) combined PM_{10} pie graphs of source contributions at Penrose

The biomass burning source contributions were consistent across both datasets and was primarily a $PM_{2.5}$ source. As with other sites the PM_{10} motor vehicle source contribution is significantly higher than the corresponding $PM_{2.5}$ due to the inclusion of the coarse particle road dust component in PM_{10}. The Penrose motor vehicle source contributions for $PM_{2.5}$ and PM_{10} was consistent with the Takapuna site as both sites are dominated by emissions from motor vehicles on a nearby motorway (each site is about the same distance from the motorway).

It would appear that there was a local source of secondary sulphate in the Penrose area. The marine aerosol contribution is consistent with other sites in the Auckland region and indicates that marine aerosol is a regional source. The crustal matter source contributions were probably a combination of specific industrial activities such as aggregate and soil handling as well as wind-blown dust and the generations and re-suspension of road dust by vehicles on the Southern motorway and other local roads.

9.8.1 Identification of industrial source contributions at the Penrose site

The receptor modelling analysis of eight years of Penrose $PM_{2.5}$ and PM_{10} elemental composition data has revealed a number of sources that have been identified as originating from industrial sources. While there are likely to be a number of other industrial sources that emit particles to atmosphere in the Penrose area, they may not have been identified as a separate contributor for a variety of reasons, for example:

- Emissions do not (or rarely) impact on the monitoring (receptor) site;
- The contribution of emissions to particulate matter concentrations is too low (i.e. within the range of analytical noise);
- The chemical signature (source profile) is not distinct enough from other sources;
- The nature of the emissions change over time

As an illustration of the changing nature of activities in the Penrose area and therefore the relative source contributions to particulate matter, Figure 9.38 presents a time-series of aerial photographs of the immediate environs around the Gavin Street monitoring site. This shows that initially, when speciation sampling began at the end of 2005, there was an aggregate and landscaping supplies activity immediately next to the Gavin Street substation site and across Gavin Street was a quarry and asphalt production facility. By 2007 the quarry had been disestablished and a major concrete batching facility built between Gavin Street and the asphalt production facility. At the time of the last image was taken in 2013 the same activities as in 2007 appeared to still be in operation. Significant building development and sealing of previously unsealed yards may explain the evident decreasing trend in crustal matter contributions to PM_{10} as shown in Figure 9.29.

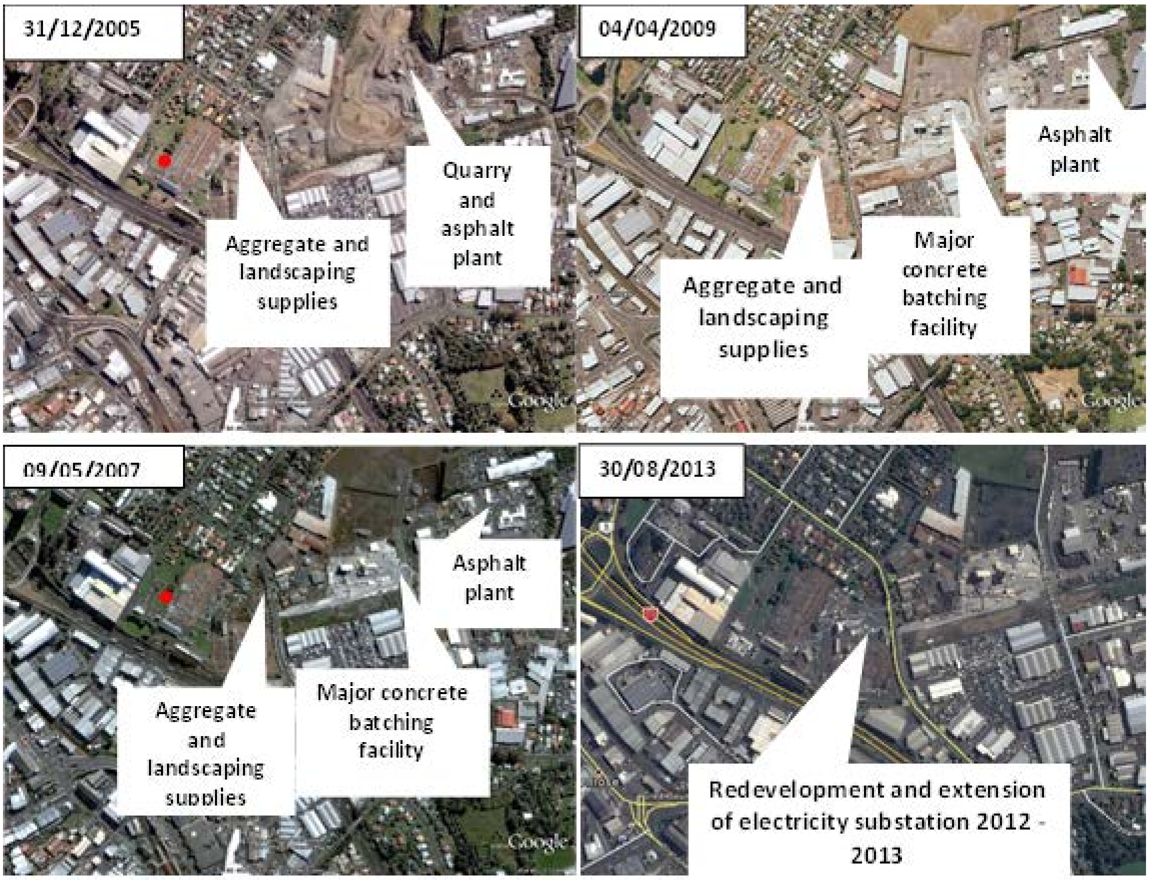

Figure 9.38 Aerial views of Penrose monitoring site (●) identifying the changes in activities over time. Image dates are given in the top left hand corner (Source: Google Earth)

One industry specific source contribution to $PM_{2.5}$ and PM_{10} with a distinctive chemical signature is the source profile with a high relative zinc concentration that was identified as associated with hot-dip galvanising processes. This source has been present since the first analysis (Davy, Trompetter et al. 2007) and mass contributions from galvanising were relatively low but consistent over time in both $PM_{2.5}$ and PM_{10}.

10.0 HENDERSON INTERMEDIATE SCHOOL, HENDERSON

10.1 DESCRIPTION

Samples of airborne particles were collected at an ambient air quality monitoring station located within the grounds of Henderson Intermediate School, off Lincoln Road, Henderson (Latitude -36.8681; Longitude 174.6284). Figure 10.1 shows a map of the local area.

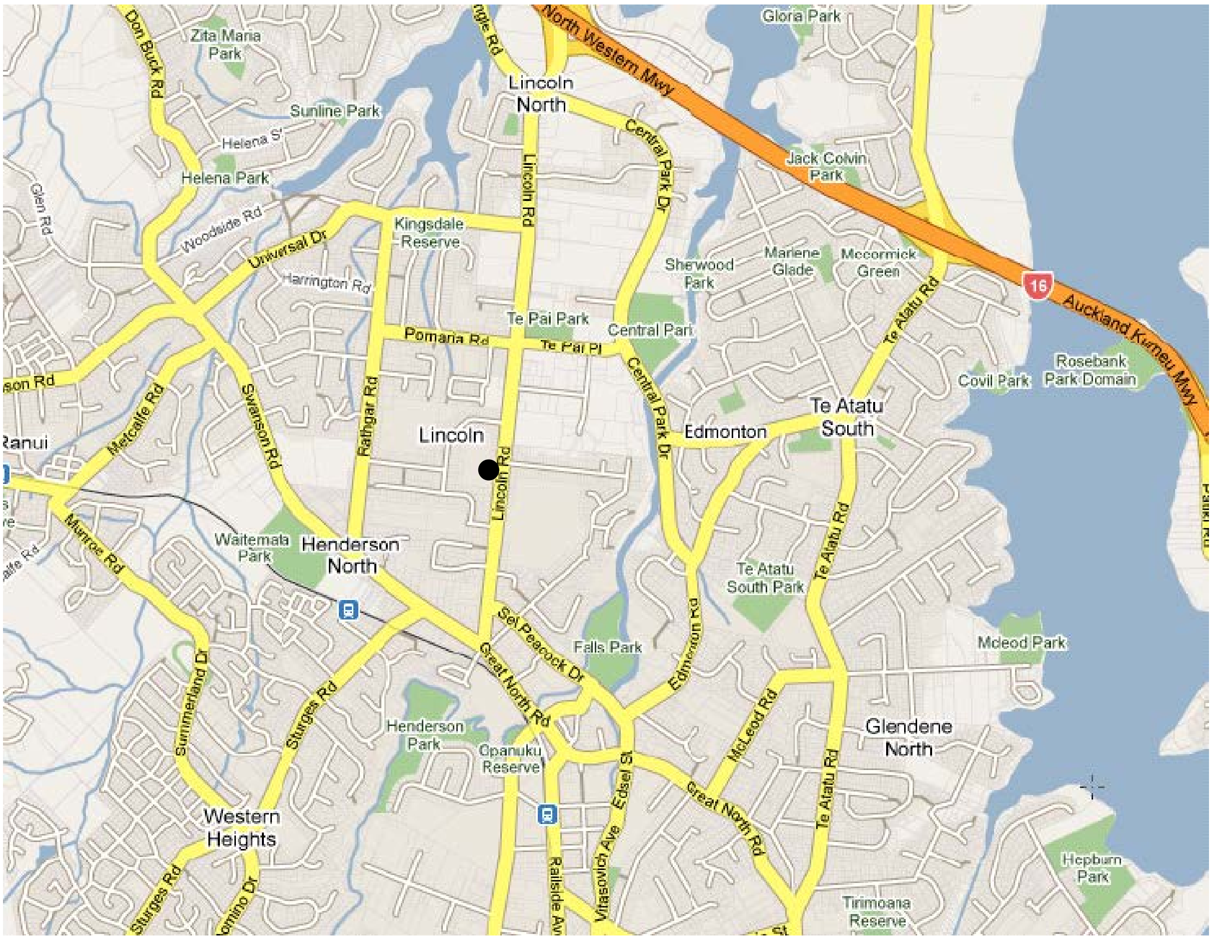

Figure 10.1 Map showing location of Henderson monitoring site (●) (Source Google Maps 2008)

The Henderson site is operated by WSL for AC as part of the AC ambient air quality monitoring programme. The site was established at the end of 1993 and is classed as a residential – peak site. Pollutants monitored at the site include CO, NO_x, PM_{10} (Beta Gauge and Partisol) as well as meteorological parameters.

The Henderson site is approximately 2 km northwest of the Henderson shopping and commercial centre. Land use in the area is a mixture of residential and commercial activities with Te Pai Park industrial area (mainly warehousing and light industrial activities) 500 m to the northeast where the Te Pai Park meteorological monitoring site is located and Waitakere Hospital 300 m southeast of the site. The eastern side of the monitoring station is adjacent to Lincoln Road. To the west is the school, and beyond that are residential properties. Figure 10.2 is an aerial view of the Henderson Intermediate School site and Te Pai Park meteorological site locations.

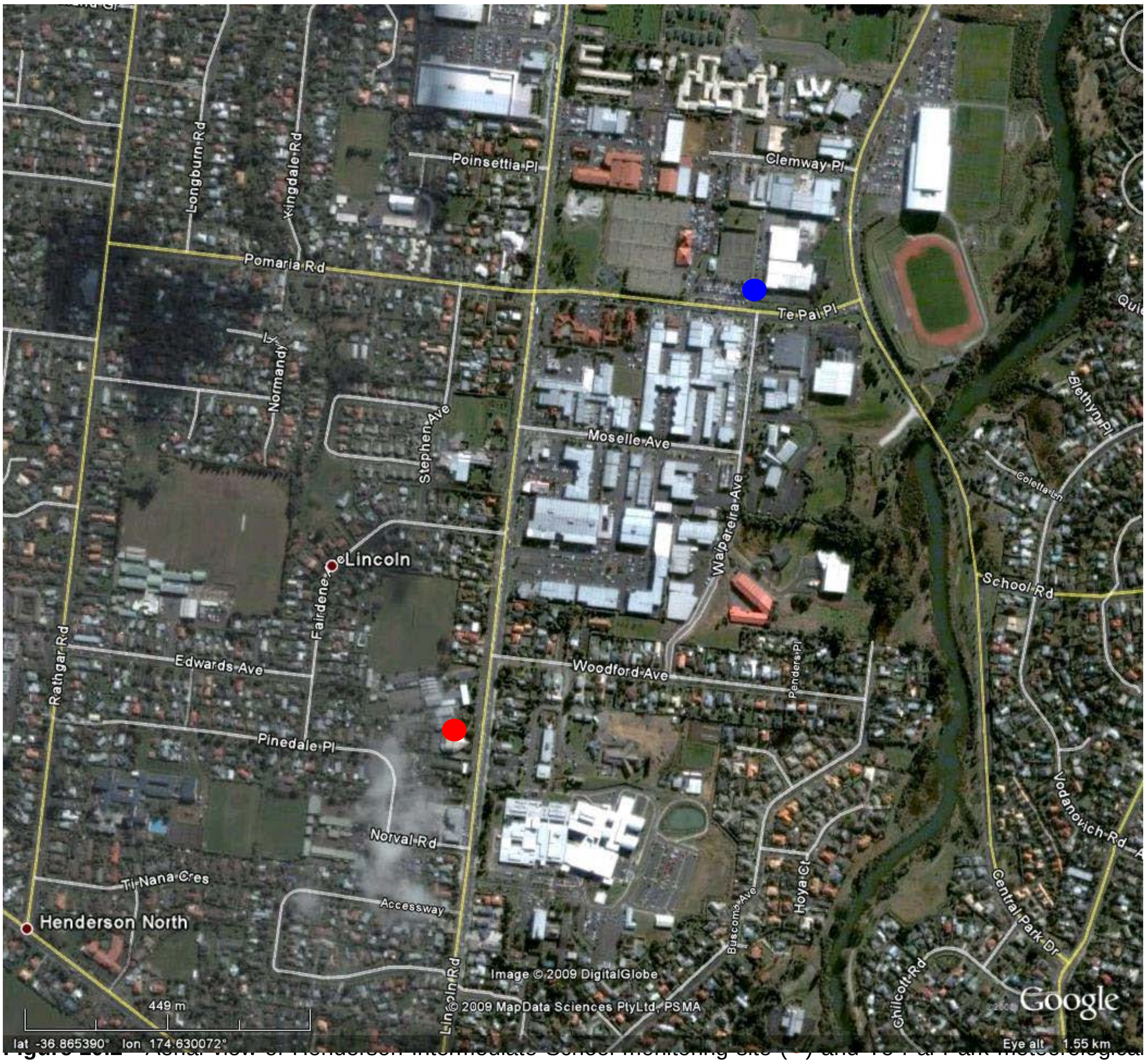

Figure 10.2 Aerial view of Henderson Intermediate School monitoring site (●) and Te Pai Park meteorological monitoring site (●) (Source: Google Maps 2007)

10.2 AIR PARTICULATE MATTER SAMPLES AND MONITORING PERIOD

Filter samples from a sampler located at the Henderson air quality monitoring station were supplied by AC for analysis:

1. 798 PM_{10} samples from a Partisol 2000 sampler on a one-day-in-three sampling regime for the period August 2006 – December 2013.

A receptor modelling study was carried out for the PM_{10} sample set and is reported in Section 10.6.

10.3 PM_{10} CONCENTRATIONS AT THE HENDERSON SITE

The particulate matter results (24-hour average) from the continuous PM_{10} B-gauge monitor (BAM) at Henderson presented in Figure 10.3 show that PM_{10} concentrations are highest during winter months (June - August). Peak PM_{10} concentrations are also evident during summer (December-January) and the summer-winter variations are explained by the relative contributions to ambient concentrations from different sources at different times of the year.

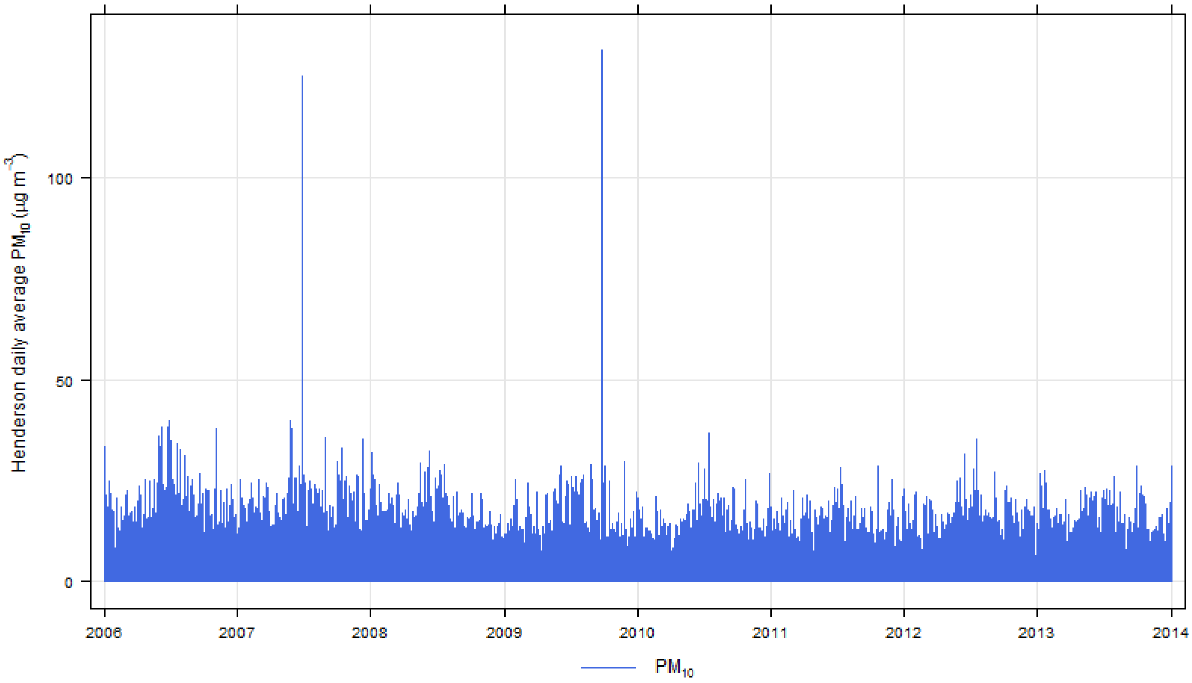

Figure 10.3 BAM PM_{10} concentrations (24-hour average) at the Henderson site

Two exceedances of the NES for PM_{10} (50 $\mu g\ m^{-3}$) were recorded (up to December 2013) at the Henderson site, the first on 27 May 2007 and the next on 25 September 2009. The latter was an extraordinary event due to an Australian dust storm (Davy, Trompetter et al. 2011). Further discussion is provided in Section 10.6.2.

10.4 CONCEPTUAL RECEPTOR MODEL FOR PARTICULATE MATTER AT HENDERSON

The following initial conceptual model for Henderson includes local emission sources:

- Domestic activities – likely to be dominated by biomass burning such as emissions from solid fuel fires used for domestic heating during the winter;
- Motor vehicles – all roads in the area act as line sources and roads with higher density traffic will dominate particularly the motorway immediately to the west;
- Local wind blown soil or road dust sources;
- Local industrial activities
- Activities at the school.

Longer range sources may also contribute to ambient particle loadings and these include:

- Marine aerosol;
- Secondary particulate matter resulting from atmospheric gas-to-particle conversion processes (sulphate and nitrate species, organic particle species resulting from photochemical smog events);
- Potential for long range transport of industrial emissions
- Trans-boundary events such as Australian bush fires or dust storms

Another category of emission sources that may contribute are those considered as ‘one-off’ emission sources, for example:

- Fireworks displays and other special events;
- Short-term road works and demolition/construction activities.

The variety of sources described above can be recognised and accounted for by appropriate data analysis methods, such as examination of seasonal differences, temporal variations and receptor modelling itself.

10.5 LOCAL METEOROLOGY AT THE HENDERSON SITE

The meteorological data used for analysis of meteorology associated with the Henderson Intermediate School air quality monitoring site has been obtained from the Te Pai Park meteorological station (see Figure 10.2) as the presence of adjacent large trees is likely to have affected meteorological data collected at the school location. The predominant wind direction at the Henderson site is from the southwesterly quarter as shown by the wind roses in Figure 10.4.

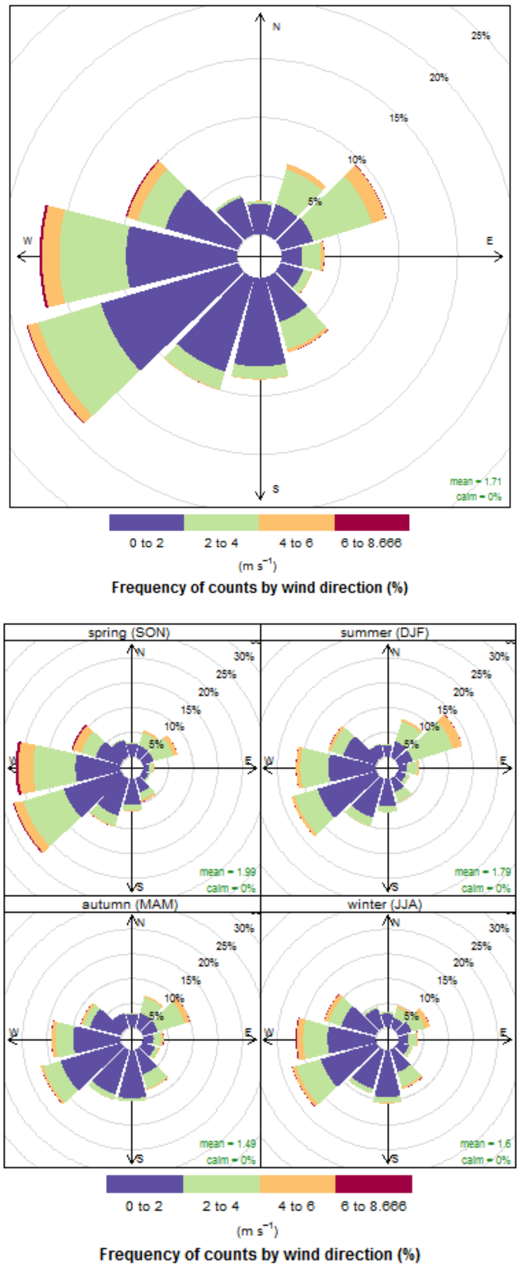

Figure 10.4 (Top) Wind rose for 2006-2013; (Bottom) Wind roses for each season

Meteorological differences between seasons at the Henderson site can be seen in the wind roses presented in Figure 10.4. The predominance of southwesterly winds was markedly more significant in winter and spring, with a greater component of winds originating from the northeast during the summer.

10.6 ANALYSIS OF PM_{10} SAMPLES FROM THE HENDERSON SITE

The Henderson PM_{10} samples from the Henderson Intermediate School monitoring site refer to those PM_{10} samples collected using a Partisol 2000 Sampler (Andersen Instruments Inc.) from August 2006 to December 2013. Gravimetric results for the Partisol PM_{10} samples as presented in Figure 10.5 show distinct peaks in PM_{10} concentrations during winter months (June – August) at Henderson similar to the BAM PM_{10}. Gaps in the data are due to missed or excluded sample periods for quality assurance purposes.

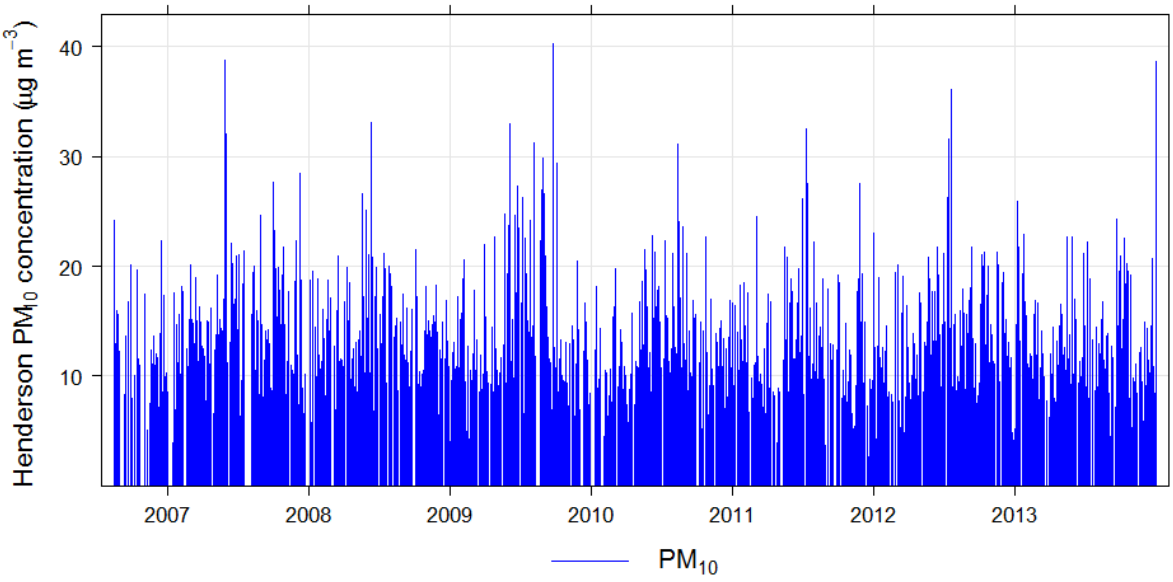

Figure 10.5 Gravimetric results for Partisol PM_{10} (24-hour average) at the Henderson site

Peak concentrations in Partisol PM_{10} correspond with peaks in BAM PM_{10} concentrations (see Figure 10.3).

10.6.1 Composition of PM_{10} at the Henderson site

Elemental concentrations for Partisol PM_{10} at the Henderson site are presented in Table 10.1 and a box and whisker plot of those concentrations is presented in Figure 10.6.

Table 10.1 Elemental analysis results for Partisol PM_{10} at the Henderson site (798 samples)

Species	Average (ngm^{-3})	Max (ngm^{-3})	Min (ngm^{-3})	Median (ngm^{-3})	Std Dev (ngm^{-3})	Av LOD (ngm^{-3})	#>LOD
PM_{10} ($\mu g\ m^{-3}$)	**14**	**40**	**4**	**13**	**5**		
H	143	847	-24	116	121	45	665
BC	2004	10463	0	1590	1646	171	785
Na	1939	7731	0	1647	1328	441	765
Mg	169	623	0	147	103	34	782
Al	81	2384	0	60	128	15	770
Si	213	5847	31	159	260	11	798
P	13	94	0	10	13	15	344
S	349	1549	54	323	163	12	798
Cl	2781	11231	2	2315	2002	6	797
K	126	2055	20	107	101	7	798
Ca	130	473	21	123	58	7	798
Sc	2	15	0	1	3	9	51
Ti	8	140	0	6	9	8	378
V	1	9	0	0	2	9	27
Cr	1	85	0	0	4	8	45
Mn	4	33	0	3	4	7	201
Fe	140	1551	4	110	125	5	795
Co	2	23	0	1	3	10	73
Ni	2	80	0	1	4	9	69
Cu	5	47	0	4	6	10	216
Zn	41	2301	0	10	136	11	388
Ga	3	20	0	0	4	18	55
Ge	3	29	0	0	6	23	43
As	8	77	0	0	13	29	123
Se	7	76	0	0	10	36	68
Br	10	66	0	0	14	45	88
Sr	17	154	0	0	26	93	63
I	9	185	0	4	13	29	75
Ba	13	99	0	9	14	31	136
Hg	11	107	0	0	19	66	48

Pb	15	166	0	0	26	81	56

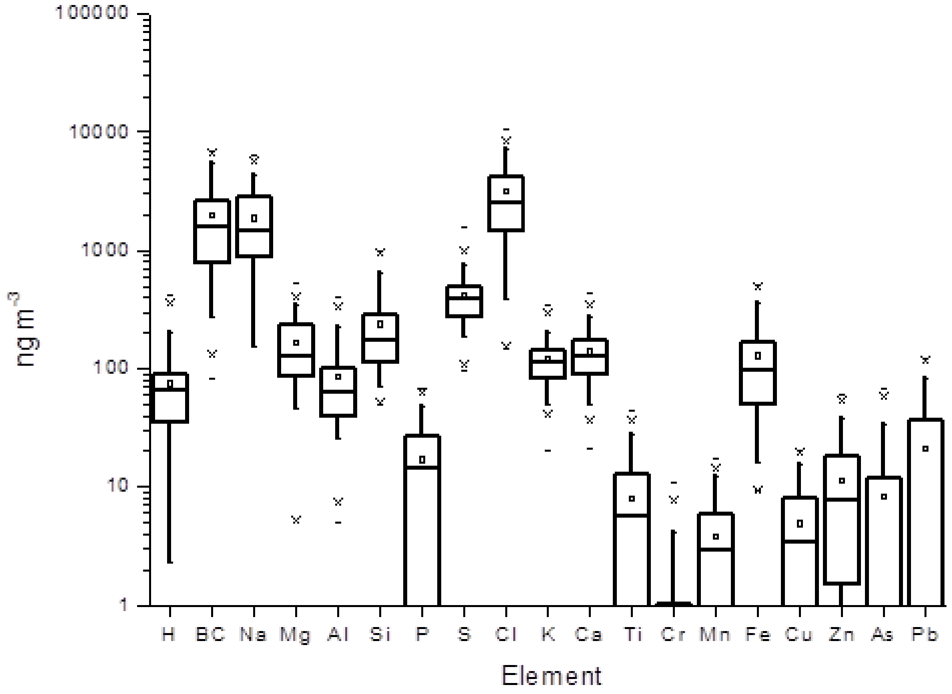

Figure 10.6 Box and whisker plot of PM_{10} elemental concentrations at the Henderson site (logarithmic scale)

Table 10.1 shows a number of measured species being generally close to or below the limits of detection. Carbonaceous species (represented by BC), sodium and chlorine were found to dominate PM_{10} elemental mass concentrations indicating that combustion processes and marine aerosol are important contributors to ambient PM_{10} at Henderson. A correlation matrix of the species in Table 10.1 is presented in Appendix 6.

10.6.2 Source contributions to PM_{10} at Henderson

Six primary source contributors were determined from the PMF receptor modelling analysis of PM_{10} elemental composition at Henderson. These are identified as presented in Table 10.2 along with the mass of PM_{10} and elemental species associated with each source.

Table 10.2 Elemental composition of source profiles and contribution to PM_{10} at the Henderson site

	Factor 1	**Factor 2**	**Factor 3**	**Factor 4**	**Factor 5**	**Factor 6**
Species	**Biomass burning (ngm^{-3})**	**Motor vehicles (ngm^{-3})**	**Sulphate (ngm^{-3})**	**Marine aerosol (ngm^{-3})**	**Soil (ngm^{-3})**	**Zinc (ngm^{-3})**
PM_{10} ($\mu g\ m^{-3}$)	**2.3**	**2.0**	**1.4**	**6.0**	**1.2**	**0.1**
H	96	0	0	21	11	4
BC	1053	842	61	0	7	6
Na	33	10	116	1676	58	29
Mg	8	3	11	130	13	1
Al	8	0	14	2	52	0
Si	16	21	39	0	132	0
S	0	39	169	124	11	3
Cl	0	55	96	2493	86	26
K	42	2	7	50	13	1
Ca	2	31	8	57	28	1
Ti	0	4	0	0	3	0
Mn	0	2	0	1	1	0
Fe	7	95	1	3	29	0
Cu	1	3	1	1	0	0
Zn	4	7	2	2	0	25
As	7	0	1	1	0	0
Pb	7	2	2	2	0	0

Table 10.2 represents the summary results for a reiterative process that examines the effect of each species on the PMF receptor modelling process using the modelling diagnostics presented in Appendix 6. Species that were poorly modelled (slope, $r^2 < 0.6$) were removed from the analyses unless considered vital for source identification.

The source contributors identified in Table 10.2 were found on average to explain 95 % of PM_{10} gravimetric mass. Figure 10.7 presents the source profiles extracted from the PMF analysis of Henderson PM_{10} data.

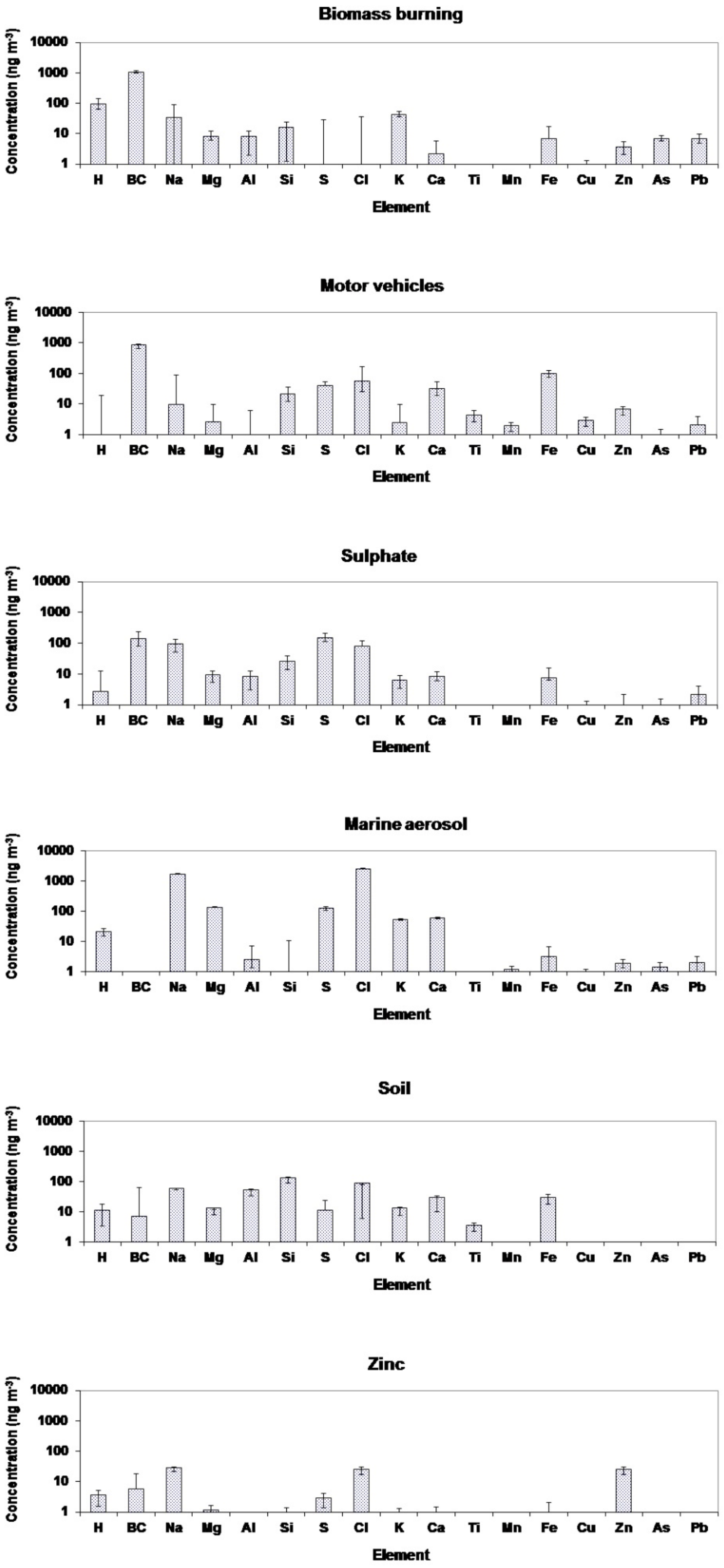

Figure 10.7 Source profiles and elemental concentrations for PM_{10} at the Henderson site (showing 5th and 95th confidence intervals in mean concentration derived from the receptor modelling)

- The first factor is from biomass burning due to the association of H, BC and K. The majority of arsenic and lead were also associated with the profile.
- The second factor represents the contribution from motor vehicle emission sources
- The third factor has been identified as a secondary sulphate aerosol source due to the predominance of S.
- The fourth factor represents the contribution from marine aerosol due to the dominance of Na and Cl.
- The fifth source is from crustal matter (wind blown dust and road dust).
- The sixth factor had a high zinc content and is thought to be associated with local industrial emissions.

Figure 10.8 presents the average (August 2006 – December 2013) source contributions to PM_{10} concentrations and includes standard deviations of average mass contributions from each of the sources indicating the variability in source strength.

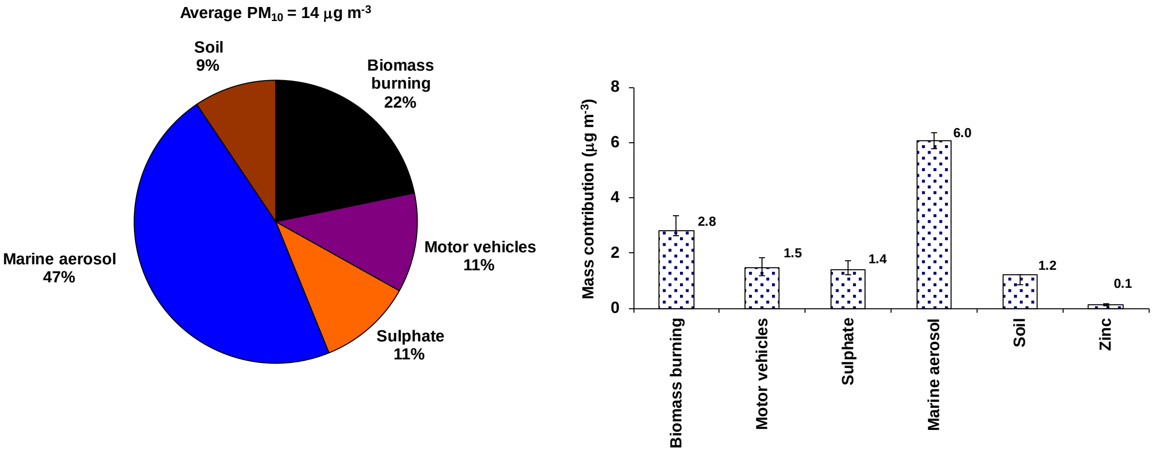

Figure 10.8 Average (August 2006 – December 2013) source contributions to PM_{10} at Henderson (showing 5th and 95th confidence intervals in mean concentration derived from the receptor modelling)

The average source contributions estimated by the receptor modelling shows that marine aerosol, biomass burning and motor vehicle emissions are the most significant contributors (46 %, 18 % and 16 % respectively) to PM_{10} concentrations at Henderson, with lesser contributions from crustal matter (9 %) and secondary sulphate particles (9 %). The Zinc source was present at low PM_{10} concentrations.

Figure 10.9 shows the mass contribution of sources to PM_{10} mass for each sample collected at Henderson. The temporal variation indicates that marine aerosol is an important contributor throughout the year while biomass burning and motor vehicles have peak contributions during winter months. A peak in crustal matter contributions (41 µg m^{-3}) occurred on 24 September 2009 as a result of a trans-boundary Australian dust event following a dust storm in the Australian desert. Further discussion and analysis of this event provided in (Davy, Trompetter et al. 2011).

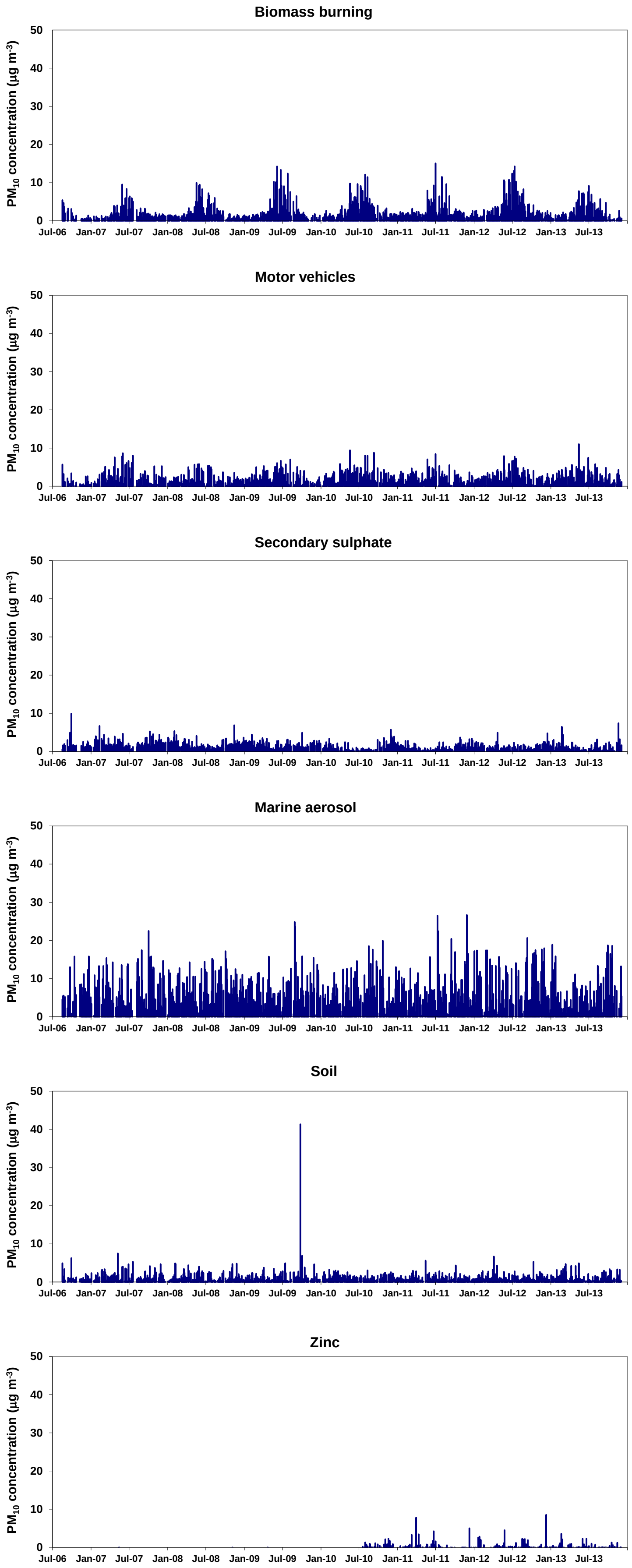

Figure 10.9 Time-series for source contributions to PM$_{10}$ mass at Henderson

The Zinc source appears to have only started impacting at the monitoring site from mid-2010 onwards. This can be seen clearly in the time-series plot for elemental zinc concentrations at the Henderson monitoring site where there was a significant jump in elemental zinc concentrations as presented in Figure 10.10. Analysis of the data indicates that elemental zinc comprises approximately 19% of the PM_{10} mass attributed to the Zinc emission source.

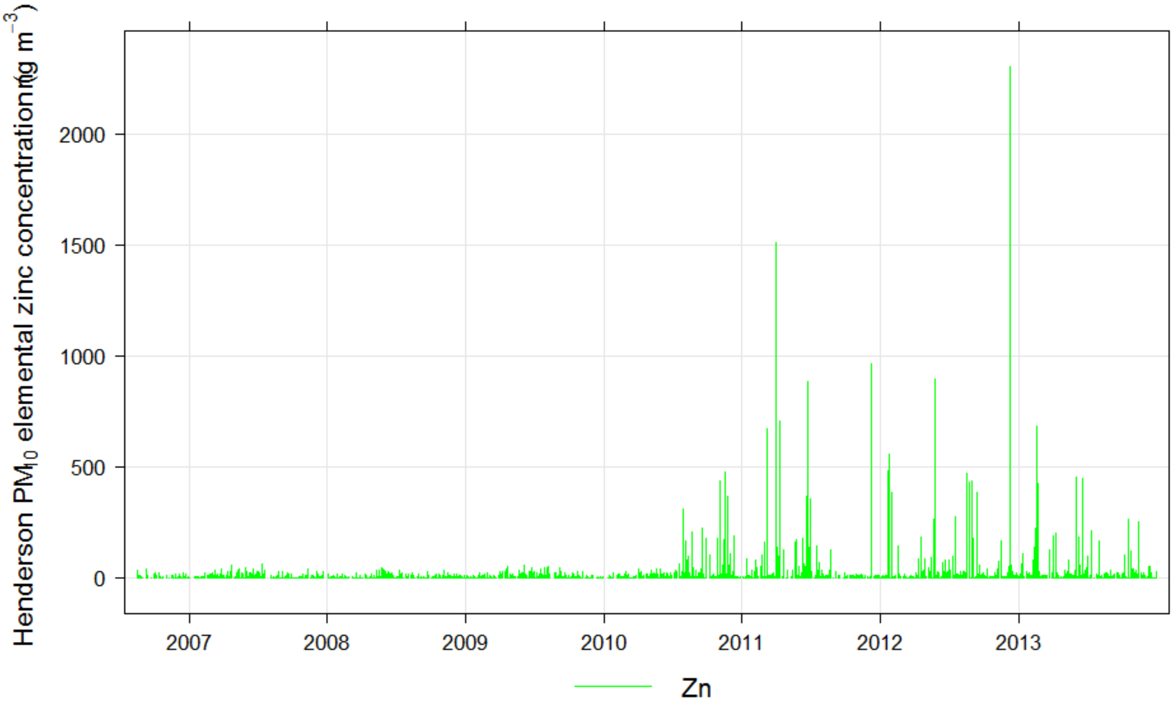

Figure 10.10 Time-series for elemental zinc concentrations in PM_{10} at the Henderson site

10.6.3 Temporal variations in PM_{10} source contributions at the Henderson site

The primary source of PM_{10} during winter (June-August) at Henderson was marine aerosol (39 %) and biomass burning (29 %). The biomass burning contributions are most likely due to emissions from solid fuel fires for domestic heating. Figure 10.11 presents the monthly and weekday average source mass contributions for the Henderson site. Average PM_{10} concentrations were found to be higher in winter months than in other seasons primarily due to mass contributions from biomass burning sources.

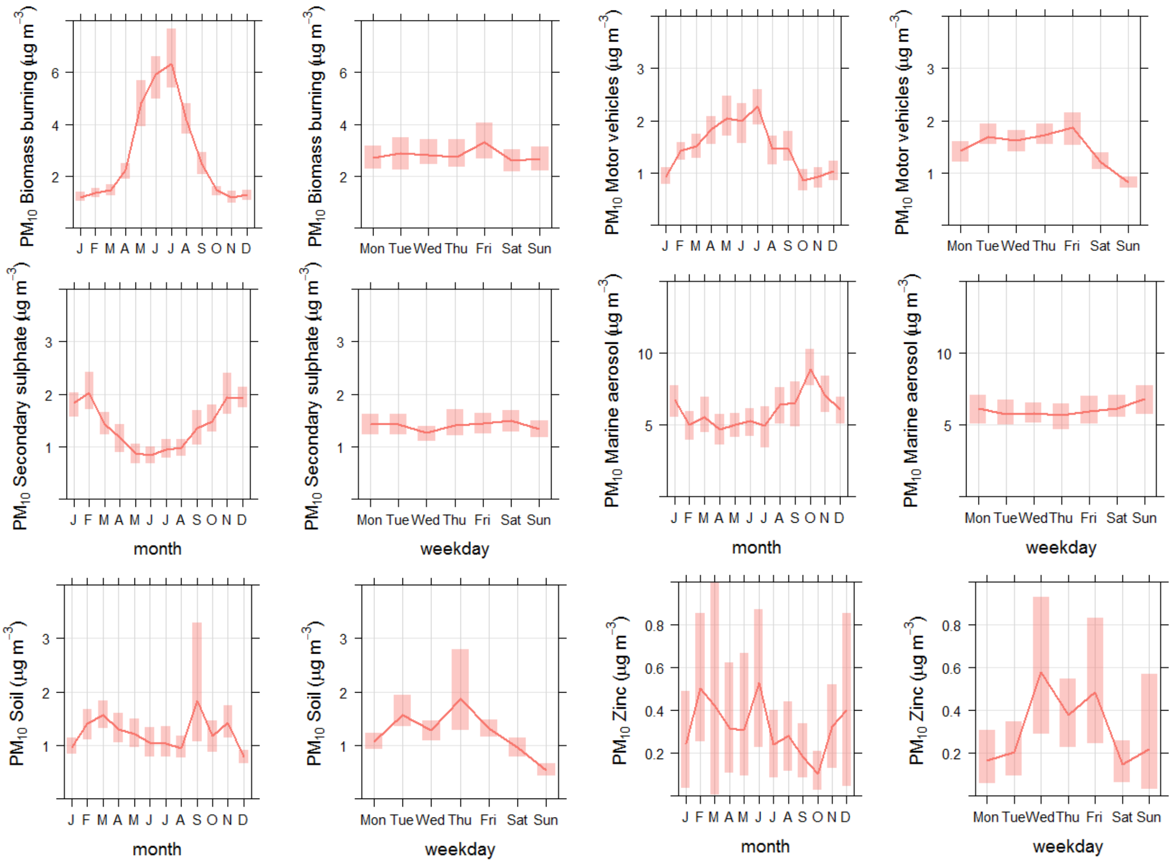

Figure 10.11 Temporal variations (2006-2013) in PM_{10} source contributions at the Henderson site (the shaded bars are the 95 percentile confidence limits in the mean)

Average PM_{10} concentrations (12 - 14 µg/m^3) during autumn (March-May), spring (September-November) and summer (December-February) were relatively similar. Marine aerosol was the predominant source during spring, summer and autumn. Motor vehicle and soil mass contributions were found to be higher during weekdays. This result is indicative of higher motor vehicle activity during weekdays aligned to typical working week commuter activity. The soil source is likely in part to be associated with road dust generated by motor vehicles and source contributions match motor vehicle weekday activity. The only significant anomaly is the Australian dust storm event (Thursday 24 September 2009) that is evident in the September and Thursday averages presented in Figure 10.11. No significant difference in mass contributions for the weekday/weekend categories was found for the biomass burning, secondary sulphate, marine aerosol or zinc sources. The strong variability (large 95 percentile confidence limits) in the Zinc source suggests some intermittency for the impacts on the monitoring site that is likely to be consistent with occasional plume touchdown depending on wind direction and source activity.

10.6.4 Trends in PM_{10} concentrations and source contributions at Henderson

The temporal trends in PM_{10} source contributions at Henderson were explored using the Thielsen functionality available in *openair*. Figure 10.12 presents the deseasonailsed trend in PM_{10} concentrations showing that there was a small but statistically significant decreasing trend (95 % CI) over the monitoring period.

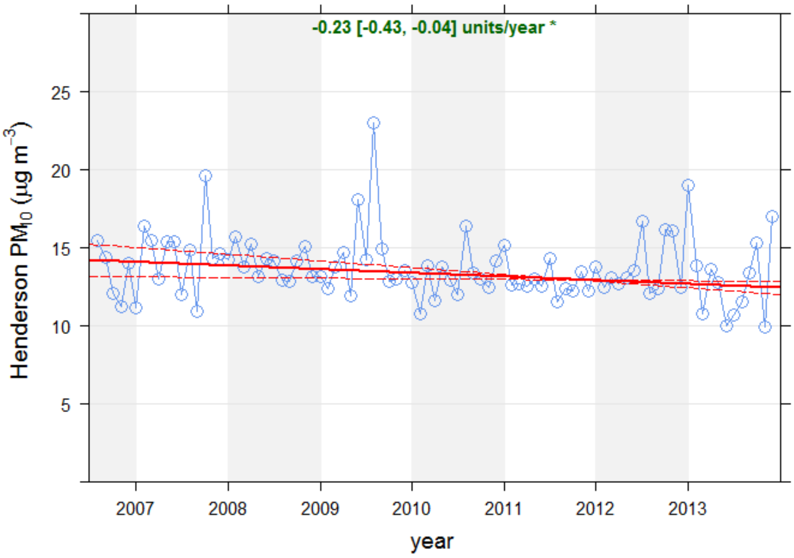

Figure 10.12 Trend in PM_{10} concentrations at Henderson (statistically significant at the 95 % confidence interval)

The trends in PM_{10} source contributions are presented in Figure 10.13 and indicate that contributions from motor vehicles (95 % CI) and biomass burning (90 % CI) appear to have increased over the monitoring period. The decrease in secondary sulphate (99.9 % CI) was consistent with a reduction in the sulphur content of fuels as discussed in Chapter 5. The increase in PM_{10} associated with motor vehicles may be due to a traffic volume increases on Lincoln Road, an arterial route immediately adjacent the Henderson monitoring site. There were no statistically significant trends for the PM_{10} crustal matter and marine aerosol sources. No trend was apparent for the Zinc source contributions but essentially there was only four years of data available so care should be taken until a longer time-series is available.

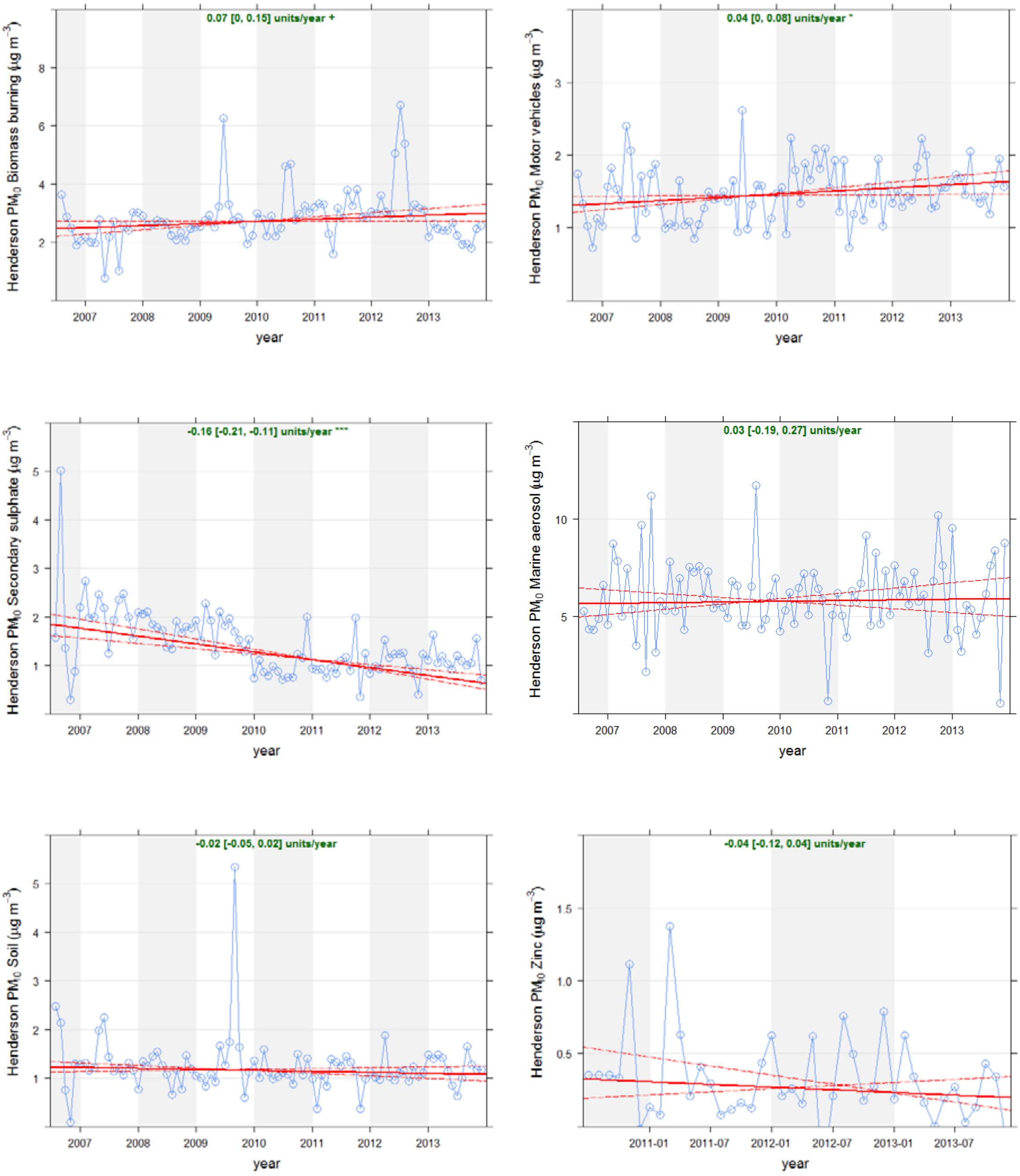

Figure 10.13 Trends in PM_{10} source contributions at Henderson

10.6.5 Analysis of individual PM_{10} events at Henderson

Peak PM_{10} events during the sampling period at Henderson have been chosen for further analysis. Peak PM_{10} events are defined as those that were higher than 66 % (33 µg m^{-3}) of the NES (50 µg m^{-3} 24-hour average). It was found that there were 33 days over the monitoring period where PM_{10} concentrations were higher than 66 % of the NES.

Figure 10.14 presents the mass contributions of individual sources to each of the peak PM_{10} days (> 33 µg m^{-3}).

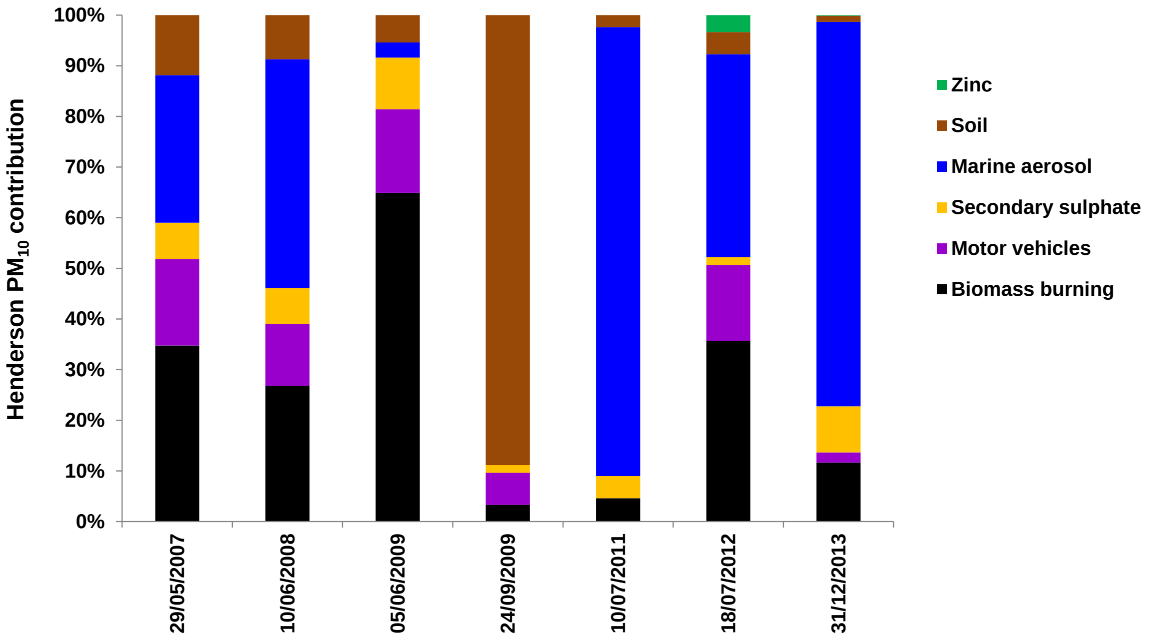

Figure 10.14 Source contributions to peak PM_{10} concentrations at Henderson

Figure 10.14 shows that biomass burning and motor vehicle emission sources (during winter) were primarily responsible for elevated PM_{10} concentrations at Henderson, while at other times coarse particle sources (marine aerosol, crustal matter) dominated peak concentrations. The high crustal matter contribution on 24 September 2009 was due to an Australian dust storm event.

10.6.6 Variation of PM_{10} source contributions with wind direction at the Henderson site

The CPF analysis of the relationship between the source contributions and wind direction is presented and discussed in the following sections. Note that the figures are presented in polar coordinates with north as 0 degrees and the axes are in relative probability units (i.e. maximum = 1.0).

10.6.6.1 Biomass Burning

Biomass burning source contributions to PM_{10} at Henderson are considered to be primarily due to emissions from domestic solid fuel fires during winter. Peak contributions are highest on cold calm winter days under inversion conditions or with a light southerly wind, particularly for anticyclonic synoptic conditions. The CPF analysis for biomass burning presented in Figure 10.15 shows a northerly and southerly component and is aligned with the air flows up and down Henderson Valley.

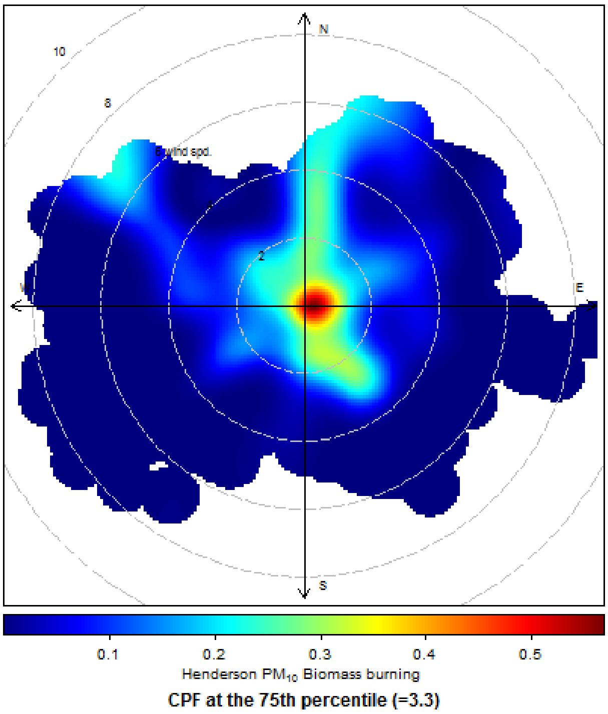

Figure 10.15 Henderson PM_{10} Biomass burning CPF analysis

10.6.6.2 Motor Vehicles

The motor vehicle source for PM_{10} shows a north-south component as presented in Figure 10.16 and is aligned with Lincoln Road which is adjacent to the monitoring site, and is a major arterial feeder road to the Northwestern Motorway (SH16).

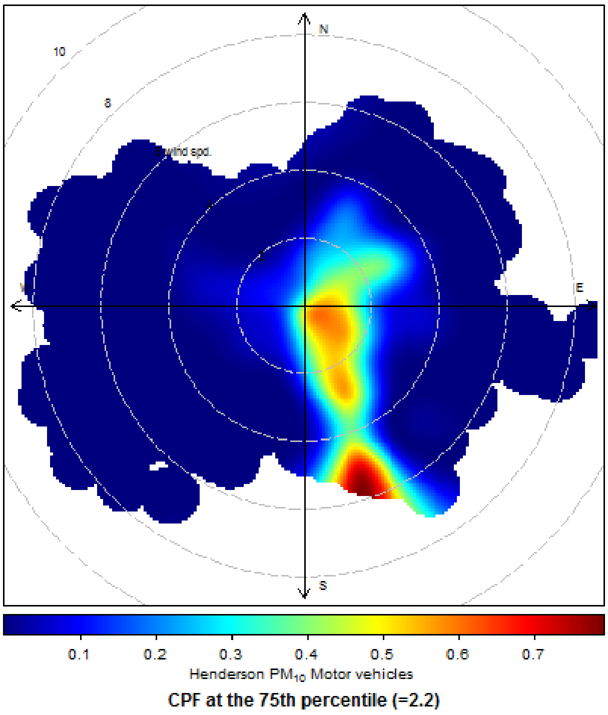

Figure 10.16 Henderson PM_{10} Motor vehicle CPF analysis

10.6.6.3 Secondary sulphate

The PM_{10} secondary sulphate contribution was found to primarily originate from the northwest and easterly sectors (Figure 10.17). This supports the case that an originating source is likely to be emissions from ships moving in and out of the Port of Auckland (easterly component for Henderson).

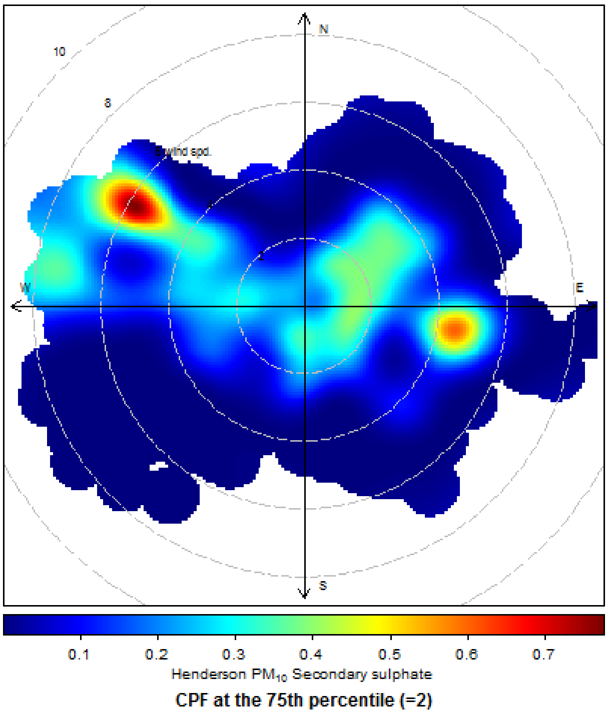

Figure 10.17 Henderson PM_{10} Secondary sulphate CPF analysis

10.6.6.4 Marine aerosol

The Henderson PM_{10} marine aerosol contribution presented in Figure 10.18 originates from the westerly and easterly directions. The most likely source of the PM_{10} marine aerosol is the Tasman Sea and Pacific Ocean.

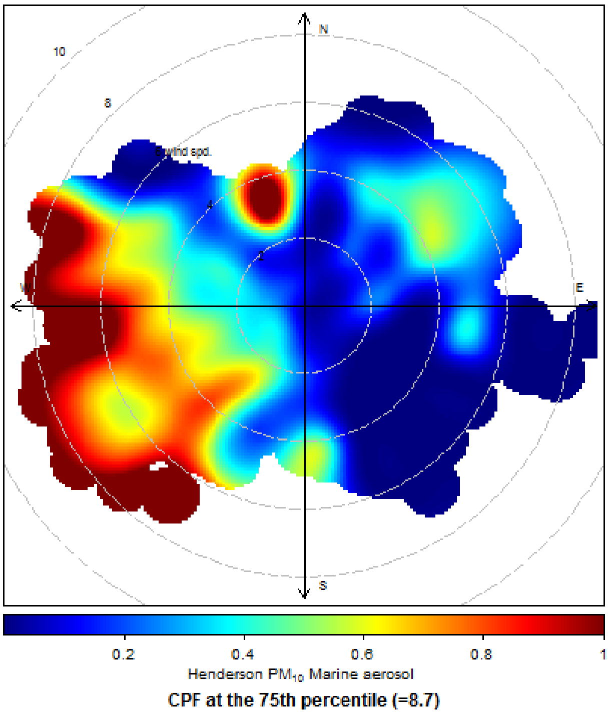

Figure 10.18 Henderson PM$_{10}$ Marine aerosol CPF analysis

10.6.6.5 Crustal matter

The crustal matter source for PM$_{10}$ shows north-south components as presented in Figure 10.19 and is likely to have originated from Lincoln Road as road dust. Dusts would also originate from the school grounds immediately northwest of the monitoring station.

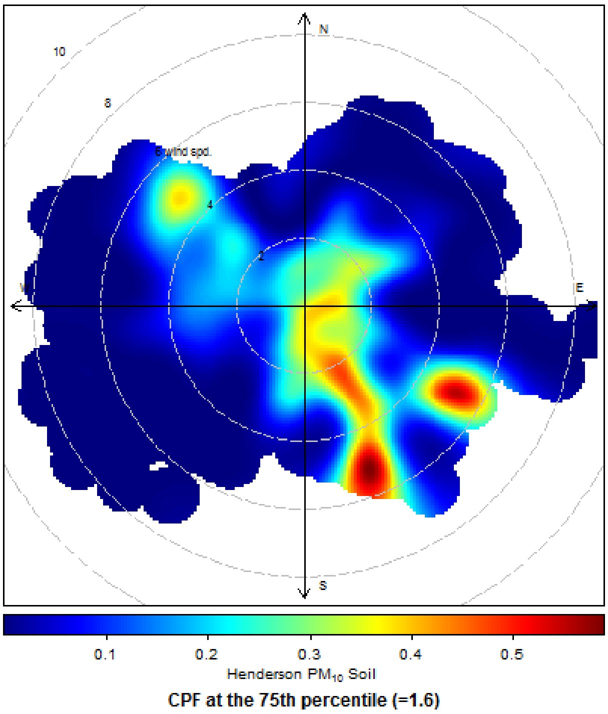

Figure 10.19 Henderson PM$_{10}$ Soil CPF analysis

10.6.6.6 Zinc

The Zinc source for PM_{10} shows a west to southwesterly dependence for source strength and wind direction as presented in Figure 10.20. The potential source of the zinc is as-yet unidentified but it is most likely to be associated with an industrial process. The zinc source at Penrose (see Chapter 9) was identified to be due to hot-dip galvanising activities in the local area. There appear to be no hot dip galvanising facilities near the Henderson site but there are surface coating activities in the industrial area to the west of the monitoring site and also a pharmaceuticals plant manufacturing topical uv-protection formulations (containing zinc oxide) to the northeast. It would seem activities to the west of the monitoring site are having the greatest influence on peak concentrations. A similar source profile containing zinc was observed at Tahunanui in Nelson and that was also surmised to be associated with anti-corrosion surface coating activities in the near-by industrial area (Davy, Trompetter et al. 2010, Ancelet, Davy et al. 2014).

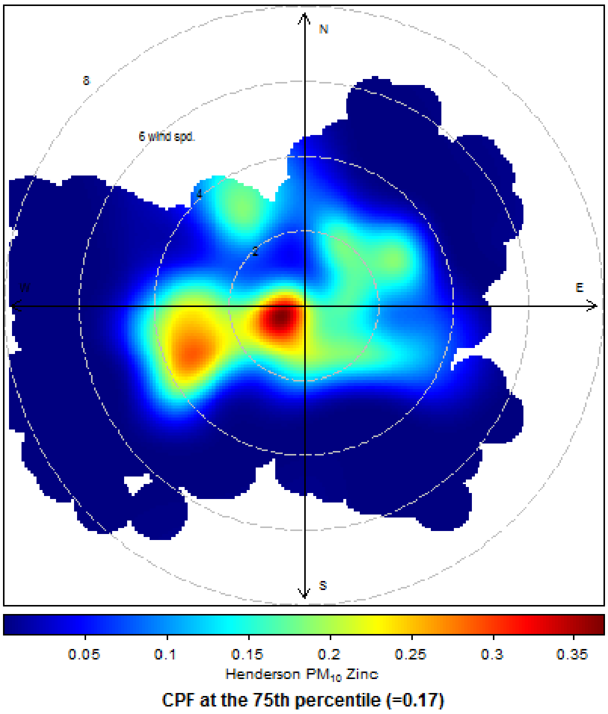

Figure 10.20 Henderson PM_{10} Zinc CPF analysis

10.7 SUMMARY OF HENDERSON SOURCE APPORTIONMENT ANALYSES

Marine aerosol was found to dominate source mass contributions to PM_{10} at the Henderson site and along with biomass burning and motor vehicles were the primary source during peak PM_{10} events. Arsenic and lead were found to be associated with the biomass burning source and it suggests there may be a significant component of CCA (copper chrome arsenate) treated timber and old painted timber (lead based paints) burnt in local wood burners producing the co-emission of arsenic and lead with other biomass burning elemental components (e.g. H, BC and K). Similar associations have been observed in elemental data from other monitoring sites across New Zealand (Davy, Ancelet et al. 2012, Ancelet, Davy et al. 2014, Davy, Ancelet et al. 2014, Ancelet, Davy et al. 2015).

11.0 REFERENCES

Agrawal, H., Q. G. J. Malloy, W. A. Welch, J. Wayne Miller and D. R. Cocker Iii (2008). "In-use gaseous and particulate matter emissions from a modern ocean going container vessel." Atmospheric Environment **42**(21): 5504-5510.

Agrawal, H., W. A. Welch, J. W. Miller and D. R. Cocker (2008). "Emission measurements from a crude oil tanker at sea." Environmental Science and Technology **42**(19): 7098-7103.

Ancelet, T., P. K. Davy, T. Mitchell, W. J. Trompetter, A. Markwitz and D. C. Weatherburn (2012). "Identification of particulate matter sources on an hourly time-scale in a wood burning community." Environmental Science and Technology **46**(9): 4767-4774.

Ancelet, T., P. K. Davy and W. J. Trompetter (2014). Hourly concentrations of arsenic associated with Particulate Matter. 5th International Congress on Arsenic in the Environment, As 2014, Buenos Aires, CRC Press/Balkema.

Ancelet, T., P. K. Davy and W. J. Trompetter (2015). "Particulate matter sources and long-term trends in a small New Zealand city." Atmospheric Pollution Research **6**(6): 1105-1112.

Ancelet, T., P. K. Davy, W. J. Trompetter and A. Markwitz (2014). "Sources of particulate matter pollution in a small new zealand city." Atmospheric Pollution Research **5**(4): 572-580.

Anlauf, K., S.-M. Li, R. Leaitch, J. Brook, K. Hayden, D. Toom-Sauntry and A. Wiebe (2006). "Ionic composition and size characteristics of particles in the Lower Fraser Valley: Pacific 2001 field study." Atmospheric Environment **40**(15): 2662-2675.

Ault, A. P., M. J. Moore, H. Furutani and K. A. Prather (2009). "Impact of emissions from the Los Angeles Port region on San Diego air quality during regional transport events." Environmental Science and Technology **43**(10): 3500-3506.

Begum, B. A., P. K. Hopke and W. X. Zhao (2005). "Source identification of fine particles in Washington, DC, by expanded factor analysis modeling." Environ. Sci. Technol. **39**(4): 1129-1137.

Brimblecombe, P. (1986). Air: Composition and Chemistry.

Brown, S. G., S. Eberly, P. Paatero and G. A. Norris (2015). "Methods for estimating uncertainty in PMF solutions: Examples with ambient air and water quality data and guidance on reporting PMF results." Science of the Total Environment **518-519**: 626-635.

Brown, S. G. and H. R. Hafner (2005). Multivariate Receptor Modelling Workbook. Research Triangle Park, NC, USEPA.

Cahill, T. A., R. A. Eldred, N. Motallebi and W. C. Malm (1989). "Indirect measurement of hydrocarbon aerosols across the United States by nonsulfate hydrogen-remaining gravimetric mass correlations." Aerosol Sci. Technol. **10**(2): 421-429.

Carslaw, D. C. (2012). The openair manual - open-source tools for analysing air pollution data. Manual for version 0.7-0, King's College London.

Carslaw, D. C. (2015). The openair manual — open-source tools for analysing air pollution data. Manual for version 1.1-4,, King's College London.

Carslaw, D. C. and K. Ropkins (2012). "openair - an R package for air quality data analysis." Environmental Modelling & Software **27-28**: 52-61.

Chueinta, W., P. K. Hopke and P. Paatero (2000). "Investigation of sources of atmospheric aerosol at urban and suburban residential areas in Thailand by positive matrix factorization." Atmos. Environ. **34**(20): 3319-3329.

Cohen, D. (1998). "Characterisation of atmospheric fine particles using IBA techniques." Nucl. Inst. Meth. Phys. Res. B **136-138**: 14-22.

Cohen, D., G. Bailey and R. Kondepudi (1996). "Elemental analysis by PIXE and other IBA techniques and their application to source fingerprinting of atmospheric fine particle pollution." Nucl. Inst. Meth. Phys. Res. B **109/110**: 218-226.

Cohen, D., G. Taha, E. Stelcer, D. Garton and G. Box (2000). The measurement and sources of fine particle elemental carbon at several key sites in NSW over the past eight years. 15th Clean Air Conference, Sydney, Clean air Society of Australia and New Zealand.

Cohen, D. D. (1999). "Accelerator based ion beam techniques for trace element aerosol analysis." Advances in Environmental, Industrial and Process Control Technologies **1**(Elemental Analysis of Airborne Particles): 139-196.

Davy, P., K. (2007). Composition and Sources of Aerosol in the Wellington Region of New Zealand. PhD Thesis. School of Chemical and Physical Sciences. Wellington, Victoria University of Wellington**:** 429 pages.

Davy, P., K., W. Trompetter and A. Markwitz (2009). Source apportionment of airborne particles at Wainuiomata, Lower Hutt. Wellington, GNS Science Client Report 2009/188.

Davy, P., K., W. Trompetter and A. Markwitz (2009). Source apportionment of airborne particles in the Auckland region: 2008 Update. Wellington, GNS Science Client Report 2009/165.

Davy, P., K., W. J. Trompetter and A. Markwitz (2007). Source apportionment of airborne particles in the Auckland region. Wellington, GNS Science Client Report 2007/314.

Davy, P., K., W. J. Trompetter and A. Markwitz (2008). Source apportionment of airborne particles at Seaview, Lower Hutt. Wellington, GNS Science Client Report 2008/160.

Davy, P., K., W. J. Trompetter and A. Markwitz (2011). Source apportionment of airborne particles at Patumahoe, South Auckland, GNS Science Client Report 2011/258.

Davy, P. K., T. Ancelet, W. J. Trompetter and A. Markwitz (2014). Arsenic and air pollution in New Zealand. 5th International Congress on Arsenic in the Environment, As 2014, Buenos Aires, CRC Press/Balkema.

Davy, P. K., T. Ancelet, W. J. Trompetter, A. Markwitz and D. C. Weatherburn (2012). "Composition and source contributions of air particulate matter pollution in a New Zealand suburban town." Atmospheric Pollution Research **3**(1): 143-147.

Davy, P. K., W. J. Trompetter and A. Markwitz (2009). Elemental analysis of wood burner emissions, GNS Science Client Report 2009/258.

Davy, P. K., W. J. Trompetter and A. Markwitz (2010). Source apportionment of PM10 at Tahunanui, Nelson, GNS Science Client Report 2010/198.

Davy, P. K., W. J. Trompetter and A. Markwitz (2011). Source apportionment of airborne particles in the Auckland region: 2010 Analysis. Wellington, GNS Science Client Report 2010/262.

Draxler, R. R. and G. D. Rolph (2003). HYSPLIT (HYbrid Single-Particle Lagrangian Integrated Trajectory) Model, NOAA Air Resources Laboratory, Silver Spring, MD.

Eberly, S. (2005). EPA PMF 1.1 User’s Guide, USEPA.

Endresen, Ø., E. Sørgård, J. K. Sundet, S. B. Dalsøren, I. S. A. Isaksen, T. F. Berglen and G. Gravir (2003). "Emission from international sea transportation and environmental impact." Journal of Geophysical Research D: Atmospheres **108**(17): ACH 14-11 ACH 14-22.

Eyring, V., I. S. A. Isaksen, T. Berntsen, W. J. Collins, J. J. Corbett, O. Endresen, R. G. Grainger, J. Moldanova, H. Schlager and D. S. Stevenson (2010). "Transport impacts on atmosphere and climate: Shipping." Atmospheric Environment **44**(37): 4735-4771.

Fine, P. M., G. R. Cass and B. R. Simoneit (2001). "Chemical characterization of fine particle emissions from fireplace combustion of woods grown in the northeastern United States." Environ. Sci. Technol. **35**(13): 2665-2675.

Fine, P. M., G. R. Cass and B. R. T. Simoneit (2004). "Chemical Characterization of Fine Particle Emissions from the Wood Stove Combustion of Prevalent United States Tree Species." Environmental Engineering Science **21**(6): 705-721.

Fine, P. M., G. R. Cass and S. B. R. T. (2002). "Chemical characterzation of fine particle emissions from the fireplace combustion of woods grown in the Southern United States." Environmental Science and Technology **36**(7): 1442-1451.

Fitzgerald, J. W. (1991). "Marine aerosols: A review." Atmospheric Environment - Part A General Topics **25**(3-4): 533-545.

Fridell, E., E. Steen and K. Peterson (2008). "Primary particles in ship emissions." Atmospheric Environment **42**(5): 1160-1168.

Gard, E. E., M. J. Kleeman, D. S. Gross, L. S. Hughes, J. O. Allen, B. D. Morrical, D. P. Fergenson, T. Dienes, M. E. Galli, R. J. Johnson, G. R. Cass and K. A. Prather (1998). "Direct observation of heterogeneous chemistry in the atmosphere." Science (Washington, D. C.) **279**(5354): 1184-1187.

George, I. J. and J. P. D. Abbatt (2010). "Heterogeneous oxidation of atmospheric aerosol particles by gas-phase radicals." Nature Chemistry **2**(9): 713-722.

Hays, M. D., S.-H. Cho, R. Baldauf, J. J. Schauer and M. Shafer (2011). "Particle size distributions of metal and non-metal elements in an urban near-highway environment." Atmospheric Environment **45**(4): 925-934.

Healy, R. M., I. P. O'Connor, S. Hellebust, A. Allanic, J. R. Sodeau and J. C. Wenger (2009). "Characterisation of single particles from in-port ship emissions." Atmospheric Environment **43**(40): 6408-6414.

Hellebust, S., A. Allanic, I. P. O'Connor, C. Jourdan, D. Healy and J. R. Sodeau (2010). "Sources of ambient concentrations and chemical composition of PM2.5-0.1 in Cork Harbour, Ireland." Atmospheric Research **95**(2-3): 136-149.

Hopke, P. K. (1999). "An introduction to source receptor modeling." Adv. Environ. Indust. Process Control Technol. **1**(Elemental Analysis of Airborne Particles): 273-315.

Hopke, P. K. (2003). "Recent developments in receptor modeling." J. Chemomet. **17**(5): 255-265.

Hopke, P. K., Y. L. Xie and P. Paatero (1999). "Mixed multiway analysis of airborne particle composition data." J. Chemomet. **13**(3-4): 343-352.

Horvath, H. (1993). "Atmospheric Light Absorption - A Review." Atmos. Environ, **27A**: 293-317.

Horvath, H. (1997). "Experimental calibration for aerosol light absorbtion measurements using the integrating plate method **-** Summary of the data." Aerosol Science **28**: 2885-2887.

Hsu, Y.-K., T. M. Holsen and P. K. Hopke (2003). "Comparison of hybrid receptor models to locate PCB sources in Chicago." Atmos. Environ. **37**(4): 545-562.

Huebert, B. J. (1999). "Sulphur emissions from ships." Nature **400**(6746): 713-714.

Hwang, I. and P. K. Hopke (2007). "Estimation of source apportionment and potential source locations of PM2.5 at a west coastal IMPROVE site." Atmospheric Environment **41**(3): 506-518.

Jacobson, M. C., H. C. Hansson, K. J. Noone and R. J. Charlson (2000). "Organic atmospheric aerosols: review and state of the science." Reviews of Geophysics **38**(2): 267-294.

Jeong, C.-H., P. K. Hopke, E. Kim and D.-W. Lee (2004). "The comparison between thermal-optical transmittance elemental carbon and Aethalometer black carbon measured at multiple monitoring sites." Atmos. Environ. **38**(31): 5193.

Kim, E., P. K. Hopke and E. S. Edgerton (2003). "Source identification of Atlanta aerosol by positive matrix factorization." J. Air Waste Manage. Assoc. **53**(6): 731-739.

Kim, E., P. K. Hopke, T. V. Larson, N. N. Maykut and J. Lewtas (2004). "Factor analysis of Seattle fine particles." Aerosol Sci. Technol. **38**(7): 724-738.

Lee, E., C. K. Chan and P. Paatero (1999). "Application of positive matrix factorization in source apportionment of particulate pollutants in Hong Kong." Atmos. Environ, **33**(19): 3201-3212.

Lee, J. H., Y. Yoshida, B. J. Turpin, P. K. Hopke, R. L. Poirot, P. J. Lioy and J. C. Oxley (2002). "Identification of sources contributing to Mid-Atlantic regional aerosol." J. Air Waste Manag. Assoc. **52**(10): 1186-1205.

Lide, D. R. (1992). CRC Handbook of Chemistry and Physics, CRC Press Inc.

Lough, G. C., J. J. Schauer, J.-S. Park, M. M. Shafer, J. T. Deminter and J. P. Weinstein (2005). "Emissions of metals associated with motor vehicle roadways." Environmental Science and Technology **39**(3): 826-836.

Maenhaut, W. and K. Malmqvist, G. (2001). Particle Induced X-ray Emission Analysis. Handbook of x-ray spectrometry. R. V. Grieken. Antwerp, Marcel Dekker Inc.

Malm, W. C., J. F. Sisler, D. Huffman, R. A. Eldred and T. A. Cahill (1994). "Spatial and seasonal trends in particle concentration and optical extinction in the United States." J. Geophys. Res. Atmos. **99**(D1): 1347-1370.

Matthias, V., I. Bewersdorff, A. Aulinger and M. Quante (2010). "The contribution of ship emissions to air pollution in the North Sea regions." Environmental Pollution **158**(6): 2241-2250.

Maxwell, J. A., J. L. Cambell and W. J. Teesdale (1989). "The Guelph PIXE software package." Nucl. Instr. And Meth. B **43**: 218.

Maxwell, J. A., W. J. Teesdale and J. L. Cambell (1995). "The Guelph PIXE software package II." Nucl. Instr. And Meth. B **95**: 407.

MfE (2002). New Zealand Ambient Air Quality Guidelines. Wellington, New Zealand Government.

Moldanová, J., E. Fridell, O. Popovicheva, B. Demirdjian, V. Tishkova, A. Faccinetto and C. Focsa (2009). "Characterisation of particulate matter and gaseous emissions from a large ship diesel engine." Atmospheric Environment **43**(16): 2632-2641.

Norris, G., R. Duvall, S. Brown and S. Bai (2014). EPA Positive Matrix Factorization (PMF) 5.0 Fundamentals and User Guide. USEPA.

O'Dowd, C. D., J. A. Lowe, N. Clegg, M. H. Smith and S. L. Clegg (2000). "Modeling heterogeneous sulphate production in maritime stratiform clouds." J. Geophys. Res.- Atmos. **105**(D6): 7143-7160.

Paatero, P. (1997). "Least squares formulation of robust non-negative factor analysis." Chemom. Intell. Lab. Syst. **18**: 183-194.

Paatero, P. (2000). PMF User's Guide. Helsinki, University of Helsinki.

Paatero, P., S. Eberly, S. G. Brown and G. A. Norris (2014). "Methods for estimating uncertainty in factor analytic solutions." Atmos. Meas. Tech. **7**(3): 781-797.

Paatero, P. and P. K. Hopke (2002). "Utilizing wind direction and wind speed as independent variables in multilinear receptor modeling studies." Chemometrics and Intelligent Laboratory Systems **60**(1-2): 25-41.

Paatero, P. and P. K. Hopke (2003). "Discarding or downweighting high-noise variables in factor analytic models." Analytica Chimica Acta **490**(1-2): 277-289.

Paatero, P., P. K. Hopke, B. A. Begum and S. K. Biswas (2005). "A graphical diagnostic method for assessing the rotation in factor analytical models of atmospheric pollution." Atmospheric Environment **39**(1): 193-201.

Paatero, P., P. K. Hopke, X. H. Song and Z. Ramadan (2002). "Understanding and controlling rotations in factor analytic models." Chemometrics and Intelligent Laboratory Systems **60**(1-2): 253-264.

Pandis, S. N., R. A. Harley, G. R. Cass and J. H. Seinfeld (1992). "Secondary organic aerosol formation and transport." Atmos. Environ. Pt. A: Gen. Topics **26A**(13): 2269-2282.

Polissar, A. V., P. K. Hopke and J. M. Harris (2001). "Source regions for atmospheric aerosol measured at Barrow, Alaska." Environ. Sci. Technol. **35**(21): 4214-4226.

Ramadan, Z., B. Eickhout, X.-H. Song, L. M. C. Buydens and P. K. Hopke (2003). "Comparison of Positive Matrix Factorization and Multilinear Engine for the source apportionment of particulate pollutants." Chemomet. Intellig. Lab. Syst. **66**(1): 15-28.

Salma, I., X. Chi and W. Maenhaut (2004). "Elemental and organic carbon in urban canyon and background environments in Budapest, Hungary." Atmos. Environ. **38**(1): 27-36.

Schauer, J. J., G. C. Lough, M. M. Shafer, W. F. Christensen, M. F. Arndt, J. T. Deminter and J.-S. Park (2006). "Characterisation of metals emitted from motor vehicles. Research Report 133. Health Effects Institute, Boston."

Scott, A. J. (2006). Source Apportionment and Chemical Characterisation of Airborne Fine Particulate Matter in Christchurch, New Zealand. PhD Thesis, University of Canterbury.

Seinfeld, J. H. and S. N. Pandis (2006). Atmospheric Chemistry and Physics: From Air Pollution to Climate Change. New York, John Wiley & Sons, Inc.

Selleck, P. and M. D. Keywood (2012). PM2.5 Chemical Composition at Takapuna and Penrose 2011.

Song, X. H., A. V. Polissar and P. K. Hopke (2001). "Sources of fine particle composition in the northeastern US." Atmospheric Environment **35**(31): 5277-5286.

Team, R. D. C. (2011). R: A language and environment for statistical computing. R Foundation for Statistical Computing, Vienna, Austria.

Thorpe, A. and R. M. Harrison (2008). "Sources and properties of non-exhaust particulate matter from road traffic: A review." Science of the Total Environment **400**(1-3): 270-282.

Trompetter, W., A. Markwitz and P. Davy, K. (2005). "Air particulate research capability at the New Zealand Ion Beam Analysis Facility using PIXE and IBA Techniques." International Journal of PIXE **15**(3&4): 249-255.

Trompetter, W. J. (2004). Ion Beam Analysis results of air particulate filters from the Wellington Regional Council. Wellington, Geological and Nuclear Sciences Limited.

Trompetter, W. J. and P. K. Davy (2005). Air Particulate Research Capability at the New Zealand Ion Beam Analysis facility using PIXE and IBA techniques. BioPIXE 5, Wellington, New Zealand.

Watson, J. G., T. Zhu, J. C. Chow, J. Engelbrecht, E. M. Fujita and W. E. Wilson (2002). "Receptor modeling application framework for particle source apportionment." Chemosphere **49**(9): 1093-1136.

Xie, S., P. Davy, K., S. Sridhar and J. Metcalfe (2015). Quantifying trends of particulate matter emissions from motor vehicles in Auckland. 22nd Clean Air & Environment Conference, Melbourne, Clean Air Society of Australia and New Zealand (CASANZ).

APPENDICES

A1.0 APPENDIX 1: SAMPLE ANALYSIS AND DATA QUALITY ASSURANCE

A1.1 ELEMENTAL ANALYSIS OF AIRBORNE PARTICLES

A1.1.1 Ion beam analysis

Ion beam analysis (IBA) was used to measure the elemental concentrations of particulate matter on the size-resolved filter samples from the Auckland monitoring sites. IBA is based on the measurement of characteristic X-rays and γ-rays of an element produced by ion-atom interactions using high-energy protons in the 2–5 million electron volt (MeV) range. IBA is a mature and well developed science, with many research groups around the world using IBA in a variety of routine analytical applications, including the analysis of atmospheric aerosols (Maenhaut and Malmqvist 2001, Trompetter, Markwitz et al. 2005). IBA techniques do not require sample preparation and are fast, non-destructive and sensitive (Cohen 1999, Maenhaut and Malmqvist 2001, Trompetter, Markwitz et al. 2005).

IBA measurements for this study were carried out at the New Zealand IBA facility operated by GNS Science. Figure A1.1 shows the PM analysis chamber with its associated X-ray, γ-ray and particle detectors for Proton-Induced X-ray Emission (PIXE), Proton-Induced Gamma-ray Emission (PIGE), Proton Elastic Scattering Analysis (PESA) and Rutherford Back Scattering (RBS) measurements.

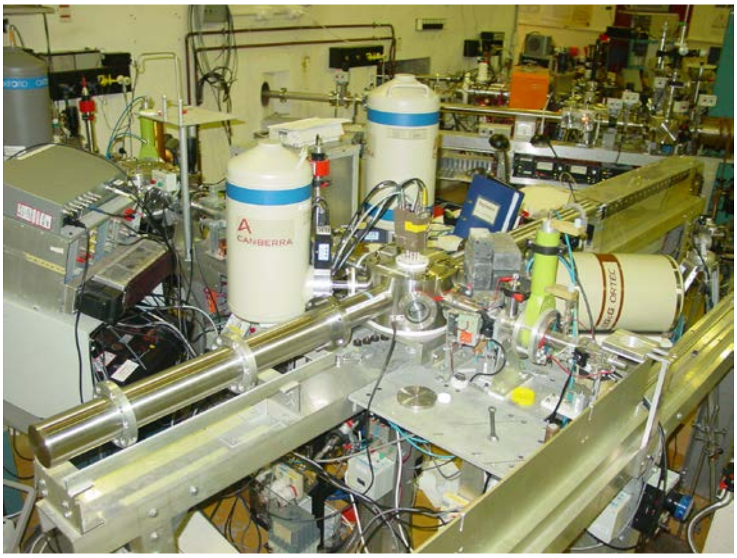

Figure A1.1 Particulate matter analysis chamber with its associated detectors.

The following sections provide a generalised overview of the IBA techniques used for elemental analysis and the analytical setup at GNS Science (Cohen, Bailey et al. 1996, Cohen 1998, Trompetter 2004, Trompetter and Davy 2005). Figure A1.2 presents a schematic diagram of the typical experimental setup for IBA of air particulate filters at GNS Science.

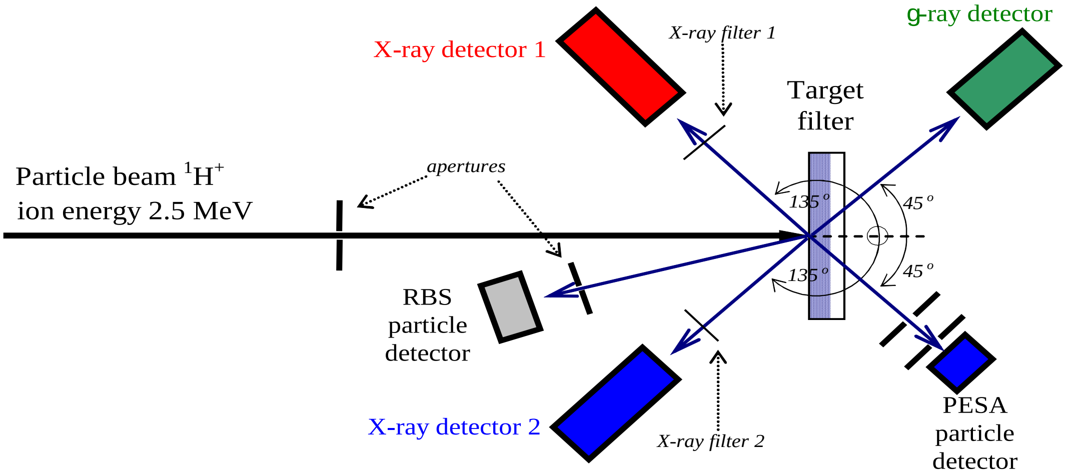

Figure A1.2 Schematic of the typical IBA experimental setup at GNS Science.

A1.1.1.1 Particle-induced X-ray emission

Particle induced X-ray emission (PIXE), is used to determine elemental concentrations heavier than neon by exposing the filter samples to a proton beam accelerated to 2.5 million volts (MeV) by the GNS 3 MeV van-de-Graaff accelerator. When high energy protons interact with atoms in the sample, characteristic X-rays (from each element) are emitted by ion-electron processes. These X-rays are recorded in an energy spectrum. While all elements heavier than boron emit K X-rays, their production become too few to satisfactorily measure elements heavier than strontium. Elements heavier than strontium are detected via their lower energy L X-rays. The X-rays are detected using a Si(Li) detector and the pulses from the detector are amplified and recorded in a pulse height analyser. In practice, sensitivities are further improved for the lighter elements by using two X-ray detectors, one for light element X-rays and the other for heavier element X-rays, each with different filtering and collimation. Figure A1.3 shows an example of a PIXE spectrum for airborne particles collected on a filter and analysed at the GNS IBA facility.

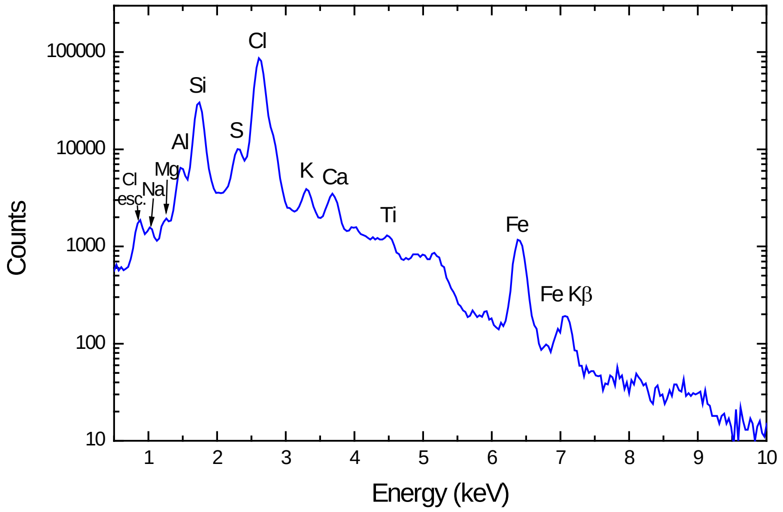

Figure A1.3 Typical PIXE spectrum for an aerosol sample analysed by PIXE.

As the PIXE spectrum consists of many peaks from different elements (and a Bremsstrahlung background), some of them overlapping, the spectrum is analysed with quantitative X-ray analysis software. In the case of this study, Gupix Software was used to perform the deconvolution with high accuracy (Maxwell, Cambell et al. 1989, Maxwell, Teesdale et al. 1995). The number of pulses (counts) in each peak for a given element is used by the Gupix software to calculate the concentration of that element. The background and neighbouring elements determine the statistical error and the limit of detection. Note, that Gupix provides a specific statistical error and limit of detection (LOD) for each element in any filter, which is essential for source apportionment studies.

Typically 20–25 elements from Mg–Pb are routinely determined above their respective LODs. Sodium (and fluorine) was determined using both PIXE and PIGE (see next section). Specific experimental details, where appropriate, are given in the results and analysis section.

A1.1.1.2 Particle-induced gamma-ray emission

Particle Induced Gamma-Ray Emission (PIGE) refers to γ-rays produced when an incident beam of protons interacts with the nuclei of an element in the sample (filter). During the de-excitation process, nuclei emit γ-ray photons of characteristic energies specific to each element. Typical elements measured with γ-ray are:

Element	*nuclear reaction*	*gamma ray energy (keV)*
Sodium	$^{23}\mathrm{Na}(p,\alpha\gamma)^{20}\mathrm{Ne}$	440, 1634
Fluorine	$^{19}\mathrm{F}(p,\alpha\gamma)^{16}\mathrm{O}$	197, 6129

Gamma rays are higher in energy than X-rays and are detected with a germanium detector. Measurements of a light element such as sodium can be measured more accurately using PIGE because the γ-rays are not attenuated to the same extent in the filter matrix or the detector material, a problem in the measurement of low energy X-rays of sodium. Figure A1.4 shows a typical PIGE spectrum.

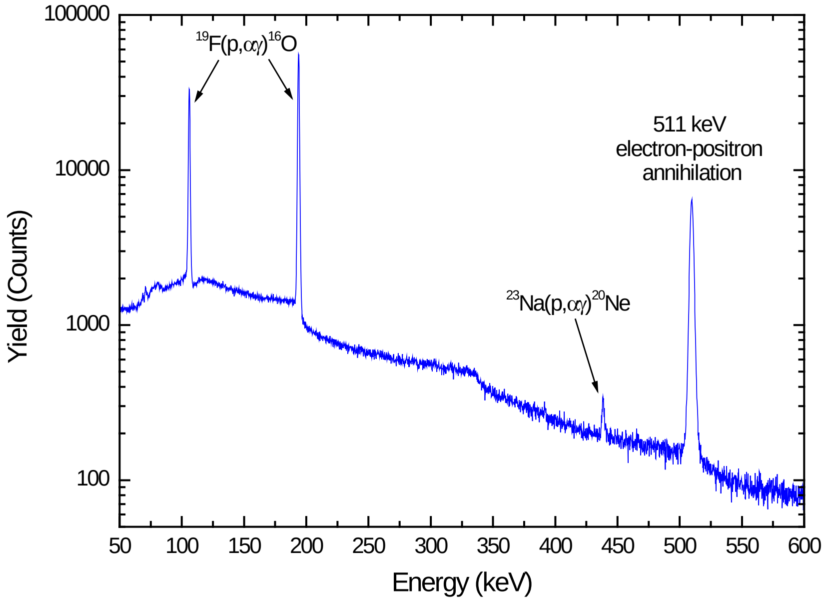

Figure A1.4 Typical PIGE spectrum for an aerosol sample.

A1.1.1.3 IBA data reporting

Most filters used to collect particulate matter samples for IBA analysis are sufficiently thin that the ion beam penetrates the entire depth producing a quantitative analysis of elements present. Because of the thin nature of the air particulate matter filters, the concentrations reported from the IBA analyses are therefore in aerial density units (ng cm^{-2}) and the total concentration of each element on the filters is calculated by multiplying with the exposed area of the filter. Typically the exposed area is 0.16 cm^2 (0.8 cm x 0.2 cm) for the sample deposit on the filters collected with the Streaker sampler used in this study. For example, to convert from Cl (ng cm^{-2}) into Cl (ng m^{-3}) for filter samples, the equation is:

$$\mathrm{Cl\ (ng\ m^{-3})} = 0.16(\mathrm{cm}^2) \times \mathrm{Cl\ (ng\ cm^{-2})} / \mathrm{Vol(m^3)} \tag{A1.1}$$

A1.1.1.4 Limits of detection for elements determined by IBA

The exact limits of detection for reporting the concentration of each element depends on a number of factors such as:

- the method of detection;
- filter composition;
- sample composition;
- the detector resolution;
- spectral interference from other elements.

To determine the concentration of each element the background is subtracted and peak areas fitted and calculated. The background occurs through energy loss, scattering and interactions of the ion beam as it passes through the filter material or from γ-rays produced in the target and scattered in the detector system (Cohen 1999). The peaks of elements in spectra that have interferences or backgrounds from other elements present in the air particulate matter, or filter matrix itself, will have higher limits of detection. Choice of filter material is an important consideration with respect to elements of interest as is avoiding sources of contamination. The GNS IBA laboratory routinely runs filter blanks to correct for filter derived analytical artefacts as part of their QA/QC procedures. Figure A1.5 shows the LODs typically achieved by PIXE for each element at the GNS IBA facility. All IBA elemental concentrations determined in this work were accompanied by their respective LODs. The use of elemental LODs is important in receptor modeling applications and is discussed further in Section A1.4.2.

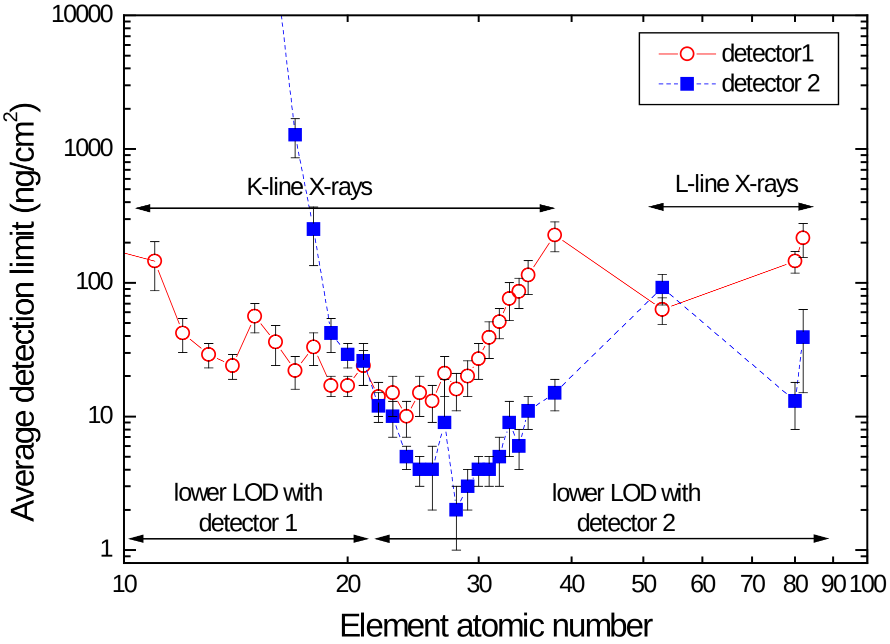

Figure A1.5 Elemental limits of detection for PIXE routinely achieved as the GNS IBA facility for air filters.

A1.2 BLACK CARBON MEASUREMENTS

Black carbon (BC) has been studied extensively, but it is still not clear to what degree it is elemental carbon (EC (or graphitic) C(0)) or high molecular weight refractory weight organic species or a combination of both (Jacobson, Hansson et al. 2000). Current literature suggests that BC is likely a combination of both, and that for combustion sources such as petrol and diesel fuelled vehicles and Biomass burning (wood burning, coal burning), EC and organic carbon compounds (OC) are the principle aerosol components emitted (Jacobson, Hansson et al. 2000, Fine, Cass et al. 2001, Watson, Zhu et al. 2002, Salma, Chi et al. 2004).

Determination of carbon (soot) on filters was performed by light reflection to provide the BC concentration. The absorption and reflection of visible light on particles in the atmosphere or collected on filters is dependent on the particle concentration, density, refractive index and size. For atmospheric particles, BC is the most highly absorbing component in the visible light spectrum with very much smaller components coming from soils, sulphates and nitrate (Horvath 1993, Horvath 1997). Hence, to the first order it can be assumed that all the absorption on atmospheric filters is due to BC. The main sources of atmospheric BC are anthropogenic combustion sources and include biomass burning, motor vehicles and industrial emissions (Cohen, Taha et al. 2000). Cohen and co-workers found that BC is typically 10–40% of the fine mass ($PM_{2.5}$) fraction in many urban areas of Australia.

When measuring BC by light reflection/transmission, light from a light source is transmitted through a filter onto a photocell. The amount of light absorption is proportional to the amount of black carbon present and provides a value that is a measure of the black carbon on the filter. Conversion of the absorbance value to an atmospheric concentration value of BC requires the use of an empirically derived equation (Cohen, Taha et al. 2000):

$$\text{BC } (\mu\text{g cm}^{-2}) = (100/2(F\varepsilon)) \ln[R_0/R] \qquad \textbf{(A1.2)}$$

where:

ε is the mass absorbent coefficient for BC (m^2 g^{-1}) at a given wavelength;

F is a correction factor to account for other absorbing factors such as sulphates, nitrates, shadowing and filter loading. These effects are generally assumed to be negligible and F is set at 1.00;

R_0, R are the pre- and post-reflection intensity measurements, respectively.

Black carbon was measured at GNS Science using the M43D Digital Smoke Stain Reflectometer. The following equation (from Willy Maenhaut, Institute for Nuclear Sciences, University of Gent Proeftuinstraat 86, B-9000 GENT, Belgium) was used for obtaining BC from reflectance measurements on Nucleopore polycarbonate filters or Pall Life Sciences Teflon filters:

$$\text{BC } (\mu\text{g cm}^{-2}) = [1000 \times \text{LOG}(R_{blank}/R_{sample}) + 2.39] / 45.8 \qquad \textbf{(A1.3)}$$

where:

R_{blank}: the average reflectance for a series of blank filters; R_{blank} is close (but not identical) to 100. GNS always use the same blank filter for adjusting to 100.

R_{sample}: the reflectance for a filter sample (normally lower than 100).

With: 2.39 and 45.8 constants derived using a series of 100 Nuclepore polycarbonate filter samples which served as secondary standards; the BC loading (in µg cm^{-2}) for these samples had been determined by Prof. Dr. M.O. Andreae (Max Planck Institute of Chemistry, Mainz, Germany) relative to standards that were prepared by collecting burning acetylene soot on filters and determining the mass concentration gravimetrically (Trompetter 2004).

A1.3 POSITIVE MATRIX FACTORISATION

Positive matrix factorisation (PMF) is a linear least-squares approach to factor analysis and was designed to overcome the receptor modeling problems associated with techniques like principal components analysis (PCA) and the *a priori* knowledge required for chemical mass balance approaches (Paatero, Hopke et al. 2005). With PMF, sources are constrained to have non-negative species concentrations, no sample can have a negative source contribution and error estimates for each observed data point are used as point-by-point weights. This feature is a distinct advantage, in that it can accommodate missing and below detection limit data that is a common feature of environmental monitoring results (Song, Polissar et al. 2001). In fact, the signal to noise ratio for an individual elemental measurement can have a significant influence on a receptor model and modeling results. For the weakest (closest to detection limit) species, the variance may be entirely from noise (Paatero and Hopke 2002). Paatero and Hopke strongly suggest down-weighting or discarding noisy variables that are always below their detection limit or species that have a lot of error in their measurements relative to the magnitude of their concentrations (Paatero and Hopke 2003). The distinct advantage of PMF is that mass concentrations can be included in the model and the results are directly interpretable as mass contributions from each factor (source).

A1.3.1 PMF model outline

The mathematical basis for PMF is described in detail by Paatero (Paatero 1997, Paatero 2000). Briefly, PMF uses a weighted least-squares fit with the known error estimates of measured elemental concentrations used to derive the weights. In matrix notation this is indicated as:

$$X = GF + E \tag{A1.4}$$

where:

X is the known n x m matrix of m measured elemental species in n samples;

G is an n x p matrix of source contributions to the samples;

F is a p x m matrix of source compositions (source profiles).

E is a residual matrix – the difference between measurement X and model Y.

E can be defined as a function of factors G and F:

$$e_{\mathrm{ij}} = x_{\mathrm{ij}} - y_{\mathrm{ij}} = x_{\mathrm{ij}} - \sum_{k=1}^{p} g_{\mathrm{ik}} \, f_{\mathrm{kj}} \tag{A1.5}$$

where:

$i = 1,\ldots\ldots,n$ elements

$j = 1,\ldots\ldots,m$ samples

$k = 1,\ldots\ldots,p$ sources

PMF constrains all elements of G and F to be non-negative, meaning that elements cannot have negative concentrations and samples cannot have negative source contributions as in real space. The task of PMF is to minimise the function Q such that:

$$Q(E) = \sum_{\mathrm{i}=1}^{n} \sum_{\mathrm{j}=1}^{m} (e_{\mathrm{ik}} / \sigma_{\mathrm{kj}})^2 \tag{A1.6}$$

where σ_{ij} is the error estimate for x_{ij}. Another advantage of PMF is the ability to handle extreme values typical of air pollutant concentrations as well as true outliers that would normally skew PCA. In either case, such high values would have significant influence on the solution (commonly referred to as leverage). PMF has been successfully applied to receptor modeling studies in a number of countries around the world (Hopke, Xie et al. 1999, Lee, Chan et al. 1999, Chueinta, Hopke et al. 2000, Song, Polissar et al. 2001, Lee, Yoshida et al. 2002, Kim, Hopke et al. 2003, Jeong, Hopke et al. 2004, Kim, Hopke et al. 2004, Begum, Hopke et al. 2005) including New Zealand (Scott 2006, Davy 2007, Davy, Trompetter et al. 2007, Davy, Trompetter et al. 2008, Davy, Trompetter et al. 2009, Davy, Trompetter et al. 2009, Ancelet, Davy et al. 2012).

A1.3.2 PMF model used

Two programs have been written to implement different algorithms for solving the least squares PMF problem, these are PMF2 and EPAPMF, which incorporates the Multilinear Engine (ME-2) (Hopke, Xie et al. 1999, Ramadan, Eickhout et al. 2003). In effect, the EPAPMF program provides a more flexible framework than PMF2 for controlling the solutions of the factor analysis with the ability of imposing explicit external constraints.

This study used EPAPMF 5.0 (version 14.0), which incorporates a graphical user interface (GUI) based on the ME-2 program. Both PMF2 and EPAPMF programs can be operated in a robust mode, meaning that “outliers” are not allowed to overly influence the fitting of the contributions and profiles (Eberly 2005). The user specifies two input files, one file with the concentrations and one with the uncertainties associated with those concentrations. The methodology for developing an uncertainty matrix associated with the elemental concentrations for this work is discussed in Section A1.4.2.

A1.3.3 PMF model inputs

The PMF programs provide the user with a number of choices in model parameters that can influence the final solution. Two parameters, the ‘signal-to-noise ratio’ and the ‘species category’ are of particular importance and are described below.

Signal-to-noise ratio (S/N) - this is a useful diagnostic statistic estimated from the input data and uncertainty files. Two calculations are performed to determine S/N, where concentrations below uncertainty are determined to have no signal, and for concentrations above uncertainty, the difference between concentration (x_i) and uncertainty (s_i) is used as the signal

$$d_{ij} = \left(\frac{x_{ij} - s_{ij}}{s_{ij}} \right) \text{ if } x_{ij} > s_{ij}$$

$$d_{ij} = 0 \qquad \text{if } x_{ij} \le s_{ij}$$

S/N is then calculated using Equation A1.8:

$$\left(\frac{S}{N} \right)_j = {}^1\!/_n \sum_{i=1}^{n} d_{ij}$$

(A1.7)

The result with this S/N calculation is that species with concentrations always below their uncertainty have a S/N of 0. Species with concentrations that are twice the uncertainty value have a S/N of 1. S/N greater than 1 may often indicate a species with “good” signal, though this depends on how uncertainties were determined. Negative concentration values do not contribute to the S/N, and species with a handful of high concentration events will not have artificially high S/N (Norris, Duvall et al. 2014).

The signal-to-noise ratios (S/N ratio) for each element are reported alongside other statistical data in the results section.

Species category – this enables the user to specify whether the elemental species should be considered:

- Strong – whereby the element is generally present in concentrations well above the LOD (high signal to noise ratio) and the uncertainty matrix is a reasonable representation of the errors.
- Weak – where the element may be present in concentrations near the LOD (low signal to noise ratio); there is doubt about some of the measurements and/or the error estimates; or the elemental species is only detected some of the time. If ‘Weak’ is chosen EPA.PMF increases the user-provided uncertainties for that variable by a factor of 3.
- Bad – that variable is excluded from the model run.

For this work, an element with concentrations at least 3 times above the LOD, a high signal to noise ratio (> 2) and present in all samples was generally considered ‘Strong’. Variables were labelled as weak if their concentrations were generally low, had a low signal to noise ratio, were only present in a few samples or there was a lower level of confidence in their measurement. Mass concentration gravimetric measurements and BC were also down weighted as ‘Weak’ depending on the dataset because their concentrations are generally several orders of magnitude above other species, which can have the tendency to ‘pull’ the model. Paatero and Hopke recommend that such variables be down weighted and that it doesn’t particularly affect the model fitting if those variables are from real sources (Paatero and Hopke 2003). What does affect the model severely is if a dubious variable is over-weighted. Elements that had a low signal to noise ratio (< 0.5) were examined using bivariate correlation plots to determine interspecies relationships. Those low S/N variables with little or no association with other species, or had mostly zero values, or were doubtful for any reason, were labelled as ‘Bad’ and were subsequently not included in the analyses.

If the model is appropriate for the data and if the uncertainties specified are truly reflective of the uncertainties in the data, then Q (according to Eberly) should be approximately equal to the number of data points in the concentration data set (Eberly 2005):

$$\textit{Theoretical } Q = \# \textit{ samples } \mathbf{x} \# \textit{ species measured} \qquad \textbf{(A1.8)}$$

However, a slightly different approach to calculating the Theoretical Q value was recommended (Brown and Hafner 2005), which takes into account the degrees of freedom in the PMF model and the additional constraints in place for each model run. This theoretical Q calculation Q_{th} is given as:

$$Q_{th} = (\# \textit{ samples } \mathbf{x} \# \textit{ good species}) + [(\# \textit{ samples } \mathbf{x} \# \textit{ weak species})/3] - (\# \textit{ samples } \mathbf{x} \textit{ factors estimated}) \qquad \textbf{(A1.9)}$$

Both approaches have been taken into account for this study and it is likely that the actual value lies somewhere between the two. Further guidance has more recently been provided by Paatero and co-workers (Paatero, Eberly et al. 2014, Brown, Eberly et al. 2015) where a third parameter, $Q_{expected}$ should also be calculated, but only the “good” or non-weak variables should be taken into account:

> *The expected value of Q is approximately = (number of non-weak data values in X) − (numbers of elements in G and F, taken together).* **(A1.10)**

A downweighted weak variable has only a small, rarely significant contribution to $Q_{expected}$, and for simplicity is excluded here. If the Q value of the chosen model differs significantly from what is expected (e.g., by a factor of ten o rmore), then DISP error analysis becomes invalid and BS-DISP is likely questionable.

In PMF, it is assumed that only the x_{ij}’s are known and that the goal is to estimate the contributions (g_{ik}) and the factors (or profiles) (f_{kj}). It is assumed that the contributions and mass fractions are all non-negative, hence the “constrained” part of the least-squares. Additionally, EPAPMF allows the user to say how much uncertainty there is in each x_{ij}. Species-days with lots of uncertainty are not allowed to influence the estimation of the contributions and profiles as much as those with small uncertainty, hence the “weighted” part of the least squares and the advantage of this approach over PCA.

Diagnostic outputs from the PMF models were used to guide the appropriateness of the number of factors generated and how well the receptor modelling was accounting for the input data. Where necessary, initial solutions have been ‘rotated’ to provide a better separation of factors (sources) that were considered physically reasonable (Paatero, Hopke et al. 2002). Each PMF model run reported in this study is accompanied by the modelling statistics along with comments where appropriate.

A1.4 DATASET QUALITY ASSURANCE

Quality assurance of sample elemental datasets is vital so that any dubious samples, measurements and outliers are removed as these will invariably affect the results of receptor modelling. In general, the larger the dataset used for receptor modelling, the more robust the analysis. The following sections describe the methodology used to check data integrity and provide a quality assurance process that ensured that the data being used in subsequent factor analysis was as robust as possible.

A1.4.1 Mass reconstruction and mass closure

Once the sample analysis for the range of analytes has been carried out, it is important to check that total measured mass does not exceed gravimetric mass (Cohen 1999). Ideally, when elemental analysis and organic compound analysis has been undertaken on the same sample one can reconstruct the mass using the following general equation for ambient samples as a first approximation (Cahill, Eldred et al. 1989, Malm, Sisler et al. 1994, Cohen 1999):

$$\text{Reconstructed mass} = [\text{Soil}] + [\text{OC}] + [\text{BC}] + [\text{Smoke}] + [\text{Sulphate}] + [\text{Seasalt}] \qquad \textbf{(A1.11)}$$

where:

$[\text{Soil}] = 2.20[\text{Al}] + 2.49[\text{Si}] + 1.63[\text{Ca}] + 2.42[\text{Fe}] + 1.94[\text{Ti}]$

$[\text{OC}] = \Sigma[\text{Concentrations of organic compounds}]$

[BC] = Concentration of black carbon (soot)

[Smoke] = [K] – 0.6[Fe]

[Seasalt] = 2.54[Na]

[Sulphate] = 4.125[S]

The reconstructed mass (RCM) is based on the fact that the six composite variables or 'pseudo' sources given in equation A1.12 are generally the major contributors to fine and coarse particle mass and are based on geochemical principles and constraints. The [Soil] factor contains elements predominantly found crustal matter (Al, Si, Ca, Fe, Ti) and includes a multiplier to correct for oxygen content and an additional multiplier of 1.16 to correct for the fact that three major oxide contributors (MgO, K_2O, Na_2O) carbonate and bound water are excluded from the equation.

[BC] is the concentration of black carbon, measured in this case by light reflectance/absorbance. [Smoke] represents K not included as part of crustal matter and tends to be an indicator of biomass burning. Where a direct measure of [OC] was not available, it was estimated by using equation A.11 where PESA was used to determine the hydrogen concentration on filters. In this case total hydrogen on the filter was assumed to be comprised mainly of H from organic material and ammonium sulphate (assuming sulphate is in fully neutralised form) and therefore organic content (designated [OMH]) was calculated from total H by the following equation (Malm, Sisler et al. 1994, Cohen 1999):

$$[OMH] = 11([H] - 0.25[S]) \qquad \textbf{(A1.12)}$$

Equation A.12 assumes that average particulate organic matter is composed of 11% H, 71% C, and 20 % O by weight. It was assumed that the 'remaining mass' (the difference between RCM and gravimetric mass) includes water and nitrates as major components (Cahill, Eldred et al. 1989).

[Seasalt] represents the marine aerosol contribution and assumes that the NaCl weight is 2.54 times the Na concentration. Na is used as it is well known that Cl can be volatilised from aerosol or from filters in the presence of acidic aerosol, particularly in the fine fraction via the following reactions (Lee, Chan et al. 1999):

$$NaCl(p) + HNO_3(ag) \rightarrow NaNO_3(p) + HCL(g) \qquad \textbf{(A1.13)}$$

$$2NaCl(p) + H_2SO_4(ag) \rightarrow Na_2SO_4(p) + 2HCL(g) \qquad \textbf{(A1.14)}$$

Alternatively, where Cl loss is likely to be minimal, such as in the coarse fraction or for both size fractions near coastal locations and relatively clean air in the absence of acid aerosol, then the reciprocal calculation of [Seasalt] = 1.65[Cl] can be substituted, particularly where Na concentrations are uncertain.

Most fine sulphate particles are the result of oxidation of SO_2 gas to sulphate particles in the atmosphere (Malm, Sisler et al. 1994). It is assumed that sulphate is present in fully neutralised form as ammonium sulphate. [Sulphate] therefore represents the ammonium sulphate contribution to aerosol mass with the multiplicative factor of 4.125[S] to account for ammonium ion and oxygen mass (i.e., $(NH_4)_2SO_4 = ((14 + 4)2 + 32 + (16x4)/32))$.

Additionally, the sulphate component not associated with seasalt can be calculated from equation A1.14 (Cohen 1999):

$$\text{Non-seasalt sulphate (NSS-Sulphate)} = 4.125\,([S_{tot}] - 0.0543[Cl]) \qquad \textbf{(A1.15)}$$

Where the sulphur concentrations contributed by seasalt are inferred from the chlorine concentrations, i.e., [S/Cl]seasalt = 0.0543 and the factor of 4.125 assumes that the sulphate has been fully neutralised and is generally present as $(NH_4)_2SO_4$ (Cahill, Eldred *et al*. 1990; Malm, Sisler *et al*. 1994; Cohen 1999).

The RCM and mass closure calculations using the pseudo-source and pseudo-element approach are a useful way to examine initial relationships in the data and how the measured mass of species in samples compares to gravimetric mass. Note that some scatter is possible because not all aerosols are necessarily measured and accounted for, such as all OC, ammonium species, nitrates and unbound water.

A1.4.2 Dataset preparation

Careful preparation of a dataset is required because serious errors in data analysis and receptor modeling results can be caused by erroneous individual data values. The general methodology followed for dataset preparation was as recommended by (Brown and Hafner 2005) and the EPAPMF 5.0 User Guide (Norris, Duvall et al. 2014). For this study, all data were checked for consistency with the following parameters:

1. Individual sample collection validation;
2. Gravimetric mass validation;
3. Analysis of RCM versus gravimetric mass to assess mass closure and linearity;
4. Identification of unusual values including noticeably extreme values and values that normally track with other species (e.g., Al and Si) but deviate in one or two samples. Scatter plots and time series plots were used to identify unusual values. One-off events such as fireworks displays, forest fires or vegetative burn-offs may affect a receptor model as it is forced to find a profile that matches only that day;
5. Species were included in a dataset if at least 70% of data was above the LOD and signal-to-noise ratios were checked to ensure data had sufficient variability. Important tracers of a source where less than 70% of data was above the LOD were included but model runs with and without the data were used to assess the effect;

In practice during data analyses, the above steps were a reiterative process of cross checking as issues were identified and corrected for, or certain data excluded and the effects of this were then studied.

A1.4.2.1 PMF data matrix population

The following steps were followed to produce a final dataset for use in the PMF receptor model (Brown and Hafner 2005).

Below detection limit data: For given values, the reported concentration used and the corresponding uncertainty checked to ensure it had a high value.

Missing data: Substituted with the dataset median value for that species.

A1.4.2.2 PMF uncertainty matrix population

Uncertainties can have a large effect on model results so that they must be carefully compiled. The effect of underestimating uncertainties can be severe, while overestimating uncertainties does not do too much harm (Paatero and Hopke 2003).

Uncertainties for data: Data was multiplied by % fit error provided by IBA analysis to produce an uncertainty in ng m^{-3}. Where uncertainties were zero, then this was replaced with 5/6 LOD value.

Below detection limit data: Below detection limit data was generally provided with a high % fit error and this was used to produce an uncertainty in ng m^{-3}.

Missing data: Uncertainty was calculated as 4 × median value over the entire species dataset.

PM gravimetric mass: Uncertainty derived by multiplying mass concentration by a factor of four to downweight the variable.

Reiterative model runs were used to examine the effect of including species with high uncertainties or low concentrations. In general it was found that the initial uncertainty estimations were sufficient and that adjusting the 'additional modelling uncertainty' function accommodated any issues with modelled variables such as those with residuals outside ± 3 standard deviations.

A2.0 APPENDIX 2: TAKAPUNA DATA ANALYSIS

A2.1 TAKAPUNA $PM_{2.5}$

Using the methodology outlined in Section A1.4.1, Figure A2.1 presents the mass reconstruction results for Takapuna $PM_{2.5}$ and Figure A2.2 presents a correlation plot matrix for key elemental species.

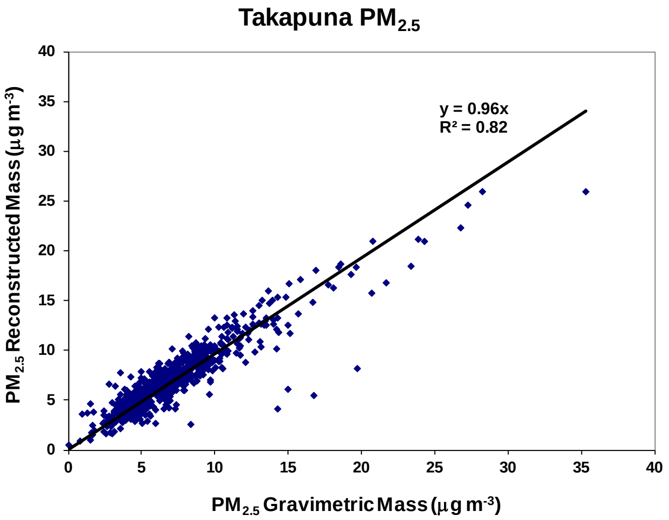

Figure A2.1 Plot of Takapuna $PM_{2.5}$ elemental mass reconstruction against gravimetric $PM_{2.5}$ mass.

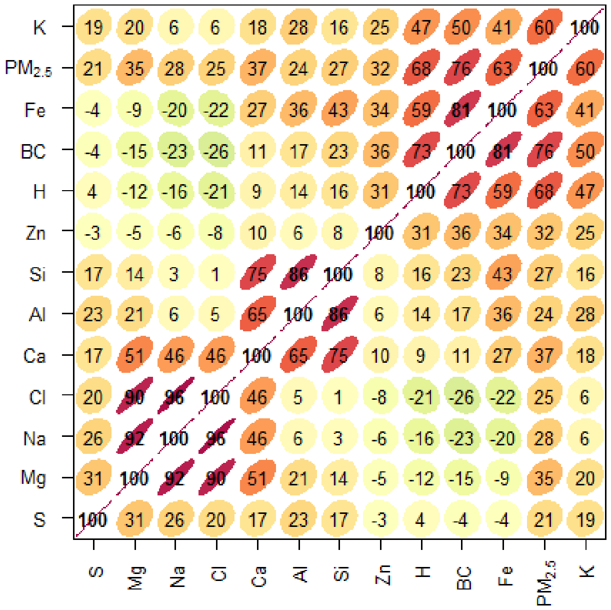

	S	Mg	Na	Cl	Ca	Al	Si	Zn	H	BC	Fe	$PM_{2.5}$	K
K	19	20	6	6	18	28	16	25	47	50	41	60	100
$PM_{2.5}$	21	35	28	25	37	24	27	32	68	76	63	100	60
Fe	-4	-9	-20	-22	27	36	43	34	59	81	100	63	41
BC	-4	-15	-23	-26	11	17	23	36	73	100	81	76	50
H	4	-12	-16	-21	9	14	16	31	100	73	59	68	47
Zn	-3	-5	-6	-8	10	6	8	100	31	36	34	32	25
Si	17	14	3	1	75	86	100	8	16	23	43	27	16
Al	23	21	6	5	65	100	86	6	14	17	36	24	28
Ca	17	51	46	46	100	65	75	10	9	11	27	37	18
Cl	20	90	96	100	46	5	1	-8	-21	-26	-22	25	6
Na	26	92	100	96	46	6	3	-6	-16	-23	-20	28	6
Mg	31	100	92	90	51	21	14	-5	-12	-15	-9	35	20
S	100	31	26	20	17	23	17	-3	4	-4	-4	21	19

Figure A2.2 Correlation plot matrix for key Takapuna $PM_{2.5}$ elemental species.

Takapuna $PM_{2.5}$ PMF RECEPTOR MODELLING DIAGNOSTICS

PMF analyses involve many details about the development of the data, decisions of what data to include/exclude, determination of a solution, and evaluation of robustness of that solution. The following diagnostics for the PMF solutions are reported as recommended by Paatero and co-workers (Paatero, Eberly et al. 2014, Brown, Eberly et al. 2015) and should be read in conjunction with Section 3.2 and Appendix 1.

Summary of EPA PMF settings for receptor modelling of Takapuna $PM_{2.5}$

Parameter	Setting
Data type; averaging timeframe	$PM_{2.5}$, 1-day-in-three
N samples	765
N factors	6
Treatment of missing data	No missing data
Treatment of data below detection limit (BDL)	Data used as reported, no modification or censoring of BDL data
Lower limit for normalized factor contributions gik	-0.2
Robust mode	Yes
Constraints	None
Seed value	Random
N bootstraps in BS	200
r^2 for BS	0.6
DISP dQmax	4, 8, 16, 32
DISP active species	PM2.5, Na, Mg, Al,, Si, S, Cl, K, Ca, Fe, Zn
N bootstraps; r^2 for BS in BS-DISP	200; 0.6
BS-DISP active species	Na, Mg, Al,, Si, S, Cl, K, Ca, Fe, Zn
BS-DISP dQmax	0.5, 1, 2, 4
Extra modelling uncertainty	25%

Output diagnostics for receptor modelling of Takapuna $PM_{2.5}$

Diagnostic	5 factors
$Q_{Theoretical}$	2805
$Q_{Expected}$	2241
Q_{true}	1160.3
Q_{robust}	1160.3
$Q_{robust}/Q_{expected}$	0.518
DISP Diagnostics:	
Error code	0
Largest decrease	
DISP % dQ	-0.0085
DISP swaps by factor	0
BS-DISP Diagnostics:	
BS mapping (Fpeak BS) - Unmapped	99% (100%) - 0
BS-DISP % cases accepted	96%
Largest Decrease in Q:	-18.937
BS-DISP % dQ	-1.63
# of Decreases in Q:	3
# of Swaps in Best Fit:	1

# of Swaps in DISP:	5
BS-DISP swaps by factor	2,0,0,0,0,2,0

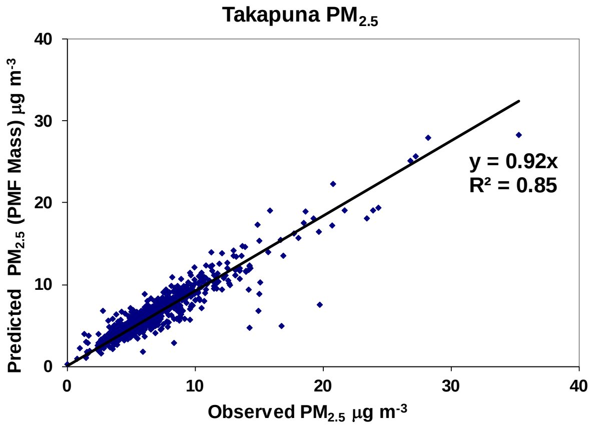

Figure A2.3 Plot of Takapuna $PM_{2.5}$ predicted (PMF mass) against observed gravimetric $PM_{2.5}$ mass.

A2.2 TAKAPUNA PM_{10}

Using the methodology outlined in Section A1.4.1, Figure A2.4 presents the mass reconstruction results for Takapuna PM_{10} and Figure A2.5 presents a correlation plot matrix for key elemental species.

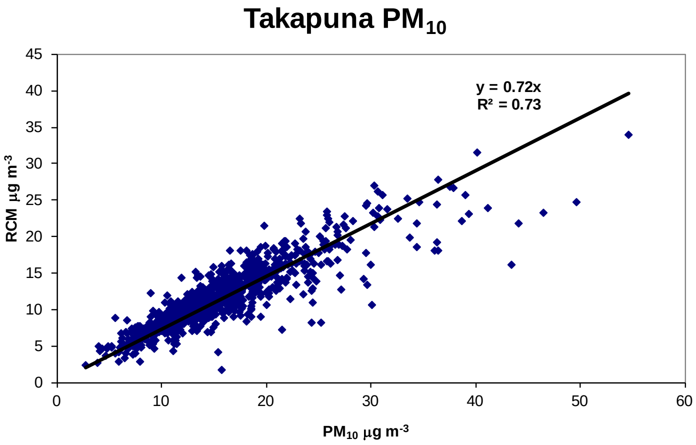

Figure A2.4 Plot of Takapuna PM_{10} elemental mass reconstruction against gravimetric PM_{10} mass.

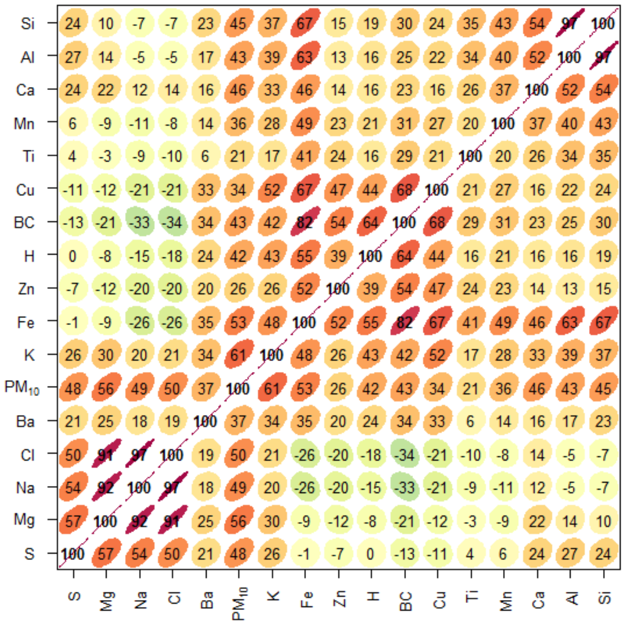

Figure A2.5 Correlation plot matrix for key Takapuna PM_{10} elemental species.

Takapuna PM_{10} PMF RECEPTOR MODELLING DIAGNOSTICS

Summary of EPA PMF settings for receptor modelling of Takapuna PM_{10}

Parameter	Setting
Data type; averaging timeframe	PM_{10}, 1-day-in-three
N samples	877
N factors	7
Treatment of missing data	No missing data
Treatment of data below detection limit (BDL)	Data used as reported, no modification or censoring of BDL data
Lower limit for normalized factor contributions gik	-0.2
Robust mode	Yes
Constraints	None
Seed value	Random
N bootstraps in BS	200
r^2 for BS	0.6
DISP dQmax	4, 8, 16, 32
DISP active species	PM10, BC, Na, Mg, Al,, Si, S, Cl, K, Ca, Fe, Cu, Zn
N bootstraps; r^2 for BS in BS-DISP	200; 0.6
BS-DISP active species	BC, Na, Mg, Al,, Si, S, Cl, K, Ca, Fe, Cu, Zn
BS-DISP dQmax	0.5, 1, 2, 4
Extra modelling uncertainty	15%

Output diagnostics for receptor modelling of Takapuna PM_{10}

Diagnostic	7 factors
$Q_{Theoretical}$	6431.33
$Q_{Expected}$	5171
Q_{true}	2353.33
Q_{robust}	2352.31
$Q_{robust}/Q_{expected}$	0.455
DISP Diagnostics:	
Error code	0
Largest Decrease in Q:	-0.03
DISP % dQ	-0.0013
DISP swaps by factor	0
BS-DISP Diagnostics:	
BS mapping (Fpeak BS) - unmapped	93% (98%) - 0
BS-DISP % cases accepted	82%
Largest Decrease in Q:	-35.267
BS-DISP % dQ	-1.50
# of Decreases in Q:	6
# of Swaps in Best Fit:	6
# of Swaps in DISP:	25
BS-DISP swaps by factor	9,0,7,0,3,0,1

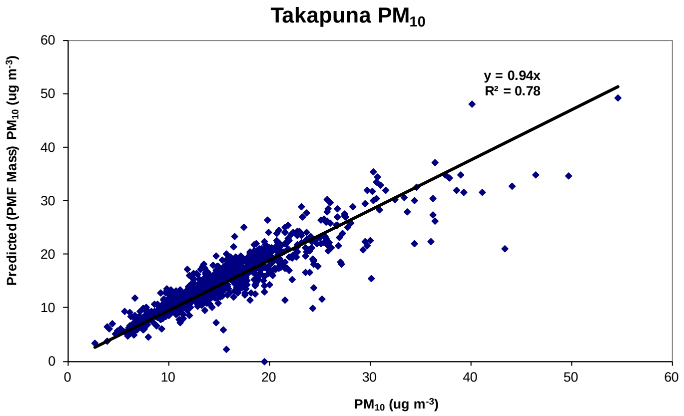

Figure A2.6 Plot of Takapuna PM_{10} predicted (PMF mass) against observed gravimetric PM_{10} mass.

A3.0 APPENDIX 3: QUEEN STREET DATA ANALYSIS

A3.1 QUEEN STREET PM$_{2.5}$

Using the methodology outlined in Section A1.4.1, Figure A3.1 presents the mass reconstruction results for Queen Street PM$_{2.5}$ and Figure A3.2 presents a correlation plot matrix for key elemental species.

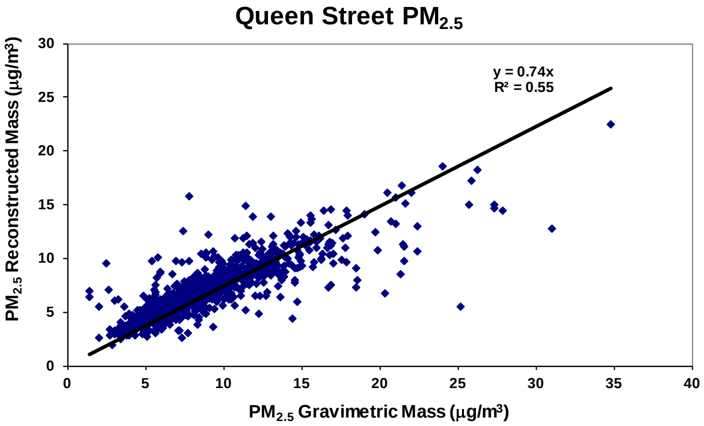

Figure A3.1 Plot of Queen Street PM$_{2.5}$ elemental mass reconstruction against gravimetric PM$_{2.5}$ mass.

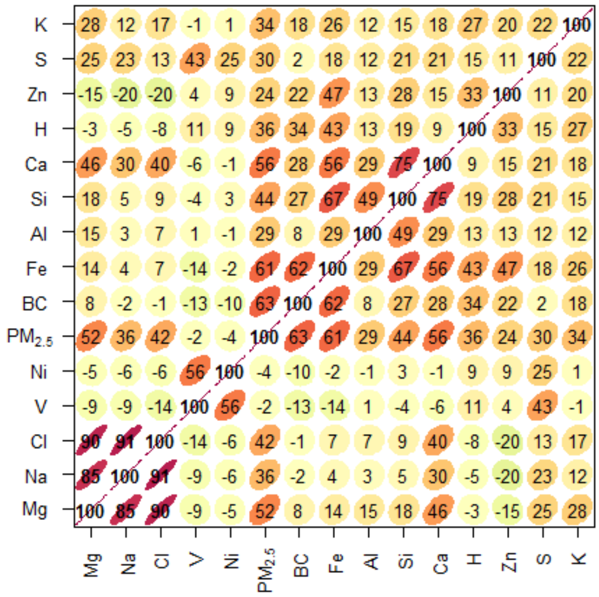

	Mg	Na	Cl	V	Ni	PM$_{2.5}$	BC	Fe	Al	Si	Ca	H	Zn	S	K
K	28	12	17	-1	1	34	18	26	12	15	18	27	20	22	100
S	25	23	13	43	25	30	2	18	12	21	21	15	11	100	22
Zn	-15	-20	-20	4	9	24	22	47	13	28	15	33	100	11	20
H	-3	-5	-8	11	9	36	34	43	13	19	9	100	33	15	27
Ca	46	30	40	-6	-1	56	28	56	29	75	100	9	15	21	18
Si	18	5	9	-4	3	44	27	67	49	100	75	19	28	21	15
Al	15	3	7	1	-1	29	8	29	100	49	29	13	13	12	12
Fe	14	4	7	-14	-2	61	62	100	29	67	56	43	47	18	26
BC	8	-2	-1	-13	-10	63	100	62	8	27	28	34	22	2	18
PM$_{2.5}$	52	36	42	-2	-4	100	63	61	29	44	56	36	24	30	34
Ni	-5	-6	-6	56	100	-4	-10	-2	-1	3	-1	9	9	25	1
V	-9	-9	-14	100	56	-2	-13	-14	1	-4	-6	11	4	43	-1
Cl	90	91	100	-14	-6	42	-1	7	7	9	40	-8	-20	13	17
Na	85	100	91	-9	-6	36	-2	4	3	5	30	-5	-20	23	12
Mg	100	85	90	-9	-5	52	8	14	15	18	46	-3	-15	25	28

Figure A3.2 Correlation plot matrix for key Queen Street PM$_{2.5}$ elemental species.

Queen Street PM$_{2.5}$ PMF RECEPTOR MODELLING DIAGNOSTICS

PMF analyses involve many details about the development of the data, decisions of what data to include/exclude, determination of a solution, and evaluation of robustness of that solution. The following diagnostics for the PMF solutions are reported as recommended by Paatero and co-workers (Paatero, Eberly et al. 2014, Brown, Eberly et al. 2015) and should be read in conjunction with Section 3.2 and Appendix 1.

Summary of EPA PMF settings for receptor modelling of Queen Street $PM_{2.5}$

Parameter	Setting
Data type; averaging timeframe	$PM_{2.5}$, 1-day-in-three
N samples	900
N factors	8
Treatment of missing data	No missing data
Treatment of data below detection limit (BDL)	Data used as reported, no modification or censoring of BDL data
Lower limit for normalized factor contributions gik	-0.2
Robust mode	Yes
Constraints	None
Seed value	Random
N bootstraps in BS	200
r^2 for BS	0.6
DISP dQmax	4, 8, 16, 32
DISP active species	PM2.5, Na, Mg, Si, S, Cl, K, Ca, V, Ni, Zn
N bootstraps; r^2 for BS in BS-DISP	200; 0.6
BS-DISP active species	Na, Si, S, Cl, K, Ca, V, Ni, Zn
BS-DISP dQmax	0.5, 1, 2, 4
Extra modelling uncertainty	25%

Output diagnostics for receptor modelling of Queen Street $PM_{2.5}$

Diagnostic	8 factors
$Q_{Theoretical}$	3900
$Q_{Expected}$	2612
Q_{true}	1280.99
Q_{robust}	1280.99
$Q_{robust}/Q_{expected}$	0.49
DISP Diagnostics:	
Error code	0
Largest decrease in Q	-0.012
DISP % dQ	-0.00094
DISP swaps by factor	0
BS-DISP Diagnostics:	
BS mapping (Fpeak BS) - Unmapped	99% (99.8%) - 0
BS-DISP % cases accepted	94%
Largest Decrease in Q:	-23.748
BS-DISP % dQ	-1.85
# of Decreases in Q:	2
# of Swaps in Best Fit:	2
# of Swaps in DISP:	9
BS-DISP swaps by factor	2,1,0,1,0,0,0,0

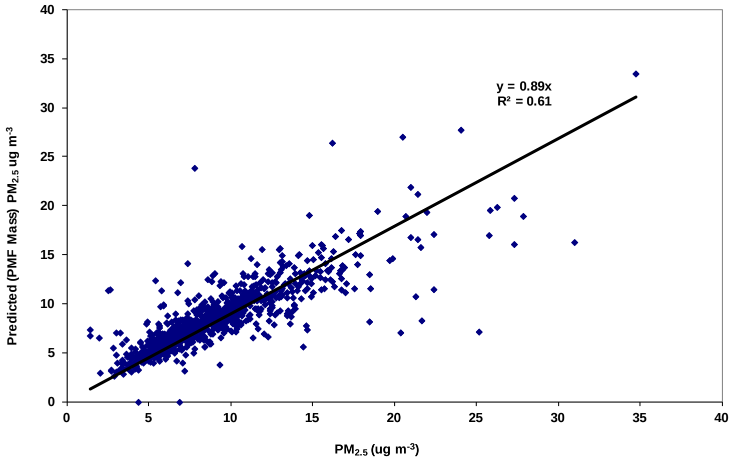

Figure A3.3 Plot of Queen Street $PM_{2.5}$ predicted (PMF mass) against observed gravimetric $PM_{2.5}$ mass.

A3.2 QUEEN STREET PM_{10}

Using the methodology outlined in Section A1.4.1, Figure A2.3 presents the mass reconstruction results for Queen Street PM_{10} and Figure A3.5 presents a correlation plot matrix for key elemental species.

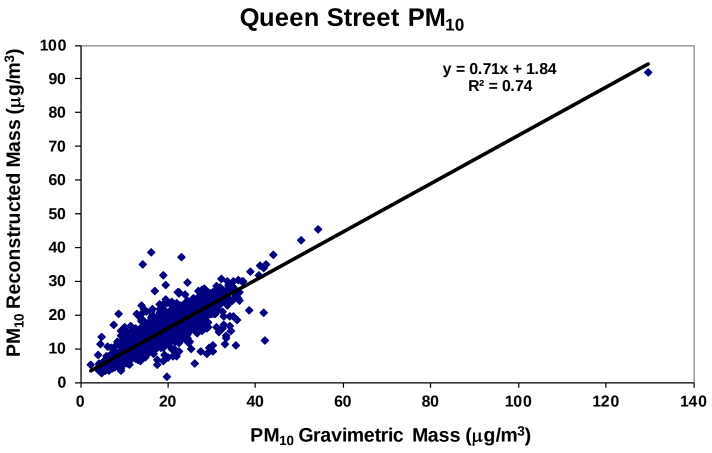

Figure A3.4 Plot of Queen Street PM_{10} elemental mass reconstruction against gravimetric PM_{10} mass.

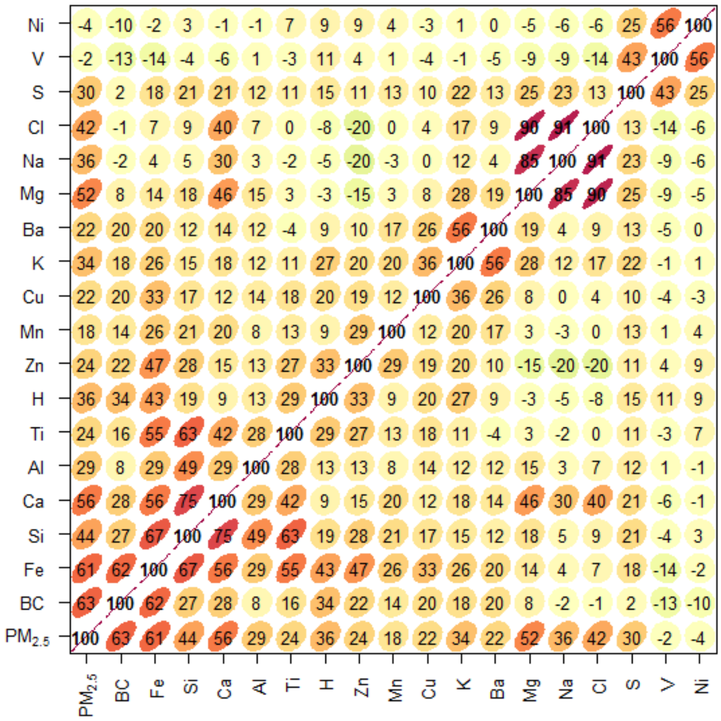

Figure A3.5 Correlation plot matrix for key Queen Street PM_{10} elemental species.

Queen Street PM_{10} PMF RECEPTOR MODELLING DIAGNOSTICS

Summary of EPA PMF settings for receptor modelling of Queen Street PM_{10}

Parameter	**Setting**
Data type; averaging timeframe	PM_{10}, Daily
N samples	2596
N factors	8
Treatment of missing data	No missing data
Treatment of data below detection limit (BDL)	Data used as reported, no modification or censoring of BDL data
Lower limit for normalized factor contributions gik	-0.2
Robust mode	Yes
Constraints	None
Seed value	Random
N bootstraps in BS	200
r^2 for BS	0.6
DISP dQmax	4, 8, 16, 32
DISP active species	PM10, BC, Na, Mg, Al, Si, S, Cl, K, Ca,, Ti, V, Mn, Ni, Zn, Ba
N bootstraps; r^2 for BS in BS-DISP	200; 0.6
BS-DISP active species	BC, Si, S, Cl, K, Ca, V, Zn
BS-DISP dQmax	0.5, 1, 2, 4
Extra modelling uncertainty	15%

Output diagnostics for receptor modelling of Queen Street PM_{10}

Diagnostic	**8 factors**
$Q_{Theoretical}$	26825
$Q_{Expected}$	25816
Q_{true}	13625
Q_{robust}	13413
$Q_{robust}/Q_{expected}$	0.528
DISP Diagnostics:	
Error code	0
Largest Decrease in Q:	0
DISP % dQ	0
DISP swaps by factor	0
BS-DISP Diagnostics:	
BS mapping (Fpeak BS) - unmapped	82% (100%) - 0
BS-DISP % cases accepted	82%
Largest Decrease in Q:	-32.314
BS-DISP % dQ	-0.321
# of Decreases in Q:	11
# of Swaps in Best Fit:	6
# of Swaps in DISP:	20
BS-DISP swaps by factor	10,1,0,3,1,2,0,6

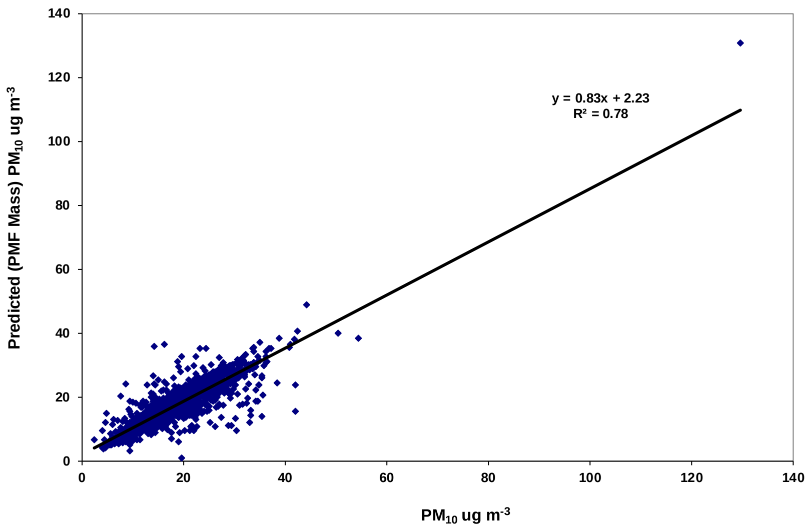

Figure A3.6 Plot of Queen Street PM_{10} predicted (PMF mass) against observed gravimetric PM_{10} mass.

A4.0 APPENDIX 4: KHYBER PASS ROAD DATA ANALYSIS

A4.1 KHYBER PASS ROAD $PM_{2.5}$

Using the methodology outlined in Section A1.4.1, Figure A4.1 presents the mass reconstruction results for Khyber Pass Road $PM_{2.5}$ and Figure A4.2 presents a correlation plot matrix for key elemental species.

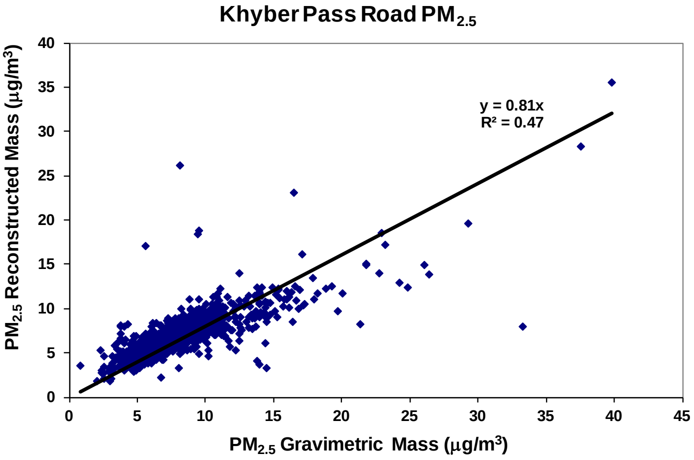

Figure A4.1 Plot of Khyber Pass Road $PM_{2.5}$ elemental mass reconstruction against gravimetric $PM_{2.5}$ mass.

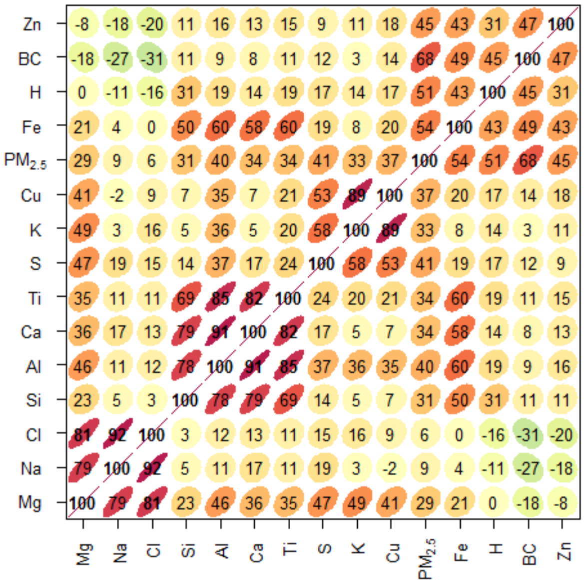

	Mg	Na	Cl	Si	Al	Ca	Ti	S	K	Cu	$PM_{2.5}$	Fe	H	BC	Zn
Zn	-8	-18	-20	11	16	13	15	9	11	18	45	43	31	47	100
BC	-18	-27	-31	11	9	8	11	12	3	14	68	49	45	100	47
H	0	-11	-16	31	19	14	19	17	14	17	51	43	100	45	31
Fe	21	4	0	50	60	58	60	19	8	20	54	100	43	49	43
$PM_{2.5}$	29	9	6	31	40	34	34	41	33	37	100	54	51	68	45
Cu	41	-2	9	7	35	7	21	53	89	100	37	20	17	14	18
K	49	3	16	5	36	5	20	58	100	89	33	8	14	3	11
S	47	19	15	14	37	17	24	100	58	53	41	19	17	12	9
Ti	35	11	11	69	85	82	100	24	20	21	34	60	19	11	15
Ca	36	17	13	79	91	100	82	17	5	7	34	58	14	8	13
Al	46	11	12	78	100	91	85	37	36	35	40	60	19	9	16
Si	23	5	3	100	78	79	69	14	5	7	31	50	31	11	11
Cl	81	92	100	3	12	13	11	15	16	9	6	0	-16	-31	-20
Na	79	100	92	5	11	17	11	19	3	-2	9	4	-11	-27	-18
Mg	100	79	81	23	46	36	35	47	49	41	29	21	0	-18	-8

Figure A4.2 Correlation plot matrix for key Khyber Pass Road $PM_{2.5}$ elemental species.

Khyber Pass Road $PM_{2.5}$ PMF RECEPTOR MODELLING DIAGNOSTICS

PMF analyses involve many details about the development of the data, decisions of what data to include/exclude, determination of a solution, and evaluation of robustness of that solution. The following diagnostics for the PMF solutions are reported as recommended by

Paatero and co-workers (Paatero, Eberly et al. 2014, Brown, Eberly et al. 2015) and should be read in conjunction with Section 3.2 and Appendix 1.

Summary of EPA PMF settings for receptor modelling of Khyber Pass Road $PM_{2.5}$

Parameter	Setting
Data type; averaging timeframe	$PM_{2.5}$, 1-day-in-three
N samples	905
N factors	6
Treatment of missing data	No missing data
Treatment of data below detection limit (BDL)	Data used as reported, no modification or censoring of BDL data
Lower limit for normalized factor contributions gik	-0.2
Robust mode	Yes
Constraints	None
Seed value	Random
N bootstraps in BS	200
r^2 for BS	0.6
DISP dQmax	4, 8, 16, 32
DISP active species	PM2.5, BC, Na, Mg, Al, Si, S, Cl, K, Ca, Fe, Zn
N bootstraps; r^2 for BS in BS-DISP	200; 0.6
BS-DISP active species	BC, Na, Mg, Al, Si, S, Cl, Ca, Fe, Zn
BS-DISP dQmax	0.5, 1, 2, 4
Extra modelling uncertainty	25%

Output diagnostics for receptor modelling of Khyber Pass Road $PM_{2.5}$

Diagnostic	6 factors
$Q_{Theoretical}$	6335
$Q_{Expected}$	5358
Q_{true}	1714.28
Q_{robust}	1714.3
$Q_{robust}/Q_{expected}$	0.320
DISP Diagnostics:	
Error code	0
Largest decrease in Q	0
DISP % dQ	0
DISP swaps by factor	0
BS-DISP Diagnostics:	
BS mapping (Fpeak BS) - Unmapped	98% (100%) - 0
BS-DISP % cases accepted	94%
Largest Decrease in Q:	-28.578
BS-DISP % dQ	-1.67
# of Decreases in Q:	8
# of Swaps in Best Fit:	1
# of Swaps in DISP:	7
BS-DISP swaps by factor	2,1,7,2,4,0

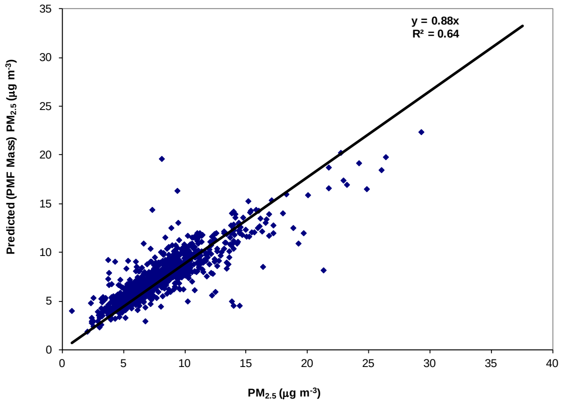

Figure A4.3 Plot of Khyber Pass Road $PM_{2.5}$ predicted (PMF mass) against observed gravimetric $PM_{2.5}$ mass.

A4.2 KHYBER PASS ROAD PM_{10}

Using the methodology outlined in Section A1.4.1, Figure A4.4 presents the mass reconstruction results for Khyber Pass Road PM_{10} and Figure A4.5 presents a correlation plot matrix for key elemental species.

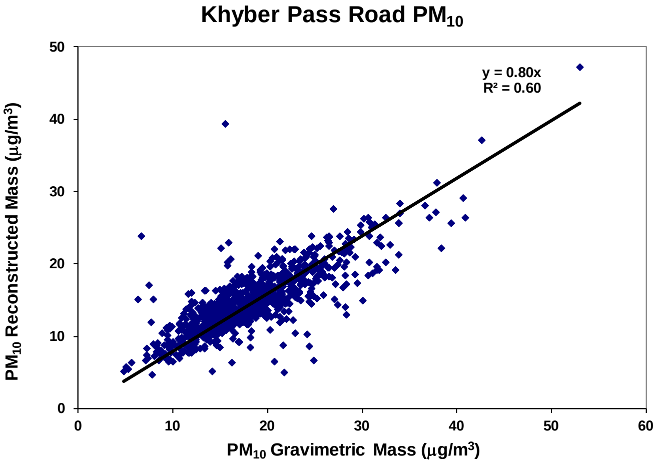

Figure A4.4 Plot of Khyber Pass Road PM_{10} elemental mass reconstruction against gravimetric PM_{10} mass.

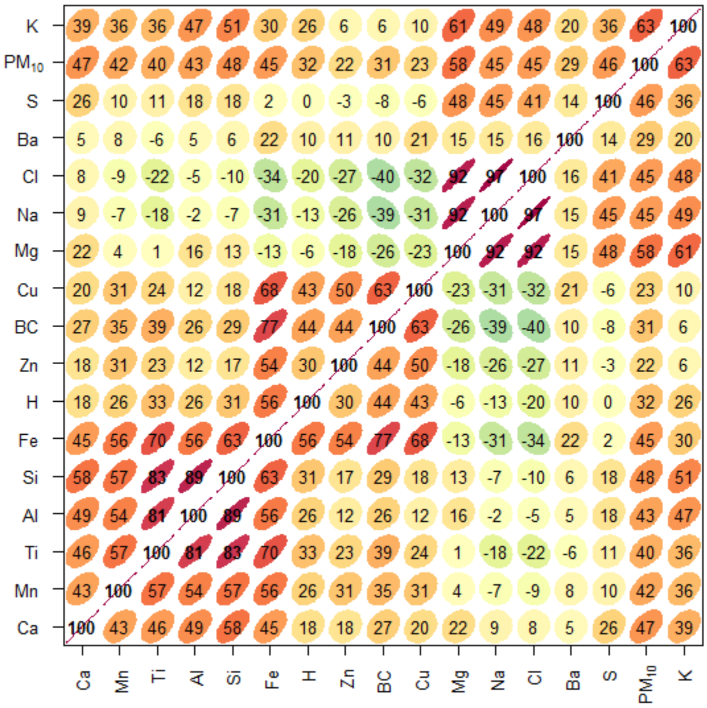

	Ca	Mn	Ti	Al	Si	Fe	H	Zn	BC	Cu	Mg	Na	Cl	Ba	S	PM$_{10}$	K
K	39	36	36	47	51	30	26	6	6	10	61	49	48	20	36	63	100
PM$_{10}$	47	42	40	43	48	45	32	22	31	23	58	45	45	29	46	100	63
S	26	10	11	18	18	2	0	-3	-8	-6	48	45	41	14	100	46	36
Ba	5	8	-6	5	6	22	10	11	10	21	15	15	16	100	14	29	20
Cl	8	-9	-22	-5	-10	-34	-20	-27	-40	-32	92	97	100	16	41	45	48
Na	9	-7	-18	-2	-7	-31	-13	-26	-39	-31	92	100	97	15	45	45	49
Mg	22	4	1	16	13	-13	-6	-18	-26	-23	100	92	92	15	48	58	61
Cu	20	31	24	12	18	68	43	50	63	100	-23	-31	-32	21	-6	23	10
BC	27	35	39	26	29	77	44	44	100	63	-26	-39	-40	10	-8	31	6
Zn	18	31	23	12	17	54	30	100	44	50	-18	-26	-27	11	-3	22	6
H	18	26	33	26	31	56	100	30	44	43	-6	-13	-20	10	0	32	26
Fe	45	56	70	56	63	100	56	54	77	68	-13	-31	-34	22	2	45	30
Si	58	57	83	89	100	63	31	17	29	18	13	-7	-10	6	18	48	51
Al	49	54	81	100	89	56	26	12	26	12	16	-2	-5	5	18	43	47
Ti	46	57	100	81	83	70	33	23	39	24	1	-18	-22	-6	11	40	36
Mn	43	100	57	54	57	56	26	31	35	31	4	-7	-9	8	10	42	36
Ca	100	43	46	49	58	45	18	18	27	20	22	9	8	5	26	47	39

Figure A4.5 Correlation plot matrix for key Khyber Pass Road PM$_{10}$ elemental species.

Khyber Pass Road PM$_{10}$ PMF RECEPTOR MODELLING DIAGNOSTICS

Summary of EPA PMF settings for receptor modelling of Khyber Pass Road PM$_{10}$

Parameter	Setting
Data type; averaging timeframe	PM$_{10}$, 1-day-in-3
N samples	885
N factors	6
Treatment of missing data	No missing data
Treatment of data below detection limit (BDL)	Data used as reported, no modification or censoring of BDL data
Lower limit for normalized factor contributions gik	-0.2
Robust mode	Yes
Constraints	None
Seed value	Random
N bootstraps in BS	200
r^2 for BS	0.6
DISP dQmax	4, 8, 16, 32
DISP active species	PM10, Na, Mg, Al, Si, S, Cl, K, Ca, Ti, Mn, Fe, Cu, Zn, Ba
N bootstraps; r^2 for BS in BS-DISP	200; 0.6
BS-DISP active species	Na, Mg, Al, Si, S, Cl, K, Ca, Ti, Mn, Fe, Cu, Zn, Ba
BS-DISP dQmax	0.5, 1, 2, 4
Extra modelling uncertainty	25%

Output diagnostics for receptor modelling of Khyber Pass Road PM_{10}

Diagnostic	6 factors
$Q_{Theoretical}$	8555
$Q_{Expected}$	7875
Q_{true}	2244.05
Q_{robust}	2244.05
$Q_{robust}/Q_{expected}$	0.285
DISP Diagnostics:	
Error code	0
Largest Decrease in Q:	-0.014
DISP % dQ	-0.00062
DISP swaps by factor	0
BS-DISP Diagnostics:	
BS mapping (Fpeak BS) - unmapped	99% (100%) - 0
BS-DISP % cases accepted	100%
Largest Decrease in Q:	-11.309
BS-DISP % dQ	-0.504
# of Decreases in Q:	0
# of Swaps in Best Fit:	0
# of Swaps in DISP:	1
BS-DISP swaps by factor	0

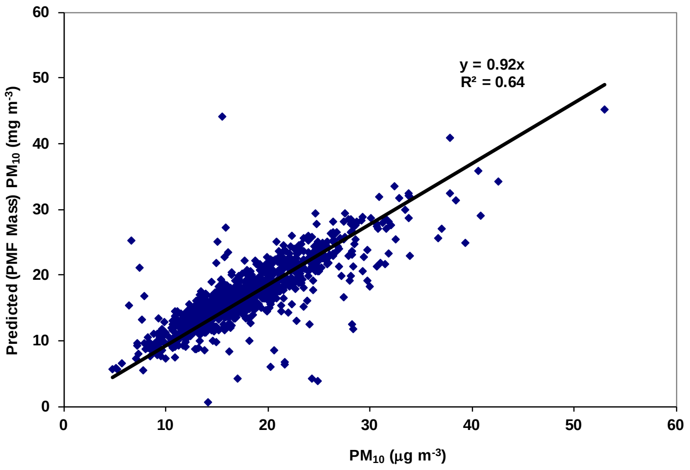

Figure A4.6 Plot of Khyber Pass Road PM_{10} predicted (PMF mass) against observed gravimetric PM_{10} mass.

A5.0 APPENDIX 5: PENROSE DATA ANALYSIS

A5.1 PENROSE $PM_{2.5}$

Using the methodology outlined in Section A1.4.1, Figure A5.1 presents the mass reconstruction results for Penrose $PM_{2.5}$ and Figure A5.2 presents a correlation plot matrix for key elemental species.

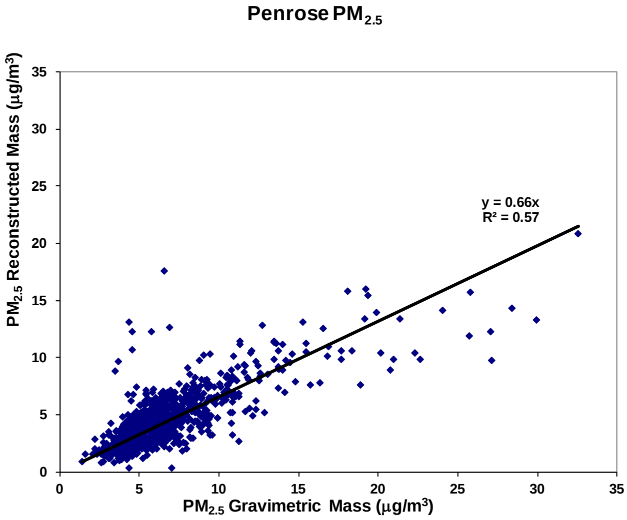

Figure A5.1 Plot of Penrose $PM_{2.5}$ elemental mass reconstruction against gravimetric $PM_{2.5}$ mass.

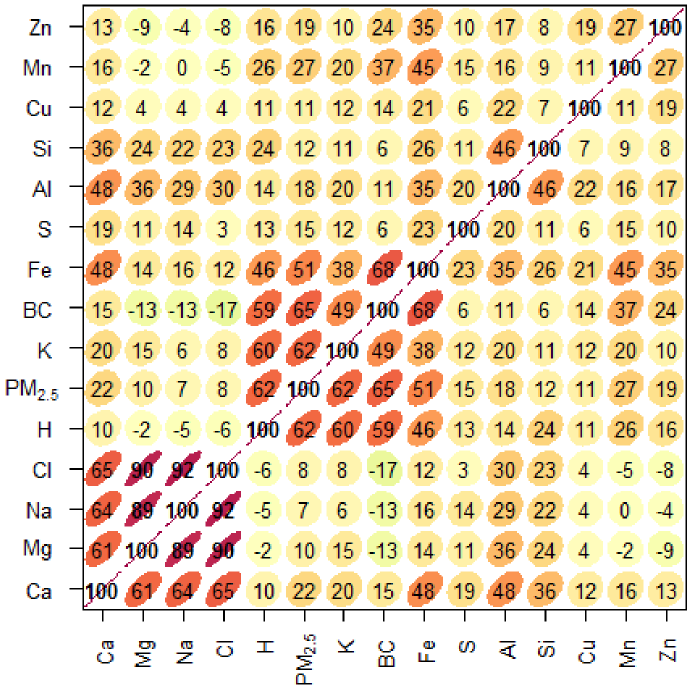

	Ca	Mg	Na	Cl	H	$PM_{2.5}$	K	BC	Fe	S	Al	Si	Cu	Mn	Zn
Zn	13	-9	-4	-8	16	19	10	24	35	10	17	8	19	27	100
Mn	16	-2	0	-5	26	27	20	37	45	15	16	9	11	100	27
Cu	12	4	4	4	11	11	12	14	21	6	22	7	100	11	19
Si	36	24	22	23	24	12	11	6	26	11	46	100	7	9	8
Al	48	36	29	30	14	18	20	11	35	20	100	46	22	16	17
S	19	11	14	3	13	15	12	6	23	100	20	11	6	15	10
Fe	48	14	16	12	46	51	38	68	100	23	35	26	21	45	35
BC	15	-13	-13	-17	59	65	49	100	68	6	11	6	14	37	24
K	20	15	6	8	60	62	100	49	38	12	20	11	12	20	10
$PM_{2.5}$	22	10	7	8	62	100	62	65	51	15	18	12	11	27	19
H	10	-2	-5	-6	100	62	60	59	46	13	14	24	11	26	16
Cl	65	90	92	100	-6	8	8	-17	12	3	30	23	4	-5	-8
Na	64	89	100	92	-5	7	6	-13	16	14	29	22	4	0	-4
Mg	61	100	89	90	-2	10	15	-13	14	11	36	24	4	-2	-9
Ca	100	61	64	65	10	22	20	15	48	19	48	36	12	16	13

Figure A5.2 Correlation plot matrix for key Penrose $PM_{2.5}$ elemental species.

Penrose $PM_{2.5}$ PMF RECEPTOR MODELLING DIAGNOSTICS

PMF analyses involve many details about the development of the data, decisions of what data to include/exclude, determination of a solution, and evaluation of robustness of that solution. The following diagnostics for the PMF solutions are reported as recommended by Paatero and co-workers (Paatero, Eberly et al. 2014, Brown, Eberly et al. 2015) and should be read in conjunction with Section 3.2 and Appendix 1.

Summary of EPA PMF settings for receptor modelling of Penrose $PM_{2.5}$

Parameter	Setting
Data type; averaging timeframe	$PM_{2.5}$, 1-day-in-three
N samples	798
N factors	8
Treatment of missing data	No missing data
Treatment of data below detection limit (BDL)	Data used as reported, no modification or censoring of BDL data
Lower limit for normalized factor contributions gik	-0.2
Robust mode	Yes
Constraints	None
Seed value	Random
N bootstraps in BS	200
r^2 for BS	0.6
DISP dQmax	4, 8, 16, 32
DISP active species	PM2.5, BC, Na, Mg, Al, Si, S, Cl, K, Ca, Fe, Zn
N bootstraps; r^2 for BS in BS-DISP	200; 0.6
BS-DISP active species	BC, Na, Mg, Al, Si, S, Cl, K, Ca, Fe, Zn
BS-DISP dQmax	0.5, 1, 2, 4
Extra modelling uncertainty	25%

Output diagnostics for receptor modelling of Penrose $PM_{2.5}$

Diagnostic	6 factors
$Q_{Theoretical}$	6335
$Q_{Expected}$	5358
Q_{true}	1714.28
Q_{robust}	1714.3
$Q_{robust}/Q_{expected}$	0.320
DISP Diagnostics:	
Error code	0
Largest decrease in Q	0
DISP % dQ	0
DISP swaps by factor	0
BS-DISP Diagnostics:	
BS mapping (Fpeak BS) - Unmapped	100% (100%) - 0
BS-DISP % cases accepted	99%
Largest Decrease in Q:	-20.75
BS-DISP % dQ	-2.056
# of Decreases in Q:	1
# of Swaps in Best Fit:	0
# of Swaps in DISP:	1
BS-DISP swaps by factor	0

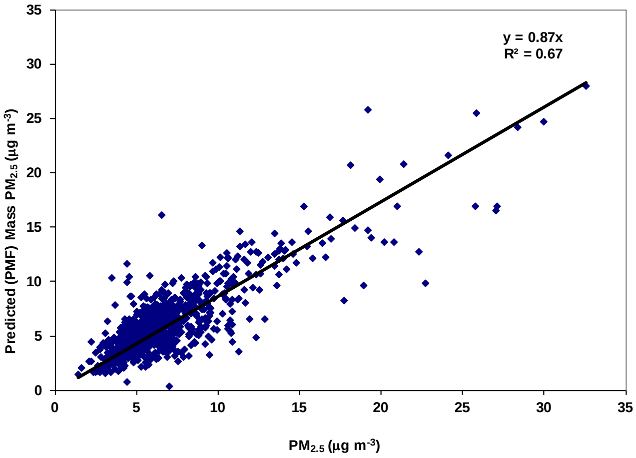

Figure A5.3 Plot of Penrose $PM_{2.5}$ predicted (PMF mass) against observed gravimetric $PM_{2.5}$ mass.

A5.2 PENROSE PM_{10}

Using the methodology outlined in Section A1.4.1, Figure A5.3 presents the mass reconstruction results for Penrose PM_{10} and Figure A5.5 presents a correlation plot matrix for key elemental species.

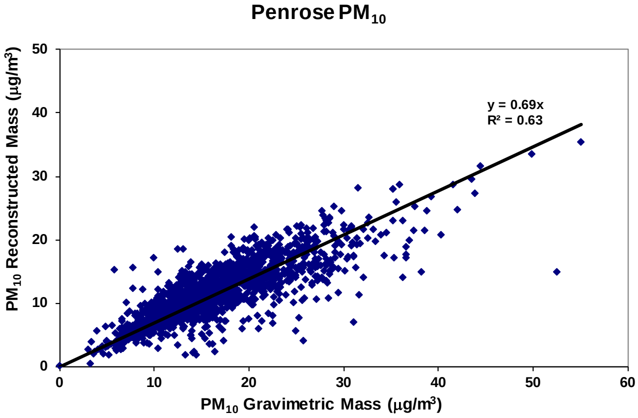

Figure A5.4 Plot of Penrose PM_{10} elemental mass reconstruction against gravimetric PM_{10} mass.

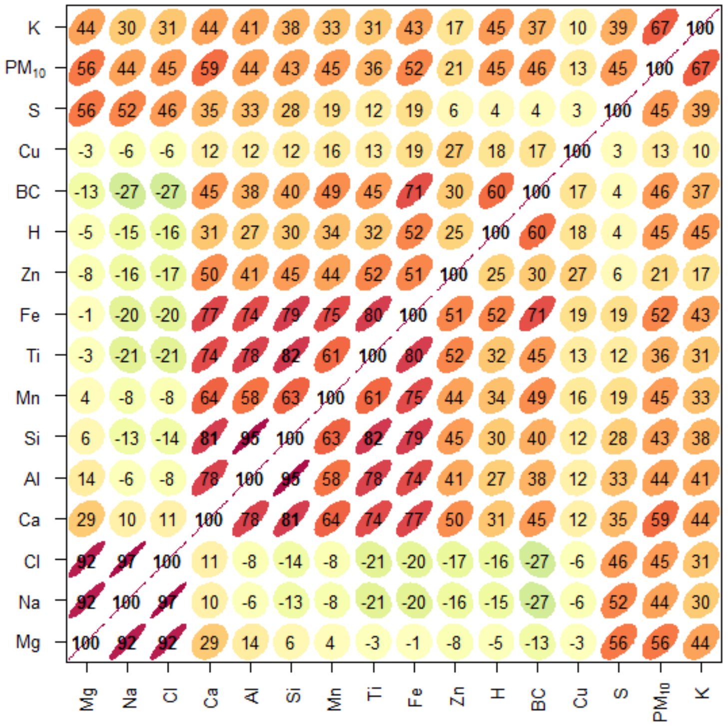

	Mg	Na	Cl	Ca	Al	Si	Mn	Ti	Fe	Zn	H	BC	Cu	S	PM_{10}	K
K	44	30	31	44	41	38	33	31	43	17	45	37	10	39	67	100
PM_{10}	56	44	45	59	44	43	45	36	52	21	45	46	13	45	100	67
S	56	52	46	35	33	28	19	12	19	6	4	4	3	100	45	39
Cu	-3	-6	-6	12	12	12	16	13	19	27	18	17	100	3	13	10
BC	-13	-27	-27	45	38	40	49	45	71	30	60	100	17	4	46	37
H	-5	-15	-16	31	27	30	34	32	52	25	100	60	18	4	45	45
Zn	-8	-16	-17	50	41	45	44	52	51	100	25	30	27	6	21	17
Fe	-1	-20	-20	77	74	79	75	80	100	51	52	71	19	19	52	43
Ti	-3	-21	-21	74	78	82	61	100	80	52	32	45	13	12	36	31
Mn	4	-8	-8	64	58	63	100	61	75	44	34	49	16	19	45	33
Si	6	-13	-14	81	95	100	63	82	79	45	30	40	12	28	43	38
Al	14	-6	-8	78	100	95	58	78	74	41	27	38	12	33	44	41
Ca	29	10	11	100	78	81	64	74	77	50	31	45	12	35	59	44
Cl	92	97	100	11	-8	-14	-8	-21	-20	-17	-16	-27	-6	46	45	31
Na	92	100	97	10	-6	-13	-8	-21	-20	-16	-15	-27	-6	52	44	30
Mg	100	92	92	29	14	6	4	-3	-1	-8	-5	-13	-3	56	56	44

Figure A5.5 Correlation plot matrix for key Penrose PM_{10} elemental species.

Penrose PM_{10} PMF RECEPTOR MODELLING DIAGNOSTICS

Summary of EPA PMF settings for receptor modelling of Penrose PM_{10}

Parameter	Setting
Data type; averaging timeframe	PM_{10}, 2-day-in-3 (RAAS and Partisol PM_{10} samples combined)
N samples	1559
N factors	6
Treatment of missing data	No missing data
Treatment of data below detection limit (BDL)	Data used as reported, no modification or censoring of BDL data
Lower limit for normalized factor contributions gik	-0.2
Robust mode	Yes
Constraints	None
Seed value	Random
N bootstraps in BS	200
r^2 for BS	0.6
DISP dQmax	4, 8, 16, 32
DISP active species	PM10, BC, Na, Mg, Al, Si, S, Cl, K, Ca, Fe, Zn
N bootstraps; r^2 for BS in BS-DISP	200; 0.6
BS-DISP active species	BC, Na, Mg, Al, Si, S, Cl, K, Ca, Fe, Zn
BS-DISP dQmax	0.5, 1, 2, 4
Extra modelling uncertainty	25%

Output diagnostics for receptor modelling of Penrose PM_{10}

Diagnostic	6 factors
$Q_{Theoretical}$	11432
$Q_{Expected}$	9282
Q_{true}	2902.68
Q_{robust}	2902.68
$Q_{robust}/Q_{expected}$	0.313
DISP Diagnostics:	
Error code	0
Largest Decrease in Q:	-0.02
DISP % dQ	-0.00069
DISP swaps by factor	0
BS-DISP Diagnostics:	
BS mapping (Fpeak BS) - unmapped	100% (100%) - 0
BS-DISP % cases accepted	99%
Largest Decrease in Q:	-9.641
BS-DISP % dQ	-0.332
# of Decreases in Q:	0
# of Swaps in Best Fit:	0
# of Swaps in DISP:	2
BS-DISP swaps by factor	0,1,0,1,0,0

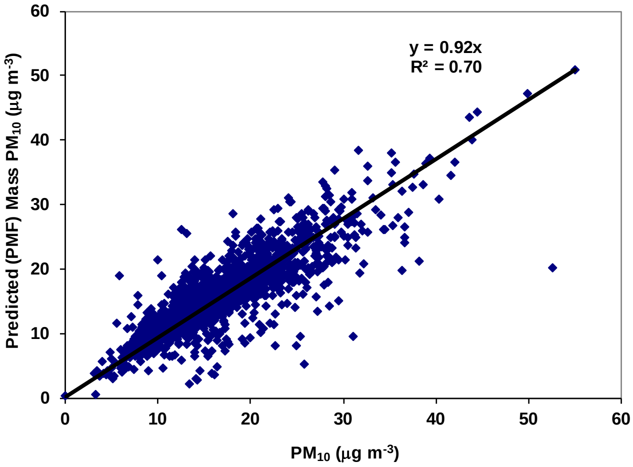

Figure A5.6 Plot of Penrose PM_{10} predicted (PMF mass) against observed gravimetric PM_{10} mass.

A6.0 APPENDIX 6: HENDERSON DATA ANALYSIS

A6.1 HENDERSON PM_{10}

Using the methodology outlined in Section A1.4.1, Figure A6.1 presents the mass reconstruction results for Henderson PM_{10} and Figure A6.2 presents a correlation plot matrix for key elemental species.

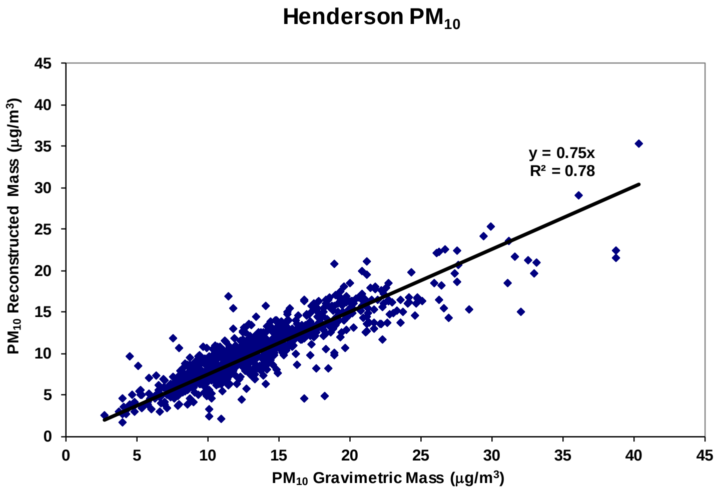

Figure A6.1 Plot of Henderson PM_{10} elemental mass reconstruction against gravimetric PM_{10} mass.

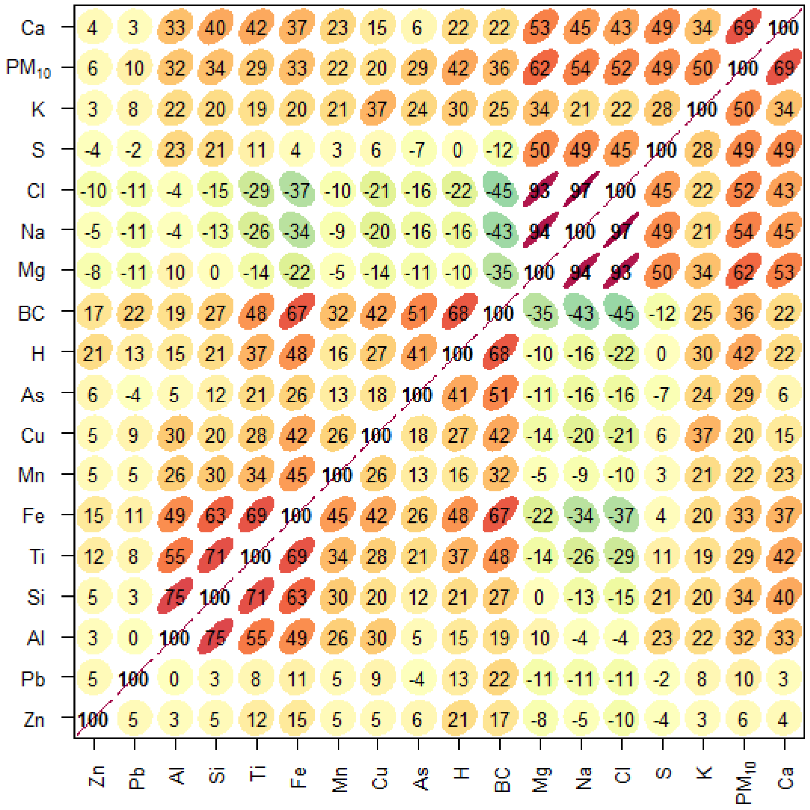

	Zn	Pb	Al	Si	Ti	Fe	Mn	Cu	As	H	BC	Mg	Na	Cl	S	K	PM_{10}	Ca
Ca	4	3	33	40	42	37	23	15	6	22	22	53	45	43	49	34	69	100
PM_{10}	6	10	32	34	29	33	22	20	29	42	36	62	54	52	49	50	100	69
K	3	8	22	20	19	20	21	37	24	30	25	34	21	22	28	100	50	34
S	-4	-2	23	21	11	4	3	6	-7	0	-12	50	49	45	100	28	49	49
Cl	-10	-11	-4	-15	-29	-37	-10	-21	-16	-22	-45	93	97	100	45	22	52	43
Na	-5	-11	-4	-13	-26	-34	-9	-20	-16	-16	-43	94	100	97	49	21	54	45
Mg	-8	-11	10	0	-14	-22	-5	-14	-11	-10	-35	100	94	93	50	34	62	53
BC	17	22	19	27	48	67	32	42	51	68	100	-35	-43	-45	-12	25	36	22
H	21	13	15	21	37	48	16	27	41	100	68	-10	-16	-22	0	30	42	22
As	6	-4	5	12	21	26	13	18	100	41	51	-11	-16	-16	-7	24	29	6
Cu	5	9	30	20	28	42	26	100	18	27	42	-14	-20	-21	6	37	20	15
Mn	5	5	26	30	34	45	100	26	13	16	32	-5	-9	-10	3	21	22	23
Fe	15	11	49	63	69	100	45	42	26	48	67	-22	-34	-37	4	20	33	37
Ti	12	8	55	71	100	69	34	28	21	37	48	-14	-26	-29	11	19	29	42
Si	5	3	75	100	71	63	30	20	12	21	27	0	-13	-15	21	20	34	40
Al	3	0	100	75	55	49	26	30	5	15	19	10	-4	-4	23	22	32	33
Pb	5	100	0	3	8	11	5	9	-4	13	22	-11	-11	-11	-2	8	10	3
Zn	100	5	3	5	12	15	5	5	6	21	17	-8	-5	-10	-4	3	6	4

Figure A6.2 Correlation plot matrix for key Henderson PM_{10} elemental species.

Henderson PM_{10} PMF RECEPTOR MODELLING DIAGNOSTICS

Summary of EPA PMF settings for receptor modelling of Henderson PM_{10}

PMF analyses involve many details about the development of the data, decisions of what data to include/exclude, determination of a solution, and evaluation of robustness of that solution. The following diagnostics for the PMF solutions are reported as recommended by Paatero and co-workers (Paatero, Eberly et al. 2014, Brown, Eberly et al. 2015) and should be read in conjunction with Section 3.2 and Appendix 1.

Parameter	Setting
Data type; averaging timeframe	PM_{10}, 1-day-in-3
N samples	789
N factors	6
Treatment of missing data	No missing data
Treatment of data below detection limit (BDL)	Data used as reported, no modification or censoring of BDL data
Lower limit for normalized factor contributions gik	-0.2
Robust mode	Yes
Constraints	None
Seed value	Random
N bootstraps in BS	200
r^2 for BS	0.6
DISP dQmax	4, 8, 16, 32
DISP active species	PM10, Na, Mg, Al, Si, S, Cl, K, Ca, Ti, Fe, Cu, Zn, As
N bootstraps; r^2 for BS in BS-DISP	200; 0.6
BS-DISP active species	Na, Mg, Al, Si, S, Cl, K, Ca, Ti, Fe, Cu, Zn
BS-DISP dQmax	0.5, 1, 2, 4
Extra modelling uncertainty	25%

Output diagnostics for receptor modelling of Henderson PM_{10}

Diagnostic	6 factors
$Q_{Theoretical}$	7627
$Q_{Expected}$	6228
Q_{true}	1674.77
Q_{robust}	1674.77
$Q_{robust}/Q_{expected}$	0.269
DISP Diagnostics:	
Error code	0
Largest Decrease in Q:	-0.037
DISP % dQ	-0.00221
DISP swaps by factor	0
BS-DISP Diagnostics:	
BS mapping (Fpeak BS) - unmapped	99% (100%) - 0
BS-DISP % cases accepted	96%
Largest Decrease in Q:	-82.214
BS-DISP % dQ	-4.909
# of Decreases in Q:	2
# of Swaps in Best Fit:	0
# of Swaps in DISP:	5
BS-DISP swaps by factor	0,0,0,0,1,1

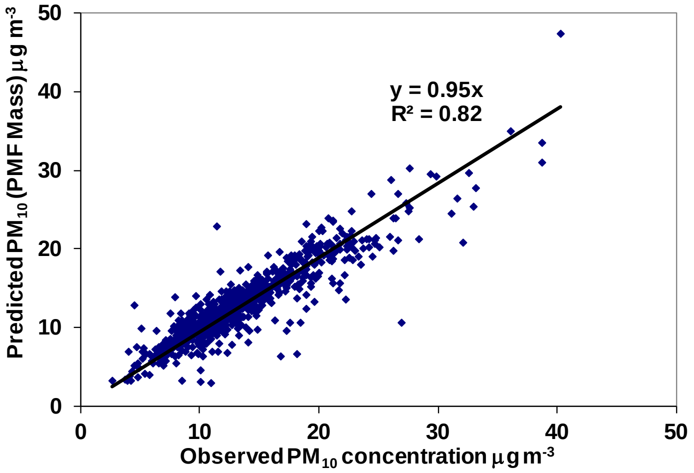

Figure A6.3 Plot of Henderson PM_{10} predicted (PMF mass) against observed gravimetric PM_{10} mass.

The Henderson PM_{10} data was run as a constrained model run in order to pull down any contribution from the Zinc source before the appearance of significant elemental zinc concentrations in July 2010 (see Section 10.6.2). The table below contains the constrained run diagnostics.

Output diagnostics for receptor modelling of Henderson PM_{10}

Constraint	6 factors
Factor	Factor 5 (Zinc source)
Element	17/8/2006 – 12/7/2010
Type	Pull Down
Value	NA
dQ	8.37
%dQ	0.5
Q_{true}	1862.6
Q_{robust}	2723.7
$Q_{robust}/Q_{expected}$	0.269
Constrained DISP Diagnostics:	
Error code	0
DISP % dQ	-0.00018
DISP swaps by factor	0
Constrained BS-DISP Diagnostics:	
BS mapping - unmapped	100% - 0
BS-DISP % cases accepted	99%
BS-DISP % dQ	-0.0278
BS-DISP swaps by factor	0

Find out more: phone 09 301 0101, email rimu@aucklandcouncil.govt.nz or visit aucklandcouncil.govt.nz and knowledgeauckland.org.nz

Auckland Council
Te Kaunihera o Tāmaki Makaurau